

---

# A “Trojan horse” strategy to reverse drug- resistance in brain tumors

---

Martha Leonor Pinzón Daza

---

Doctorado en Ciencias  
Biomédicas Universidad del  
Rosario 2014

---



UNIVERSIDAD DEL ROSARIO  
Colegio Mayor de Nuestra Señora del Rosario - 1653

UNIVERSITÀ  
DEGLI STUDI  
DI TORINO  
ALMA UNIVERSITAS  
TAURINENSIS



UNIVERSIDAD DEL ROSARIO  
DOCTORADO EN CIENCIAS BIOMEDICAS

UNIVERSITÀ DEGLI STUDI DI TORINO  
DOTTORATO IN MEDICINA MOLECOLARE

**A "Trojan horse" strategy to reverse drug-resistance in brain tumors**

***Martha Leonor Pinzón Daza***

**DIRECTOR:**

**Chiara Riganti, PhD**

**Assitant Professor of Biochemistry  
of Oncology**

**Medicine School, University of Turin, Italy**

**CO-DIRECTOR:**

**Ruth Garzón, PhD**

**Principal Professor of Biochemistry Departament  
Faculty of Natural Science and Mathematics**

**Universidad del Rosario, Bogotá, Colombia**

**BOGOTA, 2014**

UNIVERSIDAD DEL ROSARIO  
DOCTORADO EN CIENCIAS BIOMEDICAS

UNIVERSITÀ DEGLI STUDI DI TORINO  
DOTTORATO IN MEDICINA MOLECOLARE

**A "Trojan horse" strategy to reverse drug-resistance in brain tumors**

**BOGOTA, 2014**

**CONTENT**

<b>ABSTRACT (English)</b>	<b>2</b>
<b>ABSTRACT (Italian)</b>	<b>4</b>
<b>ABSTRACT (RESUMEN) (Spanish)</b>	<b>6</b>
<b>LIST OF PUBLICATIONS</b>	<b>8</b>
<b>ABREVIATIONS</b>	<b>9</b>
<b>ACKNOWLEDGEMENTS</b>	<b>11</b>
<b>1. Justification</b>	<b>12</b>
<b>2. Theoretical framework</b>	<b>14</b>
<b>2.1. Brain tumors</b>	<b>14</b>
<b>2.2. Blood Brain Barrier</b>	<b>15</b>
<b>2.3. Multidrug resistance genes and ABC transporters</b>	<b>17</b>
<b>2.4. ABC transporters and hypoxia</b>	<b>20</b>
<b>2.5. Therapeutic approach to brain cancer, the use of nanoparticles         and liposomes (Article II)</b>	<b>21</b>
<b>2.5.1. Statins and mechanism of action</b>	<b>25</b>
<b>2.6. ABC transporters and signaling pathway</b>	<b>27</b>
<b>3. Hypothesis</b>	<b>29</b>
<b>4. General objective</b>	<b>30</b>
<b>4.1. Specific objectives</b>	<b>30</b>
<b>5. General discussion</b>	<b>30</b>
<b>6. Conclusions and perspectives</b>	<b>35</b>
<b>7. References</b>	<b>37</b>

## **ABSTRACT**

Malignant gliomas represent one of the most aggressive forms of Central Nervous System (CNS) tumors. According to the WHO classification of brain tumors, astrocytomas have been categorized into four grades, determined by the underlying pathology. Malignant (or high-grade) gliomas include anaplastic glioma (WHO grade III) as well as glioblastoma multiforme (GBM; WHO grade IV). These are the most aggressive brain tumors with the worst prognosis (1). The therapeutic management of CNS tumors is based on surgery, radiotherapy and chemotherapy, depending on the characteristics of the tumor, the clinical stage and age (2), (3), however none of the standard treatments is completely safe and compatible with an acceptable quality of life (3), (4). Chemotherapy is the first choice in disseminated tumors, like invasive glioblastoma, high-risk medulloblastoma or multiple metastasis, but the prognosis in these patients is very poor (2),(3). New targeted therapies (2), anti-angiogenic therapies (3), (4) or gene therapies show a real benefit only in limited groups of patients with known specific molecular defects (4). Thereby, the development of new pharmacological therapies for brain tumors is mandatory. Malignant gliomas are frequently chemoresistant and this resistance seems to depend on at least two mechanisms: first, the poor penetration of many anticancer drugs across the blood-brain barrier (BBB), the blood-cerebrospinal fluid barrier (BCSFB) and the blood-tumor barrier (BTB), due to their interaction with several ATP-binding cassette (ABC) drug efflux transporters that are overexpressed by the endothelial or epithelial cells of these barriers. Second, ABC drug efflux transporters in tumor cells confer multidrug resistance (MDR) on several other solid tumors; they are present on CNS tumors too and their role in gliomas is under investigation (5). Drug delivery across the blood-brain barrier (BBB) is one of the vital problems in targeted therapy treatments. Recent studies have shown that some small molecules used in these therapies are substrates of P-glycoprotein (Pgp), as well as other efflux pumps like multidrug resistance-related proteins (MRPs) and breast-cancer resistance related protein (BCRP), which extrude several anticancer drugs and will not allow drugs to reach the tumor (1).

DOXOrubicin (DOXO), a drug widely used in anti-cancer therapy, is a substrate of Pgp and BCRP, and it is very effective to attack the vitro brain tumor cells, but has a limited clinical use for its low delivery across BBB and the resistance of tumors. On the other hand BBB cells and brain tumor cells also have surface proteins, such as Low Density Lipoprotein Receptor (LDLR), which could be used as a therapeutic target. The importance of this study is based on the generation of therapeutical strategies to promote the passage of drugs through the BBB and the intratumoral accumulation, and at the same time, on the analysis of cellular mechanisms that induce increased expression of ABC transporters, to be used as therapeutic targets.

In this work we demonstrated that the use of a new strategy based on the "Trojan horse", which combines DOXOrubicin introduced into a liposome, could safeguards the drug to prevent its recognition by the ABC transporters in both the BBB and the tumor cells. The construction of liposome allowed using the LDLR receptor cells as docking receptor, ensuring the entrance through the BBB and into the tumor cells through a process of endocytosis. This mechanism was associated with the use of statins, anti-cholesterol drugs which favoured the expression of LDLR and decreased the activity of ABC transporters, increasing the efficiency of our Trojan horse. Accordingly, I demonstrated that the use of a new DOXOrubicin liposomal formulation mimicking LDLs, called ApolipoDOXO, further favors drug delivery

### ***A "Trojan Horse" strategy to reverse drug-resistance in brain tumors***

through the BBB, overcoming the resistance of tumor and reducing the side effects of DOXOrubicin dose. In addition this strategy can be considered as a new strategy to increase the effectiveness of different drugs in several brain tumors and ensures high efficiency even in a hypoxic environment, characteristic of cancer cells, where the expression of Pgp transporter was increased.

Taking advantage of another signaling pathway recognized as a modulator of Pgp activity this study presents not only the strategy of the Trojan horse, but also a second therapeutic proposal related to the use of Temozolomide plus DOXOrubicin. This strategy showed that temozolomide (TMZ) penetrated the BBB in a way involved the Wnt/GSK3/ $\beta$ -catenin signaling pathway, which modulates the expression of Pgp transporter. It was demonstrated that the TMZ reduces Wnt3 protein and mRNA allowing raising the hypothesis that this drug decreases Wnt3 gene transcription in BBB cells, decreasing  $\beta$ -catenin pathway activation by its phosphorylation, reducing  $\beta$ -catenin nuclear translocation and binding to the promoter of the *mdr1* gene. Taking together the results of this study allowed the recognition of three basic mechanisms related to the down-regulation of Pgp and associated strategies: the first was the use of statins, which led to the transporter nitration decreasing its activity by NF $\kappa$ B pathway; the second one was based on the use of temozolomide, which by methylating Wnt3 gene reduces the activity of the  $\beta$ -catenin signaling pathway, decreasing the expression of Pgp transporter; the third one consisted on the cross-talk between the Wnt/GSK3/ $\beta$ -catenin axis and the Wnt/RhoA/RhoA kinase as a modulator of *mdr1* transcription: we demonstrated that RhoA protein kinase promoted the activation of the protein PTB1, which by phosphorylating GSK3 induced phosphorylation of  $\beta$ -catenin, priming it for destruction by the proteasome, avoiding the binding to the promoter of the *mdr1* gene and therefore reducing Pgp expression. In conclusion, the therapeutic strategies proposed in this work increased the cytotoxicity of tumour cells by increasing permeability not only in the BBB, but also in tumor barrier. Also, the "Trojan horse" strategy could be useful for the therapy of other diseases associated with the central nervous system. On the other hand, these studies indicate that recognition of mechanisms associated with the expression of ABC transporters could be a key tool in the development of new anti-cancer therapies.

## **ABSTRACT**

Il glioma maligno rappresenta una delle forme più aggressive di tumore del sistema nervoso centrale (SNC). In base alla classificazione WHO dei tumori cerebrali, gli astrocitomi sono stati suddivisi in quattro gradi, in base ai loro caratteri patologici. I gliomi maligni o di altro grado comprendono il glioma anaplastico (grado III WHO) ed il glioblastoma multiforme (GBM; gradi IV WHO). Questi sono i tumori più aggressivi e dalla prognosi peggiore (1). Il trattamento terapeutico dei tumori del SNC è basato su chirurgia, radioterapia e chemioterapia, in base alle caratteristiche del tumore, allo stadio clinico ed all'età (2), (3), tuttavia nessuno di questi trattamenti standard è sicuro e compatibile con una qualità di vita accettabile (3), (4). La chemioterapia è la prima scelta terapeutica nei tumori disseminati, come il glioblastoma invasivo, il medulloblastoma ad alto rischio o le metastasi multiple, ma la prognosi di questi pazienti è molto scadente (2), (3). Le nuove "targeted therapies" (2), le terapie anti-angiogeniche (3), (4) o le terapie geniche mostrano un reale beneficio solo in un gruppo limitato di pazienti con specifici difetti molecolari (4). Pertanto, è necessario sviluppare nuove strategie farmacologiche per i tumori cerebrali. I gliomi maligni sono spesso chemioresistenti e tale resistenza è dovuta a due fattori: primo, la bassa penetrazione di molti farmaci antitumorali attraverso la barriera ematoencefalica (BEE), la barriera emato-cerebrospinale (BECS) e la barriera emato-tumorale (BET), a causa della loro interazione con numerosi trasportatori di efflusso ATP Binding Cassette (ABC), che sono iperespressi nelle cellule endoteliali o epiteliali di queste barriere. In secondo luogo, i trasportatori di efflusso ABC conferiscono un fenotipo multidrug resistance (MDR) a molti tumori solidi; essi sono presenti anche nei tumori del SNC e la loro funzione nei gliomi è oggetto di studio (5). Il delivery di farmaci attraverso la BBB è uno dei problemi critici nelle "targeted therapies". Studi recenti hanno mostrato che molte molecole usate in tali terapie sono substrati della glicoproteina P (Pgp) e di altre pompe di efflusso, come le MDR-related proteins (MRP) e la breast-cancer resistance related protein (BCRP), che estrudono numerosi farmaci antitumorali impedendo loro di raggiungere il tumore (1).

La DOXOrubicina (DOXO), un farmaco ampiamente usato nella terapia antitumorale, è substrato di Pgp e BCRP; è molto efficiente in vitro contro le cellule derivate da tumori cerebrali, ma ha un uso clinico limitato a causa del suo basso passaggio attraverso la BBB e della resistenza tumorale. D'altra parte, le cellule di BBB e dei tumori cerebrali hanno anche proteine di superficie, come il recettore per le lipoproteine a bassa densità (RLDL) che può essere usato come bersaglio terapeutico. Questo studio è stato incentrato sulla creazione di strategie terapeutiche che incrementino il passaggio dei farmaci attraverso la BEE ed il loro accumulo intratumorale e sull'analisi dei meccanismi molecolari che inducono l'aumentata espressione dei trasportatori ABC, al fine di sfruttarli come bersagli terapeutici.

In questo lavoro ho dimostrato che l'uso di una nuova strategia "cavallo di Troia", basata sulla DOXO liposomiale, può evitare che il farmaco sia estruso dai trasportatori ABC presenti sia sulla BEE sia sulle cellule tumorali. La formulazione liposomiale ha permesso di sfruttare il RLDL come punto di attracco, per garantire l'entrata nella BEE e nelle cellule tumorali mediante endocitosi. Tale approccio è stato combinato con l'uso di statine, farmaci anti-colesterolemici che hanno favorito l'espressione del RLDL e diminuito l'attività dei trasportatori ABC, aumentando ulteriormente l'efficacia del mio approccio. In linea con questo, ho dimostrato che l'uso di una nuova DOXO liposomiale mimante le LDL, chiamata ApolipoDOXO, aumenta ulteriormente il passaggio del farmaco attraverso la BEE, bypassa la resistenza delle cellule tumorali e riduce gli effetti collaterali legati alla DOXO. Questa strategia può essere usata per aumentare l'efficacia di diversi farmaci nei tumori cerebrali e

## *A "Trojan Horse" strategy to reverse drug-resistance in brain tumors*

per garantire una buona efficienza anche in ambienti ipossici, caratteristici dei tumori, dove l'espressione della Pgp è aumentata.

Sfruttando un'altra via di segnale riconosciuta come modulatrice dell'attività di Pgp, il mio lavoro presenta anche un secondo approccio terapeutico basato sulla combinazione di temozolomide (TMZ) e DOXO. Tale studio ha mostrato che la TMZ può modulare sulla BEE la via di segnale Wnt/GSK3/ $\beta$ -catenina, che regola l'espressione della Pgp. Ho dimostrato che la TMZ riduce sia il mRNA che la proteina Wnt3, lasciando ipotizzare che tale farmaco riduca la trascrizione di Wnt3 nelle cellule di BEE, diminuendo di conseguenza l'attivazione della  $\beta$ -catenina tramite fosforilazione, la sua traslocazione nucleare ed il suo legame sul promotore del gene *mdr1*.

Nell'insieme lo studio ha permesso di identificare tre meccanismi che possono ridurre la quantità di Pgp e possono essere usati come strategie terapeutiche: primo, l'uso di statine, che inducono nitratozione di Pgp e diminuzione della sua attività, tramite la via di NF $\kappa$ B; secondo, l'uso della TMZ, che metilando il gene Wnt3, riduce l'attività della  $\beta$ -catenina e l'espressione della Pgp. Il terzo si basa sul cross-talk tra la via Wnt/GSK3/ $\beta$ -catenina e la via Wnt/RhoA/RhoA cinasi, come modulatore della trascrizione del gene *mdr1*: ho dimostrato che RhoA cinasi attiva la proteina PTPB1; quest'ultima - tramite defosforilazione di GSK3 - promuove la fosforilazione di  $\beta$ -catenina, indirizzandola alla degradazione proteasomiale, impedendone il legame sul promotore del gene *mdr1* e riducendo così l'espressione di Pgp.

In conclusione, le strategie terapeutiche proposte in questo lavoro hanno aumentato la citotossicità da chemioterapici nelle cellule tumorali aumentando la permeabilità non solo della BEE, ma anche del tumore. La strategia "cavallo di Troia" proposta può essere utile per la terapia anche di altre patologie del SNC. Inoltre, questo studio suggerisce che la conoscenza dei meccanismi che regolano l'espressione dei trasportatori ABC può essere un utile strumento per sviluppare nuove terapie anti-tumorali.

## RESUMEN

Los gliomas malignos representan una de las formas más agresivas de los tumores del sistema nervioso central (SNC). De acuerdo con la clasificación de los tumores cerebrales de la Organización Mundial de la Salud (OMS), los astrocitomas han sido categorizados en cuatro grados, determinados por la patología subyacente. Es así como los gliomas malignos (o de alto grado) incluyen el glioma anaplásico (grado III) así como el glioblastoma multiforme (GBM, grado IV), estos últimos los más agresivos con el peor pronóstico (1). El manejo terapéutico de los tumores del SNC se basa en la cirugía, la radioterapia y la quimioterapia, dependiendo de las características del tumor, el estadio clínico y la edad (2),(3), sin embargo ninguno de los tratamientos estándar es completamente seguro y compatible con una calidad de vida aceptable (3), (4). En general, la quimioterapia es la primera opción en los tumores diseminados, como el glioblastoma invasivo y el meduloblastoma de alto riesgo o con metástasis múltiple, pero el pronóstico en estos pacientes es muy pobre (2),(3). Solamente nuevas terapias dirigidas (2) como las terapias anti-angiogénicas (4); o terapias génicas muestran un beneficio real en grupos limitados de pacientes con defectos moleculares específicos conocidos (4). De este modo, se hace necesario el desarrollo de nuevas terapias farmacológicas para atacar los tumores cerebrales. Frente a las terapias los gliomas malignos son con frecuencia quimioresistentes, y esta resistencia parece depender de al menos dos mecanismos: en primer lugar, la pobre penetración de muchas drogas anticáncer a través de la barrera hematoencefálica (BBB: Blood Brain Barrier), la barrera del fluido sangre-cerebroespinal (BCSFB: Blood-cerebrospinal fluid barrier) y la barrera sangre-tumor (BTB: blood-tumor barrier). Dicha resistencia se debe a la interacción de la droga con varios transportadores o bombas de eflujo de droga ABC (ABC: ATP-binding cassette) que se sobre expresan en las células endoteliales o epiteliales de estas barreras. En segundo lugar, estos transportadores de eflujo de drogas ABC propios de las células tumorales confieren un fenotipo conocido como resistencia a multidrogas (MDR: multidrug resistance), el cual es característico de varios tumores sólidos. Este fenotipo también está presente en los tumores del SNC y su papel en gliomas es objeto de investigación (5). Por consiguiente el suministro de medicamentos a través de la BBB es uno de los problemas vitales en los tratamientos de terapia dirigida. Estudios recientes han demostrado que algunas moléculas pequeñas utilizadas en estas terapias son sustratos de la glicoproteína P (Pgp: P-glycoprotein), así como también de otras bombas de eflujo como las proteínas relacionadas con la resistencia a multidrogas (MRPs: multidrug resistance-related proteins (MRPs) o la proteína relacionada con cáncer de seno (BCRP: breast-cancer resistance related protein)) que no permiten que las drogas de este tipo alcancen el tumor (1). Un sustrato de Pgp y BCRP es la DOXOrubicina (DOXO), un fármaco utilizado en la terapia anti cáncer, el cual es muy eficaz para atacar las células del tumor cerebral *in vitro*, pero con un uso clínico limitado por la poca entrega a través de la barrera hematoencefálica (BBB) y por la resistencia propia de los tumores. Por otra parte las células de BBB y las células del tumor cerebral tienen también proteínas superficiales, como el receptor de la lipoproteína de baja densidad (LDLR), que podría utilizarse como blanco terapéutico en BBB y tumores cerebrales. Es así como la importancia de este estudio se basa en la generación de estrategias terapéuticas que promuevan el paso de las drogas a través de la barrera hematoencefálica y tumoral, y a su vez, se reconozcan mecanismos celulares que induzcan el incremento en la expresión de los transportadores ABC, de manera que puedan ser utilizados como blancos terapéuticos.

## ***A "Trojan Horse" strategy to reverse drug-resistance in brain tumors***

Este estudio demostró que el uso de una nueva estrategia basada en el "Caballo de Troya", donde se combina la droga DOXOrubicina, la cual es introducida dentro de un liposoma, salvaguarda la droga de manera que se evita su reconocimiento por parte de los transportadores ABC tanto de la BBB como de las células del tumor. La construcción del liposoma permitió utilizar el receptor LDLR de las células asegurando la entrada a través de la BBB y hacia las células tumorales a través de un proceso de endocitosis. Este mecanismo fue asociado al uso de estatinas o drogas anticolesterol las cuales favorecieron la expresión de LDLR y disminuyeron la actividad de los transportadores ABC por nitración de los mismos, incrementando la eficiencia de nuestro Caballo de Troya. Por consiguiente demostramos que el uso de una nueva estrategia o formulación denominada ApolipoDOXO más el uso de estatinas favorece la administración de fármacos a través de la BBB, venciendo la resistencia del tumor y reduciendo los efectos colaterales dosis dependiente de la DOXOrubicina. Además esta estrategia del "Caballo de Troya", es un nuevo enfoque terapéutico que puede ser considerado como una nueva estrategia para aumentar la eficacia de diferentes fármacos en varios tumores cerebrales y garantiza una alta eficiencia incluso en un medio hipóxico, característico de las células cancerosas, donde la expresión del transportador Pgp se vio aumentada. Teniendo en cuenta la relación entre algunas vías de señalización reconocidas como moduladores de la actividad de Pgp, este estudio presenta no solo la estrategia del Caballo de Troya, sino también otra propuesta terapéutica relacionada con el uso de Temozolomide más DOXOrubicina. Esta estrategia demostró que el temozolomide logra penetrar la BBB por que interviene en la via de señalización de la Wnt/GSK3/ $\beta$ -catenina, la cual modula la expresión del transportador Pgp. Se demostró que el TMZ disminuye la proteína y el mRNA de Wnt3 permitiendo plantear la hipótesis de que la droga al disminuir la transcripción del gen *Wnt3* en células de BBB, incrementa la activación de la vía fosforilando la  $\beta$ -catenina y conduciendo a disminuir la  $\beta$ -catenina nuclear y por tanto su unión al promotor del gen *mdr1*. Con base en los resultados este estudio permitió el reconocimiento de tres mecanismos básicos relacionados con la expresión de los transportadores ABC y asociados a las estrategias empleadas: el primero fue el uso de las estatinas, el cual condujo a la nitración de los transportadores disminuyendo su actividad por la via del factor de transcripción NF $\kappa$ B; el segundo a partir del uso del temozolomide, el cual metila el gen de *Wnt3* reduciendo la actividad de la via de señalización de la  $\beta$ -catenina, disminuyendo la expresión del transportador Pgp. El tercero consistió en la determinación de la relación entre el eje RhoA/RhoA quinasa como un modulador de la via (no canónica) GSK3/ $\beta$ -catenina. Se demostró que la proteína quinasa RhoA promovió la activación de la proteína PTB1, la cual al fosforilar a GSK3 indujo la fosforilación de la  $\beta$ -catenina, lo cual dio lugar a su destrucción por el proteosoma, evitando su unión al promotor del gen *mdr1* y por tanto reduciendo su expresión. En conclusión las estrategias propuestas en este trabajo incrementaron la citotoxicidad de las células tumorales al aumentar la permeabilidad no solo de la barrera hematoencefálica, sino también de la propia barrera tumoral. Igualmente, la estrategia del "Caballo de Troya" podría ser útil para la terapia de otras enfermedades asociadas al sistema nervioso central. Por otra parte estos estudios indican que el reconocimiento de mecanismos asociados a la expresión de los transportadores ABC podría constituir una herramienta clave en el desarrollo de nuevas terapias anticáncer.

## LIST OF PUBLICATIONS

This thesis is based on the following publications, which are indicated in the text by the corresponding Roman numerals:

- I. **Pinzón-Daza M**, Garzón R, Couraud P, Romero Ia, Weksler B, Ghigo D, Bosia A, Riganti C. The association of statins plus LDL receptor-targeted liposome-encapsulated DOXOrubicin increases in vitro drug delivery across blood-brain barrier cells. *Br J Pharmacol*. 2012 Dec; 167(7):1431-47.
- II. **Pinzon-Daza ML**, Campia I, Kopecka J, Garzon R, Ghigo D, Riganti C. Nanoparticle- and liposome-carried drugs: new strategies for active targeting and drug delivery across blood-brain barrier. *Current drug metabolism*. 2013;14(6):625-40.
- III. **Pinzón-Daza M.L.**, Kopecka J., Campia I., Garzon R., Riganti C. The “LDL-masked DOXOrubicin”: an effective strategy for drug delivery across hypoxic blood brain barrier. *ScienceJet* 2014, 3: 49.
- IV. Riganti, C., I. C. Salaroglio, **M. L. Pinzon-Daza**, V. Caldera, I. Campia, J. Kopecka, M. Mellai, L. Annovazzi, P. O. Couraud, A. Bosia, D. Ghigo and D. Schiffer (2014). "Temozolomide down-regulates P-glycoprotein in human blood-brain barrier cells by disrupting Wnt3 signaling." *Cell Mol Life Sci* 71(3): 499-516.
- V. **Martha L. Pinzón-Daza**, Iris C. Salaroglio, Joanna Kopecka, Ruth Garzon, Pierre-Olivier Couraud, Dario Ghigo, Chiara Riganti. The cross-talk between canonical and non canonical Wnt-dependent pathways regulates Pglycoprotein expression in human blood brain barrier cells. *J Cereb Blood Flow Metab* 34: 1258-1269; advance online publication, June 4, 2014; doi:10.1038/jcbfm.2014.100.

**ABBREVIATIONS**

ATP	ADENOSIN TRIPHOSPHATE
AJ	ADHERENT JUNCTIONS
ABC	ATP BINDING CASSETTE
BBB	BLOOD BRAIN BARRIER
BCRP	BREAST CANCER RELATED PROTEIN
BCSF	BLOOD CEREBRO-SPINAL FLUID
CNS	CENTRAL NERVOUS SYSTEM
DAU	DAUNORUBICIN
DOXO	DOXORUBICIN
DNA	DEOXIRIBONUCLEIC ACID
FPP	FARNESYL PIROPHOSPHATE
GSH	GLUTATHION
GGPP	GERANYL GERANYL PIROPHOSPHATE
GBM	GLIOBLASTOMA
HMG-CoAR	3-HYDROXY-3-METHYLGLUTARYL-COENZYME A REDUCTASE
HRE	HYPOXIA RESPONSE ELEMENT
HIF-1 $\alpha$	HYPOXIA INDUCIBLE FACTOR-1 ALPHA
HA	HUMAN ALBUMIN
LDL	LOW DENSITY LIPOPROTEIN
LDLR	LOW DENSITY LIPOPROTEIN RECEPTOR
LEF	LINFOIDS ENHANCED FACTOR
LDH	LACTATE DESHYDROGENASE
MDR	MULTIDRUG RESISTANCE
MRP	MULTIDRUG RESISTANCE RELATED PROTEIN
NOS	NITRIC OXIDE SYNTHASE
NP	NANOPARTICLES
Pgp	P-GLYCOPROTEIN
PCP	PLANAR CELLULAR POLARITY
SREBP	STEROL REGULATORY ELEMENT-BINDING PROTEIN
SLN	SOLID LIPIDIC NANOPARTICLES
TJ	TIGHT JUNCTIONS
TMZ	TEMOZOLOMIDE
WHO	WORLD HEALTH ORGANIZATION

To the memory of my father, my guide, my example, my light, my support, my friend and certainly the most wonderful human being I've ever met in my life.....

## **ACKNOWLEDGEMENTS**

My sincere and deep gratitude, who with their voice, their hand, their support, their teachings allowed me conclude this work. First of all I thank the University of Rosario for the opportunity to develop my dissertation work with the ERASMUS MUNDUS COLOMBIA ERACOL programme for which I was granted a scholarship for three years to work at the University of Turin, Italy. The University of Rosario not only gives me the time but also its financial support during my stay abroad.

I also thank the Department of Oncology of the Medical School and the Doctoral program in Molecular Medicine of the University of Turin, Italy: by opening their doors and allow me the full development of the thesis work. I am especially grateful to Dr. Dario Ghigo and the Dr. Amalia Bosia for allowing me to be part of their working group.

I give a very special thanks to my tutor and guide in this process, Dr. Chiara Riganti who gives me her full support, her energy, her time and all the will to make this work not only possible but give important fruits. Her unconditional attitude, her optimism, her permanent support and human warmth were always what drove me, so also the desire to give the best permanently. I thank also my coworkers of the laboratory Ivana Campia, for her permanent help, Johana Kopecka for her warmth, Carolina Belisario for her support inside and outside the laboratory, and especially moments shared in Italy. To my great friend Sophie Doublie who gave me the opportunity to get to know another face of Italy and by offering me a wonderful friendship. Thanks to Iris, Loredana and the other collaborators of the laboratory who I will always remember deeply.

A special thank you is directed to research BIO-BIO group colleagues who gave me their support and accompaniment in this doctorate: Lilia, Fabio, Alejandro, Albita, Alejandrina. I especially thank my boss, colleague and friend Ruth Garzón who has co-directed this thesis and who has always given me their support. Thank you especially for all her suggestions, her desire to promote new ideas and her generous attitude with the entire working group, for her friendship and being a person that so comprehensive: thank you.

My PhD is one of the biggest challenges that I've had in my life and that had not been achieved without fundamental support from my family. My father who is accompanying me from the heaven, my mother who has always urged me to do new things, giving me their love and support; my brothers: Javier, Patricia, Camilo, Elizabeth, Teresa, Enrique, Mauricio and Angie have been unconditional and motivated me to grow; my nephews: Juan Camilo, Santiago, Sara and Pablo who always give me their love. Because they gave me the strength to get this new achievement, I dedicate all this work because I love them and they love me and are always by my side.

## **1. Justification**

It is estimated that each year more than 11 million new cases of cancer, of which about 80% occur in developing countries are present in the world. In Colombia cancer is the third leading cause of death, after cardiovascular diseases and violence, so as in 2010, there were 33.450 deaths by cancer, which accounted for 16.9% of all deaths: 16.381 were men and 17.069 women, with a crude rate of 72.9 per 100,000 and 74.1 per 100,000 cancer mortality respectively, according to documents reported in the ten-year plan for the control of cancer of Colombia describe in the period of 2012-2021 (<http://www.cancer.gov.co/documentos/Plandecenalparaelcontroldelcancer>). Worldwide, deaths caused by tumors account for almost 15% of the total (rate of 65/100,000 people (1). This incidence depends on different factors: the zone, the age, among other epidemiological characteristics. It is the case of leukemia and tumors of the central nervous system which are the main causes of death from cancer among the population under the age of 30 (2, 3). This incidence in young people is characteristic of brain tumors, i.e. 1 per 1300 in habitants develops brain cancer before the age of 20. In young people, 25% of cancer mortality is secondary to a tumor of the central nervous system (6, 7). On the other hand the 23% of pediatric cancers are brain where medulloblastoma is the most common cause of death related to cancer in children (8). Taking into account the adult population, 7 cases of malignant brain cancer per 100 thousand people are diagnosed every year and this rate is among the 10 leading causes of death due to cancer. (9).

Whitin the 5 fundamental kinds of tumors of the CNS (neuronal tumors, poorly differentiated neoplasms, meningiomas, gliomas and metastasis), it has been shown that aggressive glioblastoma, and low and high grade gliomas account for 78% of primary brain tumors among adults (5), while brain metastasis of solid tumors are also frequent and occur in approximately 25% of patients with cancer (10).

In addition, the analysis of the demographic characteristics of these lesions has been studied in Colombia and it is very similar to the world. Each tumor set occurs in a specific demographic group. Meningiomas and schwannomas appear most commonly in women as astrocytomas are more frequent in men. Germ cell tumors and astrocytomas are diagnosed more in children and teens while meningiomas, adenomas and glioblastomas are detected

### ***A "Trojan Horse" strategy to reverse drug-resistance in brain tumors***

more in adults (2). Regarding patient's sex, it has been shown that gliomas occur in men 40% more than women (11) and the average age of presentation is 45 years old.

Taking the above data, it is estimated that the high levels of incidence/mortality for cancer of the central nervous system and especially gliomas, indicate a poor prognosis, which could be attributed to very advanced stages at the time of diagnosis or to the lack of efficacy in the treatment. From these observations, it is important to understand that the high prevalence of this disease is not only due to the aggressiveness of the tumor but also to deficiency in therapies that can control it. This limitation can be explained from the presence of a natural mechanism- the blood brain barrier (BBB) - that the brain uses to regulate the entry of substances, including anti cancer therapies. In this way the BBB acts as a neuroprotective shield in order to protect the brain from most substances, maintaining a balanced supply of nutrients to the brain tissues and filtering the harmful compounds from the brain to the blood stream (11). Anti cancer drugs such as anthracyclines, used for a long time, do not show a high effectiveness and the resistance to these agents has become a failure of chemotherapy, promoting a low prognosis. One of the mechanisms that are postulated as possible cause of this failure relies on the multidrug resistance (MDR) phenotype, which leads to a low cytotoxicity by anticancer agents; because they can not cross the BBB and can not accumulate in tumor. Studies based on cells in vitro and clinical studies have shown that MDR occurs in central nervous system (CNS) (12) cancer cells. In addition it has been recognized that the key mechanism of the MDR is based on the overexpression of human tumors membrane transporters, such as: the P-glycoprotein (Pgp) and the related MDR (MRPs), known as ABC transporters proteins (ABC: ATP binding cassette), which function as ATP-dependent pumps that bind to anti cancer drugs and pump them outside the BBB or tumor. The CNS tumors have a MDR phenotype, due to overexpression of Pgp and MRPs, which may be constitutive or induced by own chemotherapy (4). Therefore, this phenotype is a strong barrier to the diffusion of chemotherapeutic drugs. This study contributes to increase the efficiency of anti cancer drugs using the association between ApolipoDOXO and Statins to improve administration of drugs through BBB, in order to overcome the resistance of the tumor and reduce the dose-dependent side effects of DOXO in vitro. Additionally this work serves as basis to contribute to the decrease in deaths from brain cancer affecting a large percentage of the Colombian and world population.

## **2. Theoretical framework**

### **2.1. Brain tumors**

Brain tumors or Gliomas are named in different ways depending on histological features observed and compared with mature glial cells. Brain tumors with cells resembling astrocytes were termed astrocytomas; the tumor cells of ependymoma shared an appearance with ependymal cells; pinealoma was composed of tumor cells resembling those of the pineal gland. The names of several tumor entities related to cell types are no longer recognized today. Examples are spongioblastoma to the spongioblast (or by other authors glioblastoma referring to the glioblast) and medulloblastoma to the medulloblast. It is noteworthy that this first comprehensive classification system already outlined the concept of tumors arising from immature precursor cells or from neuroectodermal stem cells (6). Low grade gliomas, mostly astrocytomas (World Health Organization (WHO) grade II) are progressively transforming into malignant gliomas, that is, anaplastic tumors (WHO grade III) and glioblastoma multiforme (GBM; WHO grade IV). However, most GBM are diagnosed without any prior record of a tumor of lower grade (7). GBM is a complex mixture of cell types that includes astrocyte-like and stem-like cells, characterized by rapid growth and diffuse invasiveness into adjacent brain parenchyma. Resection possibility depends on tumor location and only the nodular component can be surgically controlled. The infiltrative component of the tumor, however, is left to chemotherapy and radiotherapy that can impede tumor progression for a limited time only. GBM patient survival is less than 1 year (8). GBM has a severe mutated phenotype that consists of large chromosomal alterations; at the genetic level, the most frequent mutations affect genes involved in the control of cell cycle, growth, apoptosis, invasion and neovascularization (9). Glioblastoma multiforme refers to a malignant neoplasm with abundant glial pleomorphism, numerous mitotic figures and giant cells, vascular hyperplasia, and focal areas of necrosis. It grows as an irregular mass in the white matter and infiltrates the surrounding parenchyma by coursing along white matter tracts, frequently involving the corpus callosum and crossing the midline to produce the characteristic “butterfly” appearance (10). Of the estimated 17,000 primary brain tumors diagnosed in the United States each year, approximately 60% are gliomas (11). GBM accounts for approximately half of all newly diagnosed primary brain tumors with an incidence of 2–3 cases per 100,000 people each year (8). It is the most frequent primary brain

## *A "Trojan Horse" strategy to reverse drug-resistance in brain tumors*

tumor, accounting for approximately 12–15% of all intracranial neoplasms and 50–60% of all astrocytic tumors (12).

Malignant Gliomas are the most common and deadly tumors, however, the survival of patients with GBM, although it varies individually, has improved from an average of 10 months to 14 months after the diagnosis in the past 5 years since it has improved the level of care (13). It has been recognized that the origin of brain cancers can be directly in the brain or outside the CNS in other parts of the body and spread to the brain such as metastasis (14). Approximately 25% of cancer patients develop brain metastases, and although usually appear late in the course of the disease, a brain metastasis may cause early symptoms, until the primary cancer has been identified. In this way the diagnostic and therapeutic management approach depends on the quantity and location of brain injury and the stage of the cancer. Patients with brain cancer metastases are rarely cured (15) and this may be due to the role played by the tumor barrier and the BBB to obstruct the chemotherapeutic treatment with agents such as paclitaxel and DOXOrubicin (DOXO) . Given the failure of many chemotherapy drugs that do not permeate the BBB, a new class of agents that have a good chemotherapeutic activity against metastases in the brain is required. These agents must be not only BBB permeable and active against metastatic cancer cells, but also non-toxic to the cells of the CNS (14).

In general, the brain tumors derived from the cells glial respond differentially to treatment with surgery and radiotherapy or radiotherapy alone, combined with or without chemotherapy (7). The treatment of malignant brain tumors with conventional approaches is usually unsuccessful since curative doses generally lead to excessive toxicity in normal cells of the brain (10).

### **2.2. Blood Brain Barrier**

BBB is constituted by the brain endothelial cells which form the anatomical substrate called cerebral microvascular endothelium (16). BBB regulates the transport of solutes and other substances including drugs in and out of the brain, controls leukocyte migration, and maintains the homeostasis of the brain microenvironment, which is crucial for neuronal activity and proper functioning of CNS. The cerebral microvascular endothelium, together

with astrocytes, pericytes, neurons, and extracellular matrix, constitute a “neurovascular unit” that is essential for the health and function of the CNS (17). The transport of solutes and other substances across BBB is strictly constrained through both physical tight junctions (TJs) and adherent’s junctions (AJs) and metabolic barriers (enzymes, diverse transport systems) and excludes also very small, electrically neutral and lipid soluble molecules. Thus, conventional pharmacological drugs or chemotherapeutic agents are unable to pass through the barrier (17).

The main structural differences between the endothelium of brain capillaries and other capillary endothelium are the TJs between adjacent endothelial cells (18), the lack of hollow fenestrations and pinocytotic vesicles (19). The TJs are multiproteic complex located on the lateral surface of the brain endothelial cells, they are composed of transmembrane proteins, as claudin-3, occludin, adhesion molecules and cytosolic proteins, such as zonula occludens-1/2/3, AF6, 7 H 6, cingulin, claudin-5. In the BBB the presence of TJs and the absence of fenestrations prevent paracellular molecules delivery (20). The AJs, other complexes of basolateral membranes composed of vascular endothelial cadherin, p120 and complex  $\alpha$ -/  $\beta$ -catenin, contribute to strong cellular adhesion and are required for the assembly of the TJs (20). They further decrease the paracellular permeability of many substances. Finally, the absence of pinocytotic vesicles increases the strict control over the processes of transcytosis through BBB. In general, both the luminal (into the blood) surfaces and the basolateral (to the brain), contribute to the function of "barrier" of the brain microvascular endothelium (Figure 1).

Several mentioned features are induced in the endothelial cells by the close proximity and multiple contacts with pericytes, astrocytes and neurons; also, the simultaneous presence of endothelial cells, extracellular matrix and cells of the CNS form a physiologically competent BBB (17).

In addition to the BBB, other crucial barriers to maintain the homeostasis of the brain parenchyma are the barrier blood - cerebrospinal fluid (BSCF), which is formed by the epithelial cells of the choroid plexus and regulates the transport of molecules between the CNS and cerebrospinal fluid (21) and the blood-retina barrier (22). In all these barriers, the mechanisms of passive diffusion, facilitated diffusion and active transport of substrates are

strictly regulated. Here ABC transporters are crucial in the process of active transport through the cells of the BBB.

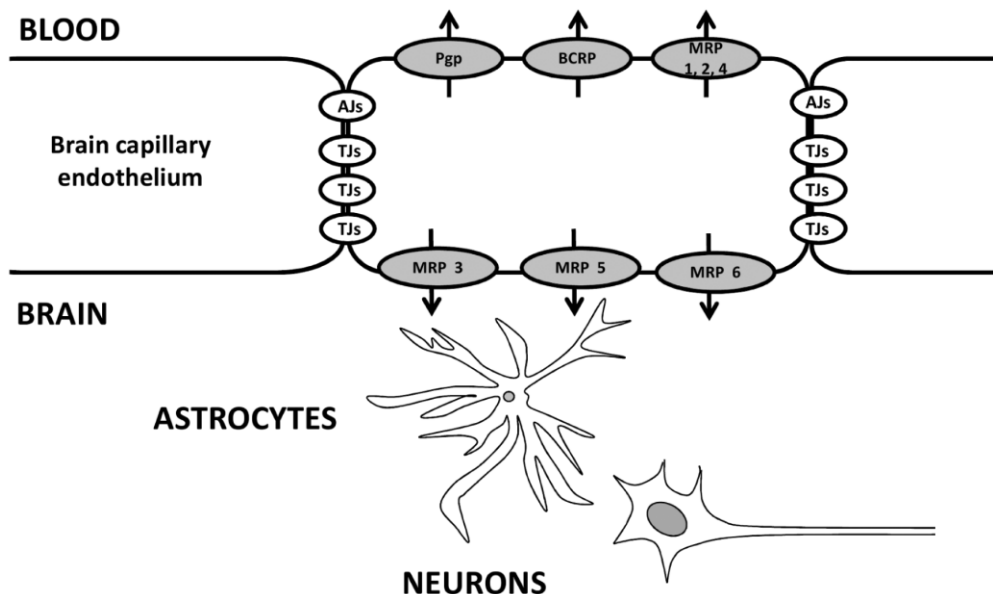


**Figure No. 1. Schematic representation of the blood-brain barrier (BBB). BBB is a structural-functional unit composed by peculiar brain microvascular endothelial cells, devoid of fenestrations, rich of tight junctions (TJs) and adherent junctions (AJs) on lateral surface, and ABC transporters, such as Pgp, MRP1-6, BCRP, on luminal and basolateral side. Most of these features, which determine a tight control on the bi-directional transport of metabolites and xenobiotics, are maintained by the close proximity and multiple contacts between endothelial cells and CNS cells, such as astrocytes and neurons (23).**

### **2.3. Multidrug resistance genes and ABC transporters**

The multidrug resistance (MDR), which is the cross resistance toward chemotherapeutic drugs unrelated for chemical structure and mechanism of action, is the main cause of failure of the pharmacological therapy in human cancers. Tumors of CNS have often a MDR phenotype, due to the overexpression of Pgp and MRPs, which can be constitutive or induced by the chemotherapy itself. Moreover CNS is surrounded by brain-blood barrier (BBB), which is reach of both Pgp and MRPs. This abundance is a further obstacle to the diffusion of chemotherapeutic drugs toward brain tumors (24). The MDR gene product Pgp is a 170-kDa transmembrane protein associated with tumor resistance to chemotherapeutic drugs such as DOXO. The Pgp drug efflux pump serves to lower intracellular concentrations of drugs to sub-

lethal levels by actively transporting them out of the cells. Currently, the ABC transporters family includes more than 200 prokaryotes and eukaryotes proteins, and many of them are still unknown. The function of ABC transporters is not limited to drug transport, and many important human ABC transporters are involved in transport and/or regulation of ions or other substances (25, 26) (Table No.1). Initially discovered in the 1970s as a prototypic transporter involved in multidrug resistance (MDR) of cancer cells (27), Pgp was also the first ABC transporter that was detected in endothelial cells of the human BBB in 1989 (24), (28). Subsequently Pgp was localized in brain capillary endothelial cells of several species, including monkeys, rats, mice, cattle, and pigs, suggesting that Pgp may serve as general defense mechanism in the mammalian BBB, protecting the brain from intoxication by potentially harmful lipophilic compounds from natural sources and other lipophilic xenobiotics which otherwise could penetrate the BBB by simple diffusion without any limitation (29). The exact localization of Pgp in the BBB has been the object of numerous investigations using various experimental approaches such as *in situ* hybridization and immunohistochemistry. In the absence of Pgp in the BBB in *mdr1a* knockout mice, the brain penetration of Pgp substrate drugs can increase up to 10- to 100-fold (30).

Furthermore, blockade of BBB Pgp by cerebral application of Pgp inhibitors significantly increases the brain concentration of various drugs, again being in line with Pgp functioning as an efflux transporter in the BBB. Expression of Pgp confers drug resistance to numerous antitumor agents, including DOXOrubicin, daunorubicin, actinomycin D, etoposide, teniposide, colchicine, taxol, vincristine, and vinblastine (31). In contrast to Pgp, details about other BBB ABC transporters are much more limited (32). The ABCC family (with the first member, MRP1, discovered in cancer cells in 1992) currently has 12 members (including MRP1-9), which act as organic anion transporters, but can also transport neutral organic drugs (33). As a consequence, Pgp and MRPs have overlapping substrate specificity, so that several drugs are substrates for both transporter families (34).

Like Pgp, MRPs are located in several normal tissues, including the BBB and BCSFB. Resistance to numerous anticancer agents is associated with overexpression of the 170-kDa Pgp or the 190-kDa MRPs. The role of MRPs in BBB permeability has been demonstrated by experiments in which inhibitors of MRPs, such as probenecid or MK-571, were shown to enhance drug penetration into the brain or to inhibit drug efflux from isolated brain

## *A “Trojan Horse” strategy to reverse drug-resistance in brain tumors*

endothelial cells (35). It is of great importance also the expression of BCRP (Breast Cancer Related Protein) transporter in BBB and tumor cells. BCRP was first discovered in a chemotherapy-resistant breast cancer cell line, but there is no indication that its expression is specific for breast cancer cells or that BCRP should play a significant role only in chemotherapy resistance in breast cancer.

**Table 1. Substrates of ATP-binding cassette (ABC) transporters present in blood-brain barrier (BBB)**

ABC transporter	Localization on BBB	Endogenous substrates	Xenobiotics and drugs
Pgp (ABCB1)	luminal	neutral/cationic organic compounds, amyloid $\beta$ peptide	doxorubicin, daunorubicin, vincristine, vinblastine, actinomycin-D, paclitaxel, docetaxel, etoposide, teniposide, topotecan, mitoxantrone, methotrexate, imatinib, lapatinib, dasatinib, sorafenib, gefitinib, erlotinib, zidovudine, lamivudine, saquinavir, indinavir, nelfinavir, ketoconazole
MRP1 (ABCC1)	luminal	GSH-conjugated and anionic organic compounds, leukotriene C4	etoposide, teniposide, vincristine, vinblastine, paclitaxel, docetaxel, doxorubicin, daunorubicin, epirubicin, mitoxantrone, methotrexate, topotecan, irinotecan
MRP2 (ABCC2)	luminal	anionic organic compounds	cisplatin, methotrexate, doxorubicin, daunorubicin, etoposide, paclitaxel, docetaxel, topotecan, irinotecan
MRP3 (ABCC3)	basal	glucuronic acid- and GSH-conjugated compounds, bile salts	etoposide, teniposide, methotrexate, cisplatin, doxorubicin, vincristine
MRP4 (ABCC4)	luminal	nucleotide derivatives, organic anionic compounds	methotrexate, 6-mercaptopurine, 6-thioguanine, topotecan, cisplatin
MRP5 (ABCC5)	basal	nucleotide derivatives, organic anionic compounds	6-mercaptopurine, 6-thioguanine, gemcitabine
MRP6 (ABCC6)	basal	anionic cyclic pentapeptide	unknown
BCRP (ABCG2)	luminal	hydrophobic and hydrophilic anionic compounds	prazosin, mitoxantrone, doxorubicin, daunorubicin, topotecan, 7-ethyl-10-hydroxycamptothecin (SN-38), methotrexate, imatinib, lapatinib, dasatinib, sorafenib, gefitinib, erlotinib

Pgp: P-glycoprotein; MRP: multidrug resistance related protein; BCRP: breast cancer related protein; GSH: glutathione.

The tissue distribution of BCRP shows extensive overlap with that of Pgp, suggesting that both transporters similarly confer protection from potentially harmful xenobiotics in various tissues (26). In the brain, BCRP has been detected in capillary endothelial cells of humans mainly at the luminal surface (36). Based on mRNA analysis, BCRP was more strongly expressed on BBB than Pgp or MRP1 (33). The role of BCRP in brain uptake was recently demonstrated by using *mdr1a* knockout mice, in which BCRP was inhibited by GF120918, resulting in reduced brain uptake of prazosin and mitoxantrone. Interestingly, *mdr1a* knockout mice had about three times more BCRP in the brain microvessels than normal mice, indicating an up regulation of BCRP to compensate for the lack of Pgp in the BBB (37). ABC

transporters also share a low specificity for substrates, i.e. each transporter can recognize different molecules and the same substrate can be extracted by different transporters (38) (Table 1). The vast majority of ABC transporters involved in multidrug resistance or their mRNAs have been identified in cells of the BBB and BSCF; the relative abundance in these barriers and the prevalent location luminal or basolateral membrane, is unknown for all transporters (23). Cells overexpressing ABC transporters have a different intracellular drug distribution and the reasons of this are not so clear. There are several possibilities involving both direct and indirect effects. First, the transporter may be expressed not only on the plasma membrane, but also on the vesicular membranes, where it actively contributes to drug transport from the cytoplasm into the vesicles. Another explanation is suggested by the observation that vesicular sequestration is a saturable process strongly dependent on the cytoplasmic drug concentration (39).

There are a limited number of studies on high-grade brain tumors identifying subtypes of MDR, the level of expression of these transporters, with a lacking functional detailed and pharmacological analysis. This lack of knowledge has contributed in large part to the poor effectiveness of therapies targeting cancer in the CNS. Recently some factors associated with the expression of ABC transporters have been identified, among which are: 1) hypoxia; 2) oxidative stress, 3) the use of chemotherapy; (4) the use of radiotherapy. In some cases the combination of these effects leads to an increase in the MDR (40).

#### **2.4. ABC transporters and hypoxia**

Many reports have demonstrated an increased chemoresistance and radioresistance in hypoxic cancer cells by activation of the Hypoxia-Inducible Factor-1  $\alpha$  (HIF-1 $\alpha$ ) mediated pathway (40) HIF-1 $\alpha$  is composed of two subunits:  $\beta$ , which is constitutively expressed, and  $\alpha$ , which is rapidly degraded under normal conditions but becomes stable when the oxygen or iron supply decreases, leading to a net increase in Hypoxia inducible factor alpha. This factor is constitutively high in the hypoxic areas of tumours. When active, HIF-1 $\alpha$  up regulates several genes involved in processes such as cellular growth, glucose and iron metabolism, pH control, angiogenesis, matrix remodelling and drug resistance. Since HIF-1 $\alpha$  promotes cellular proliferation, inhibition of apoptosis, invasion and MDR, its expression in tumours is related to poor prognosis (41).

Thus, different therapeutic approaches have been attempted in order to reduce HIF-1 $\alpha$  expression. In the lung, most cell types, including bronchial and alveolar epithelium, smooth muscle and vascular endothelium, overexpress HIF-1 $\alpha$  under hypoxic conditions. High levels of HIF-1 $\alpha$  have been described in mesothelioma biopsies of patients, one of the most highly chemoresistant and aggressive tumor, whereas mesothelial cells contain low amounts of HIF-1 $\alpha$  (41). HIF-1 $\alpha$  is associated with multidrug resistance because could regulate transcription of ABC transporter genes in cancer cells and promote overexpression of Pgp and MRPs in cancer tissues. These facts have been demonstrated to efflux the intracellular anticancer drugs outside the cancer cells, resulting in promotion of chemoresistance to taxanes (paclitaxel or docetaxel) and anthracyclines (DOXO or daunorubicin) (42).

## **2.5. Therapeutic approach to brain cancer, the use of nanoparticles and liposomes (Article II)**

The antineoplastic drugs have been one of the major successes of cancer medicine. Their use has helped to increase life, in childhood cancer has increased from more than 30% in the 1960s to 70 and 80% today (43), (44). The first two anthracyclines, daunorubicin (also known as daunomycin and rubidomycin) and DOXOrubicin (DOXO, also known as Adriamycin), were isolated in the 1960s from *Streptomyces peucetius*, a species of actinobacteria. While DAU has been shown to be highly effective against acute lymphoblastic and myeloblastic leukemias, DOXO has been found to have a much broader anticancer spectrum, which includes numerous solid tumors in addition to hematological malignancies. Although more than 40 years old, anthracyclines are still frequently used in clinical practice, and DOXO in particular, remains as an important component of many current chemotherapy protocols for treating breast cancer, sarcomas, childhood solid tumors (e.g., Wilms' tumor), leukemias, Hodgkin's disease, non-Hodgkin's lymphomas, and many other cancers. Interestingly, rather than being replaced with novel progressive “targeted” agents, current clinical practice tends to combine them with the novel therapeutics to maximize the therapeutic response (45). Despite their extensive use, the mechanism of anthracyclines antineoplastic action is still a subject of debate and apparently it is a combination of several different mechanisms, which accounts for the high efficiency of this class of anticancer drugs (46), (47), (48).

Mechanism of action of anthracyclines is attributed to their intercalation between base pairs of the DNA strands, which prevents replication of rapidly growing cancer cells. However, more recent studies have shown that at clinically relevant concentrations, intercalation is unlikely to play a major role. Anthracyclines are called “topoisomerase poisons” because they act by stabilizing a reaction intermediate in which DNA strands are cut and covalently linked to topoisomerase II- tyrosine residues, which blocks subsequent DNA resealing. Failure to relax the supercoiled DNA blocks DNA replication and transcription. Furthermore, breaking DNA strands may trigger apoptosis of cancer cells, apparently *via* the p53-dependent pathway. Some studies have also suggested that reactive oxygen species (ROS) formation and lipid peroxidation participate in the anticancer effects of anthracyclines (45).

According with their structure DOXO differs from daunorubicin only by a single hydroxyl group. This fact has spurred researchers worldwide to find analogs of DOXO that have less acute toxicity, e.g. causing less cardiomyopathy, and can be administered orally, and/or have different, or greater antitumor efficacy. None of these analogs have stronger antitumor efficacy than the original two anthracyclines, but there are some differences in toxicity. Methods have been fashioned to keep the peak plasma level of DOXO muted to minimize cardiotoxicity, but the only apparently effective method available so far (prolonged drug infusion) is cumbersome. The bisoxopiperazine class of drugs (especially dexrazoxane) provides protection against anthracycline-induced cardiomyopathy and has much promise for helping mitigate this major obstacle to prolonged use of the anthracyclines. The DOXO analogs being evaluated in the 1990s have been selected for their ability to overcome multidrug resistance in cancer cells. Thirty years after discovery of the anticancer activity of the first anthracycline, some means of reducing anthracycline toxicity have been devised. Current studies are evaluating increased doses of epirubicin to improve anthracycline cytotoxicity, while limiting cardiotoxicity, but at present DOXO still remains in this drug class as the one having the most proven anticancer effect (49).

Different methods have been developed in order to maintain an effective amount of DOXO which minimizes the cardiotoxicity; it has been developed derivatives of the drug, to prevent this and other effects in plasma. Some systems can protect DOXO by macrophages phagocytosis and favor the entrance in the tumor cells to evade the presence of ABC

## ***A “Trojan Horse” strategy to reverse drug-resistance in brain tumors***

transporters (47), (48). Some DOXO analogues have been evaluated in recent years and have proven to be effective to prevent resistance to drugs in cancer cells. This is how many strategies offer a promising alternative therapy for brain cancers (13) (50). Within these include nanoparticles or liposomes as key elements that used to allow access to the drug to the brain.

In recent years the nanoparticles (NPs), emerged as a very efficient way of transporting the drug, due to small size, high solubility and multifunctionality (51). Size ranges between 10 and 1000 nm; they are made with a variety of materials, including carbohydrates like malto-dextrins or chitosan derivatives (52); fatty acids as beenic and palmitic acid are assembled in the solid lipid NPs (SLNs)(53); proteins such as human albumin (HA)(54), among others, are also conjugated. Some of them are amphiphilic molecules micelles with their oriented towards the external surface hydrophilic and hydrophobic towards the inner center groups. Tumor specific drug delivery has become increasingly interesting in cancer therapy, as the use of chemotherapeutics is often limited due to severe side effects. Conventional drug delivery systems have shown low efficiency and a continuous search for more advanced drug delivery principles is therefore of great importance (50).

Liposomes were suggested as drug transporters in cancer chemotherapy by Gregoriadis et al. in 1974. Since then, the interest in liposomes has increased and liposome systems are now being extensively studied as drug transporters. Three basic requirements need to be fulfilled if liposomes are to be successful in delivering drugs specifically to cancerous tissue: (i) prolonged blood circulation, (ii) sufficient tumor accumulation, (iii) controlled drug release and uptake by tumor cells with a release profile matching the pharmacodynamics of the drug. This system is part of the called nanoparticles. In nano aqueous polymeric particles made of natural or artificial polymers ranging in size between about 10 and 1000 nm, drugs may be adsorbed to the surface or chemically attached. Drug delivery systems such as microspheres, liposomes or polymeric NPs may improve the effectiveness and decrease the side effects of cancer chemotherapy. Some of these transporters possess moderate MDR reversal activity on their own. To further enhance chemotherapy of drug-resistant malignancies, some investigators have integrated the approach of encapsulation with the combination of cytotoxic drugs and chemosensitizer (13). The exact strategy implemented, however, has varied among studies. In some cases, only the chemosensitizer was encapsulated (55),

whereas in other studies, encapsulated cytotoxic drug was administered with free chemosensitizer (55). Co-encapsulation of anticancer drugs and chemosensitizers by polymeric particles has been reported to have good efficacy (56). Moreover, lower normal tissue drug toxicity and fewer drug-drug interactions have generally been observed in the combination treatments. However, so far, there has been no consensus regarding which strategy provides the optimal treatment outcome (57).

There have been used many ways to present drug to BBB, especially focusing on DOXO for its low penetration across BBB. One strategy is the pegylated liposomal DOXO developed to maintain or enhance the demonstrated antineoplastic effects of DOXO, while improving the toxicity profile associated with this important cytotoxic agent. Accumulating clinical data have confirmed the activity of pegylated liposomal DOXO in cancers of the breast and ovary (49).

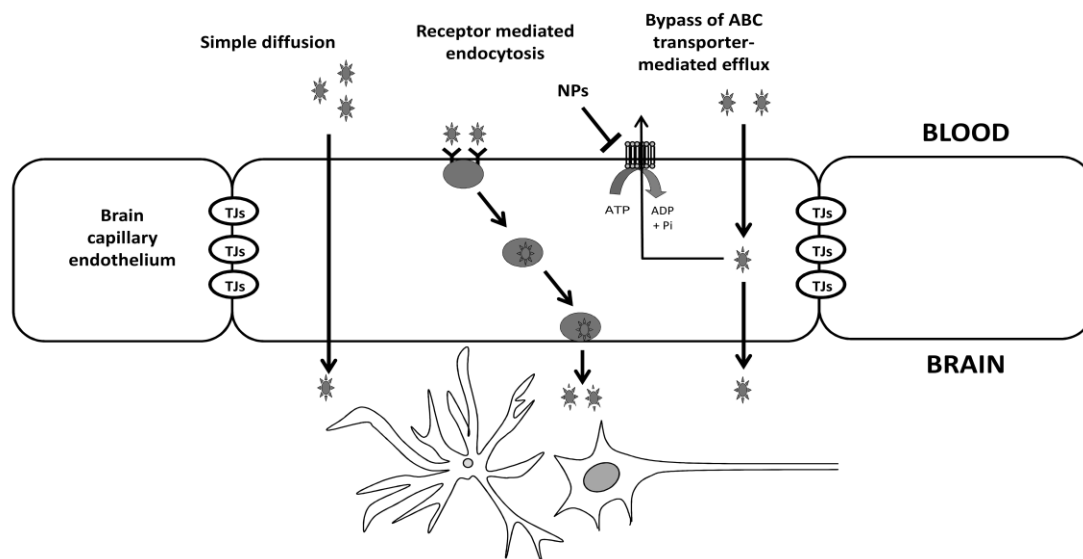


**Figure No. 2. Nanoparticles- and liposomes-loaded drugs are more easily delivered across blood-brain barrier (BBB) than free drugs with at least three mechanisms: 1) they are favored to enter cells by simple diffusion; 2) they are uptaken by a receptor-triggered endocytosis, if conjugated with specific ligands; 3) they are less effluxed by ABC transporters: indeed nanoparticles and liposomes can directly inhibit the catalytic cycle of ABC transporters and alter the optimal physico-chemical properties of the plasma membrane in which the transporters work. Overall, the drugs loaded on these delivery systems can pass through the BBB and reach the brain parenchyma at therapeutically relevant concentrations (23).**

## ***A “Trojan Horse” strategy to reverse drug-resistance in brain tumors***

The abundance of ABC transporters in endothelial cells of brain capillaries of bovine, murine and human origin may help to clarify by which mechanisms NPs and liposomes protect drugs from the ABC transporters-mediated efflux (Figure 2). This information could be then translated into the design of NPs/liposomes with specific physico-chemical properties, useful not only to increase the delivery across BBB, but to increase the pharmacological efficacy in every condition for which the ABC transporters represent an obstacle.

The major advantage of using NPs/liposomes-based strategies is their great versatility: once synthesized a specific carrier formulation, the cargo can be easily varied and can include drugs, siRNA, gene-delivering systems, and radiotracers. Such versatility enlarges the number of applications, from the therapeutic use of drug-delivery systems in diseases such as cancer, epilepsy, infective or neurodegenerative disorders, to the diagnostic use and to theranostic applications, which couples diagnosis and therapy. If these are the benefits of NPs- and liposome-based strategies, there are also many unsolved issues, such as the lack of consistent information about their long term toxicity or the lack of effective strategies assuring a strong tropism for BBB or CNS cells. These gaps have to be considered as challenges, which will give the opportunity to continue developing new drug delivery systems, progressively more effective and selective (58, 59).

### **2.5.1. Statins and mechanism of action**

Statins are competitive inhibitors of 3-hydroxy-3-methylglutaryl coenzyme A (HMG-CoA) reductase, which catalyzes the rate limiting step in cholesterol synthesis. Therefore, statins dramatically decrease both cholesterol and isoprenoid intermediates, impairing the isoprenylation and activity of different enzymes, such as the small G-protein families Ras and Rho (60). Farnesylpyrophosphate (FPP) and geranylgeranylpyrophosphate (GGPP) serve as important lipid attachments for the posttranslational modification of heterotrimeric G-proteins and small GTP binding proteins (61). Isoprenylation converts small GTPases from a cytosolic (inactive) state to a membrane-bound (active) state. Statins reduce the risk of myocardial infarction and stroke. Increasing evidence suggests that protection conferred by statins relates not only to cholesterol-lowering but rather to direct effects on endothelium function as well as antithrombotic and antiinflammatory effects. In humans, improvement of

endothelium function is one the earliest clinical effects after initiation of statin treatment (62).

Most statins are given in the active  $\alpha$ -hydroxy acid form except for lovastatin and simvastatin, which are administered as inactive lactone prodrugs. Both lactone and acid forms were observed in the systemic circulation after oral administration of atorvastatin, lovastatin, simvastatin, and cerivastatin in humans and/or animals, indicating that interconversion occurs between the lactone and acid forms of these statins. The 2 forms of these statins are substrates for Pgp transporter (63). To date, there are several lines of preclinical and epidemiologic evidences to support the anticancer potential of statins. (64). Some epidemiologic analyses have demonstrated up to a 50% reduction in cancer risk among statin users and partial or complete responses have been observed in some, but not all, patients undergoing early phase 1/2 trials. These mixed responses underscore the importance of reliably identifying the appropriate subset of patients who stand to benefit most from statin-based anticancer therapy. To ultimately advance statins as anticancer agents, it is therefore crucial to understand the molecular mechanisms involved in their anticancer activity and to delineate markers that distinguish the subset of tumors that are sensitive to statin-induced apoptosis. Statin-induced apoptosis results directly from inhibiting HMGCoA reductase (64), Once statins have blocked it and depleted the intracellular end-products of the mevalonate pathway, cytoplasmic transcription factors known as sterol regulatory element-binding proteins are activated. These transcription factors translocate to the nucleus, bind DNA at promoter regions containing sterol response elements (SREs), and induce the transcription of several key target genes, including *HMGCR* and the low-density lipoprotein receptor (*LDLR*). Up-regulated LDLR on the cell surface then binds and internalizes extracellular LDL-loaded cholesterol, thus reducing plasma cholesterol. It is this extraordinary feedback mechanism that has been successfully exploited to control hypercholesterolemia with statins (63).

A well-characterized pleiotropic effect of statins is the upregulation and activation of endothelial nitric oxide synthase (eNOS), one of the three NOS isoforms that catalyze the conversion of L-arginine to L-citrulline and nitric oxide (NO) with a 1:1 stoichiometry (62). Statins regulate eNOS via inhibition of geranylgeranylation of the small G-protein Rho (65). Translocation of inactive Rho from the cytosol to the membrane depends on geranylgeranylation. Activated Rho binds and activates Rho-associated kinases, which in turn

## ***A “Trojan Horse” strategy to reverse drug-resistance in brain tumors***

leads to phosphorylation of myosin light chains required for the formation of actin stress fibers and focal adhesion complexes. Anchoring of mRNAs to the actin cytoskeleton is necessary for their stability and translational expression (66). Consequently, Rho-mediated reorganization of the actin cytoskeleton may regulate the trafficking and subcellular localization of specific mRNAs.

Rho GTPases play a key role in the regulation of tumor growth, migration, and sensitivity to anticancer drugs. Some of these functions are dependent on the activity of the transcription factor nuclear factor- $\kappa$ B (NF $\kappa$ B) (67), (68) or Wnt3a / $\beta$ -catenin (non canonical) signaling pathway (69). NF- $\kappa$ B is composed of protein dimers, such as the heterodimer p50/p65, and regulates the expression of genes involved in inflammation, cellular proliferation, and apoptosis (70). In resting cells, members of the inhibitory I $\kappa$ B family proteins, like I $\kappa$ B $\alpha$ , bind directly to NF- $\kappa$ B dimer in the cytoplasm, preventing its nuclear localization. NF- $\kappa$ B is free to translocate and bind to DNA on the target genes when I $\kappa$ B $\alpha$  is phosphorylated by the I $\kappa$ B kinase (IKK) complex, ubiquitinated, and degraded by S26 proteasome (71). Statins, by inhibiting RhoA and its effector Rho kinase, can activate the IKK/NF- $\kappa$ B pathway (72). In addition, DOXO can induce NF- $\kappa$ B translocation in cancer cells via different mechanisms (73). By activating NF- $\kappa$ B, statins and DOXO may enhance the transcription of the inducible nitric-oxide synthase (iNOS) (70). NO is a signaling molecule involved in the control of cellular growth, differentiation, and apoptosis (70). In previous studies Riganti et al. suggested that NO is implicated in the DOXO cytotoxicity in HT29 cells and reverts DOXO resistance via the tyrosine nitration of Pgp and MRP3, two ATP-binding cassette transporters that recognize DOXO as a substrate. Such a nitration reduces the drug efflux in DOXO-resistant cells (74).

### **2.6. ABC transporters and signaling pathway**

Statins have been recognized as regulators of iNOS expression, nitration and modulation of the activity of ABC transporters, via RhoA protein and NF- $\kappa$ B transcription factor (74). However it is necessary to study other pathways that may be involved in the expression and/or activity of ABC transporters modulation, in order to find therapeutic targets associated with the use of new therapies (systems of nanoparticles or liposomes) to increase their effectiveness. In this way it has been considered the activity of the protein Rho as a modulator of Wnt3/ $\beta$ -catenin signaling pathway. Activation of signaling pathways by the

Wnt family secreted glycoproteins is central to a wide array of developmental events across all animal taxa, including cell proliferation, migration, establishment of cell polarity, and specification of cell fate (75). Dysregulation of Wnt signaling is known to result in human disease, and aberrant Wnt activation is a critical step in oncogenesis in many human tumors (76). Furthermore it has been shown a correlation between Wnt/ $\beta$ -catenin signaling activation and ABC transporters expression (77) which induce multidrug resistance. Wnt ligands bind to cellular receptors to activate diverse signaling events, including  $\beta$ -catenin-dependent transcriptional induction (the canonical pathway), stimulated release of intracellular calcium (the Wnt-Ca<sup>2+</sup> pathway), and initiation of the planar cell polarity/convergent extension pathway (the PCP pathway) (76) (72). There are ~20 members of the Wnt family in mammals that can be divided into two major categories: transforming and non-transforming factors. Transforming Wnts possess the ability to transform mammary epithelial cells and can induce secondary axis formation in *Xenopus*. Transforming Wnts generally activate the canonical,  $\beta$ -catenin-dependent signaling wherein Wnt stimulation regulates cellular  $\beta$ -catenin to ultimately induce transcription of target genes (78). Cytosolic  $\beta$ -catenin is continuously degraded in unstimulated cells via phosphorylation-ubiquitination-coupled proteasomal degradation. Receptor binding of canonical Wnts inhibits this degradation resulting in the accumulation of stabilized  $\beta$ -catenin, which can then shuttle into the nucleus. Nuclear  $\beta$ -catenin interacts with members of the T-cell factor (TCF)/lymphoid enhancing factor (LEF) family of HMG-box transcription factors to induce expression of Wnt target genes (79). Non-transforming Wnts neither transform cells nor induce secondary axis formation and are associated with the non-canonical Wnt-Ca<sup>2+</sup> and PCP pathways. Wnt signaling in these pathways is  $\beta$ -catenin-independent. Non-transforming Wnts control cytoskeletal changes to affect movement and polarity and do so in part by promoting the activation of the Rho family of GTPases, including Rho and Rac, which are important regulators of cytoarchitecture, cell adhesion, transcriptional events, and cell cycle progression (78). Wnt-induced activation of Rho GTPases is not restricted to non-transforming Wnts, however. The canonical Wnt1 in *Xenopus* was shown to trigger the activation of both Rho and Rac, and, in several studies, Wnt3A was reported to promote both canonical  $\beta$ -catenin dependent signaling as well as the activation of RhoA (69). While the importance of Wnt-triggered Rho activation of non-canonical signaling is well appreciated, its contribution to canonical signaling has not been examined. For that reason it is important to verify this pathway as a critical actor of  $\beta$ -catenin-induced transcription of target genes like

## *A "Trojan Horse" strategy to reverse drug-resistance in brain tumors*

ABC transporters. In addition a possible modulator of canonical signaling pathway could be the statins which are important Rho activity regulators.

### **3. Hypothesis**

BBB is the first obstacle for access of drugs targeting cancer cells in the brain. This impediment is represented by the expression of ABC transporters, which recognize and extrude the drugs out of the cells, decreasing the effectiveness of the chemotherapy. Taking as a basis the liposome structure, which accommodates the anti-cancer drug DOXO, it is possible to create a "Trojan horse". The liposome marked with a human peptide from APOB100, allows the recognition of the LDL (LDL-R) receptor, which is expressed in the cells of the BBB. This leads the liposome to cross the BBB, due to its low polarity by a process of simple diffusion or by endocytosis via LDL-R. In addition, the simultaneous use of statins, anti-cholesterol drugs, allows a greater expression of LDL-R and also induces a decrease in the activity of ABC transporters. Statins reduce the Rho GTPase activity and increase the activation of NOS, induce the synthesis of not favoring the nitration of ABC transporters. This combination increases the permeability of the "Trojan horse" allowing greater accumulation and toxicity of drugs in cancer cells. In hypoxia conditions there is an increasing Pgp expression however our strategy could be useful to reduce ABC transporters activity and could induce cytotoxicity in cancer cells.

In addition to recognize that Temozolomide crosses the BBB, the combined use of this drug associated with DOXO arised as an alternative therapy. Temozolomide is not substrate of ABC transporters or evades its action, it is a modulator of GSK3/ $\beta$ -catenin signalling, which is involved in the expression of Pgp transporter. This study contributes to clarify how Temozolomide reduces the activity of the GSK3/ $\beta$ -catenin pathway, lowers the expression of Pgp transporter and therefore facilitates the entrance of DOXO. By associating Temozolomide with the DOXO the permeability of the latter can be increased through the BBB, increasing the cytotoxicity of cancer cells.

#### **4. General Objective**

The objective of this work was to reverse the MDR phenotype in CNS tumors starting from the creation and use of a therapeutic strategy that improves the permeability of DOXO through the BBB, its accumulation and cytotoxic effect in tumors.

##### **4.1. Specific Objectives**

- A.** Generate a tool based on liposomes therapy that improves the permeability of DOXO through the BBB and reversed the MDR phenotype.
- B.** Verify that the LDL-mimicking liposome, ApolipoDOXO, binds the LDL receptor, reversed the MDR phenotype, i.e.:
  - 1. crosses in vitro the BBB
  - 2. accumulates in tumor cells
  - 3. exerts a strong cytotoxic effect.
- C.** Evaluate the use of combination therapies with DOXO or ApolipoDOXO, in the reversal of the MDR phenotype, associated with the use of:
  - 1. Statins
  - 2. Temozolomide
- D.** Evaluate the behavior of the ApolipoDOXO system in the tumor microenvironment under hypoxic conditions.
- E.** Determine molecular mechanisms associated with the expression of the MDR phenotype caused by overexpression of ABC transporters.

#### **5. General discussion**

Malignant gliomas, the most common brain tumors known as high-grade tumors, and systemic metastatic tumors, have high levels of ABC transporters or molecules responsible for the efflux of drugs used in chemotherapy treatments. These tumors response to chemotherapy is poor, since many anticancer drugs (DOXO, daunorubicin, etoposide, teniposide, paclitaxel, docetaxel, vincristine, vinblastine, cisplatin, methotrexate) have a permeability limited through the BBB and tumor cell membrane, and drugs able to enter the

### ***A “Trojan Horse” strategy to reverse drug-resistance in brain tumors***

cell are immediately removed by ABC transporters (1). (80). This barrier and tumor cell defense system bring as consequence that approximately 10% of patients with CNS tumours develop metastases and chemoresistance maintaining an intact BBB (15). Currently there are new strategies aimed at improving the effectiveness of primary brain tumors and metastatic conventional chemotherapies, maintaining unaltered the other cells of the CNS (14). The little possibility that drugs move through the BBB and the little accumulation in tumor cells are the main factors to consider in deficiency of therapies, which may be due to the molecular properties of the BBB, with few fenestrations, many strong unions as the tight junctions, and high levels of expression of pumps or ABC transporters (1, 5). This expression has been identified in CNS tumours (81), where they contribute to the chemoresistance. Therefore, a pharmacological therapy indicated for CNS tumors should be focused on mechanisms to evade the action of these transporters and/or recognize pathways that can promote the expression of them. In this context, my work suggests two approaches: First, it proposes strategies that evade the response of transporters in the cells of the BBB or tumor cells and second, it analyses cellular mechanisms that induce the expression of ABC transporters and that can be considered therapeutic targets.

The first approach use in this study suggests (Article I) a new combination, based on the association of statins plus DOXO encapsulated in liposomes marked with the binding peptide of LDL-R from APOB100 (ApolipoDOXO) taking into account two considerations: (a) liposomal drugs and statins have chemosensitive properties in solid tumors; (b) liposomal drugs cross the BBB more easily than free drugs. Some authors have proposed that the use of liposomes is safer than the use of nanoparticles (82), however, there are few studies based on the use of liposomes as transporters of drugs in the CNS (83). On the other hand, the liposomes are less toxic than other nanoparticles, since the former are constructed of substances such as phospholipids and cholesterol which are physiologically embedded in the cell membrane and subsequently degraded. Some studies have shown that the anti-cancer drugs loaded in liposomes are a successful alternative cancer treatment therapies and it is suggested that liposomal formulations may overcome the effect of ABC transporters. This is how it has been shown that in addition to staying a long time in tumor cells (83). Moreover liposomal drugs are not promoters of the expression of transporters as Pgp, unlike some drugs (84).

Previously it was shown the use of membrane receptors as a target for the recognition of liposomes: transferrin (Tf), lactoferrin, insulin, among others are some examples used in liposomes directed toward the cerebral parenchyma (83). This strategy has been recognized because it allows masking drug to enter the endothelial cells of the capillaries of the brain. Many liposomes enter mechanisms associated to a receiver via endocytosis. It is the case of PEG-liposome conjugated with Tf which more easily traversed BBB cells than non-conjugated liposomes. In addition the use of the boron 10-loaded liposomes in co-culture models, increased the cytotoxicity of cells of glioblastoma U87 (85). In the present study the strategy named Trojan horse, demonstrated that the use of liposomes associated with LDL, ApolipoDOXO, can be advantageous since they can be recognized, through peptide from ApoB100, not only by the endothelial cells of the BBB, but also by the tumor cells. Likewise combined administration with statins favors the increase in expression of the LDL receptor, which is consistent with the use of LDLR-associated liposomes. On the other hand ApolipoDOXO crossed through the cells of the BBB and it also induced cytotoxicity in tumor cells in co-culture.

The Trojan horse liposome system proposed in this paper, differs from other studies using nanoparticles that penetrate the BBB since this is a more "physiological" system: it takes advantage from the usual metabolic effects of statins which, by reducing the amount of cholesterol, promote the increase in LDL receptors and the synthesis of NO (favoring the nitration and inactivation of ABC transporters). On the other hand, it takes advantage also from the properties of the liposomes, which cross the BBB by diffusion or by endocytosis. The union of these two factors promotes the effectiveness against drug-resistant tumors. This final effect was demonstrated not only in conditions of normoxia, but also in hypoxic conditions, in which drug resistance is increased, since HIF-1 $\alpha$  hypoxia modulates the expression of transporters as Pgp (Article III) (86, 87). HIF-1 $\alpha$  presents a double action on the cells of the BBB; first it increases the expression of Pgp transporter, which limits the use of DOXOrubicin, reducing its permeability, and second it increases the expression of LDL receptor in the cells, therefore it favours the use of the ApolipoDOXO to be better recognized and allow their passage by endothelial cells.

In this part of the study (Article III) it was evaluated the passage of drugs such as DOXO and vinblastine, substrates of Pgp, under conditions of normoxia and hypoxia. Cells of

### ***A “Trojan Horse” strategy to reverse drug-resistance in brain tumors***

endothelial barrier have different behavior depending on the species which come from: cells murine bEND3 decrease their permeability while hCMEC/D3 human cells do not change it in hypoxia. This difference lies in the expression of Pgp, which occurs under conditions of normoxia in human cells but not in murine cells, which confirms findings of other researchers (88). However, this study demonstrated how hypoxia could modulate the activity of Pgp transporter in murine cells, while in the human cells hCMEC/D3 HIF-1 $\alpha$  is stabilized also in normoxia. There is a transporters-specific regulation under hypoxia; indeed other transporters such as MRP 1 and 6 could be invariant under these conditions. In this study it was found that HIF-1 $\alpha$  and SREBP-2 co-immunoprecipitated, HIF-1 $\alpha$  favored the nuclear translocation of SREBP-2 and the transcription of HMGCoAR. The activation of HIF-1 $\alpha$ /SREBP-2 axis determined the rate of cholesterol synthesis. Currently there are no known reports that show this dependence on cholesterol synthesis of the activity of HIF-1 $\alpha$  in cells of the BBB. Thus the study proposes that the SREBP-2 transcription factor activation dependent on HIF-1 $\alpha$  positively modulates the expression of LDLR receptor cells BBB. This effect also favoured an increased ApolipoDOXO permeability associated with the use of statins in hypoxic conditions in both BBB cells and glioblastoma cells.

Therapies associated with nanoparticles or liposomes have improve the entry of drugs such as DOXO in cancer cells seeking to improve therapies and decreasing the isolated drug (13) cardiotoxic effect. However other efforts have led to improved therapies which in principle have shown a great effectiveness not being dependent on the ABC transporters. It is the case of temozolomide (TMZ), which, despite the use of different doses, does not show sufficient efficacy to control GBM disease (18). In this study it was demonstrated that the TMZ, in similar doses to those found in blood (89), increased the permeability of the cells of the BBB to DOXO, seen by the increase in coefficients of permeability, and decreased the expression of the transporter Pgp (Article IV). In the systemic circulation the TMZ is quickly converted into its form active 3-methyl-(triazen-1-il) imidazole-4-carboxamide, so that it could be considered the latter as the reducer of Pgp expression.

Previous studies have reported that Pgp is under the transcriptional control of the  $\beta$ -catenin, whose activity is regulated by Wnt/GSK3/ $\beta$ -catenin signalling in hCMEC/D3 cells (77), an effect that I confirmed in my study (Article V). TMZ-treated cells showed an increase in the activity of GSK3 and an increase in the amount of phosphorylated  $\beta$ -catenin, leading to the

decline of the nuclear  $\beta$ -catenin and binding to the promoter of *mdr1*. The activity of GSK3/ $\beta$ -catenin signaling pathway depends on the combination of factors as Wnts to LRP5/6 or Frizzled receptors (77), in this way it was evaluated the action that could have the TMZ on this axis. It was found that the TMZ decreased protein and mRNA *Wnt3* allowing raising the hypothesis that the drug decreases the *Wnt3* gene transcription in cells of the BBB, increases the phosphorylation of the  $\beta$ -catenin and reduces nuclear and binding to the promoter of the *mdr1* gene. It is known that TMZ, an alkylating agent, methylates a guanine at position O6 and induces the double-stranded DNA breaks. Primary cytotoxic lesions of the O6 methylguanine can be removed by a direct repair mechanism by the methyltransferase (MGMT)-methylguanine in tumors expressing it, or tolerated in tumors with mismatch repair-deficient (MMR-). MGMT or deficiency in MMR confers resistance to treatments with TMZ. However, most of the methylations caused by the TMZ are methylations of another type usually non-cytotoxic (90). The consequences of these methylations have not been studied. It was found that TMZ methylates *Wnt3* gene promoter in untreated BBB cells that express a promoter fully demethylated, which is consistent with the constitutive transcription of *Wnt3*: Thus the methylation of promoter induced by the TMZ could explain the decrease in the *Wnt3*, suggesting that the TMZ is an epigenetic regulator of the *Wnt3* gene. This deregulation is not only noted on BBB endothelial cells, but also in cells of glioblastoma (91).

The combination of TMZ with DOXO proved to be effective to increase the permeability of DOXO in cells of the BBB by decreasing the expression of the Pgp transporter by methylation of *Wnt3*, which affects the GSK3/ $\beta$ -catenin pathway and the expression of the transporter Pgp. Likewise it was increased the cytotoxicity of GBM cells maintained in coculture with BBB cells.

In this work, beside identifying potential strategies that facilitate the movement of drugs through the blood-brain barrier, we identified specific molecular mechanisms associated with the expression of Pgp transporter in human cells of BBB, which are quoted below:

1. Use statins produced NOS expression through a NF $\kappa$ B-dependent mechanism (Article I) and leads to the synthesis of NO; NO nitrates ABC transporters and decreased ATPase activity. This mechanism had been previously evaluated in colon cancer cells

## ***A "Trojan Horse" strategy to reverse drug-resistance in brain tumors***

HT29 (73) and it was evidenced as a modulator mechanism of the activity of Pgp and BCRP transporters in cells of the BBB.

2. Another key mechanism presented in this study, corresponds to the modulation of the TMZ in the methylation of the gene Wnt3 (Article IV) that reduces the activity of GSK3/ $\beta$ -catenin signaling pathway and therefore reduces the expression of Pgp transporter.
3. The last mechanism corresponds to the action of the axis of the RhoA/RhoA kinase as a key element in the activity of the GSK3/ $\beta$ -catenin (non-canonical) pathway, demonstrating that this pathway associated with the activity of RhoA and RhoA protein expression kinase is an important factor that favors the Pgp transporter expression (Article V). Previous studies had shown that PTP1B tyrosine phosphatase reduces the activity of GSK3 by 216 tyrosine dephosphorylation, which is critical to the activity of GSK3 (92). PTP1B is activated by phosphorylation of serine 50 (93). In this study it was demonstrated that RhoA kinase phosphorylated PTP1B in serine 50, and decreased the GSK3 phosphorylation on tyrosine 216. Reducing the phosphorylation of GSK3 decreases phosphorylation of  $\beta$ -catenin favoring its accumulation at the nuclear level and therefore promoting its binding to *mdr1* gene promoter.

All these mechanisms contributing to modulate the expression of Pgp are of great interest considering that this transporter is the main generator of resistance to drugs in the BBB and in glioblastoma cells. Therefore, this study provides knowledge in two ways: one, in the improvement of the presentation of the drug anticancer; two, in the knowledge of mechanisms of action that promote the MDR phenotype. Our strategies can be considered not only in the modulation of brain cancer but also in the management of diseases associated with the CNS.

## **6. Conclusions and Perspectives**

The study presented in this thesis allows concluding that the use of combined chemotherapy of glioblastomas would be helpful to increase the effectiveness of the drugs by circumventing ABC transporters. Thus the strategy of the "Trojan horse", based on the administration of statins over the use of DOXO encapsulated in liposomes associated to the LDL receptor, could

have potential applications in therapy not only of brain cancer, but also of different diseases in which the BBB represents an obstacle. On the other hand, these results suggest that TMZ increases the permeability of drugs in the BBB, which are substrate of Pgp transporter. Therefore association of TMZ with DOXO could be a new combined therapy approach for glioblastoma.

Additionally it was shown evidence for apparent metabolic changes occurring in the cells of the BBB during hypoxia, which allowed posing an effective strategy that improves the permeability of the drug in BBB cells exposed to a hypoxic environment and/or with an active HIF-1 $\alpha$ . This strategy is flexible, as different drugs could be encapsulated in liposomes associated to the LDL receptor.

The understanding of new mechanisms associated with the expression of the MDR phenotype caused by overexpression of ABC transporters, was evident in this work. It was possible to demonstrate that statins reduce the activity of transporters through a process of nitration. On the other hand the use of Temozolomide favored the methylation of the gene Wnt3 promoting the inactivation of the GSK3/ $\beta$ -catenin pathway and the decrease of expression of Pgp transporter. It was shown that the expression of P-glycoprotein is controlled by a crossover between the canonical and non-canonical Wnt/ $\beta$ -catenin pathway. Alteration of this crosstalk by inhibition of RhoA/RhoA kinase could represent a strategy to decrease the expression of Pgp and increase the passage of substrates of this transporter through the BBB.

The effects of a new therapeutic strategy associated with the knowledge of mechanisms that regulate the MDR phenotype are presented in this study as an effective alternative that promotes the use of new approaches in the fight against Glioblastoma and which could be useful in the control of other diseases of the Central Nervous System.

The next phase of this work will consist of assessing mechanisms associated with resistance to drugs caused by stress. It has been recognized the reactive species of oxygen (ROS) that arise due to the use of drugs or the environment hypoxic tumor could increase the Multidrug resistance phenotype by increasing the expression of ABC transporters. The next goal will be to analyze these events and develop new therapies based on specific targets.

## 7. References

1. Mercer RW, Tyler MA, Ulasov IV, Lesniak MS. Targeted therapies for malignant glioma: progress and potential. *BioDrugs : clinical immunotherapeutics, biopharmaceuticals and gene therapy*. 2009;23(1):25-35.
2. Rossi A, Caracciolo V, Russo G, Reiss K, Giordano A. Medulloblastoma: from molecular pathology to therapy. *Clinical cancer research : an official journal of the American Association for Cancer Research*. 2008;14(4):971-6.
3. Soffietti R, Ruda R. Neuro-oncology: new insights and advances in treatment. *Lancet Neurol*. 2008;7(1):14-6.
4. Sathornsumetee S, Reardon DA, Desjardins A, Quinn JA, Vredenburgh JJ, Rich JN. Molecularly targeted therapy for malignant glioma. *Cancer*. 2007;110(1):13-24.
5. Decleves X, Amiel A, Delattre JY, Scherrmann JM. Role of ABC transporters in the chemoresistance of human gliomas. *Curr Cancer Drug Targets*. 2006;6(5):433-45.
6. Savage RE, Jr., Kanitz MH, Lotz WG, Conover D, Hennessey EM, Hanneman WH, et al. Changes in gene and protein expression in magnetic field-treated human glioma cells. *Toxicology mechanisms and methods*. 2005;15(2):115-20.
7. Tanaka Y, Fujii M, Saito T, Kawamori J. [Radiation therapy for brain tumors]. *Nihon Igaku Hoshasen Gakkai Zasshi*. 2004;64(7):387-93.
8. van Rij CM, Wilhelm AJ, Sauerwein WA, van Loenen AC. Boron neutron capture therapy for glioblastoma multiforme. *Pharm World Sci*. 2005;27(2):92-5.
9. Al-Waili NS, Butler GJ, Beale J, Abdullah MS, Hamilton RW, Lee BY, et al. Hyperbaric oxygen in the treatment of patients with cerebral stroke, brain trauma, and neurologic disease. *Advances in therapy*. 2005;22(6):659-78.
10. Zalutsky MR. Current status of therapy of solid tumors: brain tumor therapy. *J Nucl Med*. 2005;46 Suppl 1:151S-6S.
11. Al-Waili NS, Butler GJ. A combination of radiotherapy, nitric oxide and a hyperoxygenation sensitizing protocol for brain malignant tumor treatment. *Med Hypotheses*. 2007;68(3):528-37.
12. Heuer GG, Jackson EM, Magge SN, Storm PB. Surgical management of pediatric brain tumors. *Expert Rev Anticancer Ther*. 2007;7(12 Suppl):S61-8.
13. Bhaskar S, Tian F, Stoeger T, Kreyling W, de la Fuente JM, Grazu V, et al. Multifunctional Nanocarriers for diagnostics, drug delivery and targeted treatment across blood-brain barrier: perspectives on tracking and neuroimaging. *Part Fibre Toxicol*. 2010;7:3.
14. Lockman PR, Mittapalli RK, Taskar KS, Rudraraju V, Gril B, Bohn KA, et al. Heterogeneous blood-tumor barrier permeability determines drug efficacy in experimental brain metastases of breast cancer. *Clinical cancer research : an official journal of the American Association for Cancer Research*. 2010;16(23):5664-78.
15. Kamar FG, Posner JB. Brain metastases. *Seminars in neurology*. 2010;30(3):217-35.
16. Pardridge WM. Why is the global CNS pharmaceutical market so under-penetrated? *Drug Discov Today*. 2002;7(1):5-7.
17. Pardridge WM. Blood-brain barrier biology and methodology. *J Neurovirol*. 1999;5(6):556-69.
18. Hawkins BT, Davis TP. The blood-brain barrier/neurovascular unit in health and disease. *Pharmacol Rev*. 2005;57(2):173-85.
19. Saunders NR, Ek CJ, Habgood MD, Dziegielewska KM. Barriers in the brain: a renaissance? *Trends in neurosciences*. 2008;31(6):279-86.

20. Jin R, Yang G, Li G. Molecular insights and therapeutic targets for blood-brain barrier disruption in ischemic stroke: critical role of matrix metalloproteinases and tissue-type plasminogen activator. *Neurobiology of disease*. 2010;38(3):376-85.
21. Lichota J, Skjorringe T, Thomsen LB, Moos T. Macromolecular drug transport into the brain using targeted therapy. *J Neurochem*. 2010;113(1):1-13.
22. Saunders NR, Knott GW, Dziegielewska KM. Barriers in the immature brain. *Cell Mol Neurobiol*. 2000;20(1):29-40.
23. Pinzon-Daza ML, Campia I, Kopecka J, Garzon R, Ghigo D, Riganti C. Nanoparticle- and liposome-carried drugs: new strategies for active targeting and drug delivery across blood-brain barrier. *Current drug metabolism*. 2013;14(6):625-40.
24. Polli JW, Olson KL, Chism JP, John-Williams LS, Yeager RL, Woodard SM, et al. An unexpected synergist role of P-glycoprotein and breast cancer resistance protein on the central nervous system penetration of the tyrosine kinase inhibitor lapatinib (N-{3-chloro-4-[(3-fluorobenzyl)oxy]phenyl}-6-[5-{{[2-(methylsulfonyl)ethyl]amino }methyl}-2-furyl]-4-quinazolinamine; GW572016). *Drug Metab Dispos*. 2009;37(2):439-42.
25. Schinkel AH, Jonker JW. Mammalian drug efflux transporters of the ATP binding cassette (ABC) family: an overview. *Adv Drug Deliv Rev*. 2003;55(1):3-29.
26. Eisenblatter T, Huwel S, Galla HJ. Characterisation of the brain multidrug resistance protein (BMDP/ABCG2/BCRP) expressed at the blood-brain barrier. *Brain Res*. 2003;971(2):221-31.
27. de Vries NA, Zhao J, Kroon E, Buckle T, Beijnen JH, van Tellingen O. P-glycoprotein and breast cancer resistance protein: two dominant transporters working together in limiting the brain penetration of topotecan. *Clinical cancer research : an official journal of the American Association for Cancer Research*. 2007;13(21):6440-9.
28. Lagas JS, Fan L, Wagenaar E, Vlaming ML, van Tellingen O, Beijnen JH, et al. P-glycoprotein (P-gp/Abcb1), Abcc2, and Abcc3 determine the pharmacokinetics of etoposide. *Clinical cancer research : an official journal of the American Association for Cancer Research*. 2010;16(1):130-40.
29. Vlaming ML, Lagas JS, Schinkel AH. Physiological and pharmacological roles of ABCG2 (BCRP): recent findings in Abcg2 knockout mice. *Adv Drug Deliv Rev*. 2009;61(1):14-25.
30. Lagas JS, van Waterschoot RA, van Tilburg VA, Hillebrand MJ, Lankheet N, Rosing H, et al. Brain accumulation of dasatinib is restricted by P-glycoprotein (ABCB1) and breast cancer resistance protein (ABCG2) and can be enhanced by elacridar treatment. *Clinical cancer research : an official journal of the American Association for Cancer Research*. 2009;15(7):2344-51.
31. Begley DJ, Brightman MW. Structural and functional aspects of the blood-brain barrier. *Prog Drug Res*. 2003;61:39-78.
32. Bauer M, Zeitlinger M, Karch R, Matzneller P, Stanek J, Jager W, et al. Pgp-mediated interaction between (R)-[11C]verapamil and tariquidar at the human blood-brain barrier: a comparison with rat data. *Clinical pharmacology and therapeutics*. 2012;91(2):227-33.
33. Loscher W, Potschka H. Blood-brain barrier active efflux transporters: ATP-binding cassette gene family. *NeuroRx*. 2005;2(1):86-98.
34. Pardridge WM. Drug targeting to the brain. *Pharm Res*. 2007;24(9):1733-44.
35. Zhang Y, Han H, Elmquist WF, Miller DW. Expression of various multidrug resistance-associated protein (MRP) homologues in brain microvessel endothelial cells. *Brain Res*. 2000;876(1-2):148-53.
36. Cisternino S, Mercier C, Bourasset F, Roux F, Scherrmann JM. Expression, up-regulation, and transport activity of the multidrug-resistance protein Abcg2 at the mouse blood-brain barrier. *Cancer Res*. 2004;64(9):3296-301.

## ***A "Trojan Horse" strategy to reverse drug-resistance in brain tumors***

37. Agarwal S, Sane R, Ohlfest JR, Elmquist WF. The role of the breast cancer resistance protein (ABCG2) in the distribution of sorafenib to the brain. *J Pharmacol Exp Ther.* 2011;336(1):223-33.
38. Gottesman MM, Fojo T, Bates SE. Multidrug resistance in cancer: role of ATP-dependent transporters. *Nat Rev Cancer.* 2002;2(1):48-58.
39. Van Luyn MJ, Muller M, Renes J, Meijer C, Scheper RJ, Nienhuis EF, et al. Transport of glutathione conjugates into secretory vesicles is mediated by the multidrug-resistance protein 1. *Int J Cancer.* 1998;76(1):55-62.
40. Comerford KM, Wallace TJ, Karhausen J, Louis NA, Montalto MC, Colgan SP. Hypoxia-inducible factor-1-dependent regulation of the multidrug resistance (MDR1) gene. *Cancer Res.* 2002;62(12):3387-94.
41. Moeller BJ, Dewhirst MW. HIF-1 and tumour radiosensitivity. *Br J Cancer.* 2006;95(1):1-5.
42. Yasuda H. Solid tumor physiology and hypoxia-induced chemo/radio-resistance: novel strategy for cancer therapy: nitric oxide donor as a therapeutic enhancer. *Nitric Oxide.* 2008;19(2):205-16.
43. Gianni L, Herman EH, Lipshultz SE, Minotti G, Sarvazyan N, Sawyer DB. Anthracycline cardiotoxicity: from bench to bedside. *J Clin Oncol.* 2008;26(22):3777-84.
44. Simunek T, Sterba M, Popelova O, Adamcova M, Hrdina R, Gersl V. Anthracycline-induced cardiotoxicity: overview of studies examining the roles of oxidative stress and free cellular iron. *Pharmacol Rep.* 2009;61(1):154-71.
45. Gewirtz DA. A critical evaluation of the mechanisms of action proposed for the antitumor effects of the anthracycline antibiotics adriamycin and daunorubicin. *Biochem Pharmacol.* 1999;57(7):727-41.
46. L'Ecuyer T, Horenstein MS, Thomas R, Vander Heide R. Anthracycline-induced cardiac injury using a cardiac cell line: potential for gene therapy studies. *Mol Genet Metab.* 2001;74(3):370-9.
47. Minotti G, Menna P, Salvatorelli E, Cairo G, Gianni L. Anthracyclines: molecular advances and pharmacologic developments in antitumor activity and cardiotoxicity. *Pharmacol Rev.* 2004;56(2):185-229.
48. Weiss RB. The anthracyclines: will we ever find a better DOXOrubicin? *Semin Oncol.* 1992;19(6):670-86.
49. Markman M. Pegylated liposomal DOXOrubicin in the treatment of cancers of the breast and ovary. *Expert opinion on pharmacotherapy.* 2006;7(11):1469-74.
50. Andresen TL, Jensen SS, Jorgensen K. Advanced strategies in liposomal cancer therapy: problems and prospects of active and tumor specific drug release. *Prog Lipid Res.* 2005;44(1):68-97.
51. McNeil SE. Nanotechnology for the biologist. *Journal of leukocyte biology.* 2005;78(3):585-94.
52. Trapani A, Denora N, Iacobellis G, Sitterberg J, Bakowsky U, Kissel T. Methotrexate-loaded chitosan- and glycol chitosan-based nanoparticles: a promising strategy for the administration of the anticancer drug to brain tumors. *AAPS PharmSciTech.* 2011;12(4):1302-11.
53. Kim HR, Kim IK, Bae KH, Lee SH, Lee Y, Park TG. Cationic solid lipid nanoparticles reconstituted from low density lipoprotein components for delivery of siRNA. *Molecular pharmaceuticals.* 2008;5(4):622-31.
54. Owens DE, 3rd, Peppas NA. Opsonization, biodistribution, and pharmacokinetics of polymeric nanoparticles. *Int J Pharm.* 2006;307(1):93-102.

55. Kratz F, Muller-Driver R, Hofmann I, Dreves J, Unger C. A novel macromolecular prodrug concept exploiting endogenous serum albumin as a drug carrier for cancer chemotherapy. *J Med Chem.* 2000;43(7):1253-6.
56. DeFeo-Jones D, Garsky VM, Wong BK, Feng DM, Bolyar T, Haskell K, et al. A peptide-DOXOrubicin 'prodrug' activated by prostate-specific antigen selectively kills prostate tumor cells positive for prostate-specific antigen in vivo. *Nature medicine.* 2000;6(11):1248-52.
57. Wong HL, Bendayan R, Rauth AM, Wu XY. Simultaneous delivery of DOXOrubicin and GG918 (Elacridar) by new polymer-lipid hybrid nanoparticles (PLN) for enhanced treatment of multidrug-resistant breast cancer. *J Control Release.* 2006;116(3):275-84.
58. Miladi I, Duc GL, Kryza D, Berniard A, Mowat P, Roux S, et al. Biodistribution of ultra small gadolinium-based nanoparticles as theranostic agent: application to brain tumors. *Journal of biomaterials applications.* 2013;28(3):385-94.
59. Bennewitz MF, Saltzman WM. Nanotechnology for delivery of drugs to the brain for epilepsy. *Neurotherapeutics : the journal of the American Society for Experimental NeuroTherapeutics.* 2009;6(2):323-36.
60. Vaughan CJ, Delanty N. Neuroprotective properties of statins in cerebral ischemia and stroke. *Stroke.* 1999;30(9):1969-73.
61. Laufs U, Liao JK. Post-transcriptional regulation of endothelial nitric oxide synthase mRNA stability by Rho GTPase. *J Biol Chem.* 1998;273(37):24266-71.
62. Endres M, Laufs U. Effects of statins on endothelium and signaling mechanisms. *Stroke.* 2004;35(11 Suppl 1):2708-11.
63. Bogman K, Peyer AK, Torok M, Kusters E, Drewe J. HMG-CoA reductase inhibitors and P-glycoprotein modulation. *Br J Pharmacol.* 2001;132(6):1183-92.
64. Clendening JW, Pandyra A, Li Z, Boutros PC, Martirosyan A, Lehner R, et al. Exploiting the mevalonate pathway to distinguish statin-sensitive multiple myeloma. *Blood.* 2010;115(23):4787-97.
65. Rikitake Y, Liao JK. Rho GTPases, statins, and nitric oxide. *Circ Res.* 2005;97(12):1232-5.
66. Blum R, Jacob-Hirsch J, Amariglio N, Rechavi G, Kloog Y. Ras inhibition in glioblastoma down-regulates hypoxia-inducible factor-1alpha, causing glycolysis shutdown and cell death. *Cancer Res.* 2005;65(3):999-1006.
67. Fritz G, Kaina B. Rho GTPases: promising cellular targets for novel anticancer drugs. *Curr Cancer Drug Targets.* 2006;6(1):1-14.
68. Greten FR, Karin M. The IKK/NF-kappaB activation pathway-a target for prevention and treatment of cancer. *Cancer Lett.* 2004;206(2):193-9.
69. Rossol-Allison J, Stemmler LN, Swenson-Fields KI, Kelly P, Fields PE, McCall SJ, et al. Rho GTPase activity modulates Wnt3a/beta-catenin signaling. *Cell Signal.* 2009;21(11):1559-68.
70. Kraynack NC, Corey DA, Elmer HL, Kelley TJ. Mechanisms of NOS2 regulation by Rho GTPase signaling in airway epithelial cells. *Am J Physiol Lung Cell Mol Physiol.* 2002;283(3):L604-11.
71. Rattan R, Giri S, Singh AK, Singh I. Rho A negatively regulates cytokine-mediated inducible nitric oxide synthase expression in brain-derived transformed cell lines: negative regulation of IKKalpha. *Free Radic Biol Med.* 2003;35(9):1037-50.
72. Lin X, Li Q, Wang YJ, Ju YW, Chi ZQ, Wang MW, et al. Morphine inhibits DOXOrubicin-induced reactive oxygen species generation and nuclear factor kappaB transcriptional activation in neuroblastoma SH-SY5Y cells. *Biochem J.* 2007;406(2):215-21.

## ***A "Trojan Horse" strategy to reverse drug-resistance in brain tumors***

73. Riganti C, Doublier S, Costamagna C, Aldieri E, Pescarmona G, Ghigo D, et al. Activation of nuclear factor-kappa B pathway by simvastatin and RhoA silencing increases DOXOrubicin cytotoxicity in human colon cancer HT29 cells. *Mol Pharmacol*. 2008;74(2):476-84.
74. Riganti C, Orecchia S, Pescarmona G, Betta PG, Ghigo D, Bosia A. Statins revert DOXOrubicin resistance via nitric oxide in malignant mesothelioma. *Int J Cancer*. 2006;119(1):17-27.
75. Logan CY, Nusse R. The Wnt signaling pathway in development and disease. *Annu Rev Cell Dev Biol*. 2004;20:781-810.
76. Polakis P. The many ways of Wnt in cancer. *Curr Opin Genet Dev*. 2007;17(1):45-51.
77. Lim JC, Kania KD, Wijesuriya H, Chawla S, Sethi JK, Pulaski L, et al. Activation of beta-catenin signalling by GSK-3 inhibition increases p-glycoprotein expression in brain endothelial cells. *J Neurochem*. 2008;106(4):1855-65.
78. Nelson WJ, Nusse R. Convergence of Wnt, beta-catenin, and cadherin pathways. *Science*. 2004;303(5663):1483-7.
79. Takahashi-Yanaga F, Sasaguri T. The Wnt/beta-catenin signaling pathway as a target in drug discovery. *J Pharmacol Sci*. 2007;104(4):293-302.
80. Van Meir EG, Hadjipanayis CG, Norden AD, Shu HK, Wen PY, Olson JJ. Exciting new advances in neuro-oncology: the avenue to a cure for malignant glioma. *CA: a cancer journal for clinicians*. 2010;60(3):166-93.
81. Nakagawa T, Ido K, Sakuma T, Takeuchi H, Sato K, Kubota T. Prognostic significance of the immunohistochemical expression of O6-methylguanine-DNA methyltransferase, P-glycoprotein, and multidrug resistance protein-1 in glioblastomas. *Neuropathology : official journal of the Japanese Society of Neuropathology*. 2009;29(4):379-88.
82. Zhang YF, Boado RJ, Pardridge WM. Absence of toxicity of chronic weekly intravenous gene therapy with pegylated immunoliposomes. *Pharm Res*. 2003;20(11):1779-85.
83. Kobayashi T, Ishida T, Okada Y, Ise S, Harashima H, Kiwada H. Effect of transferrin receptor-targeted liposomal DOXOrubicin in P-glycoprotein-mediated drug resistant tumor cells. *Int J Pharm*. 2007;329(1-2):94-102.
84. Zalipsky S, Saad M, Kiwan R, Ber E, Yu N, Minko T. Antitumor activity of new liposomal prodrug of mitomycin C in multidrug resistant solid tumor: insights of the mechanism of action. *Journal of drug targeting*. 2007;15(7-8):518-30.
85. Doi A, Kawabata S, Iida K, Yokoyama K, Kajimoto Y, Kuroiwa T, et al. Tumor-specific targeting of sodium borocaptate (BSH) to malignant glioma by transferrin-PEG liposomes: a modality for boron neutron capture therapy. *Journal of neuro-oncology*. 2008;87(3):287-94.
86. Brahimi-Horn C, Pouyssegur J. When hypoxia signalling meets the ubiquitin-proteasomal pathway, new targets for cancer therapy. *Critical reviews in oncology/hematology*. 2005;53(2):115-23.
87. Brahimi-Horn C, Pouyssegur J. The role of the hypoxia-inducible factor in tumor metabolism growth and invasion. *Bulletin du cancer*. 2006;93(8):E73-80.
88. Uchida Y, Ohtsuki S, Katsukura Y, Ikeda C, Suzuki T, Kamiie J, et al. Quantitative targeted absolute proteomics of human blood-brain barrier transporters and receptors. *J Neurochem*. 2011;117(2):333-45.
89. Portnow J, Badie B, Chen M, Liu A, Blanchard S, Synold TW. The neuropharmacokinetics of temozolomide in patients with resectable brain tumors: potential implications for the current approach to chemoradiation. *Clinical cancer research : an official journal of the American Association for Cancer Research*. 2009;15(22):7092-8.
90. Wick W, Platten M, Weller M. New (alternative) temozolomide regimens for the treatment of glioma. *Neuro-oncology*. 2009;11(1):69-79.

91. Riganti C, Salaroglio IC, Caldera V, Campia I, Kopecka J, Mellai M, et al. Temozolomide downregulates P-glycoprotein expression in glioblastoma stem cells by interfering with the Wnt3a/glycogen synthase-3 kinase/beta-catenin pathway. *Neuro-oncology*. 2013;15(11):1502-17.
92. Mobasher MA, Gonzalez-Rodriguez A, Santamaria B, Ramos S, Martin MA, Goya L, et al. Protein tyrosine phosphatase 1B modulates GSK3beta/Nrf2 and IGFIR signaling pathways in acetaminophen-induced hepatotoxicity. *Cell death & disease*. 2013;4:e626.
93. Moeslein FM, Myers MP, Landreth GE. The CLK family kinases, CLK1 and CLK2, phosphorylate and activate the tyrosine phosphatase, PTP-1B. *J Biol Chem*. 1999;274(38):26697-704.

## RESEARCH PAPER

# The association of statins plus LDL receptor-targeted liposome-encapsulated doxorubicin increases *in vitro* drug delivery across blood–brain barrier cells

ML Pinzón-Daza<sup>1,2</sup>, R Garzón<sup>2</sup>, PO Couraud<sup>3</sup>, IA Romero<sup>4</sup>, B Weksler<sup>5</sup>, D Ghigo<sup>1,6</sup>, A Bosia<sup>1,6</sup> and C Riganti<sup>1,6</sup>

<sup>1</sup>Department of Oncology, Faculty of Medicine, University of Turin, Turin, Italy, <sup>2</sup>Unidad de Bioquímica, Facultad de Ciencias Naturales y Matemáticas, Universidad del Rosario, Bogotá, Colombia, <sup>3</sup>Institut Cochin, Centre National de la Recherche Scientifique UMR 8104, Institut National de la Santé et de la Recherche Médicale (INSERM) U567, Université René Descartes, Paris, France, <sup>4</sup>Department of Biological Sciences, The Open University, Milton Keynes, UK, <sup>5</sup>Department of Medicine, Weill Medical College, New York, USA, and <sup>6</sup>Center for Experimental Research and Medical Studies, University of Turin, Turin, Italy

### Correspondence

Dr Chiara Riganti, Department of Oncology, Via Santena 5/bis, 10126 Turin, Italy. E-mail: chiara.riganti@unito.it

### Keywords

blood–brain barrier; statins; ATP-binding cassette transporters; doxorubicin; nitric oxide; low-density lipoproteins receptor; liposomes; central nervous system tumours

### Received

8 January 2012

### Revised

20 May 2012

### Accepted

22 June 2012

## BACKGROUND AND PURPOSE

The passage of drugs across the blood–brain barrier (BBB) limits the efficacy of chemotherapy in brain tumours. For instance, the anticancer drug doxorubicin, which is effective against glioblastoma *in vitro*, has poor efficacy *in vivo*, because it is extruded by P-glycoprotein (Pgp/ABCB1), multidrug resistance-related proteins and breast cancer resistance protein (BCRP/ABCG2) in BBB cells. The aim of this study was to convert poorly permeant drugs like doxorubicin into drugs able to cross the BBB.

## EXPERIMENTAL APPROACH

Experiments were performed on primary human cerebral microvascular endothelial hCMEC/D3 cells, alone and co-cultured with human brain and epithelial tumour cells.

## KEY RESULTS

Statins reduced the efflux activity of Pgp/ABCB1 and BCRP/ABCG2 in hCMEC/D3 cells by increasing the synthesis of NO, which elicits the nitration of critical tyrosine residues on these transporters. Statins also increased the number of low-density lipoprotein (LDL) receptors exposed on the surface of BBB cells, as well as on tumour cells like human glioblastoma. We showed that the association of statins plus drug-loaded nanoparticles engineered as LDLs was effective as a vehicle for non-permeant drugs like doxorubicin to cross the BBB, allowing its delivery into primary and metastatic brain tumour cells and to achieve significant anti-tumour cytotoxicity.

## CONCLUSIONS AND IMPLICATIONS

We suggest that our 'Trojan horse' approach, based on the administration of statins plus a LDL receptor-targeted liposomal drug, might have potential applications in the pharmacological therapy of different brain diseases for which the BBB represents an obstacle.

## Abbreviations

ABC, ATP-binding cassette; AMC, amino-4-methylcumarine; BBB, blood–brain barrier; BCRP/ABCG2, breast cancer resistance protein; GAPDH, glyceraldehyde 3-phosphate dehydrogenase; GGPP, geranylgeranyl pyrophosphate; LDL, low-density lipoprotein; MRPs/ABCCs, multidrug resistance-related proteins; PEG, polyethylene glycol; Pgp/ABCB1, P-glycoprotein; PTIO, phenyl-4,4,5,5-tetramethylimidazoline-1-oxyl 3-oxide; TBS, Tris-buffered saline

## Introduction

Primary CNS tumours, like glioblastoma, and CNS metastasis of solid tumours are poorly responsive to chemotherapy, as a consequence of the intrinsic tumour resistance and of the low penetration of many anticancer drugs across the blood–brain barrier (BBB). Both tumour cells and BBB endothelial cells are rich in ATP-binding cassette (ABC) transporters, like P-glycoprotein (Pgp/ABCB1), multidrug resistance-related proteins (MRPs/ABCCs) and breast cancer resistance protein (BCRP/ABCG2) that extrude drugs from the luminal side of endothelial cells back into the blood and out of the tumour cells (Declèves *et al.*, 2006; Mercer *et al.*, 2009; Robey *et al.*, 2010). Doxorubicin, for instance, is a very effective anticancer drug against glioblastoma cells *in vitro*, but since it is a substrate of Pgp/ABCB1, MRP1/ABCC1 and BCRP/ABCG2, its delivery across the BBB is hampered and it is ineffective clinically at treating this tumour.

The effects of a pegylated liposomal doxorubicin (Doxil or Caelyx) have recently been investigated in glioblastoma, but the results obtained are unconvincing (Glas *et al.*, 2007; Beier *et al.*, 2009; Ananda *et al.*, 2011). As alternative strategy, liposome-encapsulated drugs that have shown selective intratumour drug delivery, lower side effects and particular efficacy against aggressive and chemoresistant tumours (Jabr-Milane *et al.*, 2008; Riganti *et al.*, 2011), have been proposed as vehicles able to cross the BBB (through a diffusion process or a receptor-mediated endocytosis) and deliver their cargo into the CNS (Deelen and Loscher, 2007). Certain types of drug-containing nanoparticles adsorb apoB-100 and apo-E proteins from human low-density lipoprotein (LDLs; Kim *et al.*, 2007), are recognized by the LDL receptor and achieve an efficient drug delivery into brain parenchyma (Michaelis *et al.*, 2006; Nikanjam *et al.*, 2007) because both neurons and glial cells express LDL receptors (Ambruosi *et al.*, 2006).

In addition to increasing the delivery across the BBB, an 'ideal' chemotherapy for primary and metastatic tumours of CNS must simultaneously overcome the ABC transporters-dependent drug resistance of tumour cells. To meet these two requisites, in the present study we have investigated a nanoparticle-based approach – that is, the association of cholesterol-lowering drugs like statin plus a LDL receptor-targeting liposomal doxorubicin (termed 'apo-Lipodox'; Kopecka *et al.*, 2011).

Previous works from our group has shown that statins have chemosensitizing properties in epithelial tumours (Riganti *et al.*, 2005; Riganti *et al.*, 2006; Kopecka *et al.*, 2011). Moreover statins are reported to exert cytotoxic effects against CNS tumour cells (Bababeygy *et al.*, 2009; Yanae *et al.*, 2011). To our knowledge, no data exist on the effects of statins on the metabolism and permeability of BBB cells. In this study, we investigated whether the association of statin

with LDL receptor-targeted liposome-encapsulated doxorubicin simultaneously increases the drug permeability across the BBB and the cytotoxicity against CNS tumour cells, which would meet the two requisites of an optimal chemotherapy for brain tumours.

## Methods

### Chemicals

Plasticware for cell cultures was from Falcon (Becton Dickinson, Franklin Lakes, NJ, USA). Mevastatin, simvastatin, rhodamine 123 and Hoechst 33342 were purchased from Calbiochem (San Diego, CA, USA). Electrophoresis reagents were obtained from Bio-Rad Laboratories (Hercules, CA, USA); the protein content of cell monolayers and lysates was assessed with the BCA kit from Sigma Chemical Co (St. Louis, MO, USA). When not otherwise specified, all the other reagents were purchased from Sigma Chemical Co.

### Cell lines

The hCMEC/D3 cells, a human brain microvascular endothelial cell line, were cultured as previously described (Weksler *et al.*, 2005). Human glioblastoma U87-MG cells were cultured in DMEM medium, human neuroblastoma SKNP cells and human breast cancer MDA-MB-231 cells were grown in RPMI-1640 medium, human lung cancer A549 cells were grown in Ham's F12 medium. These cell lines (purchased from American Type Cells Collection) were maintained with 1% v v<sup>-1</sup> penicillin-streptomycin and 10% v v<sup>-1</sup> FBS, at 37°C and 5% CO<sub>2</sub> and were preliminarily characterized for the amount of Pgp, MRP1, BCRP and LDL receptor and for drug-resistance parameters (intracellular doxorubicin accumulation, extracellular release of lactate dehydrogenase, LDH) as reported below.

### Cholesterol and geranylgeranyl pyrophosphate de novo synthesis

Cells grown to confluence in 35-mm diameter Petri dishes, incubated as reported in the Results section, were labelled for 24 h with 1 µCi·mL<sup>-1</sup> [<sup>3</sup>H]-acetate (3600 mCi·mmol<sup>-1</sup>; Amer-sham Bioscience, Piscataway, NJ, USA), then washed and subjected to lipid extraction with the methanol/hexane method (Kopecka *et al.*, 2011). Samples were resuspended in 30 µL chloroform and separated by TLC, using 1:1 v v<sup>-1</sup> ether/hexane as the mobile phase. Solutions of 10 mg·mL<sup>-1</sup> cholesterol and 10 mg·mL<sup>-1</sup> geranylgeranyl pyrophosphate (GGPP) were used as standards. After exposure for 1 h to an iodine-saturated atmosphere, the migrated spots were cut out and their radioactivity was measured by liquid scintillation, using a Tri-Carb Liquid Scintillation Analyzer (PerkinElmer, Waltham, MA, USA). Cholesterol and GGPP synthesis were

expressed as pmol [ $^3\text{H}$ ]-cholesterol per  $10^6$  cells or [ $^3\text{H}$ ]-GGPP per  $10^6$  cells, according to the corresponding calibration curve.

### *Spectrophotometric measurement of membrane cholesterol*

Cells were rinsed with 0.5 mL PBS, sonicated on ice with two bursts of 10 s and centrifuged at  $100\,000\times g$  for 1 h at  $4^\circ\text{C}$ . The pellets (cell membrane fractions) were resuspended in 0.25 mL PBS and the cholesterol concentration was measured with an enzymatic colorimetric assay kit (OSR6516, Olympus System Reagent, Olympus Europe Holding GmbH, Hamburg, Germany), following the manufacturer's instructions. The absorbance was measured at 540/600 nm by an Olympus Analyzers spectrophotometer (Olympus Europe Holding GmbH).  $\beta$ -Methyl-cyclodextrin ( $10\text{ mmol}\cdot\text{L}^{-1}$  for 3 h) was used as a cholesterol chelator (Kopecka *et al.*, 2011). A 50  $\mu\text{L}$  aliquot was used to determine the protein content with the BCA kit. The results are expressed in  $\mu\text{g}$  cholesterol- $\text{mg}^{-1}$  membrane proteins, according to a previously prepared titration curve.

### *RhoA and RhoA kinase activity*

To evaluate RhoA activity, the GTP-bound fraction, taken as an index of monomeric G-proteins activation (Laufs and Liao, 2000), was measured using the G-LISA<sup>TM</sup> RhoA Activation Assay Biochem Kit (Cytoskeleton Inc, Denver, CO, USA), according to the manufacturer's instructions. Absorbance was read at 450 nm, using a Packard EL340 microplate reader (Bio-Tek Instruments, Winooski, VT, USA). For each set of experiments, a titration curve was prepared, using serial dilution of the Rho-GTP positive control of the kit. Data are expressed as absorbance units- $\text{mg}^{-1}$  cell proteins. RhoA kinase activity was measured using the CycLex Rho Kinase Assay Kit (CycLex Co, Nagano, Japan), following the manufacturer's instructions. The titration curve was prepared with serial dilutions of recombinant RhoA kinase (Rock2, MBL Inc, Woburn, MA, USA). Data are expressed as absorbance units- $\text{mg}^{-1}$  cell proteins.

### *NF- $\kappa\text{B}$ activity*

Nuclear proteins were extracted using the Nuclear Extract Kit (Active Motif, Rixensart, Belgium) and quantified. The activity of NF- $\kappa\text{B}$  was assessed by the TransAM<sup>TM</sup> Flexi NF $\kappa\text{B}$  Family kit (Active Motif), by adding 1 pmol of the biotinylated probe containing the NF- $\kappa\text{B}$  consensus site 5'-GGGACTTCC-3' to 10  $\mu\text{g}$  of nuclear extract proteins. The absorbance at 450 nm was measured with a Packard EL340 microplate reader (Bio-Tek Instruments). For each set of experiments, a blank was prepared with bi-distilled water, and its absorbance was subtracted from that obtained in the presence of nuclear extracts. Data are expressed as absorbance units- $\text{mg}^{-1}$  cell proteins.

### *NOS activity and nitrite measurement*

Cells were detached by trypsin/EDTA, resuspended in 0.3 mL of assay buffer ( $20\text{ mmol}\cdot\text{L}^{-1}$  HEPES,  $0.5\text{ mmol}\cdot\text{L}^{-1}$  EDTA, and  $1\text{ mmol}\cdot\text{L}^{-1}$  dithiothreitol DTT; pH 7.2) and sonicated. NOS (EC 1.14.13.49) activity was measured in 100  $\mu\text{g}$  of cell lysates with the Ultrasensitive Colorimetric Assay for Nitric Oxide Synthase kit (Oxford Biomedical Research, Oxford, MI, USA).

Results are expressed as  $\text{nmol nitrite}\cdot\text{min}^{-1}\cdot\text{mg}^{-1}$  cell proteins. Nitrite production was measured by adding 0.15 mL of cell culture medium to 0.15 mL of Griess reagent in a 96-well plate. After a 10 min incubation at  $37^\circ\text{C}$  in the dark, the absorbance was detected at 540 nm with a Packard EL340 microplate reader. A blank was prepared for each experiment in the absence of cells, and its absorbance was subtracted from that obtained in the presence of cells. Nitrite concentration was expressed as  $\text{nmol nitrite}\cdot\text{mg}^{-1}$  cell protein.

### *Western blot analysis*

Cells were rinsed with lysis buffer ( $50\text{ mmol}\cdot\text{L}^{-1}$  Tris,  $10\text{ mmol}\cdot\text{L}^{-1}$  EDTA, 1% v v<sup>-1</sup> Triton-X100), supplemented with the protease inhibitor cocktail set III ( $80\text{ }\mu\text{mol}\cdot\text{L}^{-1}$  aprotinin,  $5\text{ mmol}\cdot\text{L}^{-1}$  bestatin,  $1.5\text{ mmol}\cdot\text{L}^{-1}$  leupeptin,  $1\text{ mmol}\cdot\text{L}^{-1}$  pepstatin; Calbiochem),  $2\text{ mmol}\cdot\text{L}^{-1}$  phenylmethylsulfonyl fluoride (PMSF) and  $1\text{ mmol}\cdot\text{L}^{-1}$  sodium orthovanadate, then sonicated and centrifuged at  $13\,000\times g$  for 10 min at  $4^\circ\text{C}$ . Extracts of protein, 20  $\mu\text{g}$ , were subjected to SDS-PAGE and probed with the following antibodies: anti-phospho-Ser(176/180)-IKK $\alpha/\beta$  (Cell Signaling Technology Inc, Danvers, MA, USA), anti-IKK $\alpha/\beta$  (Santa Cruz Biotechnology Inc., Santa Cruz, CA, USA), anti-I $\kappa\text{B}$ - $\alpha$  (Santa Cruz Biotechnology Inc.), anti-neuronal NOS (nNOS/NOS I, Transduction Laboratories, Lexington, KY, USA), anti-inducible NOS (iNOS/NOS II, Transduction Laboratories), anti-endothelial NOS (eNOS/NOS III, Transduction Laboratories), anti-phospho-(Ser 1177) eNOS (Cell Signaling Technology Inc), anti-Pgp/ABCB1 (Santa Cruz Biotechnology Inc.), anti-MRP1/ABCC1 (Abcam, Cambridge, MA, USA), anti-BCRP/ABCG2 (Santa Cruz Biotechnology Inc.), anti-glyceraldehyde 3-phosphate dehydrogenase (GAPDH, Santa Cruz Biotechnology Inc.) This procedure was followed by exposure to a peroxidase-conjugated secondary antibody (Bio-Rad). The membranes were washed with Tris-buffered saline (TBS)-Tween 0.1% v v<sup>-1</sup>, and proteins were detected by enhanced chemiluminescence (PerkinElmer).

To assess the presence of nitrated proteins, the whole cell extract was immunoprecipitated with a rabbit polyclonal anti-nitrotyrosine antibody (Millipore, Billerica, MA, USA), using the PureProteome Protein A and Protein G Magnetic Beads (Millipore). Immunoprecipitated proteins were separated by SDS-PAGE and probed with anti-Pgp/ABCB1, anti-MRP1/ABCC1 or anti-BCRP/ABCG2 antibody. Whole cells lysates, 30  $\mu\text{g}$ , were probed with the same antibodies before the immunoprecipitation step to check the total amount of Pgp, MRP1 and BCRP.

### *ABC transporters activity*

To measure the ATPase activity of Pgp/ABCB1, MRP1/ABCC1 and BCRP/ABCG2, cells were lysed in buffer A ( $50\text{ mmol}\cdot\text{L}^{-1}$  HEPES,  $750\text{ mmol}\cdot\text{L}^{-1}$  KCl,  $200\text{ mmol}\cdot\text{L}^{-1}$  sucrose,  $10\text{ mmol}\cdot\text{L}^{-1}$  NaHCO<sub>3</sub>; pH 7.4), supplemented with protease inhibitor cocktail set III, centrifuged at  $13\,000\times g$  for 5 min, then at  $100\,000\times g$  for 1 h at  $4^\circ\text{C}$ . The pellet was resuspended in 1 mL buffer B ( $20\text{ mmol}\cdot\text{L}^{-1}$  HEPES,  $160\text{ mmol}\cdot\text{L}^{-1}$  KCl,  $1\text{ mmol}\cdot\text{L}^{-1}$  MgCl<sub>2</sub>,  $1\text{ mmol}\cdot\text{L}^{-1}$  CaCl<sub>2</sub>, 0.5% v v<sup>-1</sup> Triton X-100; pH 7.4). To obtain membrane fractions enriched in Pgp/ABCB1, MRP1/ABCC1 and BCRP/ABCG2, 100  $\mu\text{g}$  of membrane proteins were immunoprecipitated overnight with the

specific primary antibodies, then washed twice with 1 mL buffer B, supplemented with 2 mmol·L<sup>-1</sup> DTT; 50 µg of each sample were mixed with 2 mmol·L<sup>-1</sup> ATP, 2.5 mmol·L<sup>-1</sup> phosphoenolpyruvate, 7.5 U pyruvate kinase and 8.0 U LDH to check ATPase activity, as previously described (Doublier *et al.*, 2008). The reaction was started by adding 0.25 mmol·L<sup>-1</sup> NADH and was followed for 10 min, measuring the absorbance at 340 nm with a Packard EL340 microplate reader. The reaction kinetics was linear throughout the time of measurement. The NADH oxidation rate (expressed as µmol NADH oxidized·min<sup>-1</sup>·mg<sup>-1</sup> cell proteins) of each sample was subtracted from the oxidation obtained in the absence of immunoprecipitated proteins. The ATP hydrolysis rate was calculated stoichiometrically and ATPase activity was expressed as µmol ATP hydrolysed·min<sup>-1</sup>·mg<sup>-1</sup> cell proteins.

The efflux of rhodamine 123, taken as an index of Pgp/ABCBI and MRP1/ABCC1 activity, and the intracellular accumulation of Hoechst 33342, taken as an index of BCRP/ABCG2 activity, were measured as reported previously (Riganti *et al.*, 2011).

### LDL receptor expression

Total RNA was extracted and reverse transcribed using the QuantiTect Reverse Transcription Kit (Qiagen, Hilden, Germany). RT-PCR was carried out using IQ<sup>TM</sup> SYBR Green Supermix (Bio-Rad), according to the manufacturer's instructions. The same cDNA preparation was used for the quantification of *LDL receptor* and *GAPDH*, used as a housekeeping gene. The sequences of *LDL receptor* primers were 5'-TGAACTGGTGAGAGACCAC-3', 5'-TGTTCTTAAGCCGCCAGTTGTT-3'; the sequences of the *GAPDH* primers were 5'-TGGTCACCAGGGCTGCTT-3', 5'-AGCTTCCCCTTCTCAGCCTT-3'. The relative quantification of each sample was obtained by comparing the LDL receptor PCR product with the GAPDH PCR product, with the Bio-Rad Software Gene Expression Quantitation (Bio-Rad).

For flow cytometry detection of surface LDL receptors, cells were washed with PBS, detached with Cell Dissociation Solution (Sigma) and resuspended at 5 × 10<sup>5</sup> cells·mL<sup>-1</sup> in 1 mL RPMI medium containing 5% v v<sup>-1</sup> FBS. Samples were washed with 0.25% w v<sup>-1</sup> BSA-PBS, incubated with the primary antibody for LDL receptors (Abcam) for 45 min at 4°C, then washed twice and incubated with secondary FITC-conjugated antibody for 30 min at 4°C. After washing and fixation with paraformaldehyde 2% w v<sup>-1</sup>, the number of LDL receptors expressed on the surface was detected on 100 000 cells by a FACSCalibur system (Becton Dickinson), using the Cell Quest software (Becton Dickinson). Control experiments included incubation of cells with non-immune isotypic antibody, followed by the appropriate labelled secondary antibody.

### Synthesis of LDL receptor-targeted liposome-encapsulated doxorubicin

LDL receptor-targeted liposome-encapsulated doxorubicin was prepared using anionic pegylated liposomes (COATSOME EL-01-PA, NOF Corporation, Tokyo, Japan) of the following composition: 1,2 distearoyl-*sn*-3-glycero-3-phosphoethanolamine conjugated with polyethylene glycol (PEG), cholesterol, 1,2 dipalmitoyl-*sn*-glycero-3-

phosphocoline, 1,2 dipalmitoyl-*sn*-glycero-3-phosphoglycerol, at a molar ratio 4.2:11.4:15.2:11.4. For each preparation, 30 mg desiccated liposomes were incubated with 1.5 mmol·L<sup>-1</sup> doxorubicin in sterile aqueous solution, according to the manufacturer's instructions. The residual non-encapsulated drug was removed by gel filtration in a Sephadex G-50 (Amersham Bioscience) column. The amount of encapsulated doxorubicin was quantified by diluting 50 µL of liposomal suspension in 0.5 mL of 1:1 v v<sup>-1</sup> ethanol/HCl 0.3 N, sonicating the liposomes and measuring the fluorescence emitted by the drug with a LS-5 spectrofluorimeter (PerkinElmer). Excitation and emission wavelengths were 475 nm and 553 nm respectively. The encapsulation efficiency was calculated as described (Wong *et al.*, 2004). The liposomes with an encapsulation efficiency higher than 85% (termed 'Lipodox') were collected, stored at a doxorubicin concentration of 0.5 mmol·L<sup>-1</sup> and used to produce apoB100-conjugated doxorubicin-loaded liposomes (termed 'apo-Lipodox'). With this aim, the following recombinant peptide from human apoB100 was used: DWLKAFYDKVAEKLKEA-FRLTRKRGLKLA (LDL receptor-binding site is underlined; GenScript, Piscataway, NJ, USA). An aqueous solution of the peptide, 2.5 µmol·L<sup>-1</sup>, was added to liposomal doxorubicin, vortexed and incubated for 30 min at room temperature, with mild agitation. The unbound peptide was removed by dialysis as described previously (Nikanjam *et al.*, 2007). The amount of peptide attached to the liposomes was detected by the QuantiPro BCA Assay kit (Sigma).

To assess the role of PEG in the peptide attachment, anionic non-pegylated liposomes (COATSOME EL01A, NOF Corporation), with the following composition: 1,2 dipalmitoyl-*sn*-glycero-3-phosphocoline, cholesterol, 1,2 dipalmitoyl-*sn*-glycero-3-phosphoglycerol (molar ratio of 3:4:3), were used in control experiments. To investigate the effects of liposomal shell alone, empty anionic pegylated liposomes (COATSOME EL-01-PA series), conjugated or not with the LDL receptor-targeted peptide, were used.

The size of the liposomes was evaluated by dynamic light scattering: 10 µL of liposome suspension were diluted in 1 mL of 120 mmol·L<sup>-1</sup> NaCl solution and analysed with an ALV-NIBS dynamic light scattering instrument (Langen, Germany) provided with a Ne-He laser and an ALV-5000 multiple tau digital correlator. The scattered light intensity was recorded for 30 s on suspensions at 37°C. The hydrodynamic radius of liposomes was evaluated by using both the cumulant method and the CONTIN algorithm (Provencher, 1982). The mean radius of each liposomal preparation is presented in Table 1.

The morphological analysis of apo-Lipodox was performed on diluted samples (5 mg·mL<sup>-1</sup> liposomes in 120 mmol·L<sup>-1</sup> NaCl solution), using a Philips CM10 transmission electron microscope (TEM; Philips Amsterdam, The Netherlands), at an acceleration voltage of 80 kV. For each sample, a minimum of three microscopic fields was examined.

### Permeability coefficient across the BBB cells

The permeability to inulin, taken as a parameter of the integrity of the tight junctions (Monnaert *et al.*, 2004), was measured on hCMEC/D3 cells seeded at 50 000·cm<sup>-2</sup> and grown for 7 days up to confluence in 6-multiwell Transwell devices (0.4 µm diameter pores-size, Corning Life Sciences, Corning, NY, USA).

**Table 1**

Dynamic light scatter analysis of liposomes

Liposomes <sup>a</sup>	Acronym <sup>b</sup>	Doxorubicin	PEG	Peptide	Radius (mean ± SD)	P.I. <sup>c</sup>
COATSOME EL01A	–	Yes	No	Yes	70.05 nm ± 22.45 nm	0.187
COATSOME EL-01-PA	Lipodox	Yes	Yes	No	70.63 nm ± 28.55 nm	0.183
COATSOME EL-01-PA	apo-Lipodox	Yes	Yes	Yes	72.05 nm ± 23.14 nm	0.180
COATSOME EL-01-PA	EL	No	Yes	No	69.57 nm ± 27.35 nm	0.171
COATSOME EL-01-PA	apoEL	No	Yes	Yes	71.77 nm ± 18.71 nm	0.177

<sup>a</sup>Commercial name (NOF Corporation).<sup>b</sup>Acronyms used in text and figures.<sup>c</sup>Polydispersity Index.

France). Cells were incubated with or without mevastatin or simvastatin (0.1  $\mu\text{mol}\cdot\text{L}^{-1}$  for 24 h) or  $\beta$ -methyl-cyclodextrin (10  $\text{mmol}\cdot\text{L}^{-1}$  for 3 h), then the culture medium was replaced in the upper and lower chambers and 2  $\mu\text{Ci}\cdot\text{mL}^{-1}$  [ $^{14}\text{C}$ ]-inulin (10  $\text{mCi}\cdot\text{mmol}^{-1}$ ; PerkinElmer) was added to the upper chamber of Transwell. After 3 h, the medium in the lower chamber was collected and the amount of [ $^{14}\text{C}$ ]-inulin was measured using a Tri-Carb Liquid Scintillation Analyzer (PerkinElmer). Radioactivity was converted to  $\text{nmol inulin}\cdot\text{cm}^{-2}$ , using a calibration curve prepared previously.

For doxorubicin permeability, hCMEC/D3 cells seeded as reported above, were incubated with or without mevastatin or simvastatin (0.1  $\mu\text{mol}\cdot\text{L}^{-1}$  for 24 or 48 h). After this period, the culture medium was replaced in the upper and lower chambers and 5  $\mu\text{mol}\cdot\text{L}^{-1}$  doxorubicin or apo-Lipodox were added in the upper chamber of Transwell for 3 h, then the medium in lower chamber was collected and the amount of doxorubicin was measured fluorimetrically, using a LS-5 spectrofluorimeter (PerkinElmer). Excitation and emission wavelengths were 475 nm and 553 nm, respectively. Fluorescence was converted in  $\text{nmol doxorubicin}\cdot\text{cm}^{-2}$ , using a calibration curve previously set.

The permeability coefficients were calculated as described previously (Siflinger-Birnboim *et al.*, 1987).

### *Intratumour drug accumulation and toxicity in co-culture models*

The hCMEC/D3 cells (50 000  $\cdot\text{cm}^{-2}$ ) were grown for 7 days up to confluence in 6-multiwell Transwell devices (0.4  $\mu\text{m}$  diameter pores-size), whereas in the lower chamber, 500 000 cells (U87-MG, SJKNP, A549 or MDA-MB-231 cells) were seeded at day 4. At day 7, 0.1  $\mu\text{mol}\cdot\text{L}^{-1}$  simvastatin was added to the upper chamber medium for 48 h, when indicated. During the final 24 h, 5  $\mu\text{mol}\cdot\text{L}^{-1}$  doxorubicin or apo-Lipodox were added into the upper chamber of Transwell, then the inserts were removed and the extracellular medium of cells in the lower chamber was checked for the LDH activity, taken as an index of cytotoxicity and necrosis (Kopecka *et al.*, 2011). Cells in the lower chamber were detached, and divided into two aliquots of 250 000 cells each: the first aliquot was lysed in 0.5 mL ethanol/HCl 0.3 N (1:1 v v<sup>-1</sup>) and analysed for the intracellular content of doxorubicin, as reported above. Results are expressed as  $\text{nmol doxorubicin}\cdot\text{mg}^{-1}$  cell proteins. The second aliquot was lysed in 0.5 mL of caspase lysis buffer

(20  $\text{mmol}\cdot\text{L}^{-1}$  HEPES/KOH, 10  $\text{mmol}\cdot\text{L}^{-1}$  KCl, 1.5  $\text{mmol}\cdot\text{L}^{-1}$   $\text{MgCl}_2$ , 1  $\text{mmol}\cdot\text{L}^{-1}$  EGTA, 1  $\text{mmol}\cdot\text{L}^{-1}$  EDTA, 1  $\text{mmol}\cdot\text{L}^{-1}$  DTT, 1  $\text{mmol}\cdot\text{L}^{-1}$  PMSF, 10  $\mu\text{g}\cdot\text{mL}^{-1}$  leupeptin; pH 7.5). Then 20  $\mu\text{g}$  cell lysates were incubated for 1 h at 37°C with 20  $\mu\text{mol}\cdot\text{L}^{-1}$  of the fluorogenic substrate of caspase 3, DEVD-7-amino-4-methylcumarine (DEVD-AMC), in 0.25 mL caspase assay buffer (25  $\text{mmol}\cdot\text{L}^{-1}$  HEPES, 0.1% w v<sup>-1</sup> 3-[(3-cholamidopropyl) dimethylammonio] - 1 - propanesulfonate CHAPS, 10% w v<sup>-1</sup> sucrose, 10  $\text{mmol}\cdot\text{L}^{-1}$  DTT, 0.01% w v<sup>-1</sup> egg albumin; pH 7.5). The reaction was stopped by adding 0.75 mL ice-cold 0.1% w v<sup>-1</sup> trichloroacetic acid and the fluorescence of the AMC fragment released by active caspase-3 was read using a LS-5 spectrofluorimeter (PerkinElmer). Excitation and emission wavelengths were 380 nm and 460 nm respectively. Fluorescence was converted in  $\text{pmol}\cdot\mu\text{g}^{-1}$  cell protein using a calibration curve prepared previously with standard solutions of AMC.

For fluorescence microscope analysis, tumour cells in the lower chamber were seeded on sterile glass coverslips and treated as reported above. At the end of the incubation time, samples were rinsed with PBS, fixed with 4% w v<sup>-1</sup> paraformaldehyde for 15 min, washed three times with PBS and incubated with 4',6-diamidino-2-phenylindole dihydrochloride (DAPI) for 3 min at room temperature in the dark. Cells were washed three times with PBS and once with water, then the slides were mounted with 4  $\mu\text{L}$  of Gel Mount Aqueous Mounting and examined with a Leica DC100 fluorescence microscope (Leica Microsystems GmbH, Wetzlar, Germany). For each experimental point, a minimum of five microscopic fields were examined.

### *Statistical analysis*

All data in the text and figures are presented as means  $\pm$  SD. The results were analysed by a one-way ANOVA. A  $P < 0.05$  was considered significant.

## **Results**

### *Statins induce the synthesis of NO in human primary BBB cells by a RhoA/RhoA kinase/NF- $\kappa$ B-dependent mechanism*

As inhibitors of 3-hydroxy-3-methylglutaryl coenzyme A reductase enzyme, statins decrease the synthesis of cholesterol

and isoprenoids like farnesyl pyrophosphate and GGPP in mammalian cells (Liao and Laufs, 2005). We observed in solid tumours that a decrease in GGPP reduces the activity of small GTPase of the RhoA family, activates the NF- $\kappa$ B transcription factor and up-regulates the inducible NO synthase (*i*NOS/*NOS II*) gene (Riganti *et al.*, 2006; Riganti *et al.*, 2008). The human brain microvascular endothelial hCMEC/D3 cells were sensitive to both mevastatin and simvastatin, two lipophilic statins that reduced the endogenous synthesis of cholesterol and GGPP in a dose- and time-dependent manner (Figure 1A). The lowest concentration that significantly decreased cholesterol and GGPP level after 24 h was  $0.1 \mu\text{mol}\cdot\text{L}^{-1}$  and this was chosen for all the subsequent experiments. The cholesterol chelator  $\beta$ -methyl-cyclodextrin significantly depleted the cell membrane of cholesterol (Supporting information Figure S1A) and in parallel disrupted the integrity of the tight junctions in hCMEC/D3 cells, as demonstrated by the increased permeability coefficient of inulin (Supporting information Figure S1B). In the experimental conditions used in this study, mevastatin and simvastatin reduced the amount of cholesterol in the cell membrane by a lesser extent than  $\beta$ -methyl-cyclodextrin (Supporting information Figure S1A) and did not affect the permeability to inulin (Supporting information Figure S1B).

In keeping with the decrease in GGPP, the activity of the geranylgeranylated protein RhoA, measured as the amount of active GTP-bound protein, was reduced by both statins, resulting in a lower activation of the downstream effector RhoA kinase (Figure 1B). In parallel, the amount of IKK $\alpha$ / $\beta$  complex phosphorylated on serine 176/180, which was nearly undetectable in untreated hCMEC/D3 cells, was increased by mevastatin and simvastatin, without significant changes in the expression of IKK $\alpha$ / $\beta$  protein (Figure 1C). Such an increase was accompanied by a decrease in the inhibitory protein I $\kappa$ -B $\alpha$  (Figure 1C) and by the activation of NF- $\kappa$ B, measured as the ability of the transcription factor translocated into the nucleus to bind its specific target sequence (Figure 1D).

Differently from the constitutive NOS isoforms (neuronal NOS/NOS I and endothelial NOS/NOS III), the inducible *i*NOS/NOS II is usually absent in non-stimulated cells and is up-regulated by different stimuli, like cytokines and bacterial lipopolysaccharide that induce the activation of NF- $\kappa$ B (Pautz *et al.*, 2010). Statins increased the expression of NOS II; this was undetectable in untreated hCMEC/D3 cells (Figure 1E). The statins did not induce NOS I and did not change the expression of NOS III, but a slight increase in the amount of the active phospho-(Ser1177)-NOS III was detected following statins treatment (Figure 1E). As a consequence of these changes, the global enzymatic activity of NOS in cell lysates and the synthesis of NO, measured as the amount of the stable NO-derivative nitrite in culture supernatant, were significantly increased in hCMEC/D3 cells treated with mevastatin or simvastatin (Figure 1F).

### *Statins reduce the activity of Pgp and BCRP and increase the permeability of doxorubicin across the BBB cells by a NO-dependent mechanism*

hCMEC/D3 cells constitutively express several ABC transporters (Carl *et al.*, 2010), like Pgp/ABCB1, MRP1/ABCC1, BCRP/

ABCG2 (Figure 2A). The immunoprecipitation of membrane extracts with an anti-nitrotyrosine antibody, followed by the Western blot detection with the specific primary antibodies, revealed that mevastatin and simvastatin promoted a nitration on tyrosine of Pgp/ABCB1 and BCRP/ABCG2, similar to the one produced by the NO donor sodium nitroprusside (Figure 2A). Both these transporters also showed a low level of nitration in untreated cells, whereas no nitration was detectable on MRP1/ABCC1 in each experimental condition. In parallel the ATPase activity of Pgp/ABCB1 and BCRP/ABCG2, but not that MRP1/ABCC1, was decreased in the presence of the statins (Figure 2B), suggesting that the nitration probably impairs the catalytic cycle of the pumps. Indeed, the intracellular retention of rhodamine 123 (Figure 2C) that is inversely related to the activity of Pgp/ABCB1, and the intracellular retention of Hoechst 33342 (Figure 2D) that is inversely related to the activity of BCRP/ABCG2, were both increased by the statins. Although the tyrosine nitration and the decrease in ATPase activity in Pgp/ABCB1 and BCRP/ABCG2 were already detectable after 24 h of incubation with mevastatin or simvastatin (Figure 2A and B) and were not lost after 48 h (data not shown), the effects of these changes on the activity of Pgp/ABCB1 and BCRP/ABCG2 were stronger after 48 h (Figure 2C and D).

As doxorubicin is transported by Pgp/ABCB1, MRP1/ABCC1 and BCRP/ABCG2, its ability to cross the BBB cells is poor *in vivo*; also in hCMEC/D3 cells, the permeability coefficient was low (Figure 2E). However, the treatment with statins for 48 h significantly increased the permeability of the drug. The presence of the NO scavenger 2-phenyl-4,4,5,5-tetramethylimidazole-1-oxyl 3-oxide (PTIO) prevented the increase in permeability to doxorubicin (Figure 2E), suggesting that NO levels play a crucial role in regulating the activity of Pgp/ABCB1 and BCRP/ABCG2 in hCMEC/D3 cells.

### *The association of statins plus a LDL receptor-targeted liposome-encapsulated doxorubicin further increases the drug transport across BBB cells*

By lowering the *de novo* synthesis of cholesterol, statins force mammalian cells to expose the LDL receptor on their surface (Liao and Laufs, 2005). In hCMEC/D3 cells treated with mevastatin and simvastatin, the mRNA level for LDL receptors was significantly increased after 24 h (Figure 3A), a time point at which the synthesis of cholesterol was decreased (Figure 1A). The amount of LDL receptor protein on the cell surface was further increased by statins after 48 h (Figure 3B).

We have previously shown that anionic pegylated liposomes loaded with doxorubicin and conjugated with a synthetic peptide containing the LDL receptor-binding site from human apo-B100 (the so-called 'apo-Lipodox') was internalized efficiently via a LDL receptor-mediated endocytosis and was less extruded by Pgp/ABCB1 in solid tumour cells (Kopecka *et al.*, 2011). We thus applied apo-Lipodox that appeared as round-shaped particles with electron-dense areas due to the doxorubicin packed inside the liposomal shell (Figure 3C), to hCMEC/D3 cells untreated or treated with mevastatin and simvastatin for 48 h. In control cells, the permeability coefficient of apo-Lipodox was higher than that

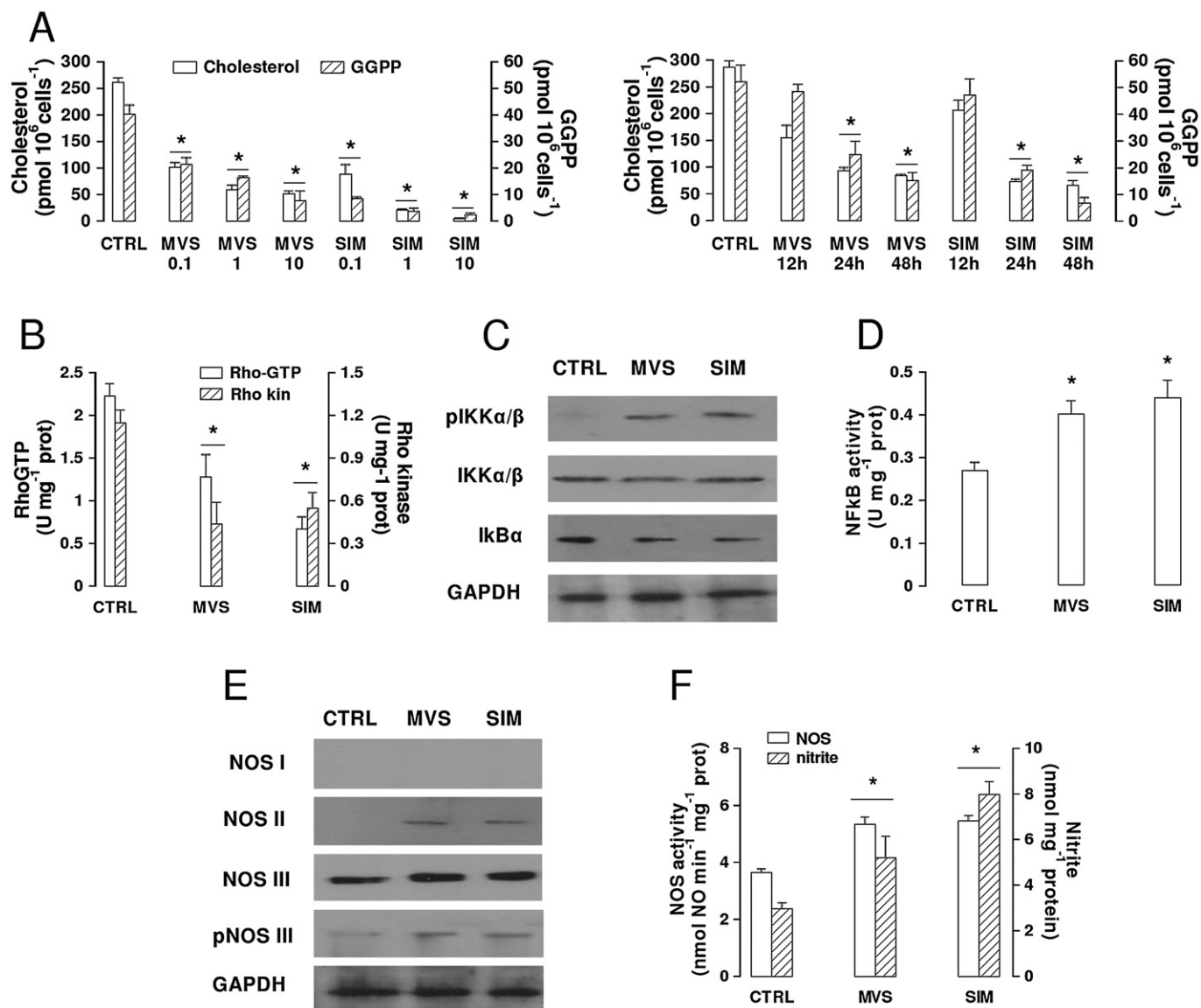


**Figure 1**

Effects of statins on cholesterol and GGPP synthesis, RhoA/RhoA kinase activity, NF- $\kappa$ B pathway and NO synthesis in BBB cells. (A) Cholesterol and GGPP synthesis. hCMEC/D3 cells were incubated in the absence (CTRL) or presence of different concentrations of 0.1, 1, 10  $\mu\text{mol}\cdot\text{L}^{-1}$  mevastatin (MVS) and simvastatin (SIM) for 24 h (left panel), or in the presence of 0.1  $\mu\text{mol}\cdot\text{L}^{-1}$  statin for 12, 24 or 48 h (right panel). In the subsequent 24 h, the cells were labelled with [ $^3\text{H}$ ]-acetate, then cholesterol (open columns) and GGPP (hatched columns) synthesis was measured as reported under Methods. Data are presented as means  $\pm$  SD ( $n = 3$ ). Versus CTRL:  $*P < 0.05$ . For the subsequent experiments, 0.1  $\mu\text{mol}\cdot\text{L}^{-1}$  MVS or SIM for 24 h was used. (B) RhoA/RhoA kinase activity. Samples were subjected to ELISA assays to measure the amount of RhoA-GTP (open bars) and the activity of RhoA kinase (hatched bars). The experiments were performed in duplicate, as described in the Methods section. Data are presented as means  $\pm$  SD ( $n = 3$ ). Versus CTRL:  $*P < 0.05$ . (C) Western blot detection of phospho-Ser(176/180)-IKK  $\alpha/\beta$ , IKK  $\alpha/\beta$  and I $\kappa$ B- $\alpha$  protein in extracts from hCMEC/D3 cells. The expression of GAPDH was used to check the equal protein loading. The figure is representative of three experiments with superimposable results. (D) NF- $\kappa$ B activity. The activity of NF- $\kappa$ B was detected in the nuclear extracts measuring the DNA-binding capacity of NF- $\kappa$ B on its target sequence (see Methods). Measurements were performed in duplicate and data are presented as means  $\pm$  SD ( $n = 3$ ). Versus CTRL:  $*P < 0.05$ . (E) Western blot detection of NOS isoforms (nNOS/NOS I; iNOS/NOS II; eNOS/NOS III) and of phospho-(Ser 1177)eNOS/NOS III protein in extracts from hCMEC/D3 cells. The expression of GAPDH was used to check the equal protein loading. The figure is representative of three experiments with superimposable results. (F) NO synthesis. NOS activity in cell lysates and nitrite accumulation in the extracellular medium were measured by use of spectrophotometric assays, as reported in Methods. Data are presented as means  $\pm$  SD ( $n = 3$ ). Versus CTRL:  $*P < 0.05$ .

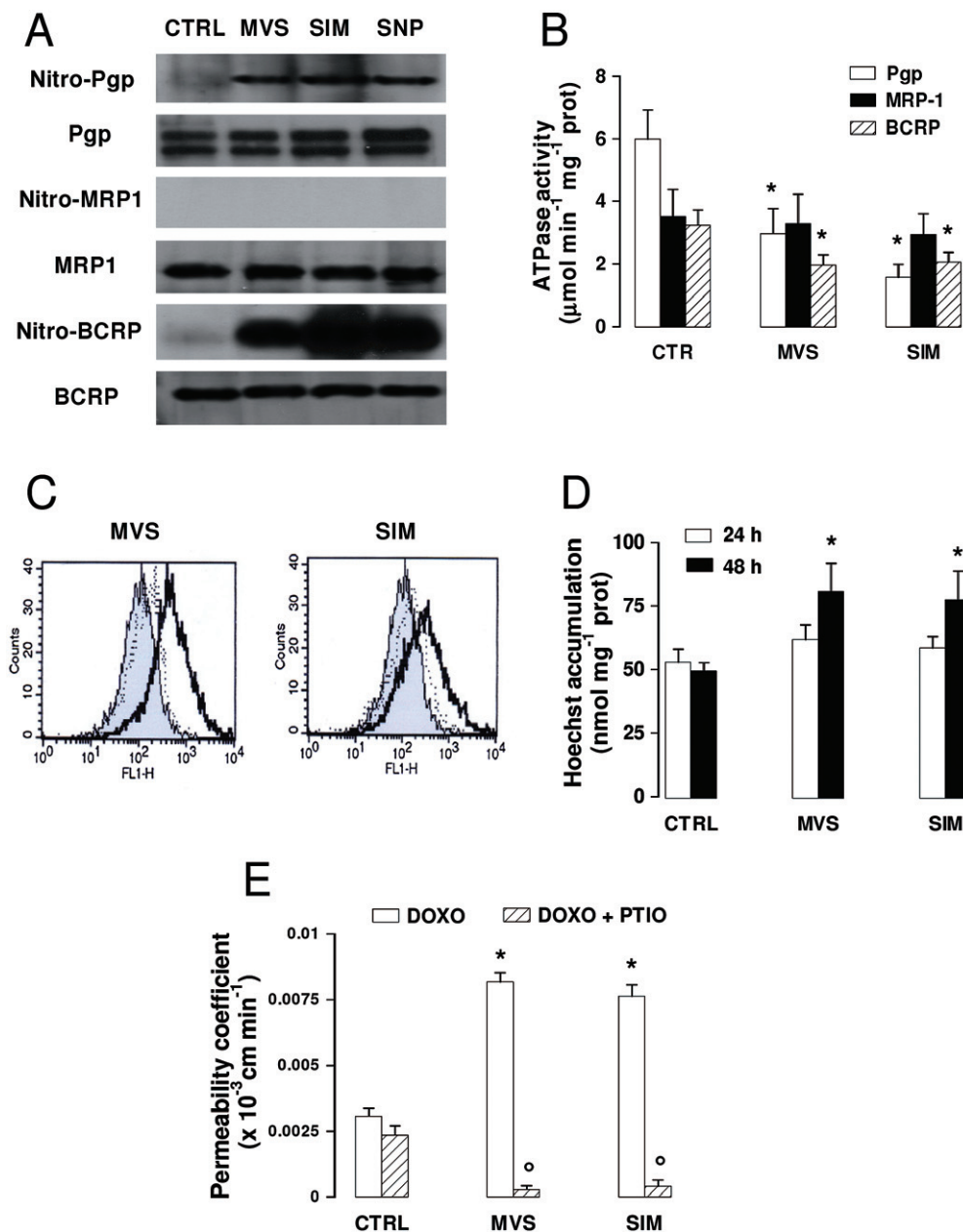


**Figure 2**

Effects of statins on ABC transporters activity and doxorubicin permeability across BBB cells. The hCMEC/D3 cells were incubated in the absence (CTRL) or presence of  $0.1 \mu\text{mol}\cdot\text{L}^{-1}$  mevastatin (MVS) or simvastatin (SIM) for 24 h or 48 h, then subjected to the following investigations. (A) Nitration of ABC transporters. After a 24 h incubation, cells were lysed and the whole cell extracts were immunoprecipitated with an anti-nitrotyrosine polyclonal antibody. The immunoprecipitated proteins were subjected to Western blotting, using an anti-Pgp, an anti-MRP1 or an anti-BCRP antibody (see Methods). The NO donor sodium nitroprusside ( $100 \mu\text{mol}\cdot\text{L}^{-1}$  for 24 h, SNP) was used as a positive control of nitration. The figure is representative of three experiments with similar results. (B) ATPase activity was measured spectrophotometrically after immunoprecipitation of Pgp, MRP1, BCRP from membrane fractions, as described in the Methods. Measurements were performed in duplicate and data are presented as means  $\pm$  SD ( $n = 3$ ). Versus CTRL: \* $P < 0.05$ . (C) Rhodamine assay. Cells were incubated for 20 min at  $37^\circ\text{C}$  with the fluorescent Pgp substrate rhodamine 123. The intracellular fluorescence was assessed by flow cytometry analysis in untreated cells (grey peak) and in cells treated with statins for 24 h (dotted line) or 48 h (continuous line). The figures shown here are representative of three similar experiments performed in duplicate. (D) Hoechst 33342 assay. Cells were incubated for 15 min at  $37^\circ\text{C}$  with Hoechst 33342, lysed and analysed fluorimetrically for the intracellular content of the dye. Measurements were performed in duplicate and data are presented as mean  $\pm$  SD ( $n = 3$ ). Versus CTRL: \* $P < 0.05$ . (E) Transport of doxorubicin across BBB monolayer. hCMEC/D3 cells were grown up to the confluence in Transwell insert, in fresh medium or in the presence of statins for 48 h, alone or co-incubated with the NO scavenger PTIO ( $100 \mu\text{mol}\cdot\text{L}^{-1}$ ).  $5 \mu\text{mol}\cdot\text{L}^{-1}$  doxorubicin was then added in the upper chamber. After 3 h, the medium was recovered by the lower chamber and the amount of doxorubicin was measured fluorimetrically. Measurements were performed in duplicate and data are presented as means  $\pm$  SD ( $n = 4$ ). Versus CTRL: \* $P < 0.05$ ; versus condition without PTIO: <sup>o</sup> $P < 0.001$ .

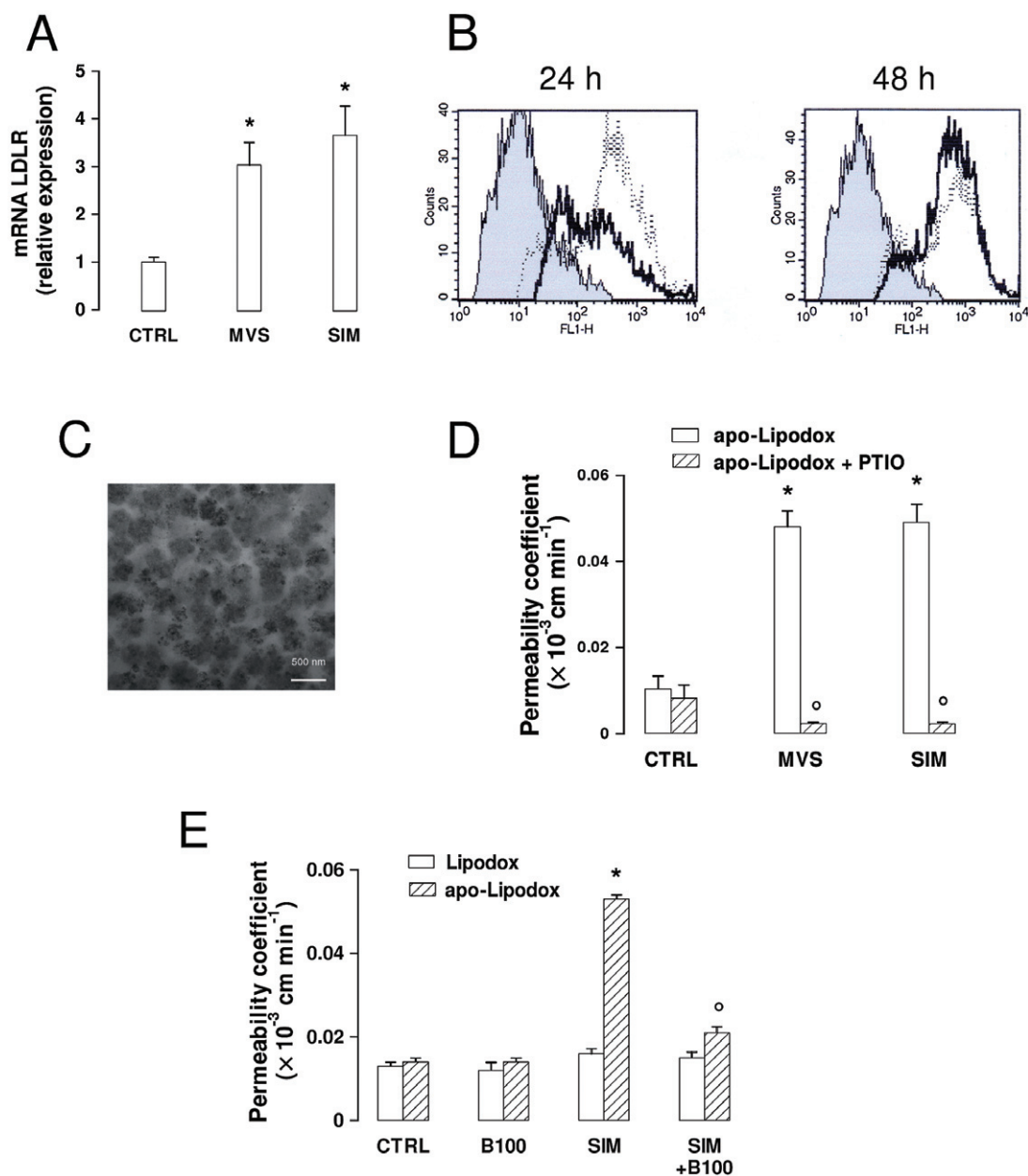


### Figure 3

Effects of statins on the expression of LDL receptors and on the permeability of LDL receptor-targeted liposomal doxorubicin across the BBB. The hCMEC/D3 cells were incubated in the absence (CTRL) or presence of  $0.1 \mu\text{mol}\cdot\text{L}^{-1}$  mevastatin (MVS) or simvastatin (SIM) for 24 h (A, B), 48 h (B, D and E), then subjected to the following investigations. (A) RT-PCR of LDL receptors. Total RNA was extracted, reverse transcribed and amplified by RT-PCR, as indicated in Methods. Measurements were performed in triplicate and data are presented as means  $\pm$  SD ( $n = 3$ ). Versus CTRL:  $*P < 0.005$ . (B) Flow cytometry analysis of surface LDL receptors in untreated cells (grey peak) or treated with MVS (continuous line) or SIM (dotted line) for 48 h. The figures shown here are representative of 3 similar experiments, performed in triplicate. (C) Apo-Lipodox imaging by TEM. The micrographs ( $28\ 500\times$  magnification) are representative of three similar experiments. (D) Transport of apo-Lipodox across the BBB monolayer. The hCMEC/D3 cells were grown to the confluence in Transwell insert, in fresh medium or in the presence of statins or of the NO scavenger PTIO ( $100 \mu\text{mol}\cdot\text{L}^{-1}$  for 48 h), then  $5 \mu\text{mol}\cdot\text{L}^{-1}$  apo-Lipodox was added in the upper chamber. After 3 h, the amount of the drug recovered by the lower chamber medium was measured fluorimetrically. Measurements were performed in duplicate and data are presented as means  $\pm$  SD ( $n = 4$ ). Versus CTRL:  $*P < 0.005$ ; versus condition without PTIO:  $^{\circ}P < 0.001$ . (E) Transport of Lipodox and apo-Lipodox across the BBB monolayer. The hCMEC/D3 cells were grown up to the confluence in Transwell insert, in fresh medium or in the presence of SIM, then  $5 \mu\text{mol}\cdot\text{L}^{-1}$  Lipodox or apo-Lipodox was added in the upper chamber. When indicated, the free LDL receptor-targeted apoB100 peptide (the same that was conjugated with apo-Lipodox), was co-incubated with the liposomes ( $100 \mu\text{mol}\cdot\text{L}^{-1}$ ; B100). After 3 h, the amount of doxorubicin recovered by the lower chamber medium was measured fluorimetrically. Measurements were performed in duplicate and data are presented as means  $\pm$  SD ( $n = 3$ ). Versus CTRL:  $*P < 0.005$ ; versus SIM:  $^{\circ}P < 0.05$ .

of free doxorubicin (see Figures 2E and 3D; comparing these data the significance of apo-Lipodox vs. doxorubicin was  $P < 0.005$ ). The transport of apo-Lipodox across the BBB monolayer was even higher than that of free doxorubicin in cells exposed to statins (Figures 2E and 3D; significance of apo-Lipodox vs. doxorubicin in statin-treated cells:  $P < 0.001$ ). Again, the addition of PTIO dramatically decreased the permeability of apo-Lipodox, suggesting that the NO levels – and the consequent status of nitration on ABC transporters – are also critical for the transport of apo-Lipodox in hCMEC/D3 cells.

In addition to the increased intracellular retention due to the inhibition of ABC transporters, we also investigated whether an increased uptake by LDL receptor-mediated endocytosis was critical in determining the greater permeability of apo-Lipodox. Apo-Lipodox exhibited a mean concentration of LDL receptor-targeted peptide of  $20 \pm 1.6 \mu\text{g}\cdot\mu\text{L}^{-1}$ , corresponding to about  $3 \times 10^{12}$  peptides $\cdot\mu\text{L}^{-1}$  ( $n = 3$ ).

The permeabilities of Lipodox (liposomal doxorubicin without the LDL receptor-targeted peptide) and apo-Lipodox were similar in untreated hCMEC/D3 cells and were unaffected by an excess of free LDL receptor-targeted peptide under basal conditions (Figure 3E). However, apo-Lipodox crossed the BBB monolayer at a significantly higher rate when cells were pre-incubated with simvastatin, which increased the amount of LDL receptors (Figure 3A and B); this transport was dramatically decreased by the competing free LDL receptor-targeted peptide (Figure 3E). In contrast, Lipodox permeability was the same in the presence of simvastatin or of the competing peptide (Figure 3E), suggesting that the uptake of non-targeted liposomes was not dependent on the LDL receptor-mediated endocytosis.

To assess whether the presence of PEG influences the attachment of the LDL receptor-targeted peptide to the liposomal shell and/or the binding to the LDL receptor, parallel experiments were performed with anionic non-pegylated liposomes. These particles did not significantly differ in their radius (Table 1) or in the amount of peptide attached ( $22 \pm 1.9 \mu\text{g}\cdot\mu\text{L}^{-1}$ ;  $n = 3$ ). The permeability of pegylated and non-pegylated apo-Lipodox was superimposable in both untreated and simvastatin-treated hCMEC/D3 cells (Supporting information Figure S2), suggesting that the presence of PEG did not interfere with the attachment of LDL receptor-targeted peptide or with the liposome uptake, either by simple endocytosis or LDL receptor-mediated endocytosis.

Empty liposomes may affect different intracellular pathways modulating the activity of Pgp/ABCB1 in epithelial cells (Riganti *et al.*, 2011). To clarify whether empty liposomes affected the activation of NF- $\kappa$ B, the synthesis of nitrite, the activity of NOS enzyme, the induction of necrosis or apoptosis, we measured these parameters (Supporting information Figure S3A–C) in hCMEC/D3 cells, exposed to the same empty anionic pegylated liposomes used for apo-Lipodox, conjugated or not with the LDL receptor-targeted peptide. None of the liposomal formulations modified the above parameters compared to the untreated cells. Furthermore, when we co-incubated free doxorubicin with empty liposomes, with or without the LDL receptor-targeted peptide, in hCMEC/D3 cells pretreated or not with simvastatin ( $0.1 \mu\text{mol}\cdot\text{L}^{-1}$  for 48 h), we did not detect a different permeability compared with free doxorubicin alone (Supporting

information Figure S3D). We thus excluded a permeabilizing effect exerted by the liposomal shell itself.

### *The association of statins plus LDL receptor-targeted liposome-encapsulated doxorubicin is effective at delivering doxorubicin into tumour cells co-cultured with BBB cells*

The abundance of ABC transporters on primary CNS tumours, on cerebral metastasis of epithelial solid tumours and on BBB cells determines a poor response to chemotherapy. To clarify if the association of statins and apo-Lipodox can overcome such resistance, we produced co-culture models by growing hCMEC/D3 cells on Transwell insert and tumour cells – that is, human glioblastoma multi-forme U87-MG cells, human neuroblastoma SJKNP cells, human invasive breast cancer MD-MBA-231 cells and human non-small cells lung cancer A549 cells – in the lower chamber.

A preliminary characterization of these cell lines showed that they all expressed at various levels Pgp/ABCB1, MRP1/ABCC1 and BCRP/ABCG2 (Figure 4A), and that simvastatin did not modify the amount of these transporters (Figure 4A) but increased the surface LDL receptors (Figure 4B). Whereas the intracellular content of free doxorubicin was low in all the cell lines (giving a fluorescence similar to the autofluorescence of untreated cells, Figure 4C) and not sufficient to elicit cytotoxicity (Figure 4C), apo-Lipodox was accumulated to higher extent, exerting significant cell damage, as revealed by the release of LDH in the culture supernatant. The addition of simvastatin to free doxorubicin enhanced the drug retention and the LDH release compared to doxorubicin alone. For all the cell lines, the maximal increase in these parameters was achieved by the combination of simvastatin plus apo-Lipodox (Figure 4C).

When added to the upper chamber of the Transwell containing confluent hCMEC/D3 cells on the insert and U87-MG in the lower chamber, doxorubicin poorly entered glioblastoma cells, as shown by the low red fluorescence in U87-MG cells recovered by the lower chamber (Figure 5A); the drug delivery into tumour cells was improved by pretreating BBB cells with simvastatin for 48 h followed by doxorubicin or apo-Lipodox in the last 24 h. The strongest fluorescent signal was achieved by the association of simvastatin (for 48 h) plus apo-Lipodox (in the last 24 h; Figure 5A).

Quantitative fluorimetric analysis of intratumour doxorubicin confirmed that the drug content was significantly higher when simvastatin was combined with apo-Lipodox rather than with doxorubicin in all the cell lines co-cultured with hCMEC/D3 cells (Figure 5B). In keeping with these results, doxorubicin alone did not exert any relevant cytotoxic effect in tumour cells, in terms of LDH release (Figure 5B) and caspase-3 activation (Figure 5C). The association of free doxorubicin plus statin or the use of apo-Lipodox, two experimental conditions that increased the intracellular amount of doxorubicin in the cell lines without a BBB monolayer (Figure 4C), were significantly less effective in the presence of BBB monolayer (Figure 5B), although apo-Lipodox increased the release of LDH in all the cell lines and induced the activation of caspase-3 in A549 and SJKNP cells (Figure 5C). Also in BBB-tumour cells co-cultures, the

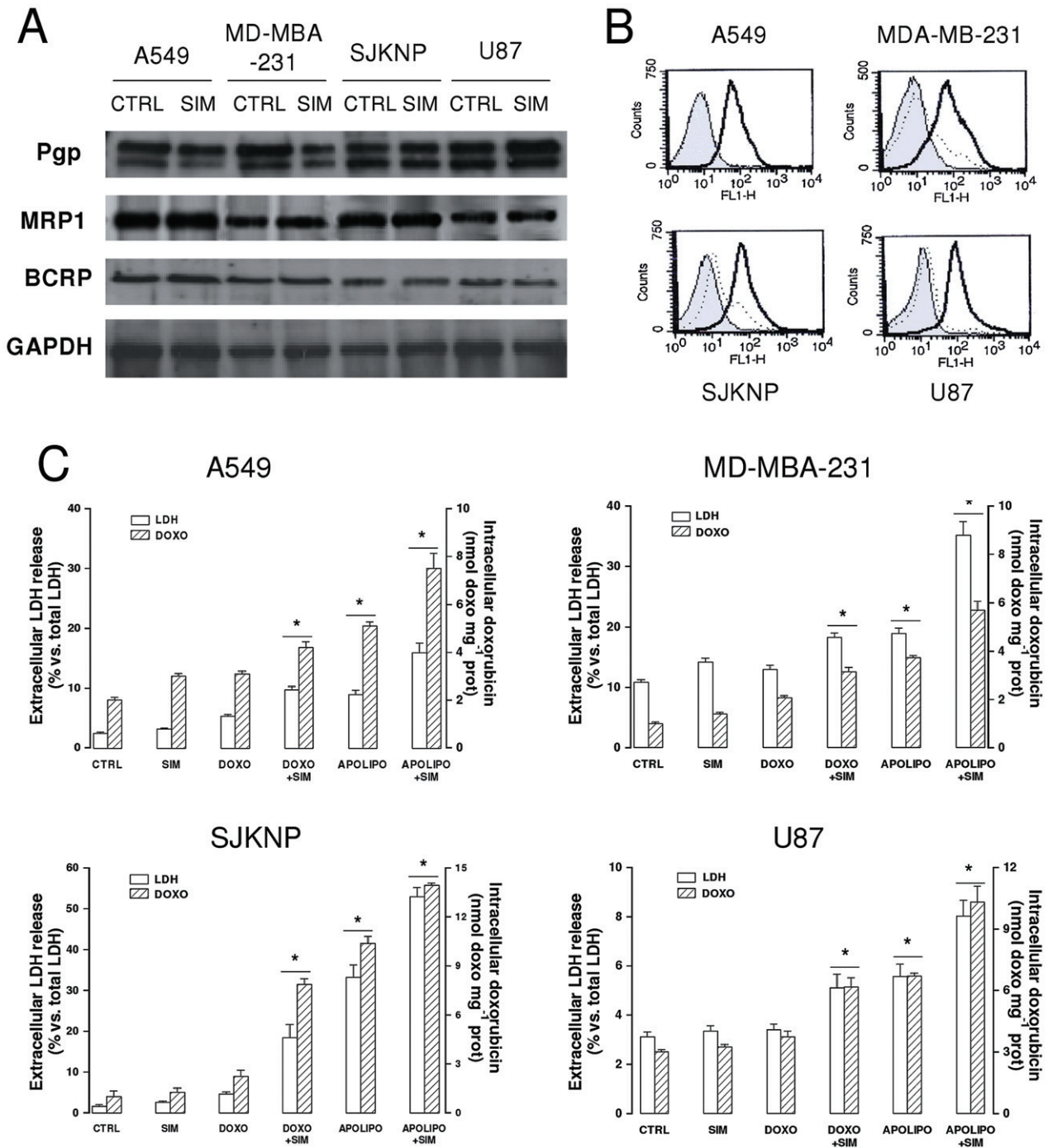


**Figure 4**

Characterization of different CNS- and non-CNS-derived tumour cells for ABC transporters expression, surface LDL receptors and resistance to doxorubicin. Human glioblastoma U87-MG cells, human neuroblastoma SJKNP cells, human breast cancer MDA-MB-231, human lung cancer A549 cells were grown in the absence (CTRL) or presence of simvastatin ( $0.1 \mu\text{mol}\cdot\text{L}^{-1}$  for 48 h; SIM). When indicated,  $5 \mu\text{mol}\cdot\text{L}^{-1}$  doxorubicin (DOXO) or apo-Lipodox (APOLIPO) were added in the last 24 h. (A) Western blot analysis of ABC transporters. The expression of Pgp, MRP1 and BCRP on whole cells extracts was detected by Western blotting. The expression of GAPDH was used to check the equal protein loading. The figure is representative of three experiments with superimposable results. (B) Flow cytometry analysis of surface LDL receptors in untreated cells (dotted line) or SIM-treated cells (continuous line). Negative controls, with non-immune isotypic antibodies, are represented by the grey peak. The figures shown here are representative of two similar experiments, each performed in duplicate. (C) Intracellular doxorubicin accumulation and toxicity. Culture supernatant was checked for the extracellular activity of LDH; cells were detached and lysed to quantify the intracellular amount of doxorubicin, as described in Methods. The hatched columns in the conditions 'CTRL' and 'SIM' refer to the cell autofluorescence, measured in the absence of doxorubicin or apo-Lipodox administration. Measurements were performed in duplicate and data are presented as means  $\pm$  SD ( $n = 3$ ). Versus CTRL: \* $P < 0.05$ .

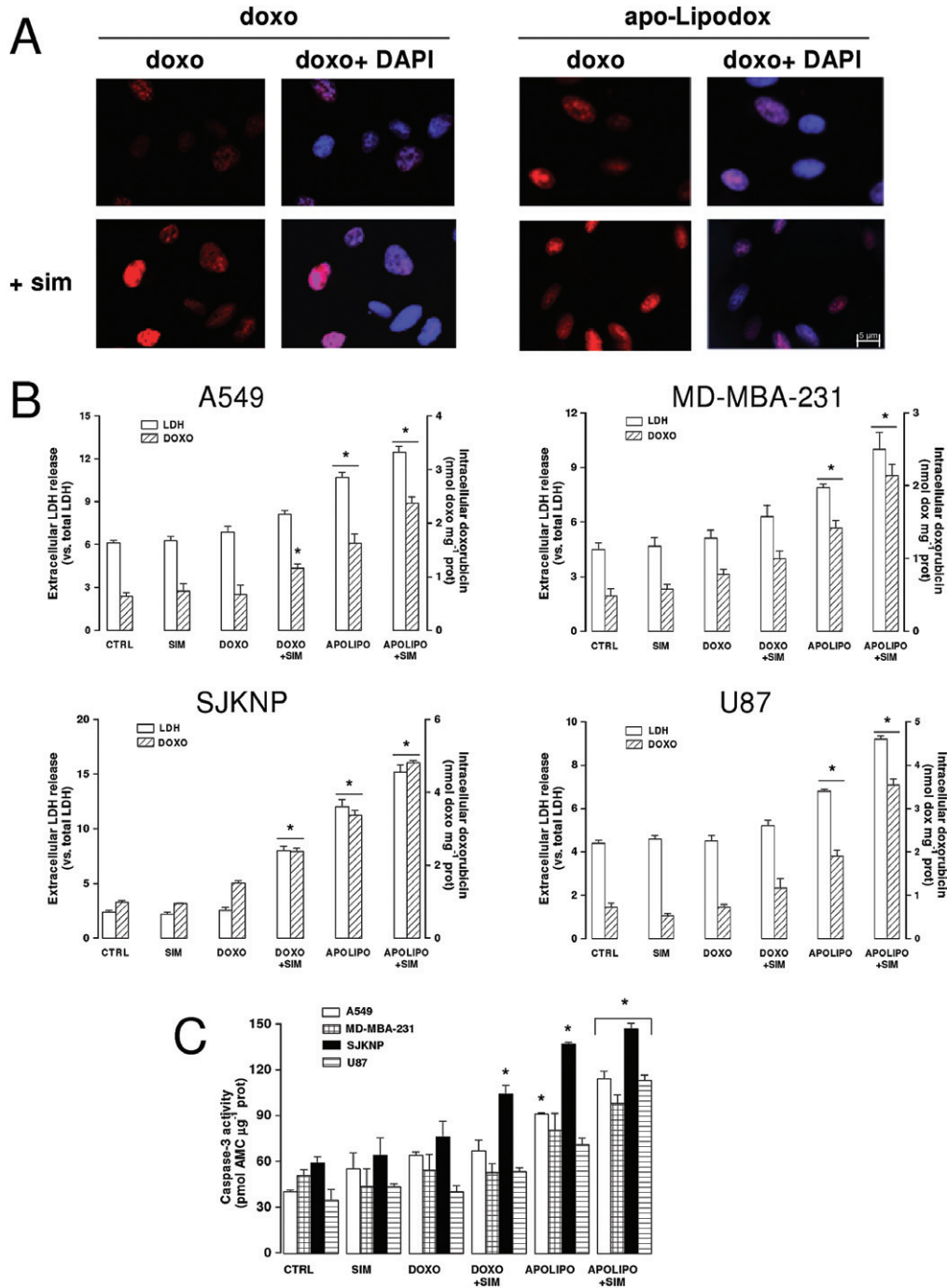


**Figure 5**

Drug delivery and antitumour efficacy of statins plus LDL receptor-targeted liposomal doxorubicin in co-culture models. The hCMEC/D3 cells were grown for 7 days up to confluence in Transwell inserts, whereas U87-MG, SJKNP, A549 or MDA-MB-231 cells were seeded at day 4 in the lower chamber. At day 0, supernatant in the upper chamber was replaced with fresh medium without (CTRL) or with simvastatin (0.1  $\mu\text{mol}\cdot\text{L}^{-1}$  for 48 h; SIM). 5  $\mu\text{mol}\cdot\text{L}^{-1}$  doxorubicin (DOXO) or apo-Lipodox (APOLIPO) were added in the upper chamber of Transwell in the last 24 h, then the following investigations were performed. (A) Microscope analysis of doxorubicin accumulation. U87-MG cells were seeded on sterile glass coverslips, treated as reported above, then analysed by fluorescence microscopy to detect the intracellular accumulation of doxorubicin. The cells were also counterstained with the nuclear fluorescent probe DAPI. The micrographs are representative of three experiments with similar results. (B) Culture supernatant of tumour cells was checked for the extracellular activity of LDH, cells were detached and lysed to quantify the intracellular amount of doxorubicin, as described in Methods. The hatched columns of the conditions 'CTRL' and 'SIM' refer to the cell autofluorescence, measured in the absence of doxorubicin or apo-Lipodox administration. Measurements were performed in duplicate and data are presented as means  $\pm$  SD ( $n = 4$ ). Versus CTRL:  $*P < 0.05$ . (C) Apoptosis induction. The activation of caspase-3 in tumour cells lysates was measured fluorimetrically as described in the Methods section. Measurements were performed in duplicate and data are presented as means  $\pm$  SD ( $n = 3$ ). Versus CTRL:  $*P < 0.05$ .

association of simvastatin plus apo-Lipodox was the most effective at achieving a significant delivery of doxorubicin (Figure 5B) and inducing cell death by both necrosis (Figure 5B) and apoptosis (Figure 5C). Free doxorubicin co-incubated with empty liposomes, with or without the LDL receptor-targeted peptide, did not accumulate within U87-MG cells more than doxorubicin alone, either in the absence or in the presence of simvastatin (Supporting information Figure S4A). Similarly, the death of glioblastoma cells, measured as release of LDH and activation of caspase-3, was not increased by the addition of free doxorubicin to empty liposomes (Supporting information Figure S4B).

## Discussion and conclusions

The therapeutic management of CNS tumours, currently based on surgery, radiotherapy and chemotherapy, is not completely safe and compatible with an acceptable quality of life. Chemotherapy is the first choice in disseminated tumours, such as invasive glioblastoma, high-risk medulloblastoma or multiple metastasis, but the percentage of success remains low. New targeted therapies, anti-angiogenic therapies or gene therapies show a real benefit only in limited groups of patients with known specific molecular defects (Sathornsumetee *et al.*, 2007; Rossi *et al.*, 2008). Thereby, the development of new pharmacological therapies for CNS tumours is still needed.

The low drug delivery across BBB and the low drug accumulation within the tumour are among the main factors that decrease the efficacy of chemotherapy in primary and metastatic brain tumours. In addition, having no fenestrations and many tight junctions, the brain microvascular endothelium has high levels of drug efflux pumps of the ABC transporter family (Declèves *et al.*, 2006; Mercer *et al.*, 2009; Robey *et al.*, 2010). The latter have also been identified in CNS tumours (Nakagawa *et al.*, 2009), where they contribute to the frequently observed chemoresistance. Therefore, an effective pharmacological therapy for CNS malignancies should overcome the extrusion of the drugs from both endothelial and tumour cells. In this perspective, we suggest a new combination approach, based on the association of statins plus LDL receptor-targeting liposomal drug, starting from two considerations: (i) both statins and liposomal drugs have chemosensitizer properties in solid tumours; (ii) liposomal drugs are delivered across the BBB more easily than free drugs.

We have previously observed that in cancer cells, statins increase the synthesis of NO, which inhibits ABC transporters efflux (Riganti *et al.*, 2005; Riganti *et al.*, 2006; Riganti *et al.*, 2008), and decrease the amount of membrane cholesterol, which also lowers the activity of Pgp/ABCB1 (Kopecka *et al.*, 2011).

In the past few years, statins have been proposed as drugs with potential benefits in cerebrovascular and neurodegenerative diseases, but to our knowledge, whether they have effects on the transport functions of brain microvascular endothelium has not been investigated. We found here that in human BBB cells, the lipophilic statins mevastatin and simvastatin decreased the synthesis of cholesterol and isoprenoids and reduced the amount of cholesterol in plasma membrane. This event has been previously linked to the loss of

integrity of tight junctions and to the increased paracellular leakage of drugs across the BBB monolayer (Monnaert *et al.*, 2004). In our work, we observed that a strong decrease in membrane cholesterol, caused by  $\beta$ -methyl-cyclodextrin, actually impaired the integrity of tight junctions in hCMEC/D3 cells, but the smaller variations of membrane cholesterol produced by statins did not. According to these data, it seems unlikely that statins – at least at the concentrations used in this study – increase the paracellular transport across BBB. At low (micromolar) concentrations, that is, in keeping with the  $K_i$  of statins for 3-hydroxy-3-methylglutaryl coenzyme A reductase (Liao and Laufs, 2005), mevastatin and simvastatin lowered the synthesis of isoprenoids in hCMEC/D3 cells and decreased the activity of RhoGTPase. In parallel, they increased the synthesis of NO, by up-regulating the IKK/NF- $\kappa$ B-mediated expression of iNOS/NOS II and by enhancing the phosphorylation on serine 1177 of eNOS/NOS III. The effects exerted by RhoA on NF- $\kappa$ B and NO synthesis are highly variable and depend on cell type (Nakata *et al.*, 2007; Ahn *et al.*, 2008; 32: Ye *et al.*, 2008). Lovastatin has been reported to inhibit RhoA, stimulate the activity of IKK- $\alpha$  and NF- $\kappa$ B and enhance the expression of iNOS in rat glioma cells (33: Rattan *et al.*, 2003); we hypothesize that such a mechanism occurs also in our model. It has been also shown that RhoA kinase reduces the stability of eNOS mRNA and prevents the Akt-dependent phosphorylation of eNOS (Rikitake and Liao, 2005). In accord with these observations, we detected an increased phosphorylation of eNOS in BBB cells treated with statins that inhibited RhoA kinase. This event, together with the up-regulation of iNOS isoform, led to a significant increase in NO levels and this suggests that this is the mechanism by which statins reduce the vascular tone and increase cerebral flow, as inhibitors of Rho kinase produce similar effects (Rikitake *et al.*, 2005).

A high blood flow usually ensures better delivery of anticancer drugs within tumour areas and better tumour oxygenation enhances the cytotoxicity of many anticancer drugs including doxorubicin. In addition to these theoretical benefits, the increased production of NO elicited by the statins reduced the activity of at least two proteins – Pgp/ABCB1 and BCRP/ABCG2 – that are involved in the apical extrusion of drugs in hCMEC/D3 cells (Tai *et al.*, 2009) and *in vivo* (Declèves *et al.*, 2006; Mercer *et al.*, 2009; Robey *et al.*, 2010).

Activators of endogenous NO synthesis, such as lipopolysaccharide, TNF- $\alpha$  and endothelin-1, as well as the NO donor SNP, are known to affect Pgp/ABCB1 in rat brain capillaries, producing a decrease in the transporter expression and activity after a 3 h incubation (Bauer *et al.*, 2007; Hartz *et al.*, 2007) followed by an increase at 6 h (Bauer *et al.*, 2007). Since the expression of Pgp/ABCB1 is subjected to rapid changes in BBB cells (Bauer *et al.*, 2007; Hawkins *et al.*, 2010), we cannot exclude the possibility that the NO synthesis induced by statins produces a decrease in Pgp/ABCB1 expression at earlier time points (e.g. less than 6 h), followed by a return to a 'steady state' at 24 h. Furthermore, the effects of NO are highly dependent on the species studied and on the amount and rate of NO released (Huerta *et al.*, 2008). This variability may explain some apparently contrasting findings, that is, a high concentration of exogenous NO for 6 h increased the expression of Pgp/ABCB1 in rat endothelial cells (Bauer *et al.*,

2007), whereas weak inducers of NOS II like statins did not produce any change of Pgp/ABCB1 expression in human hCMEC/D3 cells after 24 h (Figure 2A). Such low levels of endogenous NO, however, were sufficient to elicit a detectable nitration of the transporter, which decreased its activity. The reduction was even more pronounced after 48 h, indicating that statins induce a persistent inhibition of Pgp/ABCB1 activity after a longer time. As we considered the prolonged half-life of Pgp/ABCB1 in low-serum mediums (Zhang and Ling, 2000), the standard culture condition for hCMEC/D3 cells, we expected the reduction in activity of the ABC pumps to be higher at 48 h than at 24 h, although a clear nitration of the pump was already detectable after 24 h. The reversal of statins' effects by the NO scavenger PTIO suggests that the persistent inhibition of Pgp/ABCB1 and BCRP/ABCG2 activity was due to a continuous synthesis of NO by hCMEC/D3 cells.

Since in other models of BBB, the rate of drug efflux was NO independent (Salkeni *et al.*, 2009), we cannot exclude *a priori* that statins also reduce the activity of ABC transporters by other mechanisms, for example, by decreasing the Pgp/ABCB1 expression and glycosylation (Sieczkowski *et al.*, 2010) or by reducing the amount of cholesterol in the plasma membrane, an event that impairs the activity of Pgp/ABCB1 (Troost *et al.*, 2004; Kopecka *et al.*, 2011). Whatever the pleiotropic effects of statins on ABC transporters are, the final result of treating BBB cells with statins was a dramatic increase in the permeability of doxorubicin, a substrate of both Pgp/ABCB1 and BCRP/ABCG2.

In all mammalian cells, statins also up-regulate the transcription and surface exposure of LDL receptors, offering a flexible method of designing specific, nanoparticle-based targeted therapies. We have previously validated the efficacy of an engineered LDL receptor-targeted liposome-encapsulated doxorubicin ('apo-Lipodox') in solid tumours with high expression of LDL receptors (Kopecka *et al.*, 2011). Besides being taken up more by LDL receptor-driven endocytosis (Kopecka *et al.*, 2011), liposomal particles alter the lipid composition of the plasma membrane microdomains (i.e. lipid rafts) where Pgp/ABCB1 is active, interfere with ATP hydrolysis and substrate binding, and elicit a lower extrusion of doxorubicin in Pgp-overexpressing cells (Riganti *et al.*, 2011). In untreated hCMEC/D3 cells, the permeability for apo-Lipodox was significantly greater than that of free doxorubicin, probably as a consequence of the decreased efflux via Pgp/ABCB1 and of the increased uptake. Since both the non-LDL receptor-targeted Lipodox and the LDL receptor-targeted apo-Lipodox had a higher uptake than free doxorubicin in the absence of statins, it is likely that liposomes have a facilitated entry within BBB cells by simple endocytosis. The uptake of apo-Lipodox was unaffected by an excess of the free LDL receptor-binding apoB100 peptide under basal conditions, suggesting that the LDL receptors present on the surface of untreated hCMEC/D3 cells were too few to play a critical role in the liposome uptake. In contrast, the LDL receptor became a helpful tool to increase the endocytosis of targeted liposomes when its levels increased on the cells' surface, that is, after exposure to statins. Simvastatin, which forced BBB cells to expose more LDL receptors and simultaneously decreased the activity of Pgp/ABCB1, indeed enhanced the apo-Lipodox uptake and reduced the apical

efflux of doxorubicin, increasing the trans-cellular transport of the drug. Empty liposomal shells, which inhibited the activity of Pgp/ABCB1 in chemoresistant tumours (Riganti *et al.*, 2011), did not exert any permeabilizing activity on the delivery of doxorubicin across the BBB, suggesting that the effects of the lipidic envelope alone may be tissue-dependent.

We show here that simvastatin enhanced the number of LDL receptors exposed and induced chemosensitization in different human tumour (glioblastoma, neuroblastoma, non-small cell lung cancer, breast cancer) cells with constitutive expression of Pgp/ABCB1, MRP1/ABCC1 and BCRP/ABCG2 and different degrees of resistance to doxorubicin. Pretreatment of the tumour cells with simvastatin followed by the apo-Lipodox showed the greatest cytotoxic efficacy not only in primary CNS tumours like glioblastoma, but also in epithelial tumours, such as lung and breast cancers cells, whose metastasis within the CNS are often unresponsive to therapy. In co-culture models, the application of free doxorubicin on the luminal side of hCMEC/D3 monolayer did not yield any strong drug delivery into the tumour cells growing under the BBB. Apo-Lipodox alone or the combination of simvastatin plus free doxorubicin increased drug delivery and toxicity. However, the extent of this increase was variable, depending on the different levels and activity of ABC transporters and LDL receptors, and on the existence of other mechanisms of resistance characterizing each cell line. The presence of specific tumour cells on the basal side of hCMEC/D3 cells may also affect the permeability of the BBB differently, determining different rate and kinetics of drug delivery. Only the pretreatment of the co-cultures with simvastatin followed by apo-Lipodox elicited a clear increase in doxorubicin delivery and toxicity, consisting of both necrotic and apoptotic death, in all the models investigated, including the highly chemoresistant glioblastoma.

A direct anti-tumour activity of statins against glioblastoma cells has been reported previously (Bababeygy *et al.*, 2009; Yanae *et al.*, 2011): for instance, in rat C6 glioma cells, 5  $\mu\text{mol}\cdot\text{L}^{-1}$  mevastatin and simvastatin induced apoptosis by decreasing the intracellular availability of GGPP and the activation of ERK1/2 and Akt (Yanae *et al.*, 2011), suggesting that the effect could be mediated by a decrease in the activity of a geranylgeranylated protein. We did not detect direct cytotoxic effects of statins in co-cultured glioblastoma cells, perhaps because we used simvastatin at lower dose. It is noteworthy, however, that statins, at concentrations that are found in the blood of patients receiving anti-cholesterolemic therapy, enhanced the efficacy of a chemotherapeutic drug like doxorubicin against glioblastoma cells.

Phase I/II trials with pegylated liposomal doxorubicin have shown that the drug has very few side effects and is well tolerated, but does not offer a significant advantage in terms of overall survival or progression-free survival in comparison to the standard protocols based on radio-chemotherapy (Glas *et al.*, 2007; Beier *et al.*, 2009; Ananda *et al.*, 2011). For this reason, chemical modifications and improvements of drug-loaded nanoparticles are under intensive investigations (Michaelis *et al.*, 2006; Nikanjam *et al.*, 2007; Guo *et al.*, 2011; Wohlfart *et al.*, 2011). The approach proposed in our work differs from the other studies on CNS-penetrating nanoparticles because it is more 'physiological': it takes advantage of the usual metabolic effects of therapeutic doses of statins –

the increase in LDL receptors exposed and the synthesis of NO – and from the properties of liposomes, that induce permeability across the BBB and efficacy against drug-resistant tumours. We are currently testing this association in animal models bearing primary and metastatic CNS tumours, in order to determine the pharmacokinetic profile, the optimal administration regimen, the immunogenicity of apoLipodox, the antitumour effect and the presence of side effects. Testing our strategy in animals will add further important details about the molecular mechanisms of apo-Lipodox, inferred by these *in vitro* experiments, in order to validate the feasibility and efficacy of the association proposed.

The problem of poor permeability across the BBB is not limited to anticancer drugs, but also affects the delivery of agents used in epilepsy and neurodegenerative diseases. In a general perspective, our 'Trojan horse' approach, based on the administration of statins followed by a LDL receptor-targeting liposomal drug, might have potential applications in the pharmacological therapy of different CNS diseases.

## Acknowledgements

We thank Mr Costanzo Costamagna, Department of Genetics, Biology and Biochemistry, University of Turin, for the technical assistance and Mr Silvano Panero, Department of Vegetal Biology, University of Turin, for the help with the TEM analysis. We are grateful to Dr Marco Minella and Prof Claudio Minero, Department of Analytical Chemistry, University of Turin, for having provided the dynamic light scattering facility and for the valuable advices in the interpretation of the data. We are indebted with Prof Davide Schiffer, Neuro-Bio-Oncology Center, Vercelli, Italy, for the helpful discussion and the critical revision of the manuscript.

This work has been supported by grants from Compagnia di San Paolo, Italy (Neuroscience Program; grant 2008.1136) and Italian Association for Cancer Research (AIRC; MFAG 11475) to CR. M L P-D is a recipient of an ERACOL Erasmus Mundus fellowship.

## Conflict of in interest

None.

## References

Ahn KS, Sethi G, Chaturvedi MM, Aggarwal BB (2008). Simvastatin, 3-hydroxy-3-methylglutaryl coenzyme A reductase inhibitor, suppresses osteoclastogenesis induced by receptor activator of nuclear factor- $\kappa$ B ligand through modulation of NF- $\kappa$ B pathway. *Int J Cancer* 123: 1733–1740.

Ambrosio A, Khalansky AS, Yamamoto H, Gelperina SE, Begley DJ, Kreuter J (2006). Biodistribution of polysorbate 80-coated doxorubicin-loaded [14C]-poly(butyl cyanoacrylate) nanoparticles after intravenous administration to glioblastoma-bearing rats. *J Drug Target* 14: 97–105.

Ananda S, Nowak AK, Cher L, Dowling A, Brown C, Simes J *et al.* (2011). Phase 2 trial of temozolomide and pegylated liposomal doxorubicin in the treatment of patients with glioblastoma multiforme following concurrent radiotherapy and chemotherapy. *J Clin Neurosci* 18: 1444–1448.

Bababeygy SR, Polevaya NV, Youssef S, Sun A, Xiong A, Pruggichailers T *et al.* (2009). HMG-CoA reductase inhibition causes increased necrosis and apoptosis in an *in vivo* mouse glioblastoma multiforme model. *Anticancer Res* 29: 4901–4908.

Bauer B, Hartz AMS, Miller DS (2007). Tumor necrosis factor  $\alpha$  and endothelin-1 increase P-glycoprotein expression and transport activity at the blood-brain barrier. *Mol Pharmacol* 71: 667–675.

Beier CP, Schmid C, Gorlia T, Kleinletzenberger C, Beier D, Grauer O *et al.* (2009). RNOP-09: pegylated liposomal doxorubicine and prolonged temozolomide in addition to radiotherapy in newly diagnosed glioblastoma-a phase II study. *BMC Cancer* 9: 308–318.

Carl SM, Lindley DJ, Couraud PO, Weksler BB, Romero I, Mowery SA *et al.* (2010). ABC and SLC transporter expression and pot substrate characterization across the human CMEC/D3 blood-brain barrier cell line. *Mol Pharm* 7: 1057–1068.

Declèves X, Amiel A, Delattre JY, Scherrmann JM (2006). Role of ABC transporters in the chemoresistance of human gliomas. *Curr Cancer Drug Targets* 6: 433–445.

Deelen JF, Loscher W (2007). The blood-brain barrier and cancer: transporters, treatment, and Trojan horses. *Clin Cancer Res* 13: 1663–1674.

Doublier S, Riganti C, Voena C, Costamagna C, Aldieri E, Pescarmona G *et al.* (2008). RhoA silencing reverts the resistance to doxorubicin in human colon cancer cells. *Mol Cancer Res* 6: 1607–1620.

Glas M, Koch H, Hirschmann B, Jauch T, Steinbrecher A, Herrlinger U *et al.* (2007). Pegylated liposomal doxorubicin in recurrent malignant glioma: analysis of a case series. *Oncology* 72: 302–307.

Guo L, Fan L, Pang Z, Ren J, Ren Y, Li J *et al.* (2011). TRAIL and doxorubicin combination enhances anti-glioblastoma effect based on passive tumor targeting of liposomes. *J Control Release* 154: 93–102.

Hartz AMS, Bauer B, Fricker G, Miller DS (2007). Rapid modulation of P-glycoprotein-mediated transport at the blood-brain barrier by tumor necrosis factor- $\alpha$  and lipopolysaccharide. *Mol Pharmacol* 69: 462–470.

Hawkins BT, Sykes DB, Miller DS (2010). Rapid, reversible modulation of blood-brain barrier P-glycoprotein transport activity by vascular endothelial growth factor. *J Neurosci* 30: 1417–1425.

Huerta S, Chilka S, Bonavida B (2008). Nitric oxide donors: novel cancer therapeutics. *Int J Oncol* 33: 909–927.

Jabr-Milane LS, van Vlerken LE, Yadav S, Amiji MM (2008). Multi-functional nanocarriers to overcome tumour drug resistance. *Cancer Treat Rev* 34: 592–602.

Kim HR, Andrieux K, Gil S, Taverna M, Chacun H, Desmaele D *et al.* (2007). Translocation of poly(ethylene glycol-co-hexadecyl)cyanoacrylate nanoparticles into rat brain endothelial cells: role of apolipoproteins in receptor-mediated endocytosis. *Biomacromolecules* 8: 793–799.

Kopecka J, Campia I, Olivero P, Pescarmona G, Ghigo D, Bosia A *et al.* (2011). A LDL-masked liposomal-doxorubicin reverses drug resistance in human cancer cells. *J Control Release* 149: 196–205.

- Laufs U, Liao JK (2000). Targeting Rho in cardiovascular disease. *Circ Res* 87: 526–528.
- Liao K, Laufs U (2005). Pleiotropic effects of statins. *Annu Rev Pharmacol Toxicol* 45: 89–118.
- Mercer RW, Tyler MA, Ulasov IV, Maciej S (2009). Targeted therapies for malignant glioma. *BioDrugs* 23: 25–35.
- Michaelis K, Hoffmann MM, Dreis S, Herbert E, Alyautdin RN, Michaelis M *et al.* (2006). Covalent linkage of apolipoprotein E to albumin nanoparticles strongly enhances drug transport into the brain. *J Pharmacol Exp Ther* 317: 1246–1253.
- Monnaert V, Betbeder D, Fenart L, Bricout H, Lenfant AM, Landry C *et al.* (2004). Effects of  $\gamma$ - and hydroxypropyl- $\gamma$ -cyclodextrins on the transport of doxorubicin across an in vitro model of blood-brain barrier. *J Pharmacol Exp Ther* 311: 1115–1120.
- Nakagawa T, Ido K, Sakuma T, Takeuchi H, Sato K, Kubota T (2009). Prognostic significance of the immunohistochemical expression of O<sup>6</sup>-methylguanine-DNA methyltransferase, P-glycoprotein, and multidrug resistance protein-1 in glioblastomas. *Neuropathology* 29: 379–388.
- Nakata S, Tsutsui M, Shimokawa H, Yamashita T, Tanimoto A, Tasaki H *et al.* (2007). Statin treatment upregulates vascular neuronal nitric oxide synthase through Akt/NF- $\kappa$ B pathway. *Arterioscler Thromb Vasc Biol* 27: 92–98.
- Nikanjam M, Blakely EA, Bjornstad KA, Shu X, Budinger TF, Forte TM (2007). Synthetic nano-low density lipoprotein as targeted drug delivery vehicle for glioblastoma multiforme. *Int J Pharm* 328: 86–94.
- Pautz A, Art J, Hahn S, Nowag S, Voss C, Kleinert H (2010). Regulation of the expression of inducible nitric oxide synthase. *Nitric Oxide* 23: 75–93.
- Provencher SW (1982). A constrained regularization method for inverting data represented by linear algebraic or integral equations. *Comput Phys Commun* 27: 213–227.
- Rattan R, Giri S, Singh AK, Singh I (2003). RhoA negatively regulates cytokine-mediated inducible nitric oxide synthase expression in brain derived transformed cell lines: negative regulation of IKK $\alpha$ . *Free Radic Biol Med* 39: 1037–1050.
- Riganti C, Miraglia E, Viarisio D, Costamagna C, Pescarmona G, Ghigo D *et al.* (2005). Nitric oxide reverts the resistance to doxorubicin in human colon cancer cells by inhibiting the drug efflux. *Cancer Res* 65: 516–525.
- Riganti C, Orecchia S, Pescarmona G, Betta PG, Ghigo D, Bosia A (2006). Statins revert doxorubicin resistance via nitric oxide in malignant mesothelioma. *Int J Cancer* 119: 17–27.
- Riganti C, Doublier S, Costamagna C, Aldieri E, Pescarmona G, Ghigo D *et al.* (2008). Activation of nuclear factor-kappa B pathway by simvastatin and RhoA silencing increases doxorubicin cytotoxicity in human colon cancer HT29 cells. *Mol Pharmacol* 74: 476–484.
- Riganti C, Voena C, Kopecka J, Corsetto P, Montorfano G, Enrico E *et al.* (2011). Liposome-encapsulated doxorubicin reverses drug-resistance by inhibiting P-glycoprotein in human cancer cells. *Mol Pharm* 8: 683–700.
- Rikitake Y, Liao JK (2005). Rho GTPases, statins, and nitric oxide. *Circ Res* 97: 1232–1235.
- Rikitake Y, Kim HH, Huang Z, Seto M, Yano K, Asano T *et al.* (2005). Inhibition of Rho kinase (ROCK) leads to increased cerebral blood flow and stroke protection. *Stroke* 36: 2251–2257.
- Robey RW, Massey PR, Amiri-Kordestani L, Bates SE (2010). ABC transporters: unvalidated therapeutic targets in cancer and the CNS. *Anticancer Agents Med Chem* 10: 625–633.
- Rossi A, Caracciolo V, Russo G, Reiss K, Giordano A (2008). Medulloblastoma: from molecular pathology to therapy. *Clin Cancer Res* 14: 971–976.
- Salkeni MA, Lynch JL, Otamis-Price T, Banks WA (2009). Lipopolysaccharide impairs blood-brain barrier P-glycoprotein function in mice through prostaglandin- and nitric oxide-independent pathways. *J Neuroimmune Pharmacol* 4: 276–282.
- Sathornsumetee S, Reardon DA, Desjardins A, Quinn JA, Vredenburgh JJ, Rich JN (2007). Molecularly targeted therapy for malignant glioma. *Cancer* 110: 13–24.
- Sieczkowski E, Lehner C, Ambros PF, Hohenegger M (2010). Double impact on p-glycoprotein by statins enhances doxorubicin cytotoxicity in human neuroblastoma cells. *Int J Cancer* 126: 2025–2035.
- Siflinger-Birnboim A, Del Vecchio PJ, Cooper JA, Blumenstock FA, Shepard JM, Malik AB (1987). Molecular sieving characteristics of the cultured endothelial monolayer. *J Cell Physiol* 132: 111–117.
- Tai LM, Loughlin AJ, Male DK, Romero IA (2009). P-glycoprotein and breast cancer resistance protein restrict apical-to-basolateral permeability of human brain endothelium to amyloid- $\beta$ . *J Cereb Blood Flow Metab* 29: 1079–1083.
- Troost J, Lindenmaier H, Haefeli WE, Weiss J (2004). Modulation of cellular cholesterol alters P-glycoprotein activity in multidrug-resistant cells. *Mol Pharmacol* 66: 1329–1332.
- Weksler BB, Subileau EA, Perrière N, Charneau P, Holloway K, Leveque M *et al.* (2005). Blood-brain barrier-specific properties of a human adult brain endothelial cell line. *FASEB J* 19: 1872–1874.
- Wohlfart S, Khalansky AS, Gelperina S, Begley D, Kreuter J (2011). Kinetics of transport of doxorubicin bound to nanoparticles across the blood-brain barrier. *J Control Release* 154: 103–107.
- Wong HL, Bendayan R, Rauth AM, Wu XY (2004). Development of solid lipid nanoparticles containing ionically complexed chemotherapeutic drugs and chemosensitizers. *J Pharm Sci* 93: 1993–2008.
- Yanae M, Tsubaki M, Satou T, Itoh T, Imano M, Yamazoe Y *et al.* (2011). Statin-induced apoptosis via the suppression of ERK1/2 and Akt activation by inhibition of the geranylgeranyl-pyrophosphate biosynthesis in glioblastoma. *J Exp Clin Cancer Res* 30: 74–82.
- Ye Y, Martinez JD, Perez-Polo RJ, Lin Y, Uretsky BF, Birnbaum Y (2008). The role of eNOS, iNOS, and NF- $\kappa$ B in upregulation and activation of cyclooxygenase-2 and infarct size reduction by atorvastatin. *Am J Physiol Heart Circ Physiol* 295: H343–H351.
- Zhang W, Ling V (2000). Cell-cycle-dependent turnover of P-glycoprotein in multidrug-resistant cells. *J Cell Physiol* 184: 17–26.

## Supporting information

Additional Supporting Information may be found in the online version of this article:

**Figure S1** Effects of statins on membrane cholesterol and tight junctions integrity in hCMEC/D3 cells. (A) Cells were

incubated in the absence (CTRL) or presence of  $0.1 \mu\text{mol}\cdot\text{L}^{-1}$  mevastatin (MVS) or simvastatin (SIM) for 24 h or  $10 \text{mmol}\cdot\text{L}^{-1}$   $\beta$ -methyl cyclodextrin (MCD) for 3 h, then lysed and subjected to cell membranes isolation. The cholesterol content in membrane extracts was measured spectrophotometrically as described in the Methods section. Measurements were performed in duplicate and data are presented as means  $\pm$  SD ( $n = 3$ ). Vs CTRL:  $*P < 0.01$ . (B) Cells were seeded on Transwell insert, grown up to confluence for 7 days and incubated as reported in A;  $2 \mu\text{Ci}\cdot\text{mL}^{-1}$  [ $^{14}\text{C}$ ]-inulin was then added in the upper chamber. After 3 h the medium was recovered by the lower chamber and the amount of [ $^{14}\text{C}$ ]-inulin was measured by liquid scintillation. Measurements were performed in duplicate and data are presented as means  $\pm$  SD ( $n = 4$ ). Vs CTRL:  $*P < 0.05$ .

**Figure S2** Effects of pegylation on the permeability of LDL receptor-targeted liposomal doxorubicin across the BBB. Cells were grown up to the confluence for 7 days in Transwell insert, then incubated in the absence (CTRL) or presence of  $0.1 \mu\text{mol}\cdot\text{L}^{-1}$  simvastatin (SIM) for 48 h.  $5 \mu\text{mol}\cdot\text{L}^{-1}$  apo-Lipodox obtained from anionic non-pegylated liposomes (COATSOME EL01A series; - PEG) or from anionic pegylated liposomes (COATSOME EL-01-PA series; + PEG) was added in the upper chamber and after 3 h the amount of the drug recovered by the lower chamber medium was measured fluorimetrically. Measurements were performed in duplicate and data are presented as means  $\pm$  SD ( $n = 3$ ). Vs CTRL:  $*P < 0.005$ .

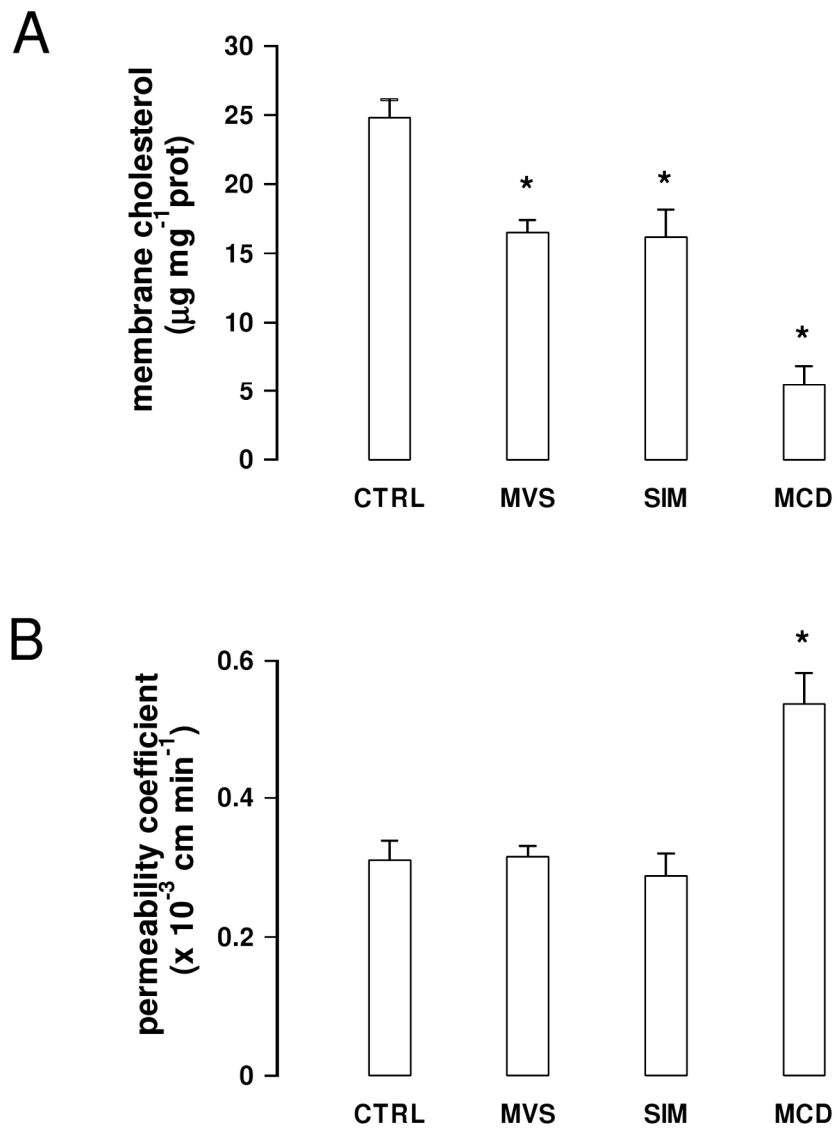
**Figure S3** Effects of empty liposomes on NF- $\kappa$ B activity, NO synthesis, cytotoxicity and permeability in hCMEC/D3 cells. The hCMEC/D3 cells were incubated in the absence (CTRL) or presence of  $5 \mu\text{mol}\cdot\text{L}^{-1}$  empty anionic pegylated liposomes (EL) or empty anionic pegylated LDL receptor-targeted conjugated-liposomes (apoEL) for 24 h, then subjected to the following investigations. (A) NF- $\kappa$ B activity. The activity of NF- $\kappa$ B was detected in the nuclear extracts measuring the DNA-binding capacity of NF- $\kappa$ B on its target sequence (see Methods). Measurements were performed in duplicate and data are presented as means  $\pm$  SD ( $n = 3$ ). (B) NO synthesis. NOS activity in cell lysates (open bars) and nitrite accumulation in the extracellular medium (hatched bars) were measured with spectrophotometric assays, as reported in the

Methods section. Data are presented as means  $\pm$  SD ( $n = 3$ ). (C) Cytotoxicity. Culture supernatant of cells was checked for the extracellular activity of LDH (open bars), cells were detached and lysed to measure the activity of caspase-3 (hatched bars), as described in the Methods section. Measurements were performed in duplicate and data are presented as means  $\pm$  SD ( $n = 3$ ). (D) Transport of doxorubicin across BBB monolayer in the presence of empty liposomes. The hCMEC/D3 cells were grown up to the confluence for 7 days in Transwell insert, in fresh medium or in the presence of simvastatin ( $5 \mu\text{mol}\cdot\text{L}^{-1}$  for 48 h; SIM); then  $5 \mu\text{mol}\cdot\text{L}^{-1}$  doxorubicin (DOXO), alone or co-incubated with  $5 \mu\text{mol}\cdot\text{L}^{-1}$  empty anionic pegylated liposomes (EL) or empty anionic pegylated LDL receptor-targeted conjugated-liposomes (apoEL), were added in the upper chamber. After 3 h the amount of the drug recovered by the lower chamber medium was measured fluorimetrically. Measurements were performed in duplicate and data are presented as means  $\pm$  SD ( $n = 3$ ). Vs the corresponding condition without SIM:  $*P < 0.005$ .

**Figure S4** Effects of empty liposomes on the delivery and cytotoxicity of free doxorubicin in co-culture models. The hCMEC/D3 cells were grown for 7 days up to confluence in Transwell inserts, whereas U87-MG cells were seeded at day 4 in the lower chamber. At day 0, supernatant in the upper chamber was replaced with fresh medium without (CTRL) or with simvastatin ( $0.1 \mu\text{mol}\cdot\text{L}^{-1}$  for 48 h; SIM).  $5 \mu\text{mol}\cdot\text{L}^{-1}$  doxorubicin (DOXO), alone or co-incubated with  $5 \mu\text{mol}\cdot\text{L}^{-1}$  empty anionic pegylated liposomes (EL) or empty anionic pegylated LDL receptor-targeted conjugated-liposomes (apoEL), were added in the upper chamber of Transwell in the last 24 h, then the following investigations were performed. (A) U87-MG cells were lysed in ethanol/HCl and the intracellular amount of doxorubicin was measured fluorimetrically (see Methods section). Measurements were performed in duplicate and data are presented as means  $\pm$  SD ( $n = 3$ ). (B) The culture supernatant of tumor cells was checked for the extracellular activity of LDH (open bars), cells were detached and lysed to measure the activity of caspase-3 (hatched bars), as described in the Methods section. Measurements were performed in duplicate and data are presented as means  $\pm$  SD ( $n = 3$ ).

**Supporting Information**

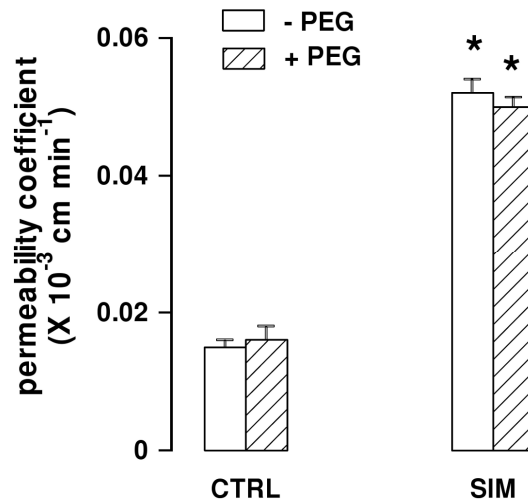
**Supporting Figure 1**



**Supporting Figure 1. Effects of statins on membrane cholesterol and tight junctions integrity in hCMEC/D3 cells.**

**A.** Cells were incubated in the absence (CTRL) or presence of  $0.1 \mu\text{mol L}^{-1}$  mevastatin (MVS) or simvastatin (SIM) for 24 h or  $10 \text{mmol L}^{-1}$   $\beta$ -methyl cyclodextrin (MCD) for 3 h, then lysed and subjected to cell membranes isolation. The cholesterol content in membrane extracts was measured spectrophotometrically as described in the Methods section. Measurements were performed in duplicate and data are presented as means  $\pm$  SD ( $n = 3$ ). Vs CTRL: \*  $p < 0.01$ . **B.** Cells were seeded on Transwell insert, grown up to confluence for 7 days and incubated as reported in **A**;  $2 \mu\text{Ci mL}^{-1}$  [ $^{14}\text{C}$ ]-inulin was then added in the upper chamber. After 3 h the medium was recovered by the lower chamber and the amount of [ $^{14}\text{C}$ ]-inulin was measured by liquid scintillation. Measurements were performed in duplicate and data are presented as means  $\pm$  SD ( $n = 4$ ). Vs CTRL: \*  $p < 0.05$ .

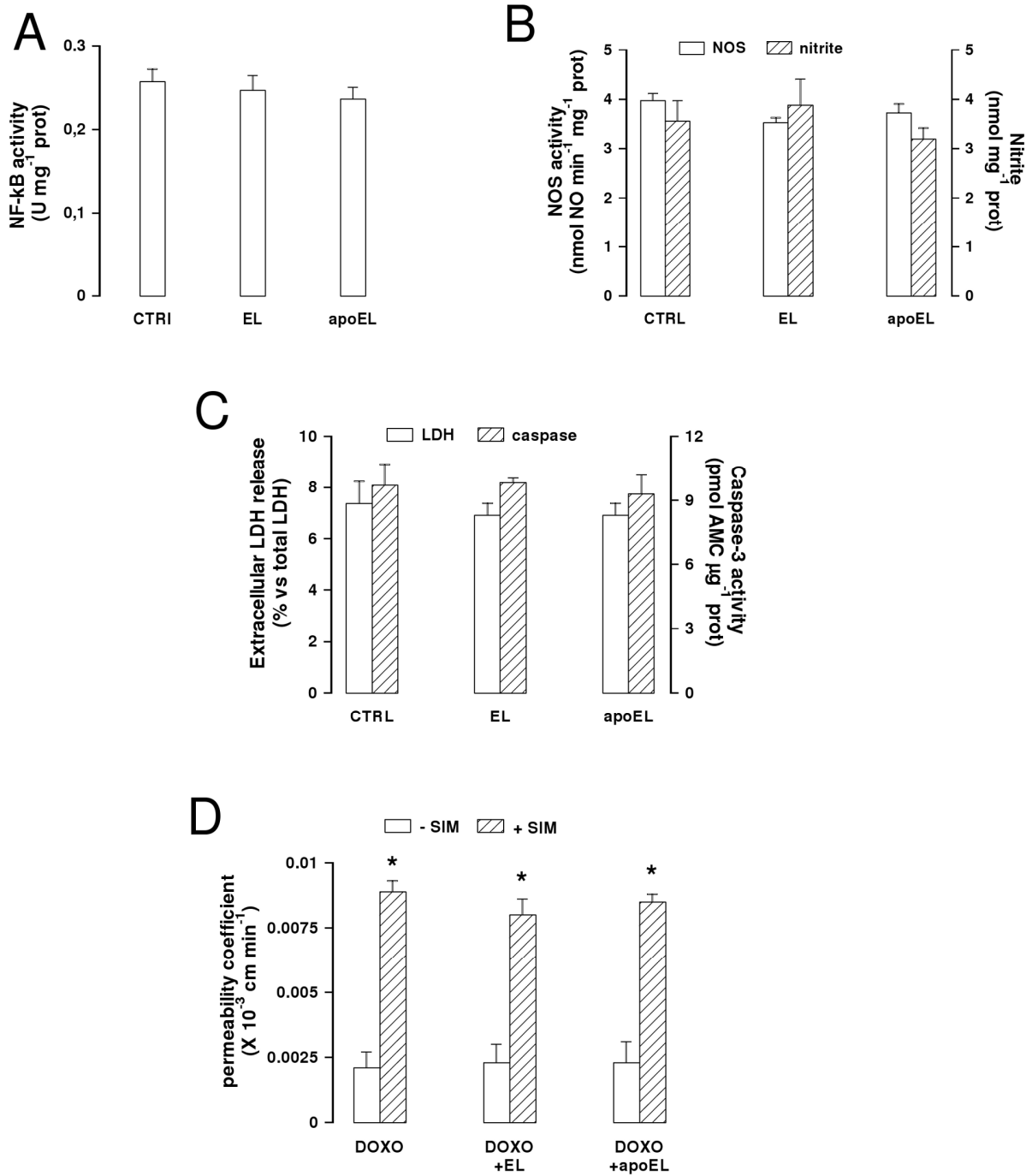
## Supporting Figure 2



### Supporting Figure 2. Effects of pegylation on the permeability of LDLR-targeted liposomal doxorubicin across the BBB.

Cells were grown up to the confluence for 7 days in Transwell insert, then incubated in the absence (CTRL) or presence of  $0.1 \mu\text{mol L}^{-1}$  simvastatin (SIM) for 48 h.  $5 \mu\text{mol L}^{-1}$  apo-Lipodox obtained from anionic non-pegylated liposomes (COATSOME EL01A series; - PEG) or from anionic pegylated liposomes (COATSOME EL-01-PA series; + PEG) was added in the upper chamber and after 3 h the amount of the drug recovered by the lower chamber medium was measured fluorimetrically. Measurements were performed in duplicate and data are presented as means  $\pm$  SD (n = 3). Vs CTRL: \* p < 0.005.

### Supporting Figure 3

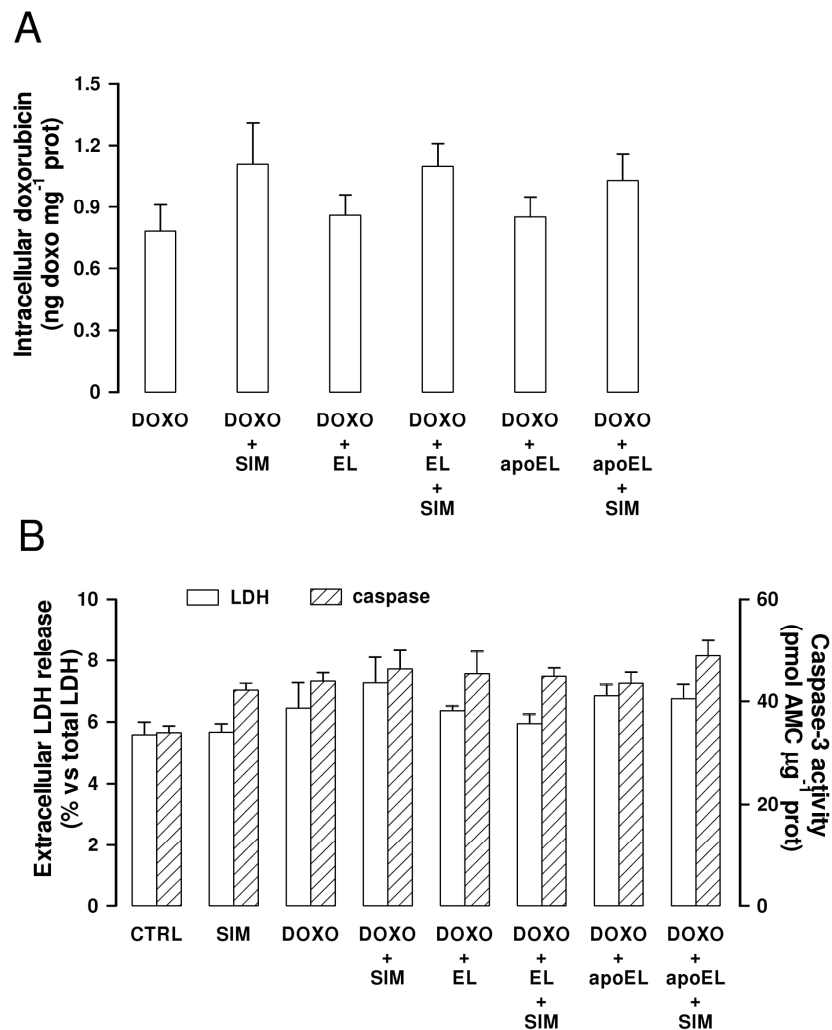


**Supporting Figure 3. Effects of empty liposomes on NF- $\kappa$ B activity, NO synthesis, cytotoxicity and permeability in hCMEC/D3 cells.**

The hCMEC/D3 cells were incubated in the absence (CTRL) or presence of  $5 \mu\text{mol L}^{-1}$  empty anionic pegylated liposomes (EL) or empty anionic pegylated LDLR-targeted conjugated-liposomes (apoEL) for 24 h, then subjected to the following investigations.

**A. NF- $\kappa$ B activity.** The activity of NF- $\kappa$ B was detected in the nuclear extracts measuring the DNA-binding capacity of NF- $\kappa$ B on its target sequence (see Methods). Measurements were performed in duplicate and data are presented as means  $\pm$  SD ( $n = 3$ ). **B. NO synthesis.** NOS activity in cell lysates (open bars) and nitrite accumulation in the extracellular medium (hatched bars) were measured with spectrophotometric assays, as reported in the Methods section. Data are presented as means  $\pm$  SD ( $n = 3$ ). **C. Cytotoxicity.** Culture supernatant of tumor cells was checked for the extracellular activity of LDH (open bars), cells were detached and lysed to measure the activity of caspase-3 (hatched bars), as described in the Methods section. Measurements were performed in duplicate and data are presented as means  $\pm$  SD ( $n = 3$ ). **D. Transport of doxorubicin across BBB monolayer in the presence of empty liposomes.** The hCMEC/D3 cells were grown up to the confluence for 7 days in Transwell insert, in fresh medium or in the presence of simvastatin ( $5 \mu\text{mol L}^{-1}$  for 48 h; SIM); then  $5 \mu\text{mol L}^{-1}$  doxorubicin (DOXO), alone or co-incubated with  $5 \mu\text{mol L}^{-1}$  empty anionic pegylated liposomes (EL) or empty anionic pegylated LDLR-targeted conjugated-liposomes (apoEL), were added in the upper chamber. After 3 h the amount of the drug recovered by the lower chamber medium was measured fluorimetrically. Measurements were performed in duplicate and data are presented as means  $\pm$  SD ( $n = 3$ ). Vs the corresponding condition without SIM: \*  $p < 0.005$ .

## Supporting Figure 4



### Supporting Figure 4. Effects of empty liposomes on the delivery and cytotoxicity of free doxorubicin in co-culture models.

The hCMEC/D3 cells were grown for 7 days up to confluence in Transwell inserts, whereas U87-MG cells were seeded at day 4 in the lower chamber. At day 0, supernatant in the upper chamber was replaced with fresh medium without (CTRL) or with simvastatin ( $0.1 \mu\text{mol L}^{-1}$  for 48 h; SIM),  $5 \mu\text{mol L}^{-1}$  doxorubicin (DOXO), alone or co-incubated with  $5 \mu\text{mol L}^{-1}$  empty anionic pegylated liposomes (EL) or empty anionic pegylated LDLR-targeted conjugated-liposomes (apoEL), were

added in the upper chamber of Transwell in the last 24 hours, then the following investigations were performed.

**A.** U87-MG cells were lysed in ethanol/HCl and the intracellular amount of doxorubicin was measured fluorimetrically (see Methods section). Measurements were performed in duplicate and data are presented as means  $\pm$  SD (n= 3). **B.** The culture supernatant of tumor cells was checked for the extracellular activity of LDH (open bars), cells were detached and lysed to measure the activity of caspase-3 (hatched bars), as described in the Methods section. Measurements were performed in duplicate and data are presented as means  $\pm$  SD (n = 3).

# Nanoparticle- and Liposome-carried Drugs: New Strategies for Active Targeting and Drug Delivery Across Blood-brain Barrier

Martha Leonor Pinzón-Daza<sup>1,2</sup>, Ivana Campia<sup>1</sup>, Joanna Kopecka<sup>1</sup>, Ruth Garzón<sup>2</sup>, Dario Ghigo<sup>1,3</sup> and Chiara Riganti<sup>1,3,\*</sup>

<sup>1</sup>Department of Oncology, University of Turin, Turin, Italy; <sup>2</sup>Unidad de Bioquímica, Facultad de Ciencias Naturales y Matemáticas, Universidad del Rosario, Bogotá, Colombia; <sup>3</sup>Center for Experimental Research and Medical Studies, University of Turin, Turin, Italy

**Abstract:** The blood-brain barrier (BBB), the unusual microvascular endothelial interface between the central nervous system (CNS) and the circulatory system, is a major hindrance to drug delivery in the brain parenchyma. Besides the absence of fenestrations and the abundance of tight junctions, ATP-binding cassette (ABC) transporters critically reduce drug entry within the CNS, as they carry many drugs back into the bloodstream. Nanoparticle- and liposome-carried drugs, because of their increased cellular uptake and reduced efflux through ABC transporters, have been developed in recent times to circumvent the low drug permeability of the BBB.

This review discusses the role of ABC transporters in controlling drug penetration into the brain parenchyma, the rationale for using nanoparticle- and liposome-based strategies to increase drug delivery across the BBB and new therapeutic strategies for using nanoparticle- and liposome-carried drugs in different conditions, ranging from CNS tumors and neurodegenerative diseases to viral infections and epilepsy.

**Keywords:** ATP-binding cassette transporters, blood-brain barrier, central nervous system, drug delivery, nanoparticles, liposomes.

## BLOOD-BRAIN BARRIER ANATOMY AND PHYSIOLOGY: AN OVERVIEW

The blood-brain barrier (BBB), the microvascular endothelial network within the capillaries of the central nervous system (CNS), maintains a constant microenvironment in the cerebral parenchyma [1]. It regulates the bi-directional transport of metabolites and xenobiotics, controls the migration of leukocytes, preserves salt homeostasis and allows toxic metabolites to be removed from the brain parenchyma and delivered back into the bloodstream [2]. Acting as a neuroprotective shield, the BBB defines the optimal conditions for neuronal and glial activity. The transport of metabolites and drugs across the BBB is strictly regulated by the presence of tight junctions (TJs), adherent junctions (AJs) and functional "metabolic barriers", such as catabolic enzymes and efflux transport systems. Only electrically neutral and hydrophobic molecules with low molecular weight can easily cross the BBB, while the vast majority of drugs (analgesics, antibiotics, antivirals, anti-epileptic and chemotherapeutic drugs) are excluded [3].

The main structural difference between the endothelium of the brain capillaries and the endothelium of other capillaries is the presence of TJs between adjacent endothelial cells [4] and the lack of fenestrations and pinocytotic vesicles [5]. TJs are multiprotein complexes localized in the lateral surface of the endothelial cells in the CNS. They are formed by transmembrane proteins, such as occludin, claudin-3, claudin-5, junctional adhesion molecule, and cytosolic proteins, such as zonula occludens-1/2/3, AF6, 7H6, and cingulin. In the physiologically competent BBB, the presence of TJs and the absence of fenestrations prevent the paracellular passage of molecules [6]. AJs, other basolateral junctions complexes made of vascular-endothelial cadherin, p120 and  $\alpha$ - $\beta$ -catenin complexes, contribute to the strong cell-cell adhesion and are required for the assembly of TJs [6], further decreasing the paracellular permeability of many substances. Finally, the lack of pinocytotic

vesicles increases even more the tight control of the transcytotic processes across the BBB.

Overall, both luminal and basolateral surfaces, facing blood and brain interstitial fluids respectively, contribute to the "barrier" role of the brain's microvascular endothelium (Fig. 1). Several of the functions described above in the endothelial cells are made possible by the close proximity and the multiple contacts with pericytes, astrocytes and neurons: it is the concurrent presence of endothelial cells, extracellular matrix and CNS cells that forms a physiologically competent BBB [7].

Besides the BBB, other barriers crucial for the homeostasis of the brain parenchyma are the blood-cerebrospinal fluid barrier (BCSF), which is formed by the epithelial cells of the choroid plexus and regulates the transport of molecules between CNS and cerebrospinal fluid [8], and the blood-retina barrier [9]. In all of these barriers, the mechanisms of passive diffusion, facilitated diffusion and active transport of substrates are tightly regulated.

The ATP-binding cassette (ABC) transporters are crucial players in the active transport processes across the BBB.

## THE ABC TRANSPORTERS SYSTEM AND THE BBB

It was originally believed that the transport of drugs across the BBB occurred through passive diffusion and depended on the specific physicochemical properties of the drug, such as lipophilicity, molecular weight and charge [3]. Yet, many lipophilic drugs do not get carried into the CNS. This observation highlights the role of the ABC transporters, as the main actors in the efflux of drugs expected to cross the BBB easily and instead showing very low level within the CNS [10].

Both the BBB and the BCSF contain several members of the ABC transporter family, such as P-glycoprotein (Pgp/ABCB1), multidrug resistance related proteins (MRPs/ABCCs), breast cancer resistance protein (BCRP/ABCG2). They are all integral membrane transporters and share the mechanism of ATP hydrolysis as the driving force for transporting substrates against their concentration gradient. ABC transporters also share a low specificity for sub-

\*Address correspondence to this author at the Department of Oncology, Via Santena 5/bis, 10126 Turin, Italy; Tel: +39-11-6705857; Fax: +39-11-6705845; E-mail: chiara.riganti@unito.it

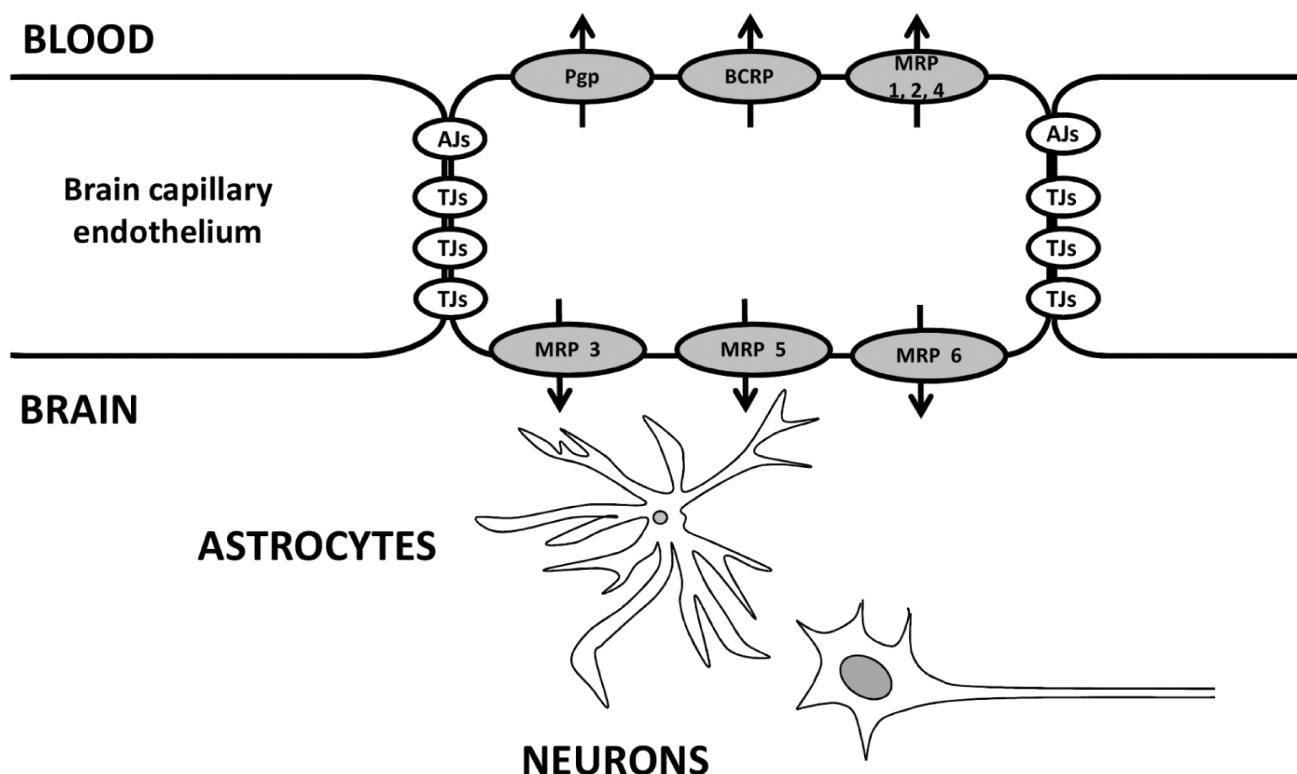


**Fig. (1).** Schematic representation of the blood-brain barrier (BBB). BBB is a structural-functional unit composed by peculiar brain microvascular endothelial cells, devoid of fenestrations, rich of tight junctions (TJs) and adherent junctions (AJs) on lateral surface, and ABC transporters, such as Pgp, MRP1-6, BCRP, on luminal and basolateral side. Most of these features, which determine a tight control on the bi-directional transport of metabolites and xenobiotics, are maintained by the close proximity and multiple contacts between endothelial cells and central nervous system cells, such as astrocytes and neurons.

strates, i.e. each transporter can recognize different molecules and the same substrate can be effluxed by more than one transporter [11] (Table 1). The vast majority of ABC transporters involved in drug resistance, or at least their mRNAs, have been identified in BBB and BCSF cells. The reason for the relative abundance of these transporters on the BBB and BCSF, as well as their prevalent localization on the luminal or basolateral cell membranes, have not yet been fully explained [12].

Pgp was the first ABC transporter detected in human BBB cells [13, 14]. Subsequently Pgp was detected in brain capillary endothelium of several species, including monkeys, rats, mice, cattle, and pigs. Its abundance across different species suggests that Pgp may represent a crucial defense mechanism in mammals, exerted by limiting the delivery of potentially dangerous lipophilic molecules, which otherwise would cross the BBB by passive diffusion [13, 14].

There are two types of human Pgp: type I (also termed “multidrug resistance-1/MDR1 Pgp”, encoded by the *mdr1* gene), responsible for the multidrug resistant phenotype in tumor cells and actively involved in the drug efflux in BBB cells; type II (encoded by *mdr2* gene), restricted to the canalicular plasma membrane of hepatocytes, where it works as a phosphatidylcholine translocase [13]. In the BBB, Pgp is located on the luminal membrane of endothelial cells (Fig. 1) and dramatically decreases the accumulation of drugs within the CNS by pumping them back to the bloodstream [15]. Moreover, Pgp is involved in the basal-apical efflux of endogenous metabolites produced by brain parenchyma, like amyloid  $\beta$  ( $A\beta$ ) peptides [16]. Therefore Pgp represents a crucial control step for the extrusion of both exogenous and endogenous compounds.

The impact of Pgp on CNS homeostasis was shown by using *mdr1a* knockout mice, where CNS levels of Pgp substrates – such as anticancer drugs, analgesics, anti-epileptics, anti-retrovirals or antibiotics' levels-increased 10-to-100-fold, causing serious toxicity [17]. Similar results were obtained when synthetic inhibitors of the transporter were used [18, 19, 20]. One major limitation of Pgp inhibitors is their low tissue specificity and subsequent high toxicity. That notwithstanding, research on Pgp inhibitors with controlled potency and higher selectivity continues in two directions. In one, drugs that exert the expected therapeutic effects on CNS cells and simultaneously inhibit Pgp are under development [21]. In the other, inhibitors of Pgp have been recently studied for diagnostic use. Marked with appropriate radiotracers in positron emission tomography (PET) or single-photon emission computed tomography (SPECT) they help visualize the localization and functional activity of Pgp within the CNS [22, 23, 24]. Some neurodegenerative diseases show reduction of Pgp in specific brain areas as an early sign of disease [25, 26]. Its detection might thus have wide applications in the early diagnosis of these conditions and could help identify those patients who might benefit from the therapeutic administration of Pgp modulators [27].

The MRP transporter family currently has 12 members (including MRP1-9), which are transporters of anionic and neutral organic molecules [28] (Table 1). Their spectrum of substrates overlaps with Pgp [11]. Like Pgp, MRPs are localized in the BBB, the BCSF and also in the blood-spinal cord barrier [29]. The role of MRPs as controllers of drug delivery across the BBB was demonstrated with pharmacological inhibitors, such as probenecid or MK-571, which enhance drug delivery within the CNS or decrease the drug efflux from isolated brain endothelial cells [30]. The contribution of MRPs to drug transport across the BBB, however, is not unidirec-

**Table 1. Substrates of ATP-binding cassette (ABC) transporters present in blood-brain barrier (BBB).**

ABC transporter	Localization on BBB	Endogenous substrates	Xenobiotics and drugs
Pgp (ABCB1)	luminal	neutral/cationic organic compounds, amyloid $\beta$ peptide	doxorubicin, daunorubicin, vincristine, vinblastine, actinomycin-D, paclitaxel, docetaxel, etoposide, teniposide, topotecan, mitoxantrone, methotrexate, imatinib, lapatinib, dasatinib, sorafenib, gefitinib, erlotinib, zidovudine, lamivudine, saquinavir, indinavir, nelfinavir, ketoconazole
MRP1 (ABCC1)	luminal	GSH-conjugated and anionic organic compounds, leukotriene C4	etoposide, teniposide, vincristine, vinblastine, paclitaxel, docetaxel, doxorubicin, daunorubicin, epirubicin, mitoxantrone, methotrexate, topotecan, irinotecan
MRP2 (ABCC2)	luminal	anionic organic compounds	cisplatin, methotrexate, doxorubicin, daunorubicin, etoposide, paclitaxel, docetaxel, topotecan, irinotecan
MRP3 (ABCC3)	basal	glucuronic acid- and GSH-conjugated compounds, bile salts	etoposide, teniposide, methotrexate, cisplatin, doxorubicin, vincristine
MRP4 (ABCC4)	luminal	nucleotide derivatives, organic anionic compounds	methotrexate, 6-mercaptopurine, 6-thioguanine, topotecan, cisplatin
MRP5 (ABCC5)	basal	nucleotide derivatives, organic anionic compounds	6-mercaptopurine, 6-thioguanine, gemcitabine
MRP6 (ABCC6)	basal	anionic cyclic pentapeptide	unknown
BCRP (ABCG2)	luminal	hydrophobic and hydrophilic anionic compounds	prazosin, mitoxantrone, doxorubicin, daunorubicin, topotecan, 7-ethyl-10-hydroxycamptothecin (SN-38), methotrexate, imatinib, lapatinib, dasatinib, sorafenib, gefitinib, erlotinib

Pgp: P-glycoprotein; MRP: multidrug resistance related protein; BCRP: breast cancer related protein; GSH: glutathione.

tional, as MRPs may have a luminal or a basolateral location (Fig. 1). This characteristic, along with the close homology of the ABC family members, makes the design of selective pharmacological inhibitors of MRPs problematic.

Greater efforts have also been made to find selective inhibitors of BCRP, which – like Pgp – is present on the luminal surface of the BBB cells [31] (Fig. 1). Based on mRNA analysis, BCRP is more expressed on the BBB than Pgp or MRP1. Interestingly, BCRP levels were three times as high in brain microvessels of *mdrl1a* knockout mice than wild-type mice, suggesting a compensative up-regulation of BCRP and a possible cross-talk between Pgp and BCRP in BBB cells. Pgp and BCRP cooperate to reduce the brain accumulation of topotecan [32], lapatinib [33], dasatinib [34], sorafenib [35]. For this reason the simultaneous inhibition of Pgp and BCRP has been proposed as a powerful strategy to increase the transport of specific drugs: for instance, the inhibition of both transporters with clinically achievable doses of canertinib and erlotinib improved the delivery of pazopanib within the CNS [36], suggesting a synergistic effect of these inhibitors. The dual inhibitors tariquidar and elacridar, that block both Pgp and BCRP in the BBB *in vivo*, have been intensively investigated as therapeutic tools [34, 37]. The chemical structure of tariquidar and elacridar has been proposed as a starting point for the synthesis of PET radiotracers, able to monitor the localization and activity of Pgp and BCRP within the CNS [23, 24].

Most of the studies on ABC transporter inhibitors were performed in animals. It should be noted that species-specific differences exist between rodents and humans for Pgp localization and activity [38], making it difficult to translate some promising results obtained in animal models into clinical applications in humans. Furthermore the localization of ABC transporters in BBB cells is not limited to the plasma membrane. In solid tumors large amounts are found in cytoplasmic vesicles, where they promote intravesicu-

lar drug sequestration. Whether these intracellular ABC transporters can also be effectively blocked by the common pharmacological inhibitors, remains unclear.

Overall, the routine use of ABC transporter inhibitors to enhance the drug delivery across the BBB *in vivo* is still controversial. The efflux of drugs from BBB cells and their vesicular sequestration depend on their cytoplasmic concentration [39]: the higher the drug concentration within the BBB cells, the lower the percentage of the drug effluxed back into the bloodstream or sequestered. With this paradigm in mind, new strategies of drug delivery have been developed, to increase drug uptake by BBB cells and reduce backward efflux. Common approaches have included the osmotic opening of the TJs [40], regional drug delivery by local catheters, drug-enriched wafers and conventionally-enhanced delivery devices [41], the use of carrier systems like antibody-conjugated drugs, nanoparticle (NP)-carried drugs or liposome-carried drugs [40, 42, 43].

#### NANOPARTICLES AND LIPOSOMES AS DRUG DELIVERY SYSTEMS: AN OVERVIEW

Owing to their small size, customizable surface, good solubility, targeted drug delivery and multifunctionality, NPs have emerged in the last decades as useful drug carriers [44].

NPs are commonly defined as carriers with a size between 10 and 1000 nm, made with a broad spectrum of materials: sugar derivatives such as malto-dextrins [45] or chitosan [46]; fatty acids such as beenic acid and palmitic acid that are assembled in the so-called solid lipidic NPs (SLNs) [47]; proteins such as human albumin (HA) and type B gelatin [48]. Some NPs are micelles of amphiphilic molecules with the peculiar orientation of the hydrophilic groups on the outer surface and the hydrophobic groups in the internal core. This structure offers the advantage to carry both water-soluble drugs, adsorbed on the hydrophilic moieties, and poorly

water-soluble drugs, hidden in the hydrophobic core, and makes amphiphilic micelles very versatile carriers [49].

Amphiphilic polymers used for micelles - such as poly(lactic acid), poly( $\beta$ -hydroxybutyrate), poly(lactic-co-glycolic acid) (PLGA), poly( $\epsilon$ -caprolactone), polyalkylcyanoacrylate, poly(butyl 2-cyanoacrylate) (PBCA), poly(isobutyl 2-cyanoacrylate), poly(methyl methacrylate), polystyrene - commanded a good deal of interest in the last few years, because they can self-assemble, are stable and have customizable features, as they can vary in length and composition of polymers [48]. These NPs are collectively termed polymeric NPs [50] and can be divided into nanospheres (if entirely made of solid components) and nanocapsules (if made of a solid shell surrounding a central cavity, containing hydrophilic or hydrophobic solvents). Polymeric micelles are usually larger than SLNs; despite their great versatility in transporting drugs, their size can sometimes limit the efficacy of drug delivery in particular tissues. To be used *in vivo*, polymeric NPs must be biocompatible. To increase the biocompatibility of synthetic polymers, cholesterol is often included in NPs. Cholesterol also helps the self-assembly of NPs and is useful for actively targeting different types of cholesterol receptors present in mammalian tissues [51].

Dendrimers, branched NPs with uniform and well-defined size and shape, and a highly controlled dendritic architecture (in terms of size, branching density, surface functionality), are another class of polymeric NPs, able to cross cell membranes and biological barriers including the BBB [52]. The most common materials used for the synthesis of dendrimers are poly(amidoamine) (PAMAM), poly(propylene imine) or polyether-copolyester. Dendrimers can transport drugs, either encapsulated or chemically bound, and are often used as carriers of pro-drugs, which are then released as active metabolites; the so-called "pH-sensitive" dendrimers are able to deliver drugs when exposed at specific pH (e.g. in the more acidic microenvironment of brain tumors). Such versatility makes dendrimers ideal carriers for the delivery of anticancer, anti-inflammatory and antibiotic agents to the CNS [53].

The main requisites that NPs must have when they are administered systemically are: 1) the preservation of their structural integrity in the bloodstream; 2) their escape from sequestration in reticulo-endothelial cells (or "stealthness"); 3) the absence of "first-passage" effect and hepatic catabolism and 4) the absence of important urinary clearance [48]. Furthermore, NPs must not induce side-effects, such as liver or kidney toxicity or abnormal immunoreactivity. Finally, the stability and the pharmacokinetic profile of each drug can widely differ, depending on its therapeutic use. Therefore NPs must be designed in such a versatile manner to prevent the early degradation/release of the drug, to allow drug delivery to the target tissue at the desired concentration and to provide a better pharmacokinetic profile than the free drug [54]. For instance the delivery of the anti-diarrheal drug loperamide with PLGA NPs conjugated with the peptide Gly-Phe-Thr-Gly-Phe-Leu-Ser-(O- $\beta$ -D-glucose)-CONH<sub>2</sub> produced stronger and more prolonged pharmacological effects than the intraventricular injection of free loperamide [55]. Similarly, the loading of paclitaxel into glutathione (GSH)-coated PLGA NPs not only lowered the drug efflux through the ABC transporters of the BBB, but also allowed a long-lasting and steady release of paclitaxel within RG2 glioma cells [56].

Besides being manufactured as drug or pro-drug containing carriers, NPs containing metallic compounds, such as titanium dioxide (TiO<sub>2</sub>), gold and iron oxide derivatives [57, 58], have been synthesized. One specific property of these NPs is in their targeting, that can be increased by the application of appropriate magnetic fields [57], using the so-called magnetic resonance imaging (MRI) guided focused ultrasound technique [59].

Liposomes are lipid vesicles with a wide range of sizes, e.g. from 20 nm to 1  $\mu$ m of diameter. They are made by one or multiple phospholipid bilayers with the typical structural organization of cell

membranes. The only exception to this definition is niosomes, which share all functional properties with the classical liposomes but are non phospholipid-based vesicles, as they contain non-ionic surfactants and cholesterol [49]. Thanks to the variety of sizes and lamellar structures, liposomes are as versatile carriers as NPs: they can be loaded with hydrophobic, hydrophilic or amphipathic drugs, using relatively simple techniques. Drugs can be encapsulated within or adsorbed on the lipid shell, depending on their hydrophobicity, and can be released from the same type of liposome with different kinetics, achieving superior therapeutic efficacy than free drugs. Liposomes, like NPs, are subjected to the enhanced permeability and retention (EPR) effect, i.e. they usually have low systemic concentration and high tumor concentration. The EPR effect and the multiple mechanisms of drug delivery make it possible for instance to carry high amounts of chemotherapeutic drugs with relatively low side-effects. For this reason, liposomes have been used against tumors unresponsive to conventional chemotherapy since 1970s.

Until now, the most commonly used carriers for drug delivery within the CNS included polymeric NPs and liposomes [49]. This review discusses the physicochemical properties that make NPs and liposomes suitable carriers for drug delivery across the BBB, the role of surface coating, the different mechanisms of uptake by BBB cells, the current hypothesis on their ability to bypass the ABC transporter-mediated efflux and the potential clinical uses of NPs and liposomes in different conditions of the CNS.

## NANOPARTICLE-BASED STRATEGIES FOR DRUG DELIVERY ACROSS THE BBB

### The Passive Targeting of NPs Across the BBB: Effects of Size, Charge Surface and Coating

Several experimental evidences have reported that NPs enhance delivery across the BBB, because of either passive targeting (non-specific endocytosis) or active targeting (by binding to specific receptors of the luminal surface of BBB cells, followed by a receptor-driven endocytosis). Confocal microscope analysis and cell fractioning studies on rat brain endothelial cells showed that indeed NPs were mostly associated with plasma membrane and vesicular compartments, and only a small fraction was associated with caveolae. These data indicate a prevalent uptake of NPs via non-specific endocytosis [60]. In the case of passive targeting, the chemical structure and the physicochemical properties of the surface are critical to make NPs suitable for the uptake within the BBB cells.

The size of the synthesized NPs is crucial. NPs smaller than 20 nm can pass through BBB endothelial cells by transcytosis and - in the case of active targeted NPs - they can easily interact with the target receptors present on the surface of the BBB cells [61].

It is generally recognized that the surface features of NPs, more than their core structure, are critical for the delivery through the BBB; changes in the surface charge and coating may influence the ability to cross biological barriers. Fenart and coworkers synthesized NPs of cross-linked malto-dextrins, derivatized with phosphate-conjugated ligands (to obtain anionic NPs), quaternary ammonium-conjugated ligands (to obtain cationic NPs) or without any modification (to obtain neutral NPs). All NPs were then coated with dipalmitoyl phosphatidyl choline and cholesterol. Whereas the coating of neutral NPs did not significantly improve their delivery through the BBB, the coating of charged NPs increased their uptake up to four folds [45]. The uptake of anionic lipid NPs was higher than neutral or cationic ones at the same concentrations [62]. These differences may underscore different uptake pathways: at 4°C, when active endocytosis was blocked and only passive diffusion was allowed, cationic NPs remained outside the BBB cells, neutral NPs were associated with cell surface, anionic NPs were detected on cell surface and in paracellular space; at 37°C, only neutral and anionic NPs had undergone endocytosis and were subjected to transcytosis [63]. The use of the caveolae-interfering agent filipin

showed that neutral and anionic NPs used in this study followed the caveolae-mediated endocytotic pathway, whereas cationic NPs did not [63].

Coating of NPs surface with hydrophilic or amphiphilic polymers, such as polyethylene glycol (PEG), pluronic, poloxamer and poloxamine, is commonly used to increase the hydration and the solubility of the NP core, and to protect it from enzymatic degradation and phagocytosis by circulating mononuclear cells and reticulo-endothelial cells [44, 48]. So far, pegylation is widely employed for the *in vivo* applications of NPs. Pegylation does not exclude encasing lipophilic drugs into the NP core. Since the solubility of the drugs carried by PEG-coated NPs is related to the NP concentration rather than the drug concentration, also hydrophobic drugs, when transported by pegylated NPs can reach the BBB at clinically relevant concentrations after systemic administration. Pegylation also facilitates the passage across the BBB: poly(methoxy-PEG-cyanoacrylate-co-hexadecyl cyanoacrylate) (PEG-PHDCA) copolymers passed the BBB more easily than the uncoated ones [60] or poloxamine 908-coated particles [54].

Beside pegylation, coating with surfactants, such as polysorbate 80 (Tween 80) has been studied for a long time as an effective tool to increase NP delivery through the BBB [54, 64]. Polysorbate 80-coated PEG-PHDCA NPs were shown to be well delivered in mice brain [54]. In this study polysorbate-80 was reported to increase the permeability to [<sup>14</sup>C]-sucrose [54], suggesting that the increased transport might be the consequence of increased paracellular, rather than transcellular transport. Other mechanisms, however, are possible: polysorbate 80 has been reported to enhance the phagocytosis of the coated NPs [64] and to reduce their efflux by Pgp [65]. As result of these findings, polysorbate 80-coated NPs allow drugs with poor CNS penetration, like doxorubicin, to be transported faster across the BBB. When we compare the CNS accumulation of doxorubicin in rats treated intravenously with free doxorubicin dissolved in 1% polysorbate 80, uncoated PBCA-doxorubicin or polysorbate 80-coated PBCA-doxorubicin, only the last formulation effectively increased the drug levels in all the CNS sections examined [66]. This study illustrates that an appropriate coating is crucial for enhanced delivery through the BBB. The presence of polysorbate 80 increased antitumor activity as well: PLGA NPs that carried doxorubicin were more cytotoxic against A172 human glioblastoma cells than non-coated NPs [67]. Differently from PEG, however, coating with polysorbate 80 did not prevent the sequestration of NPs by the reticulo-endothelial system [68].

### Active Targeting by NPs Across BBB

The presence of adsorbed or covalently-bound ligands on NPs surface further improves delivery across the BBB, by receptor-triggered endocytosis, more efficient than non-specific endocytosis [61, 69]. The most common receptors used for the active targeting by NPs on BBB cells are the insulin receptor, the transferrin (Tf) receptor, the low density lipoproteins receptor (LDLR), the LDLR-related proteins (LRPs), the folic acid receptor and the diphtheria toxin receptor [49].

Tf-conjugated NPs were delivered more effectively than unconjugated ones within the CNS [70, 71], thanks to the abundance of Tf receptor in the BBB [61]. Tf-conjugated NPs were internalized by clathrin-mediated and energy-dependent endocytosis. It was recently shown that Tf-conjugated NP transcytosis across the murine microvascular brain endothelial cells bEnd3 involves the passage through the endosomal/lysosomal compartments and the Golgi apparatus [71]. Besides Tf-conjugated NPs loaded with drugs, Tf-conjugated HA loaded with gadolinium were manufactured and proposed as sensitive tracers for MRI, due to more efficient delivery within the CNS parenchyma [72].

Also LDLR and LRPs trigger efficient receptor-driven endocytosis followed by transcytosis. They can recognize apo-lipoproteins as substrates, or synthetic peptides like Angiopep-2 [73], which

were widely used in the design of targeted NPs. HA NPs covalently bound with apolipoprotein E (apoE) were delivered more efficiently than unconjugated HA NPs in brain parenchyma after intravenous injection into SV 129 mice [74]. The imaging analysis of apoE-HA uptake in mouse brain endothelial cells bEnd3 demonstrated a typical transcytotic pathway [74]. A surprising observation reported that PEG-PHDCA NPs not conjugated with apolipoproteins were internalized via a LDLR-mediated endocytosis as well, suggesting the existence of non-specific interactions with the receptor [75]. The efficiency of internalization was however increased by the attachment of specific ligands [74, 76, 77]. When pre-incubated with rat serum, PEG-PHDCA NPs spontaneously adsorbed apolipoprotein B100 (apoB100) and apoE on their surface, and were delivered more efficiently to the CNS than apolipoprotein-free NPs [78]. However, adsorbing the whole protein on the NPs surface is neither yield- nor cost-effective. Not all the adsorbed proteins have the necessary conformation to bind to the receptor on the NP surface. To overcome these drawbacks, NPs conjugated only with the receptor-binding sequences of apoE [79] and apoB100 [80] were synthesized. These sequences were sufficient to trigger receptor-mediated endocytosis and subsequent delivery to brain parenchyma. When loaded with paclitaxel oleate, synthetic LDLs showed good anti-cancer activity in rats with glioblastoma [81]. Similarly, when a Tf-receptor targeting peptide, instead of the whole protein, was conjugated to gold NPs the efficiency of their passage across the BBB was maximized [82].

Folic acid receptor is another commonly used target: folic acid-conjugated SLNs effectively delivered docetaxel, which is otherwise undeliverable to the CNS across the BBB [83]. When  $\gamma$ -polyglutamic acid ( $\gamma$ -PGA) is attached on the surface of NPs, the length of the  $\gamma$ -PGA chain is a critical factor that determines the permeability across the BBB: PLGA NPs carrying the antiretroviral drug saquinavir conjugated with low molecular weight  $\gamma$ -PGA were more efficiently transported across the BBB than other PLGA NPs formulations [84]. This observation concurs with other evidence where PEG-PLGA NPs conjugated with serum bovine albumin had different stability and clearance rates, depending on the amount and density of the albumin molecules attached to the PEG-PLGA surface: only specific albumin/PLGA ratios allowed a good delivery within CNS [85].

Actively targeted NPs were effective not only for drug delivery, but also in the context of gene therapy. Anti-sense oligonucleotides for nuclear factor- $\kappa$ B (NF- $\kappa$ B), conjugated with a copolymer of biotin-PEG/polyethyleneimine and linked to a monoclonal antibody anti-Tf receptor were easily uptaken in brain murine microvascular endothelial cells and down-regulated the NF- $\kappa$ B-dependent pro-inflammatory pathways [86]. This strategy needs further discussion for the treatment of neuro-inflammatory diseases. DNA-carrying PAMAM dendrimers, conjugated with Angiopep-2 (a 19-mer peptide that crosses the BBB) through bifunctional PEG, were recognized by LRP1 on brain capillary endothelial cells: they were internalized through clathrin- and caveolae-mediated and energy-dependent endocytosis, and partially through macropinocytosis. *In vivo*, they showed stronger gene delivery than unconjugated PAMAM dendrimers in brain parenchyma [73]. Similarly, a good delivery of specific siRNAs with anti-tumor activity was achieved in glioma-bearing rats treated with biotinylated siRNA conjugated to a monoclonal antibody against Tf-receptor through a streptavidin linker [87]. To simultaneously increase the passage across BBB and the docking on tumor cells, dendrimers were conjugated with more than one ligand, as occurred for the dual targeting PEG-PAMAM dendrimers conjugated with Tf and wheat germ agglutinin on their surface, and loaded with doxorubicin into their core [88].

The major drawback in using Tf, folic acid or apolipoproteins as NPs ligands is that their receptors are widespread. Therefore the risk of NPs uptake by other tissues cannot be excluded. Only the design of NPs with selective tropism for brain endothelial cells

could switch this “unspecific” targeting into a BBB-specific one. In order to circumvent this problem, experiments of phage-display helped identify a number of short peptides that interacted more specifically with human cerebral microvascular endothelial cells (hCMEC/D3) than with human umbilical vein ones [89]. Although the targets of these peptides are not known, they should be investigated for the future design of more BBB-selective NPs. Similarly, a high-throughput screening of two libraries of mono- and dimethylated diketopiperazine-conjugated dipeptides identified a number of peptide shuttles with a strong ability to cross the BBB [90]. Further studies are necessary to verify the specific tropism of these peptides for the BBB endothelium and to identify their targets.

### **NPs as Effective Tools to Bypass the ABC Transporter-mediated Efflux in the BBB**

Beside showing greater uptake by the BBB cells, NP-carried drugs also show less efflux by ABC transporters. The first studies reporting this property of NPs were done on tumors that over expressed ABC transporters and showed synchronous resistance to different anti-cancer drugs, a phenotype known as multidrug resistance. The discovery of the role of ABC transporters in BBB cells gave a strong push towards the design of drug-loaded NPs less sensitive to the activity of these pumps. Methotrexate, a drug which does not cross the BBB, became highly cytotoxic against C6 rat glioma cells when carried by chitosan and glycol chitosan NPs coated with Tween 80. This formulation of methotrexate was also able to cross the monolayer of MDCKII cells overexpressing Pgp, an *in vitro* model of BBB [46]. Although these results remain to be validated *in vitro* with endothelial cells from brain capillaries and *in vivo*, they suggest that NPs can rescue the therapeutic benefit of a drug – such as methotrexate – otherwise undeliverable across the BBB. Also, docetaxel, another substrate of Pgp, is poorly transported within the CNS: it was however well delivered to brain parenchyma when loaded into folic acid-conjugated SLNs [83]. Of note, the efflux of docetaxel by Pgp increases further with the concurrent administration of other drugs interacting with Pgp, like ketoconazole. Since the co-administration of medications is common in medicine, drug-to-drug interactions and their potential negative effects on CNS delivery need investigation. Venishetty and coworkers showed that when docetaxel and ketoconazole were both loaded in SLNs, ketoconazole no longer increased the efflux of docetaxel through Pgp [83], suggesting that the SLNs formulation nullified any interaction of the substrates with Pgp. Also paclitaxel [56] and doxorubicin [66, 67, 88] were less affected by the Pgp-mediated efflux if carried by NPs.

It is not clear whether the inhibition of Pgp is caused by any specific components of the NPs. On one hand, some NPs are less effluxed than others by multidrug-resistant cancer cells: pluronic-coated NPs strongly inhibited the activity of Pgp in cancer cells as well as in BBB cells, with different mechanisms, such as ATP depletion and changes in membrane fluidity. These events forced Pgp to work with lower efficacy [91]. PEG itself inhibits the activity of Pgp, by changing the physicochemical properties of plasma membrane and altering the binding affinity of the substrates to Pgp [92]. PEG-NPs loaded with paclitaxel protected the drug from the Pgp-mediated efflux [93]. Finally, surfactants – such as Cremophor EL, Triton X-100, Nonidet P-40, Tween 20 – may inhibit Pgp, by increasing the fluidity of the lipid bilayer [91]. How polysorbate 80, one of the most commonly used surfactants in NP synthesis, inhibits Pgp remains unclear: it has been reported that polysorbate 80 modulates Pgp activity, without causing any conformational change of the transporter [94]. In *in vitro* studies surfactants inhibit Pgp at micromolar/millimolar concentrations; these conditions, however, are hardly reproducible *in vivo*, because surfactants are toxic at such concentrations. Therefore, the biochemical mechanisms that make surfactant-coated NPs more effective than uncoated NPs *in vivo* remain largely unknown. In summary, the identification of the NP

component – core compounds, PEG coating, surfactant coating – responsible for the Pgp inhibition will help optimize the design of NPs less susceptible to Pgp efflux.

While several works have reported that NPs-carried drugs bypass the efflux of Pgp, a few studies have reported the effects of NPs on the other ABC transporters [95, 96]. Since the BBB contains many different ABC transporters and the same drug can be effluxed by more than one transporter, the inhibition of Pgp alone is not enough to guarantee the delivery of the drug to the CNS. Moreover, since some ABC transporters – like MRP3, MRP5 and MRP6 – are mainly located on the basal surface of BBB cells, their inhibition by NPs would result in the drug retention within the endothelial cells rather than in their delivery to brain parenchyma. Although these issues are still largely unknown, they must command our attention if we want to improve the future design of NPs able to bypass specific ABC transporters and deliver their load to the CNS with maximum efficiency.

A recent interesting application of NPs is the delivery of peptides, like Leu-enkephalin, after oral administration: while free peptides are usually degraded within the gastro-intestinal lumen, peptides loaded into NPs were able to enter into the portal circulation, reach the systemic circulation and were delivered unaltered to the brain parenchyma [97]. From these findings it can be inferred that NPs protect peptides from the hydrolysis of proteases in the gastro-intestinal tract. It should be noted that enterocytes and hepatocytes also carry ABC transporters, which efflux drugs taken by mouth back into the intestinal lumen and in the biliary tract, respectively. We can speculate that the protective effects of NPs is caused – at least in part – by the lower efflux by ABC transporters in these tissues, which in turn cause increased systemic concentrations of the drugs to reach the BBB.

### **NP Distribution and Toxicology *In vivo***

Before we try to move on to novel NP-based therapies *in vivo*, two critical issues should be examined: 1) NPs distribution in the CNS after crossing the BBB and 2) NPs toxicology profiles.

The use of capillary depletion technique, the labeling of NPs with radioactive, magnetic or fluorescent moieties, and the subsequent analysis of brain sections with PET, SPECT, MRI and fluorescence microscopy was helpful to resolve whether NPs show uniform distribution within the brain parenchyma or are preferentially concentrated in specific areas. Notably, different NPs have different levels of distribution within the CNS. Labeled PHDCA NPs were found in the epithelial cells of choroid plexus, in pia mater, in the ventricular system and – to a minor extent – in endothelial cells, suggesting that the vast majority of NPs were not retained within BBB cells but were effectively delivered into the CNS parenchyma [54]. ApoE-conjugated HA was found in brain capillary endothelial cells and neurons [74], likely because of the presence of receptors for apolipoproteins on both endothelial cells and neurons. Since different CNS cell types and different CNS areas may have different patterns of surface receptors, the choice of appropriate ligands may direct conjugated NPs towards selected cell populations or areas. This approach could be particularly useful in diseases that arise from specific cell types or areas, such as brain tumors, neurodegenerative diseases and epilepsy. To design effective tissue specific therapies, it is imperative that we know the receptor composition of the CNS and manufacture NPs conjugated with specific ligands. Studies in CNS tumor-bearing animals have shown that NP levels are higher in tumors than in the parenchyma surrounding them [68]. This EPR effect is not specific of CNS tumors as it is common to most tumors, where the vascular architecture is different than normal tissues and acts as a “sink” for NPs. Nanotechnologies can further increase the distribution to CNS tumors by designing dual-targeted NPs, i.e. NPs which recognize BBB and CNS tumor cells at the same time. Docetaxel-carrying NPs conjugated with the TGN peptide, selected by phage-display as a molecule

targeting the BBB, and with an aptamer targeting the surface of glioma cells, has been recently proven to reach high intratumor concentrations and cytotoxic efficacy [98].

In recent years, the increasing exposure to NPs of environmental or medical origin has shown their potential toxicity for mammalian tissues especially for blood-tissue interfaces, which are heavily exposed to NPs. Until now, the effects of NPs on BBB cells are poorly described. In the case of iron-oxide NPs, it has been shown that size, concentration, agglomeration and surface physico-chemical properties are critical for neurotoxicity [99]. Recent work compared the effects of acute and repeated/chronic exposure of brain endothelial cells to TiO<sub>2</sub> NPs. While acute exposure decreased the activity of Pgp without disrupting the integrity of BBB, chronic exposure decreased the expression of ABC transporters, impaired TJ integrity and induced the synthesis of pro-inflammatory cytokines, which may in turn produce a dysfunction of microglial cells [58]. This study suggests the need to consider the long-term toxicity of drug-loaded NPs, still largely unknown, mainly because long observational *in vivo* studies have not been done. From this perspective, liposomal drugs, made of cholesterol and endogenous phospholipids, at least theoretically appear to be safer and more biocompatible tools than NPs.

## LIPOSOME-BASED STRATEGIES FOR DRUG DELIVERY ACROSS THE BBB

### The Passive Targeting of Liposomes Across BBB: Effects of Size, Charge Surface and Coating

Liposomes, like NPs, must meet three basic requirements to produce therapeutic effects when administered systemically: 1) prolonged circulation in the bloodstream, 2) sufficient accumulation in the target tissue and 3) controlled drug release and uptake by the target cells [100]. As it occurs for NPs, size, surface charge, coating with PEG and surfactants are features very important for making stealth liposomes that can be delivered efficiently to specific compartments like the BBB. PEG allows a long-lasting circulation of liposomes [101]; of note, the length of the PEG chain influences delivery across the BBB [102]. Also surface charge is critical, favoring or impairing liposomal uptake by the endothelial cells of brain capillaries. Cationic liposomes seem to be particularly well endocytosed by BBB cells: they can be produced as liposomes or as pro-liposomes, i.e. as neutral or negatively charged liposomes at pH 7.4, that can switch into cationic ones once they reach the endosomal compartment of the BBB cells [103]. Since a specific surface charge of liposomes may not be compatible with the encapsulation of charged drugs, the synthesis of pro-liposomes with a pH-dependent surface charge may widen the spectrum of the encapsulated drugs.

Just like NPs, liposomes can carry more than one drug. For instance, chemotherapeutic drugs and an inhibitors of ABC transporters were co-encapsulated within the liposomal shell in the treatment of CNS tumors, which are rich of ABC transporters [104]. The synchronous delivery of conventional chemotherapeutic agents and gene silencing or expression vectors has been recently investigated [105], as an alternative approach to the classical pharmacological therapy of CNS tumors. Also the simultaneous administration of two liposomal formulations, one containing a chemotherapeutic drug – like doxorubicin – and the other containing an adjuvant molecule – like the tumor necrosis factor-related apoptosis-inducing ligand (TRAIL), achieved good antitumor effect [106].

Pro-drugs, instead of the active drugs, have been encapsulated as well: this approach looks particularly useful when the drug is at risk of being effluxed by the BBB cells or catabolized before reaching its target, as it occurs for dopamine. An interesting study proposed the encapsulation of the dopamine pro-drug 2-amino-N-[2-(3,4-dihydroxy-phenyl)-ethyl]-3-phenyl-propionamide, within unilamellar liposomes. When packaged this way, the drug remained protected from photodegradation, stable in plasma, deliverable

across the BBB thus producing dopamine in the brain [107]. Another example comes from neurotensin-degrading enzyme inhibitors, which have potential therapeutic benefit in neuropsychiatric disorders, but are highly unstable in the blood stream and cannot cross the BBB: liposomal encapsulation overcame these limitations [108]. Similarly, cytidine 5' diphosphocholine, a neuroprotective agent in the cerebral ischemia-reperfusion syndrome, is hydrolyzed in the liver and cannot reach the BBB as is. Liposomal encapsulation allowed it to bypass liver catabolism and to reach the brain parenchyma at sufficient therapeutic concentrations [109].

Because of different pharmacokinetic profiles and different mechanisms of extravasation, drugs encapsulated in PEG-liposomes are retained in ischemic areas longer than free drugs: this observation has led to the development of liposomal-based strategies to deliver erythropoietin in areas of cerebral ischemia, attempting to prevent the ischemia/reperfusion damages that occur with stroke [110]. Methylprednisolone is a drug with potential therapeutic benefit in neuroinflammatory diseases, like multiple sclerosis, that does not cross the BBB: its liposomal encapsulation overcame this obstacle and reduced clinical symptoms in experimental autoimmune encephalomyelitis [111].

By varying the lipid composition and charge, liposomes can be easily loaded with DNA, siRNAs or anti-sense oligonucleotides, which are then kept from degrading until they reach their target cells. For obvious ethical reasons, the studies in this field have been performed only *in vitro* or in animals, but they attained striking results both in experimentally-induced CNS tumors and neurodegenerative conditions, such as Parkinson disease (PD) and Creutzfeldt-Jakob disease [112, 113].

Specific liposomes that release drugs under controlled physical stimuli have also been manufactured, such as temperature-sensitive liposomes, which release their load in a temperature-dependent manner. Of note, mild hyperthermia (i.e. 42°C) increased both the rate of delivery across the BBB and the release of doxorubicin from thermosensitive liposomes, reducing the growth of glioma in rats placed in a 42°C-bath effectively [114].

Magnetic-field sensitive liposomes can be prepared by loading Fe<sub>3</sub>O<sub>4</sub> into the liposomal envelope. The application of an external magnetic field increased the BBB passage by endocytosis and by monocyte-mediated transport. This strategy is currently under investigation to produce BBB-permeating formulations of the anti-retroviral drug azidothymidine 5'-triphosphate [115]. Lastly, liposomes were also used in diagnostics, by incorporating specific isotopes for PET imaging within liposomes: for instance, <sup>18</sup>F-labelled liposomes targeted with the Ala-Pro-Arg-Pro-Gly peptide, which recognizes angiogenic areas, were successfully used as sensitive PET tracers for the early diagnosis of glioma [116].

### The Active Targeting of Liposomes Across BBB

Liposomes, like NPs, can be conjugated with specific antibodies and ligands to enhance endocytosis by BBB cells; several studies using Tf, lactoferrin, insulin, GSH, apolipoproteins and peptides reported the successful delivery of targeted-liposomes to the brain parenchyma. This approach is known as “Trojan horse” strategy [40, 42, 112], because it allows a drug “masked” as another molecule to enter into the endothelial cells of brain capillaries. Most of these liposomes enter the BBB cells by a mechanism of receptor-triggered endocytosis, which is clathrin-dependent [103].

Tf-conjugated PEG-liposomes were uptaken by BBB cells more than unconjugated liposomes and subjected to transcytosis. In co-culture systems, Tf-conjugated PEG-liposomes effectively delivered high amounts of boron-10 into human glioma U87-MG cells, sufficient to exert cytotoxic effects in boron neutral capture therapy [117].

Liposomes conjugated with monomers or tandem dimers of the apoE-derived peptide containing the residues 141-150 were uptaken

by hCMEC/D3 cells in a manner that depended on the peptide's density, appearing promising carriers for drug delivery within the CNS [118]. We recently produced an "LDL-masked" liposomal formulation of doxorubicin, by conjugating an LDLR-targeting peptide from human apoB100 to anionic pegylated liposomes [119]. We found that the liposomal uptake was increased by a preventive stimulation with statins, which *per se* decreased the endogenous synthesis of cholesterol and forced cells to increase the amount of LDLR on their surface. This event occurred in both epithelial tumors [119] and human BBB cells [120]. Besides favoring the uptake of the LDL-masked liposomes by hCMEC/D3 cells, this approach takes advantage of the chemosensitizing properties of statins, which increase the endogenous synthesis of nitric oxide, an inhibitor of ABC transporters [121]. In the case of hCMEC/D3 cells, statins decreased the activity of Pgp and BCRP, two transporters localized on the luminal surface and thus involved in the brain-to-blood flow of drugs. Using BBB-penetrating statins, like mevastatin and simvastatin, similar effects (i.e. increased surface LDL receptor, decreased ABC transporter activity) were achieved in U87-MG glioblastoma cells cultured under hCMEC/D3 monolayer. Thanks to the concurrent targeting of BBB and tumor cells, the pre-treatment with statins allowed LDL-masked liposomal doxorubicin to cross the BBB, to accumulate within tumor cells and to exert their cytotoxic effects [120].

A similar "dual-targeting" approach – i.e. the dual ability to cross the BBB and target CNS cells – can be also achieved by conjugating liposomes with more than one ligand, i.e. one ligand specific for endothelial cells and the other specific for CNS cells. For instance, PEG-immunoliposomes conjugated with an anti-Tf receptor antibody were further conjugated with an anti-A $\beta$  antibody: these dual-targeting liposomes were well delivered across the BBB and directed to the A $\beta$  peptide in the brain parenchyma [122], thus appearing as potential tools against Alzheimer's disease (AD). Dual targeting liposomes carrying daunorubicin, conjugated with Tf and p-aminophenyl-alpha-D-manno-pyranoside (which recognize the BBB and glioma surface, respectively), were successfully used in glioma-bearing animals [123]. Dual targeting also increases the uptake of liposomes by BBB cells, because it may overcome the saturation limit observed when endocytosis is single receptor dependent [124].

The specific tropism of liposomes for BBB or CNS cells is problematic at the present, since most ligands (e.g. Tf, insulin, GSH) are not tissue-specific. Phage-display screening identified specific short peptides targeting the BBB [89]: disappointingly, when conjugated to liposomes, these peptides bound to the surface of hCMEC/D3 cells much less efficiently than when displayed by the native phage [125]. The conjugation with liposomes indeed altered the folding of the peptides, preventing them from binding to their target receptor [125]. The preservation of proper folding, as well as the ligand density on the liposomal surface, are two factors that may limit the efficiency of the BBB uptake. If these features are not carefully studied before we manufacture new targeted liposomes, then we might incorrectly judge a ligand 'ineffective', when in fact such 'ineffectiveness' might be caused by either wrong folding or wrong ligand density. Great attention must be paid to all the synthetic steps; subsequently careful validations of targeted liposomal formulations must be made, both *in vitro* and *in vivo*, to identify which conditions maximize delivery efficiency.

#### **Liposomes as Effective Tools to Bypass the ABC Transporter-mediated Efflux in the BBB**

After the successful treatment of unresponsive cancers with drug-loaded liposomes, it was hypothesized that liposomal formulations might overcome the drug efflux of ABC transporters.

Besides sustaining prolonged release within the tumor [126], liposomal drugs are less potent inducers of Pgp than free drugs [127]. One work suggested a direct interaction between liposomes

and Pgp, since liposomes inhibited the binding of free vincristine to Pgp [128]. Our group recently reported that liposomal doxorubicin acts as an allosteric inhibitor of Pgp, reduces ATP hydrolysis and competes with verapamil and colchicine for Pgp binding [129]. Site-directed mutagenesis suggested that the putative site of interaction between the liposomal drug and Pgp is a domain centered on glycine 185, overlapping with a "low-affinity drug binding site" of Pgp [129]. It is unlikely, however, that the entire structure of a liposome interacts with a specific binding site on Pgp; it is more plausible that a specific component of the liposomal shell or a lipid-associated form of doxorubicin be the actual modulator of Pgp, and that this yet unidentified compound hampers the binding and efflux of other substrates. Surprisingly, also empty liposomes inhibit the activity of Pgp, because they alter the composition of phospholipids and fatty acids in membrane microdomains (i.e. lipid rafts) where Pgp operates [129]. The increased fluidity of the plasma membrane observed in cells treated with liposomes may change the conformation of Pgp or force the protein to work in a non-optimal environment.

Only one study reported an inhibitory effect of liposomes on MRP transporters [127]; since MRPs are also highly embedded in the plasma membrane bilayer and depend on a proper lipid composition for their activity, we cannot exclude that liposomes reduce the activity of MRPs by impairing the architecture of the cell membrane, as it occurs for Pgp.

Such inhibitory properties of liposomes on ABC transporters make liposomal drugs potentially useful not only against drug-resistant tumors, but also for drug delivery across the BBB. The first few studies on the BBB focused mostly on chemotherapeutic drugs with poor BBB penetration, such as doxorubicin, which is highly effective against glioblastoma cells *in vitro* but highly effluxed by Pgp, MRP1 and BCRP in the BBB. Although different formulations of liposomal doxorubicin may have different anti-tumor efficacy, pharmacokinetic profile and side-effects [130], there is a general agreement about the higher permeability of liposomal doxorubicin across the BBB compared with free doxorubicin [131, 132].

Paradoxically, liposomal formulations of doxorubicin, vincristine and irinotecan in glioma-bearing rats decreased the growth rate of tumors but increased the BBB properties in glioma vessels [133]. The BBB is often disrupted within the core of a glioblastoma, where poorly organized vasculature develops by neo-angiogenesis. It has been shown that liposomes induce selective damages on immature and proliferating endothelial cells of solid tumors, but spare mature and quiescent endothelium [134]. In glioblastoma the rescue of a competent BBB is usually associated with tumor regression. Such observation may explain the efficacy of liposomes in this context. From this point of view, liposomes have a dual effect, being carriers of anti-cancer drugs across a competent BBB (i.e. in the brain-adjacent-to-tumor area, where metastasizing tumor cells are present), and anti-angiogenic agents where the BBB is disrupted (i.e. in the tumor core). This broad spectrum of effects makes liposomes particularly promising as anti-glioblastoma tools.

#### **Liposomes Toxicology *In vivo***

Some authors have proposed that the use of liposomes is safer than the use of NPs [135]. This observation however may be biased, as studies using liposomes as carriers of drugs within the CNS are significantly fewer than those using NPs. On the other hand, liposomes may be truly less toxic than NPs, because they are made up of phospholipid (e.g. phosphatidylcholine, phosphatidylethanolamine, phosphatidylserine, phosphatidyl glycerol) and cholesterol, which are physiologically incorporated into the cell membrane and subsequently degraded. Conversely, as we have previously observed in epithelial tumors, the liposomal envelop alters the composition of phospholipids and fatty acids of cell plasma membrane [129] and may impair the activity of integral membrane proteins,

such as transporters and receptors. So far, we cannot exclude that the prolonged exposure to liposomes may result in damages of cell plasma membrane and surface proteins. As there have been no toxicological studies on the long-term effects of liposomes to date, this issue remains unclear.

**CLINICAL IMPLICATIONS OF DRUG DELIVERY STRATEGIES ACROSS THE BBB**

In recent years, we have been watching the first few pioneering applications of NP- and liposome-based strategies for drug delivery across the BBB in CNS tumors, infections, neurodegenerative conditions and epilepsy (Table 2).

Malignant gliomas are the most common brain tumors. High-grade gliomas, such as glioblastoma multiforme, and CNS metastases of systemic tumors have high levels of ABC transporters. Their response to radio- and chemotherapy is poor, because most anti-cancer drugs (doxorubicin, daunorubicin, etoposide, teniposide, paclitaxel, docetaxel, vincristine, vinblastine, cisplatin, methotrexate) do not cross the BBB or penetrate tumor cells [136]. Moreover, approximately 10% of patients with extra-CNS tumors develop brain metastasis, also chemoresistant and usually surrounded by a competent BBB [137].

These new strategies for drug delivery may improve the efficacy of conventional chemotherapy against primary and metastatic brain tumors, provided that the delivery systems are safe for normal CNS cells [138]. The EPR effect causes rather selective accumulation of NPs and liposomes within the tumor tissue. Furthermore, tumor cells sometimes display antigens and surface markers that are not expressed or expressed at lower levels in non-transformed cells. These markers can be used as docking sites to increase the concentration of actively targeted NPs and liposomes within tumor cells [139]. Human glioblastoma for instance selectively expresses different receptors for interleukin-13 (IL-13). IL-13-conjugated liposomal doxorubicin reduced the growth of glioma in mice, without cytotoxic effects on BBB cells [140]. A few years ago, it was reported that doxorubicin-carrying NPs improved the survival of rats bearing the aggressive glioblastoma 101/8 and induced complete histological remission at 6 months in 20-40% of the animals [141]. Since then, the number of studies using formulations of doxorubicin-carrying NPs and/or liposomes has been increasing

steadily. Doxyl/Caelyx, the liposomal doxorubicin approved for breast and ovarian cancers has been used in phase I/phase II clinical trials in patients with glioblastoma: the drug was well tolerated and had few side-effects, although it did not significantly improve overall and progression-free survival when compared to the standard regimens based either on temozolomide or combination radiation therapy and chemotherapy [132, 142, 143].

Many promising studies have been performed in animal models, that used either NPs or liposomes carrying various chemotherapeutic agents [80, 114, 123, 133] or gene-targeting tools. PAMAM-PEG-Angiopep-conjugated dendrimers carrying an expression vector of TRAIL were more effective than temozolomide alone in inducing glioma regression [144]. PEG-SLN carrying c-Met siRNA effectively reduced the growth of U87-MG glioblastoma cells in orthotopic xenografts, without systemic toxicity [145].

Viral infections, in particular cerebral infection with HIV, are under active investigation, because most anti-retroviral drugs are effluxed by Pgp at the BBB level. The administration of the antiretroviral drugs zidovudine, lamivudine and nelfinavir carried by NPs coated with pluronic 85, which reduces the activity of Pgp, improved the symptoms of HIV encephalitis in mice [146]. Similarly, indinavir carried by solutol-coated NPs was delivered to mice brain significantly better than free indinavir [147]. Different drugs carried by the same NPs may be delivered differently, as suggested by work done with stavudine, delviridine and saquinavir loaded methylmethacrylate-sulfopropylmethacrylate NPs [148]. Differences in solubility and surface characteristics may explain different rates of drug uptake within the BBB cells. Differences in the affinity of each drug for ABC transporters may account for a different brain-to-blood efflux. Of note, Tf-conjugated NPs carrying saquinavir not only crossed the BBB better than the free drug, but were also more effective in reducing the replication of HIV in peripheral blood monocytes in animals [149], suggesting that NPs may have some anti-retroviral activity themselves [150]. Similarly, dendrimers carrying specific siRNA reduced the replication of the HIV strains X4-HIV NL4-3 and R5-HIV BaL in infected human astrocytes [151].

Neurodegenerative disorders, such as AD and PD, are another potential field of application for NP- and liposome-based strategies. Promising drugs and therapeutic tools for these conditions have

**Table 2. Clinical applications of nanoparticle- and liposome-based strategies in central nervous system diseases**

Disease	Biological rationale for using NPs and liposomes	Pre-clinical and clinical applications of NP- and liposome-based strategies
Malignant gliomas	Presence of surface receptors for active targeting on BBB cells Presence of ABC transporters on BBB and CNS cells	Use of NPs and liposomes carrying chemotherapeutic drugs in animal models [76, 100, 109, 129, 136,137] Use of NPs for gene therapy in animal models [140,141] Use of liposomal doxorubicin in phase I/phase II trials [108, 138,139]
HIV infections	Overexpression of Pgp on BBB cells Inhibitory effects of NPs on HIV replication	Use of NPs carrying antiretroviral drugs in animal models of HIV-induced encephalitis [142-144] Use of dendrimers for gene therapy [147]
Neurodegenerative disorders (AD, PD)	Changes in Pgp expression on BBB cells, associated with increased accumulation of Aβ in CNS and altered drug delivery across BBB	Use of NPs for immunotherapy and early diagnosis of AD [149] Use of curcumin-carrying PLGA NPs as amyloid disaggregating agents [150] Use of L-DOPA-carrying liposomes for PD treatment [152]
Epilepsy	Increase in Pgp, MRPs and BCRP on BBB cells and epileptogenic foci	Use of NPs carrying ANEP [156]

HIV: human immunodeficiency virus; AD: Alzheimer’s disease; PD: Parkinson’s disease; BBB: blood-brain barrier; CNS: central nervous system; ABC: ATP-binding cassette; Pgp: P-glycoprotein; MRP: multidrug resistance related protein; BCRP: breast cancer related protein; Aβ, amyloid β; NP: nanoparticle; PLGA: poly(lactic-co-glycolic acid); ANEP: anti-neuroexcitation peptide.

little use *in vivo*, as they do not easily cross the BBB [152]. Recent studies showed that A $\beta$  is an endogenous substrate of Pgp, that can be cleared from the brain and easily effluxed back to the bloodstream [16]. In the transgenic Tg2576 murine model of AD, which overexpresses the human amyloid precursor protein, the decrease in Pgp levels on BBB cells is responsible for the accumulation of A $\beta$  and one of the first signs of AD. Conversely, the up-regulation of Pgp through the pregnane X receptor-mediated transcription of Pgp with pregnenolone-16 $\alpha$ -carbonitrile, reduced the accumulation of A $\beta$  within the CNS in the first stages of AD [26]. Interestingly, the role of Pgp in AD is duplicitous: on one side, it prevents the early damages from the abnormal accumulation of A $\beta$ ; on the other, it represents an obstacle for potentially useful drugs to move across the BBB. For this reason, the development of NP-based strategies has been particularly active in the last few years. Several immunotherapeutic strategies based on NPs have been studied: for instance anti-A $\beta$  antibodies, which do not cross the BBB, were able to do so when carried by chitosan-coated PLGA NPs [153]. Chitosan also increased the stability and solubility of NPs, making them suitable for other applications, such as the delivery of diagnostic antibodies to detect A $\beta$  in the early stages of AD [153]. Curcumin has the interesting property to destroy amyloid aggregates and to be an anti-oxidant; unfortunately, it has low solubility in water and crosses the BBB poorly. These shortcomings were compensated by loading curcumin into PLGA NPs; the conjugation with the Tet-1 peptide, which has affinity for the neuron's surface and can trigger retrograde transport, enhanced the effective delivery of curcumin to the CNS, thus offering a potential strategy for AD treatment [154]. Several SLN and liposomes targeting A $\beta$  have been produced [155]; their efficacy has been tested *in vitro*. It is presumably only a matter of time before they get tested in animal models.

A few promising reports have been published on PD treatment: liposomes loaded with L-DOPA, for example, increase drug availability in nigrostriatal cells, where L-DOPA is converted into dopamine [156]. Moreover, liposomes containing a dopamine pro-drug, which reliably releases dopamine *in vitro*, were recently synthesized [107]: if their ability to prevent dopamine from peripheral enzymatic degradation and to deliver it to the nigrostriatal system is confirmed *in vivo*, this path might greatly improve the current therapeutic approach to PD.

Resistance to multiple antiepileptic drugs affects at least 30% of patients. It is not clear whether anti-epileptic drugs are effluxed by ABC transporters on BBB cells [157], we know, however, that Pgp is markedly increased in the epileptogenic foci of patients and murine models. Resistance to therapy seems to correlate directly with the activity of Pgp, MRPs and BCRP: the progressive increase in Pgp levels – first in brain capillaries and then in neurons – parallels the progressive loss of efficacy of antiepileptic drugs and correlates with the number and frequency of seizures before therapy [158]. Most antiepileptic drugs are highly permeable molecules and therefore should be well delivered across the BBB. Nonetheless, improving their delivery – through depot and slow-release oral formulations, and more recently by NP and liposome systems –, and developing new anti-epileptic molecules is the object of intensive investigation [159]. Recently, the anti-neuroexcitation peptide (ANEP) was identified as a promising candidate for the treatment of epilepsy. A novel formulation of ANEP loaded into trimethyl-chitosan NPs was effectively endocytosed through the BBB and delivered to the CNS [160], opening an alternative path to the use of conventional anti-epileptic drugs for refractory epilepsy.

## CONCLUSIONS

Remarkable progress has been made in the field of nanomedicine in the last few years. NPs and liposomes with controlled size, specific surface charge and surfactant coating, conjugated with selective ligands can be synthesized at low cost and with simple

laboratory equipment. Therefore, the mass of new work that describes the synthesis and validation of new drug delivery systems in this field is growing by the day.

Understanding which formulations are best for a specific condition is a challenge for many reasons. First, we still do not fully understand by which mechanisms NPs and liposomes cross the BBB. Greater knowledge on the molecular mechanisms that increase endocytosis and decrease efflux by the BBB will determine better choices of specific formulations. From this point of view, the BBB model has an undisputed advantage, as it is a model where both the endocytotic pathways and the efflux transporters are maximally active and tightly controlled. The abundance of ABC transporters in the endothelial cells of brain capillaries of bovine, murine and human origin may help explain by which mechanisms NPs and liposomes protect drugs from the ABC transporters-mediated efflux (Fig. 2). Creating *in vitro* BBB models with selective knock-down or knock-in of proteins involved in the endocytotic pathway or the efflux system is the next challenge: this approach is ideal for high throughput screening of NPs and liposomes, and might likely help unveil the preferential routes of entry and efflux of specific classes of carriers. Besides shedding light on the biological mechanisms of NP and liposome delivery across the BBB, it could also translate into the design of new NPs and liposomes with specific physico-chemical properties and better delivery across the BBB. The optimization of nanocarriers design is the next most interesting challenge for that part of medicine focused on the BBB.

With that goal in mind, standardizing the assays on BBB cells becomes a critical point. The mechanisms of endocytosis, the patterns of ABC transporters present on luminal and basal side of brain endothelial cells and the rate of cerebral flow are different among species. For this reason, results obtained in animal models will not necessarily be applicable to humans. These differences should be taken into account when we analyze the vast body of literature on drug delivery across the BBB. Furthermore these differences seem to imply that the choice of the experimental model must be rigorous and should strictly depend on the nature, be it animal or human, of the condition under study.

One major advantage of NP- and liposome-based strategies is their versatility: once a specific formulation of the carrier is synthesized, its cargo can be easily manipulated to include drugs, siRNA, gene-delivering systems or radiotracers. Such versatility broadens the uses of NPs and liposomes, from therapeutics, as drug-delivery systems in diseases like cancer, epilepsy, infective or neurodegenerative disorders, to diagnostics to, eventually, theranostics [161]. The number of studies with a theranostic focus in CNS diseases is limited and in need of development. Theranostics requires not only the design and synthesis of appropriate nanocarriers, but also the parallel improvement of imaging techniques, genetics and pharmacogenomics. Shortening the time between diagnosis and therapy is critical in rapidly growing CNS tumors, such as glioblastoma. Therefore the development of NPs for a theranostic use should have very high priority, as it appears it might change the treatment and prognosis of such critical conditions very quickly.

Nanoparticle- and liposome-based strategies may in the end be very beneficial. Many unresolved issues however remain. First, there is lack of consistent information about their long term toxicity and lack of effective strategies for adequate tissue-specificity for BBB and CNS cells. The maximal efficacy of NPs and liposomes can be achieved by active targeting strategies, but the identification of surface targets selectively expressed on BBB cells is only just beginning. Two critical actions might help filling this knowledge gap: high throughput screening of the surface proteome of primary brain endothelial cells and high throughput screening of drug and peptide libraries. The combined analysis of those screenings will likely identify a tangible number of targets and ligands selective for BBB cells, and pave the way for designing NPs and liposomes highly specific for the BBB. At the present time, all the strategies

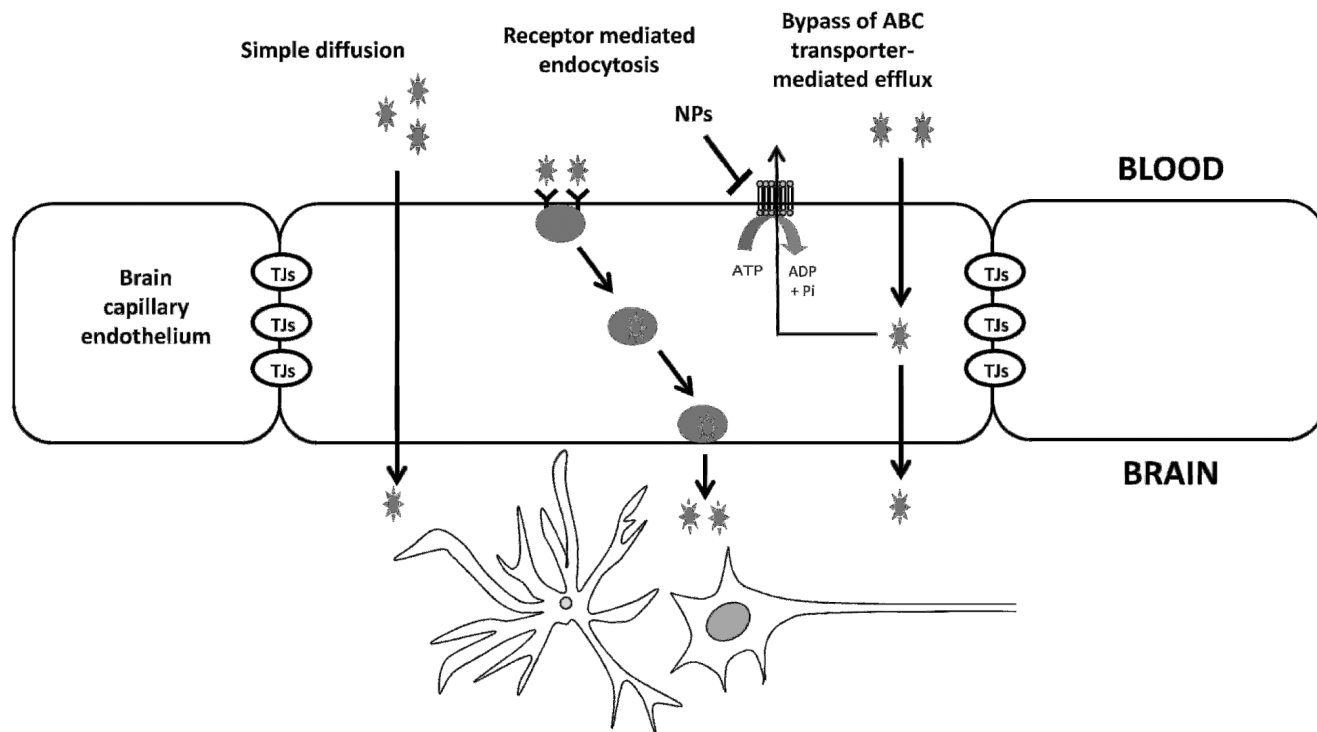


**Fig. (2).** Nanoparticle- and liposome-loaded drugs are more easily delivered across blood-brain barrier (BBB) than free drugs with at least three mechanisms: 1) they are favored to enter cells by simple diffusion (passive targeting); 2) they are uptaken by a receptor-triggered endocytosis, if conjugated with specific ligands (active targeting); 3) they are less effluxed by ABC transporters: indeed nanoparticles and liposomes can directly inhibit the catalytic cycle of ABC transporters and alter the optimal physicochemical properties of the plasma membrane in which the transporters work. Overall, the drugs loaded into these delivery systems can pass through the BBB and reach the CNS at therapeutically relevant concentrations.

for active targeting BBB cells use unspecific targets and ligands, and are not reliable, with very few exceptions [89, 90]. This knowledge gap, however, should not be considered as a limitation; rather, it should be the starting point for the next challenge, which is to develop new drug delivery systems, more and more selective and effective.

**CONFLICT OF INTEREST**

The authors confirm that this article content has no conflicts of interest.

**ACKNOWLEDGEMENTS**

This work has been supported by grants from Compagnia di San Paolo, Programma Neuroscienze (grant 2008.1136) and Italian Association for Cancer Research (AIRC; MFAG 11475) to CR.

Martha Leonor Pinzón-Daza is recipient of an ERACOL Erasmus Mundus fellowship. Joanna Kopecka is recipient of a “Mario and Valeria Rindi” fellowship from Italian Foundation for Cancer Research (FIRC).

We thanks Prof. Amalia Bosia, Dept. of Oncology, University of Turin, and Prof. Davide Schiffer, Neuro-Bio-Oncology Center, Vercelli, Italy, for the helpful discussion and advices.

**ABBREVIATIONS**

- BBB = Blood-brain barrier
- CNS = Central nervous system
- TJ = Tight junctions
- AJ = Adherent junctions
- BCSF = Blood-cerebrospinal fluid barrier

- ABC = ATP-binding cassette
- Pgp = P-glycoprotein
- MRP = Multidrug resistance related protein
- BCRP = Breast cancer resistance protein
- Aβ = Amyloid β
- PET = Positron emission tomography
- SPECT = Single-photon emission computed tomography
- NP = Nanoparticle
- SLN = Solid lipidic nanoparticle
- HA = Human albumin
- PLGA = poly(lactic-co-glycolic acid)
- PBCA = poly(butyl 2-cyanoacrylate)
- PAMAM = poly(amidoamine)
- GSH = Glutathione
- MRI = Magnetic resonance imaging
- EPR = Enhanced permeability and retention
- PEG = Polyethylene glycol
- PEG-PHDCA = poly(methoxy-PEG-cyanoacrylate-co-hexadecyl cyanoacrylate)
- Tf = Transferrin
- LDLR = Low density lipoproteins receptor
- LRP = Low-density lipoprotein receptor-related protein
- apoE = Apolipoprotein E

apoB100	=	Apolipoprotein B100
γ-PGA	=	γ-polyglutamic acid
NF-κB	=	Nuclear factor-κB
hCMEC/D3	=	Human cerebral microvascular endothelial cells
TRAIL	=	Tumor necrosis factor-related apoptosis-inducing ligand
PD	=	Parkinson's disease
AD	=	Alzheimer's disease
IL-13	=	Interleukin-13
ANEP	=	Anti-neuroexcitation peptide.

## REFERENCES

- Paulson, O.B. Blood-brain barrier, brain metabolism and cerebral blood flow. *Eur. Neuropsychopharmacol.*, **2002**, *12*, 495-501.
- Ronaldson, P.T.; Davis, T.P. Blood-brain Barrier Integrity and Glial Support: Mechanisms that can be Targeted for Novel Therapeutic Approaches in Stroke. *Curr. Pharm. Des.*, **2012**, *18*, 3624-3644.
- Bhaskar, S.; Tian, F.; Stoeger, T.; Kreyling, W.; de la Fuente, J.M.; Grazu, V.; Borm, P.; Estrada, G.; Ntziachristos, V.; Razansky, D. Multifunctional Nanocarriers for diagnostics, drug delivery and targeted treatment across blood-brain barrier: perspectives on tracking and neuroimaging. *Part. Fibre Toxicol.*, **2010**, *7*, 3-28.
- Hawkins, B.T.; Davis, T.P. The blood-brain barrier/neurovascular unit in health and disease. *Pharmacol. Rev.*, **2005**, *57*, 173-185.
- Saunders, N.R.; Ek, C.J.; Habgood, M.D.; Dziegielewska, K.M. Barriers in the brain: a renaissance? *Trends Neurosci.*, **2008**, *31*, 279-286.
- Jin, R.; Yang, G.; Li, G. Molecular insights and therapeutic targets for blood-brain barrier disruption in ischemic stroke: critical role of matrix metalloproteinases and tissue-type plasminogen activator. *Neurobiol. Dis.*, **2010**, *38*, 376-385.
- Partridge, W.M. Blood-brain barrier biology and methodology. *J. Neurovirol.*, **1999**, *5*, 556-569.
- Lichota, J.; Skjorringe, T.; Thomsen, L.B.; Moos, T. Macromolecular drug transport into the brain using targeted therapy. *J. Neurochem.*, **2009**, *113*, 1-13.
- Saunders, N.R.; Knott, G.W.; Dziegielewska, K.M. Barriers in the immature brain. *Cell Mol. Neurobiol.*, **2000**, *20*, 29-40.
- Cole, S.P.; Deeley, R.G. Multidrug resistance mediated by the ATP-binding cassette transporter protein MRP. *Bioessays*, **1998**, *20*, 931-40.
- Gottesman, M.M.; Fojo, T.; Bates, S.E. Multidrug resistance in cancer: role of ATP-dependent transporters. *Nat. Rev. Cancer*, **2002**, *2*, 48-58.
- Gazzin, S.; Strazielle, N.; Schmitt, C.; Fevre-Montange, M.; Ostrow, J.D.; Tiribelli, C.; Ghersi-Egea, J.F. Differential expression of the multidrug resistance-related proteins ABCB1 and ABCG1 between blood-brain interfaces. *J. Comp. Neurol.*, **2008**, *510*, 497-507.
- Partridge, W.M.; Golden, P.L.; Kang, Y.S.; Bickel, U. Brain microvascular and astrocyte localization of P-glycoprotein. *J. Neurochem.*, **1997**, *68*, 1278-1285.
- Loscher, W.; Potschka, H. Role of multidrug transporters in pharmacoresistance to antiepileptic drugs. *J. Pharmacol. Exp. Ther.*, **2002**, *301*, 7-14.
- Seelig, A.; Blatter, X.L.; Wohnsland, F. Substrate recognition by P-glycoprotein and the multidrug resistance-associated protein MRP1: a comparison. *Int. J. Clin. Pharmacol. Ther.*, **2000**, *38*, 111-121.
- Miller, D.S.; Bauer, B.; Hartz, A.M. Modulation of P-glycoprotein at the blood-brain barrier: opportunities to improve central nervous system pharmacotherapy. *Pharmacol. Rev.*, **2008**, *60*, 196-209.
- Borst, P.; Evers, R.; Kool, M.; Wijnholds, J. A family of drug transporters: the multidrug resistance-associated proteins. *J. Natl. Cancer Inst.*, **2000**, *92*, 1295-1302.
- Namanja, H.A.; Emmert, D.; Pires, M.M.; Hrycyna, C.A.; Chmielewski, J. Inhibition of human P-glycoprotein transport and substrate binding using a galantamine dimer. *Biochem. Biophys. Res. Commun.*, **2009**, *388*, 672-676.
- Iwanaga, K.; Yoneda, S.; Hamahata, Y.; Miyazaki, M.; Shibano, M.; Taniguchi, M.; Baba, K.; Kakemi, M. Inhibitory effects of furanocoumarin derivatives in Kambo extract medicines on P-glycoprotein at the blood-brain barrier. *Biol. Pharm. Bull.*, **2011**, *34*, 1246-1251.
- Yao, D.; Yang, Z.H.; Liu, L.; Li, J.; Yu, Y.L.; Zhang, L.L.; Pan, X.; Liu, X.D.; Xie, L.; Wang, G.J. Verapamil exerts biphasic modulation on phenobarbital transport across the blood-brain barrier: evidence from an *in vivo* and *in vitro* study. *Naunyn Schmiedeberg's Arch. Pharmacol.*, **2011**, *383*, 393-402.
- Zhou, Y.G.; Li, K.Y.; Li, H.D. Effect of the novel antipsychotic drug perospirone on P-glycoprotein function and expression in Caco-2 cells. *Eur. J. Clin. Pharmacol.*, **2008**, *64*, 697-703.
- Bankstahl, J.P.; Kuntner, C.; Abraham, A.; Karch, R.; Stanek, J.; Wanek, T.; Wadsak, W.; Kletter, K.; Muller, M.; Loscher, W.; Langer, O. Tariquidar-induced P-glycoprotein inhibition at the rat blood-brain barrier studied with (R)-11C-verapamil and PET. *J. Nucl. Med.*, **2009**, *49*, 1328-1335.
- Kuntner, C.; Bankstahl, J.P.; Bankstahl, M.; Stanek, J.; Wanek, T.; Stundner, G.; Karch, R.; Brauner, R.; Meier, M.; Ding, X.; Muller, M.; Loscher, W.; Langer, O. Dose-response assessment of tariquidar and elacridar and regional quantification of P-glycoprotein inhibition at the rat blood-brain barrier using (R)-[(11)C]verapamil PET. *Eur. J. Nucl. Med. Mol. Imaging*, **2009**, *37*, 942-953.
- Bauer, F.; Kuntner, C.; Bankstahl, J.P.; Wanek, T.; Bankstahl, M.; Stanek, J.; Mairinger, S.; Dorn, B.; Loscher, W.; Muller, M.; Erker, T.; Langer, O. Synthesis and *in vivo* evaluation of [11C]tariquidar, a positron emission tomography radiotracer based on a third-generation P-glycoprotein inhibitor. *Bioorg. Med. Chem.*, **2010**, *18*, 5489-5497.
- Dimou, E.; Booij, J.; Rodrigues, M.; Prosch, H.; Attems, J.; Knoll, P.; Zajicek, B.; Dudczak, R.; Mostbeck, G.; Kuntner, C.; Langer, O.; Brucke, T.; Mirzaei, S. Amyloid PET and MRI in Alzheimer's disease and mild cognitive impairment. *Curr. Alzheimer Res.*, **2009**, *6*, 312-319.
- Hartz, A.M.; Miller, D.S.; Bauer, B. Restoring blood-brain barrier P-glycoprotein reduces brain amyloid-beta in a mouse model of Alzheimer's disease. *Mol. Pharmacol.*, **2010**, *77*, 715-723.
- Mairinger, S.; Erker, T.; Muller, M.; Langer, O. PET and SPECT radiotracers to assess function and expression of ABC transporters *in vivo*. *Curr. Drug Metab.*, **2011**, *12*, 774-792.
- Sun, H.; Dai, H.; Shaik, N.; Elmquist, W.F. Drug efflux transporters in the CNS. *Adv. Drug Deliv. Rev.*, **2003**, *55*, 83-105.
- Campos, C.R.; Schroter, C.; Wang, X.; Miller, D.S. ABC transporter function and regulation at the blood-spinal cord barrier. *J. Cereb. Blood Flow Metab.*, **2012**, *32*, 1559-1566.
- Schinkel, A.H.; Jonker, J.W. Mammalian drug efflux transporters of the ATP binding cassette (ABC) family: an overview. *Adv. Drug Deliv. Rev.*, **2003**, *55*, 3-29.
- Eisenblatter, T.; Huwel, S.; Galla, H.J. Characterisation of the brain multidrug resistance protein (BMDP/ABCG2/BCRP) expressed at the blood-brain barrier. *Brain Res.*, **2003**, *971*, 221-231.
- de Vries, N.A.; Zhao, J.; Kroon, E.; Buckle, T.; Beijnen, J.H.; van Tellingen, O. P-glycoprotein and breast cancer resistance protein: two dominant transporters working together in limiting the brain penetration of topotecan. *Clin. Cancer Res.*, **2007**, *13*, 6440-6449.
- Polli, J.W.; Olson, K.L.; Chism, J.P.; John-Williams, L.S.; Yeager, R.L.; Woodard, S.M.; Otto, V.; Castellino, S.; Demby, V.E. An unexpected synergist role of P-glycoprotein and breast cancer resistance protein on the central nervous system penetration of the tyrosine kinase inhibitor lapatinib (N-[3-chloro-4-[(3-fluorobenzyl)oxy]phenyl]-6-[5-([2-(methylsulfonyl)ethyl]amino)methyl]-2-furyl]-4-quinazolinamine; GW572016). *Drug Metab. Dispos.*, **2009**, *37*, 439-442.
- Lagas, J.S.; van Waterschoot, R.A.; van Tilburg, V.A.; Hillebrand, M.J.; Lankheet, N.; Rosing, H.; Beijnen, J.H.; Schinkel, A.H. Brain accumulation of dasatinib is restricted by P-glycoprotein (ABCB1) and breast cancer resistance protein (ABCG2) and can be enhanced by elacridar treatment. *Clin. Cancer Res.*, **2009**, *15*, 2344-2351.
- Lagas, J.S.; van Waterschoot, R.A.; Sparidans, R.W.; Wagenaar, E.; Beijnen, J.H.; Schinkel, A.H. Breast cancer resistance protein and P-glycoprotein limit sorafenib brain accumulation. *Mol. Cancer Ther.*, **2010**, *9*, 319-326.
- Minocha, M.; Khurana, V.; Qin, B.; Pal, D.; Mitra, A.K. Enhanced brain accumulation of pazopanib by modulating P-gp and Bcrp1

- mediated efflux with canertinib or erlotinib. *Int. J. Pharm.*, **2012**, *436*, 127-134.
- [37] Breedveld, P.; Pluim, D.; Cipriani, G.; Wielinga, P.; van Tellingen, O.; Schinkel, A.H.; Schellens, J.H. The effect of Bcrp1 (Abcg2) on the *in vivo* pharmacokinetics and brain penetration of imatinib mesylate (Gleevec): implications for the use of breast cancer resistance protein and P-glycoprotein inhibitors to enable the brain penetration of imatinib in patients. *Cancer Res.*, **2005**, *65*, 2577-2582.
- [38] Bauer, M.; Zeitlinger, M.; Karch, R.; Matzner, P.; Stanek, J.; Jager, W.; Bohmdorfer, M.; Wadsak, W.; Mitterhauser, M.; Bankstahl, J.P.; Loscher, W.; Koepp, M.; Kuntner, C.; Muller, M.; Langer, O. Pgp-mediated interaction between (R)-[11C]verapamil and tariquidar at the human blood-brain barrier: a comparison with rat data. *Clin. Pharmacol. Ther.*, **2011**, *91*, 227-233.
- [39] Loscher, W.; Potschka, H. Blood-brain barrier active efflux transporters: ATP-binding cassette gene family. *NeuroRx*, **2005**, *2*, 86-98.
- [40] Deeken, J.F.; Loscher, W. The blood-brain barrier and cancer: transporters, treatment, and Trojan horses. *Clin. Cancer Res.*, **2007**, *13*, 1663-1674.
- [41] Sampson, J.H.; Raghavan, R.; Brady, M.; Friedman, A.H.; Bigner, D. Convection-enhanced delivery. *J. Neurosurg.*, **2011**, *115*, 463-466.
- [42] Partridge, W.M. Drug targeting to the brain. *Pharm. Res.*, **2007**, *24*, 1733-1744.
- [43] Singh, R.; Lillard, J.W. Jr. Nanoparticle-based targeted drug delivery. *Exp. Mol. Pathol.*, **2009**, *86*, 215-223.
- [44] McNeil, S.E. Nanotechnology for the biologist. *J. Leukoc. Biol.*, **2005**, *78*, 585-594.
- [45] Fenart, L.; Casanova, A.; Dehouck, B.; Duhem, C.; Slupek, S.; Cecchelli, R.; Betbeder, D. Evaluation of effect of charge and lipid coating on ability of 60-nm nanoparticles to cross an *in vitro* model of the blood-brain barrier. *J. Pharmacol. Exp. Ther.*, **1999**, *291*, 1017-1022.
- [46] Trapani, A.; Denora, N.; Iacobellis, G.; Sitterberg, J.; Bakowsky, U.; Kissel, T. Methotrexate-loaded chitosan- and glycol chitosan-based nanoparticles: a promising strategy for the administration of the anticancer drug to brain tumors. *AAPS PharmSciTech.*, **2011**, *12*, 1302-1311.
- [47] Kim, H.R.; Kim, I.K.; Bae, K.H.; Lee, S.H.; Lee, Y.; Park, T.G. Cationic solid lipid nanoparticles reconstituted from low density lipoprotein components for delivery of siRNA. *Mol. Pharm.*, **2008**, *5*, 622-631.
- [48] Owens, D.E. 3<sup>rd</sup>; Peppas, N.A. Opsonization, biodistribution, and pharmacokinetics of polymeric nanoparticles. *Int. J. Pharm.*, **2006**, *307*, 93-102.
- [49] Chen, Y.; Liu, L. Modern methods for delivery of drugs across the blood-brain barrier. *Adv. Drug Deliv. Rev.*, **2012**, *64*, 640-665.
- [50] Discher, D.E.; Ahmed, F. Polymersomes. *Annu. Rev. Biomed. Eng.*, **2006**, *8*, 323-341.
- [51] Liu, X.M.; Pramoda, K.P.; Yang, Y.Y.; Chow, S.Y.; He, C. Cholesterol-grafted functional amphiphilic poly(N-isopropylacrylamide-co-N-hydroxymethylacrylamide): synthesis, temperature-sensitivity, self-assembly and encapsulation of a hydrophobic agent. *Biomaterials*, **2004**, *25*, 2619-2628.
- [52] Patel, T.; Zhou, J.; Piepmeier, J.M.; Saltzman, W.M. Polymeric nanoparticles for drug delivery to the central nervous system. *Adv. Drug Deliv. Rev.*, **2012**, *64*, 701-705.
- [53] Beg, S.; Samad, A.; Alam, M.I.; Nazish, I. Dendrimers as novel systems for delivery of neuropharmaceuticals to the brain. *CNS Neurol. Disord. Drug Targets*, **2011**, *10*, 576-588.
- [54] Calvo, P.; Gouritin, B.; Chacun, H.; Desmaele, D.; D'Angelo, J.; Noel, J.P.; Georgin, D.; Fattal, E.; Andreux, J.P.; Couvreur, P. Long-circulating PEGylated polycyanoacrylate nanoparticles as new drug carrier for brain delivery. *Pharm. Res.*, **2001**, *18*, 1157-1166.
- [55] Vergoni, A.V.; Tosi, G.; Tacchi, R.; Vandelli, M.A.; Bertolini, A.; Costantino, L. Nanoparticles as drug delivery agents specific for CNS: *in vivo* biodistribution. *Nanomedicine*, **2009**, *5*, 369-377.
- [56] Geldenhuys, W.; Mbimba, T.; Bui, T.; Harrison, K.; Sutariya, V. Brain-targeted delivery of paclitaxel using glutathione-coated nanoparticles for brain cancers. *J. Drug Target.*, **2011**, *19*, 837-845.
- [57] Chertok, B.; Moffat, B.A.; David, A.E.; Yu, F.; Bergemann, C.; Ross, B.D.; Yang, V.C. Iron oxide nanoparticles as a drug delivery vehicle for MRI monitored magnetic targeting of brain tumors. *Biomaterials*, **2008**, *29*, 487-496.
- [58] Brun, E.; Carriere, M.; Mabondzo, A. *In vitro* evidence of dysregulation of blood-brain barrier function after acute and repeated/long-term exposure to TiO<sub>2</sub> nanoparticles. *Biomaterials*, **2011**, *33*, 886-896.
- [59] Etame, A.B.; Diaz, R.J.; O'Reilly, M.A.; Smith, C.A.; Mainprize, T.G.; Hynynen, K.; Rutka, J.T. Enhanced delivery of gold nanoparticles with therapeutic potential into the brain using MRI-guided focused ultrasound. *Nanomedicine*, **2012**, *8*, 1133-1142.
- [60] Garcia-Garcia, E.; Andrieux, K.; Gil, S.; Kim, H.R.; Le Doan, T.; Desmaele, D.; d'Angelo, J.; Taran, F.; Georgin, D.; Couvreur, P. A methodology to study intracellular distribution of nanoparticles in brain endothelial cells. *Int. J. Pharm.*, **2005**, *298*, 310-314.
- [61] Smith, M.W.; Gumbleton, M. Endocytosis at the blood-brain barrier: from basic understanding to drug delivery strategies. *J. Drug Target.*, **2006**, *14*, 191-214.
- [62] Lockman, P.R.; Koziara, J.M.; Mumper, R.J.; Allen, D.D. Nanoparticle surface charges alter blood-brain barrier integrity and permeability. *J. Drug Target.*, **2004**, *12*, 635-641.
- [63] Jallouli, Y.; Paillard, A.; Chang, J.; Sevin, E.; Betbeder, D. Influence of surface charge and inner composition of porous nanoparticles to cross blood-brain barrier *in vitro*. *Int. J. Pharm.*, **2007**, *344*, 103-109.
- [64] Gulyaev, A.E.; Gelperina, S.E.; Skidan, I.N.; Antropov, A.S.; Kivman, G.Y.; Kreuter, J. Significant transport of doxorubicin into the brain with polysorbate 80-coated nanoparticles. *Pharm. Res.*, **1999**, *16*, 1564-1569.
- [65] Nerurkar, M.M.; Burto, P.S.; Borchardt, R.T. The use of surfactants to enhance the permeability of peptides through Caco-2 cells by inhibition of an apically polarized efflux system. *Pharm. Res.*, **1996**, *13*, 528-534.
- [66] Wohlfart, S.; Khalansky, A.S.; Gelperina, S.; Begley, D.; Kreuter, J. Kinetics of transport of doxorubicin bound to nanoparticles across the blood-brain barrier. *J. Control. Release*, **2011**, *154*, 103-107.
- [67] Tahara, K.; Kato, Y.; Yamamoto, H.; Kreuter, J.; Kawashima, Y. Intracellular drug delivery using polysorbate 80-modified poly(D,L-lactide-co-glycolide) nanospheres to glioblastoma cells. *J. Microencapsul.*, **2010**, *28*, 29-36.
- [68] Ambruosi, A.; Khalansky, A.S.; Yamamoto, H.; Gelperina, S.E.; Begley, D.J.; Kreuter, J. Biodistribution of polysorbate 80-coated doxorubicin-loaded [14C]-poly(butyl cyanoacrylate) nanoparticles after intravenous administration to glioblastoma-bearing rats. *J. Drug Target.*, **2006**, *14*, 97-105.
- [69] Jones, A.R.; Shusta, E.V. Blood-brain barrier transport of therapeutics via receptor-mediation. *Pharm. Res.*, **2007**, *24*, 1759-1771.
- [70] Mishra, V.; Mahor, S.; Rawat, A.; Gupta, P.N.; Dubey, P.; Khatri, K.; Vyas, S.P. Targeted brain delivery of AZT via transferrin anchored pegylated albumin nanoparticles. *J. Drug Target.*, **2006**, *14*, 45-53.
- [71] Pang, Z.; Gao, H.; Yu, Y.; Chen, J.; Guo, L.; Ren, J.; Wen, Z.; Su, J.; Jiang, X. Brain delivery and cellular internalization mechanisms for transferrin conjugated biodegradable polymersomes. *Int. J. Pharm.*, **2011**, *415*, 284-292.
- [72] Korkusuz, H.; Ulbrich, K.; Welzel, K.; Koeberle, V.; Watcharin, W.; Bahr, U.; Chernikov, V.; Knobloch, T.; Petersen, S.; Huebner, F.; Ackermann, H.; Gelperina, S.; Kromen, W.; Hammerstingl, R.; Hauptenthal, J.; Gruenwald, F.; Fiehler, J.; Zeuzem, S.; Kreuter, J.; Vogl, T.J.; Piiper, A. Transferrin-Coated Gadolinium Nanoparticles as MRI Contrast Agent. *Mol. Imaging Biol.*, **2013**, *15*, 148-154.
- [73] Ke, W.; Shao, K.; Huang, R.; Han, L.; Liu, Y.; Li, J.; Kuang, Y.; Ye, L.; Lou, J.; Jiang, C. Gene delivery targeted to the brain using an Angiopep-conjugated polyethyleneglycol-modified polyamidoamine dendrimer. *Biomaterials*, **2009**, *30*, 6976-6985.
- [74] Zensi, A.; Begley, D.; Pontikis, C.; Legros, C.; Mihoreanu, L.; Wagner, S.; Buchel, C.; von Briesen, H.; Kreuter, J. Albumin nanoparticles targeted with Apo E enter the CNS by transcytosis and are delivered to neurones. *J. Control. Release*, **2009**, *137*, 78-86.
- [75] Kim, H.R.; Gil, S.; Andrieux, K.; Nicolas, V.; Appel, M.; Chacun, H.; Desmaele, D.; Taran, F.; Georgin, D.; Couvreur, P. Low-density lipoprotein receptor-mediated endocytosis of PEGylated nanoparticles in rat brain endothelial cells. *Cell. Mol. Life Sci.*, **2007**, *64*, 356-364.

- [76] Michaelis, K.; Hoffmann, M.M.; Dreis, S.; Herbert, E.; Alyautdin, R.N.; Michaelis, M.; Kreuter, J.; Langer, K. Covalent linkage of apolipoprotein e to albumin nanoparticles strongly enhances drug transport into the brain. *J. Pharmacol. Exp. Ther.*, **2006**, *317*, 1246-1253.
- [77] Kreuter, J.; Hekmatara, T.; Dreis, S.; Vogel, T.; Gelperina, S.; Langer, K. Covalent attachment of apolipoprotein A-I and apolipoprotein B-100 to albumin nanoparticles enables drug transport into the brain. *J. Control. Release*, **2007**, *118*, 54-58.
- [78] Kim, H.R.; Andrieux, K.; Gil, S.; Taverna, M.; Chacun, H.; Desmaele, D.; Taran, F.; Georgin, D.; Couvreur, P. Translocation of poly(ethylene glycol-co-hexadecyl)cyanoacrylate nanoparticles into rat brain endothelial cells: role of apolipoproteins in receptor-mediated endocytosis. *Biomacromolecules*, **2007**, *8*, 793-799.
- [79] Mousazadeh, M.; Palizban, A.; Salehi, R.; Salehi, M. Gene delivery to brain cells with apoprotein E derived peptide conjugated to polylysine (apoEdp-PLL). *J. Drug Target.*, **2007**, *15*, 226-230.
- [80] Nikanjam, M.; Blakely, E.A.; Bjornstad, K.A.; Shu, X.; Budinger, T.F.; Forte, T.M. Synthetic nano-low density lipoprotein as targeted drug delivery vehicle for glioblastoma multiforme. *Int. J. Pharm.*, **2007**, *328*, 86-94.
- [81] Nikanjam, M.; Gibbs, A.R.; Hunt, C.A.; Budinger, T.F.; Forte, T.M. Synthetic nano-LDL with paclitaxel oleate as a targeted drug delivery vehicle for glioblastoma multiforme. *J. Control. Release*, **2007**, *124*, 163-171.
- [82] Prades, R.; Guerrero, S.; Araya, E.; Molina, C.; Salas, E.; Zurita, E.; Selva, J.; Egea, G.; Lopez-Iglesias, C.; Teixido, M.; Kogan, M.J.; Giralt, E. Delivery of gold nanoparticles to the brain by conjugation with a peptide that recognizes the transferrin receptor. *Biomaterials*, **2012**, *33*, 7194-7205.
- [83] Venishetty, V.K.; Komuravelli, R.; Kuncha, M.; Sistla, R.; Diwan, P.V. Increased brain uptake of docetaxel and ketoconazole loaded folate-grafted solid lipid nanoparticles. *Nanomedicine*, **2013**, 111-121.
- [84] Kuo, Y.C.; Yu, H.W. Transport of saquinavir across human brain-microvascular endothelial cells by poly(lactide-co-glycolide) nanoparticles with surface poly( $\gamma$ -glutamic acid). *Int. J. Pharm.*, **2011**, *416*, 365-375.
- [85] Lu, W.; Wan, J.; She, Z.; Jiang, X. Brain delivery property and accelerated blood clearance of cationic albumin conjugated pegylated nanoparticle. *J. Control. Release*, **2007**, *118*, 38-53.
- [86] Bhattacharya, R.; Osburg, B.; Fischer, D.; Bickel, U. Targeted delivery of complexes of biotin-PEG-polyethylenimine and NF- $\kappa$ B decoys to brain-derived endothelial cells *in vitro*. *Pharm. Res.*, **2008**, *25*, 605-615.
- [87] Xia, C.F.; Zhang, Y.; Boado, R.J.; Pardridge, W.M. Intravenous siRNA of brain cancer with receptor targeting and avidin-biotin technology. *Pharm. Res.*, **2007**, *24*, 2309-2316.
- [88] He, H.; Li, Y.; Jia, X.R.; Du, J.; Ying, X.; Lu, W.L.; Lou, J.N.; Wei, Y. PEGylated Poly(amidoamine) dendrimer-based dual-targeting carrier for treating brain tumors. *Biomaterials*, **2010**, *32*, 478-487.
- [89] van Rooy, I.; Kadir-Tascioglu, S.; Couraud, P.O.; Romero, I.A.; Weksler, B.; Storm, G.; Hennink, W.E.; Schiffelers, R.M.; Mastrobattista, E. Identification of peptide ligands for targeting to the blood-brain barrier. *Pharm. Res.*, **2010**, *27*, 673-682.
- [90] Teixido, M.; Zurita, E.; Malakoutikhah, M.; Tarrago, T.; Giralt, E. Diketopiperazines as a tool for the study of transport across the blood-brain barrier (BBB) and their potential use as BBB-shuttles. *J. Am. Chem. Soc.*, **2007**, *129*, 11802-11813.
- [91] Kabanov, A.V.; Batrakova, E.V.; Miller, D.W. Pluronic block copolymers as modulators of drug efflux transporter activity in the blood-brain barrier. *Adv. Drug Deliv. Rev.*, **2003**, *55*, 151-164.
- [92] Li, M.; Si, L.; Pan, H.; Rabba, A.K.; Yan, F.; Qiu, J.; Li, G. Excipients enhance intestinal absorption of ganciclovir by P-gp inhibition: assessed *in vitro* by everted gut sac and *in situ* by improved intestinal perfusion. *Int. J. Pharm.*, **2010**, *403*, 37-45.
- [93] Zabaleta, V.; Ponchel, G.; Salman, H.; Agueros, M.; Vauthier, C.; Irache, J.M. Oral administration of paclitaxel with pegylated poly(anhydride) nanoparticles: Permeability and pharmacokinetic study. *Eur. J. Pharm. Biopharm.*, **2012**, *81*, 514-523.
- [94] Nagy, H.; Goda, K.; Arceci, R.; Cianfriglia, M.; Mechetner, E.; Szabo, G. Jr. P-Glycoprotein conformational changes detected by antibody competition. *Eur. J. Biochem.*, **2001**, *268*, 2416-2420.
- [95] Holpuch, A.S.; Hummel, G.J.; Tong, M.; Seghi, G.A.; Pei, P.; Ma, P.; Mumper, R.J.; Mallery, S.R. Nanoparticles for local drug delivery to the oral mucosa: proof of principle studies. *Pharm. Res.*, **2010**, *27*, 1224-1236.
- [96] Zhang, P.; Ling, G.; Pan, X.; Sun, J.; Zhang, T.; Pu, X.; Yin, S.; He, Z. Novel nanostructured lipid-dextran sulfate hybrid carriers overcome tumor multidrug resistance of mitoxantrone hydrochloride. *Nanomedicine*, **2011**, *8*, 185-193.
- [97] Lalatsa, A.; Garrett, N.L.; Ferrarelli, T.; Moger, J.; Schatzlein, A.G.; Uchegbu, I.F. Delivery of peptides to the blood and brain after oral uptake of quaternary ammonium palmitoyl glycol chitosan nanoparticles. *Mol. Pharm.*, **2012**, *9*, 1764-1774.
- [98] Gao, H.; Qian, J.; Cao, S.; Yang, Z.; Pang, Z.; Pan, S.; Fan, L.; Xi, Z.; Jiang, X.; Zhang, Q. Precise glioma targeting of and penetration by aptamer and peptide dual-functional nanoparticles. *Biomaterials*, **2012**, *33*, 5115-5123.
- [99] Rivet, C.J.; Yuan, Y.; Borca-Tasciuc, D.A.; Gilbert, R.J. Altering iron oxide nanoparticle surface properties induce cortical neuron cytotoxicity. *Chem. Res. Toxicol.*, **2011**, *25*, 153-161.
- [100] Andresen, T.L.; Jensen, S.S.; Jorgensen, K. Advanced strategies in liposomal cancer therapy: problems and prospects of active and tumor specific drug release. *Prog. Lipid Res.*, **2005**, *44*, 68-97.
- [101] Boado, R.J. Blood-brain barrier transport of non-viral gene and RNAi therapeutics. *Pharm. Res.*, **2007**, *24*, 1772-1787.
- [102] Xie, F.; Yao, N.; Qin, Y.; Zhang, Q.; Chen, H.; Yuan, M.; Tang, J.; Li, X.; Fan, W.; Wu, Y.; Hai, L.; He, Q. Investigation of glucose-modified liposomes using polyethylene glycols with different chain lengths as the linkers for brain targeting. *Int. J. Nanomedicine*, **2012**, *7*, 163-175.
- [103] Chen, H.; Tang, L.; Qin, Y.; Yin, Y.; Tang, J.; Tang, W.; Sun, X.; Zhang, Z.; Liu, J.; He, Q. Lactoferrin-modified procationic liposomes as a novel drug carrier for brain delivery. *Eur. J. Pharm. Sci.*, **2010**, *40*, 94-102.
- [104] Patel, N.R.; Rathi, A.; Mongayt, D.; Torchilin, V.P. Reversal of multidrug resistance by co-delivery of tariquidar (XR9576) and paclitaxel using long-circulating liposomes. *Int. J. Pharm.*, **2011**, *416*, 296-299.
- [105] Sun, X.; Pang, Z.; Ye, H.; Qiu, B.; Guo, L.; Li, J.; Ren, J.; Qian, Y.; Zhang, Q.; Chen, J.; Jiang, X. Co-delivery of pEGFP-hTRAIL and paclitaxel to brain glioma mediated by an angiopep-conjugated liposome. *Biomaterials*, **2011**, *33*, 916-924.
- [106] Guo, L.; Fan, L.; Pang, Z.; Ren, J.; Ren, Y.; Li, J.; Chen, J.; Wen, Z.; Jiang, X. TRAIL and doxorubicin combination enhances anti-glioblastoma effect based on passive tumor targeting of liposomes. *J. Control. Release*, **2011**, *154*, 93-102.
- [107] Carafa, M.; Marianecchi, C.; Di Marzio, L.; De Caro, V.; Giandalia, G.; Giannola, L.I.; Santucci, E. Potential dopamine prodrug-loaded liposomes: preparation, characterization, and *in vitro* stability studies. *J. Liposome Res.*, **2009**, *20*, 250-257.
- [108] van Rooy, I.; Wu, S.Y.; Storm, G.; Hennink, W.E.; Dinter-Heidorn, H.; Schiffelers, R.M.; Mastrobattista, E. Preparation and characterization of liposomal formulations of neurotensin-degrading enzyme inhibitors. *Int. J. Pharm.*, **2011**, *416*, 448-452.
- [109] Ghosh, S.; Das, N.; Mandal, A.K.; Ddung, S.R.; Sarkar, S. Mannosylated liposomal cytidine 5' diphosphocholine prevent age related global moderate cerebral ischemia reperfusion induced mitochondrial cytochrome c release in aged rat brain. *Neuroscience*, **2010**, *171*, 1287-1299.
- [110] Ishii, T.; Asai, T.; Oyama, D.; Fukuta, T.; Yasuda, N.; Shimizu, K.; Minamino, T.; Oku, N. Amelioration of cerebral ischemia-reperfusion injury based on liposomal drug delivery system with asialo-erythropoietin. *J. Control. Release*, **2012**, *160*, 81-87.
- [111] Gaillard, P.J.; Appeldoorn, C.C.; Rip, J.; Dorland, R.; van der Pol, S.M.; Kooij, G.; de Vries, H.E.; Reijkerker, A. Enhanced brain delivery of liposomal methylprednisolone improved therapeutic efficacy in a model of neuroinflammation. *J. Control. Release*, **2012**, doi: 10.1016/j.jconrel.2012.06.022.
- [112] Pardridge, W.M. Preparation of Trojan horse liposomes (THLs) for gene transfer across the blood-brain barrier. *Cold Spring Harb. Protoc.*, **2010**, pdb.prot5407.
- [113] Pulford, B.; Reim, N.; Bell, A.; Veatch, J.; Forster, G.; Bender, H.; Meyerett, C.; Hafeman, S.; Michel, B.; Johnson, T.; Wyckoff, A.C.; Miele, G.; Julius, C.; Kranich, J.; Schenkel, A.; Dow, S.; Zabel, M.D. Liposome-siRNA-peptide complexes cross the blood-brain barrier and significantly decrease PrP on neuronal cells and PrP in infected cell cultures. *PLoS One*, **2010**, *5*, 11085-11098.
- [114] Gong, W.; Wang, Z.; Liu, N.; Lin, W.; Wang, X.; Xu, D.; Liu, H.; Zeng, C.; Xie, X.; Mei, X.; Lu, W. Improving efficiency of

- adriamycin crossing blood brain barrier by combination of thermosensitive liposomes and hyperthermia. *Biol. Pharm. Bull.*, **2011**, *34*, 1058-1064.
- [115] Saiyed, Z.M.; Gandhi, N.H.; Nair, M.P. Magnetic nanoformulation of azidothymidine 5'-triphosphate for targeted delivery across the blood-brain barrier. *Int. J. Nanomedicine*, **2010**, *5*, 157-166.
- [116] Oku, N.; Yamashita, M.; Katayama, Y.; Urakami, T.; Hatanaka, K.; Shimizu, K.; Asai, T.; Tsukada, H.; Akai, S.; Kanazawa, H. PET imaging of brain cancer with positron emitter-labeled liposomes. *Int. J. Pharm.*, **2010**, *403*, 170-177.
- [117] Doi, A.; Kawabata, S.; Iida, K.; Yokoyama, K.; Kajimoto, Y.; Kuroiwa, T.; Shirakawa, T.; Kirihata, M.; Kasaoka, S.; Maruyama, K.; Kumada, H.; Sakurai, Y.; Masunaga, S.; Ono, K.; Miyatake, S. Tumor-specific targeting of sodium borocaptate (BSH) to malignant glioma by transferrin-PEG liposomes: a modality for boron neutron capture therapy. *J. Neurooncol.*, **2008**, *87*, 287-294.
- [118] Re, F.; Cambianica, I.; Zona, C.; Sesana, S.; Gregori, M.; Rigolio, R.; La Ferla, B.; Nicotra, F.; Forloni, G.; Cagnotto, A.; Salmona, M.; Masserini, M.; Sancini, G. Functionalization of liposomes with ApoE-derived peptides at different density affects cellular uptake and drug transport across a blood-brain barrier model. *Nanomedicine*, **2011**, *7*, 551-559.
- [119] Kopecka, J.; Campia, I.; Olivero, P.; Pescarmona, G.; Ghigo, D.; Bosia, A.; Riganti, C. A LDL-masked liposomal-doxorubicin reverses drug resistance in human cancer cells. *J. Control. Release*, **2010**, *149*, 196-205.
- [120] Pinzon-Daza, M.L.; Garzon, R.; Couraud, P.O.; Romero, I.A.; Weksler, B.; Ghigo, D.; Bosia, A.; Riganti, C. The association of statins plus LDL receptor-targeted liposome-encapsulated doxorubicin increases the *in vitro* drug delivery across blood-brain barrier cells. *Br. J. Pharmacol.*, **2012**, doi: 10.1111/j.1476-5381.2012.02103.x.
- [121] Riganti, C.; Orecchia, S.; Pescarmona, G.; Betta, P.G.; Ghigo, D.; Bosia, A. Statins revert doxorubicin resistance via nitric oxide in malignant mesothelioma. *Int. J. Cancer*, **2006**, *119*, 17-27.
- [122] Markoutsas, E.; Papadia, K.; Clemente, C.; Flores, O.; Antimisariis, S.G. Anti-Abeta-MAb and dually decorated nanoliposomes: effect of Abeta1-42 peptides on interaction with hCMC/D3 cells. *Eur. J. Pharm. Biopharm.*, **2012**, *8*, 49-56.
- [123] Ying, X.; Wen, H.; Lu, W.L.; Du, J.; Guo, J.; Tian, W.; Men, Y.; Zhang, Y.; Li, R.J.; Yang, T.Y.; Shang, D.W.; Lou, J.N.; Zhang, L.R.; Zhang, Q. Dual-targeting daunorubicin liposomes improve the therapeutic efficacy of brain glioma in animals. *J. Control. Release*, **2009**, *141*, 183-192.
- [124] Sharma, G.; Modgil, A.; Sun, C.; Singh, J. Grafting of cell-penetrating peptide to receptor-targeted liposomes improves their transfection efficiency and transport across blood-brain barrier model. *J. Pharm. Sci.*, **2012**, *101*, 2468-2478.
- [125] van Rooy, I.; Hennink, W.E.; Storm, G.; Schiffelers, R.M.; Mastrobattista, E. Attaching the phage display-selected GLA peptide to liposomes: factors influencing target binding. *Eur. J. Pharm. Sci.*, **2011**, *45*, 330-335.
- [126] Kobayashi, T.; Ishida, T.; Okada, Y.; Ise, S.; Harashima, H.; Kiwada, H. Effect of transferrin receptor-targeted liposomal doxorubicin in P-glycoprotein-mediated drug resistant tumor cells. *Int. J. Pharm.*, **2007**, *329*, 94-102.
- [127] Zalipsky, S.; Saad, M.; Kiwan, R.; Ber, E.; Yu, N.; Minko, T. Antitumor activity of new liposomal prodrug of mitomycin C in multidrug resistant solid tumor: insights of the mechanism of action. *J. Drug Target.*, **2007**, *15*, 518-530.
- [128] Thierry, A.R.; Dritschilo, A.; Rahman, A. Effect of liposomes on P-glycoprotein function in multidrug resistant cells. *Biochem. Biophys. Res. Commun.*, **1992**, *187*, 1098-1105.
- [129] Riganti, C.; Voena, C.; Kopecka, J.; Corsetto, P.A.; Montorfano, G.; Enrico, E.; Costamagna, C.; Rizzo, A.M.; Ghigo, D.; Bosia, A. Liposome-encapsulated doxorubicin reverses drug resistance by inhibiting P-glycoprotein in human cancer cells. *Mol. Pharm.*, **2011**, *8*, 683-700.
- [130] Cui, J.; Li, C.; Guo, W.; Li, Y.; Wang, C.; Zhang, L.; Hao, Y.; Wang, Y. Direct comparison of two pegylated liposomal doxorubicin formulations: is AUC predictive for toxicity and efficacy? *J. Control. Release*, **2007**, *118*, 204-215.
- [131] Hau, P.; Fabel, K.; Baumgart, U.; Rummele, P.; Grauer, O.; Bock, A.; Dietmaier, C.; Dietmaier, W.; Dietrich, J.; Dudel, C.; Hubner, F.; Jauch, T.; Drechsel, E.; Kleiter, I.; Wismeth, C.; Zellner, A.; Brawanski, A.; Steinbrecher, A.; Marienhagen, J.; Bogdahn, U. Pegylated liposomal doxorubicin-efficacy in patients with recurrent high-grade glioma. *Cancer*, **2004**, *100*, 1199-1207.
- [132] Glas, M.; Koch, H.; Hirschmann, B.; Jauch, T.; Steinbrecher, A.; Herrlinger, U.; Bogdahn, U.; Hau, P. Pegylated liposomal doxorubicin in recurrent malignant glioma: analysis of a case series. *Oncology*, **2007**, *72*, 302-307.
- [133] Verreault, M.; Strutt, D.; Masin, D.; Anantha, M.; Yung, A.; Kozlowski, P.; Waterhouse, D.; Bally, M.B.; Yapp, D.T. Vascular normalization in orthotopic glioblastoma following intravenous treatment with lipid-based nanoparticle formulations of irinotecan (Irinophore C), doxorubicin (Caelyx(R)) or vincristine. *BMC Cancer*, **2011**, *11*, 124-132.
- [134] Ogawara, K.; Un, K.; Tanaka, K.; Higaki, K.; Kimura, T. *In vivo* anti-tumor effect of PEG liposomal doxorubicin (DOX) in DOX-resistant tumor-bearing mice: Involvement of cytotoxic effect on vascular endothelial cells. *J. Control. Release*, **2009**, *133*, 4-10.
- [135] Zhang, Y.F.; Boado, R.J.; Pardridge, W.M. Absence of toxicity of chronic weekly intravenous gene therapy with pegylated immunoliposomes. *Pharm. Res.*, **2003**, *20*, 1779-1785.
- [136] Van Meir, E.G.; Hadjipanayis, C.G.; Norden, A.D.; Shu, H.K.; Wen, P.Y.; Olson, J.J. Exciting new advances in neuro-oncology: the avenue to a cure for malignant glioma. *CA. Cancer J. Clin.*, **2010**, *60*, 166-193.
- [137] Kamar, F.G.; Posner, J.B. Brain metastases. *Semin. Neurol.*, **2010**, *30*, 217-235.
- [138] Lockman, P.R.; Mittapalli, R.K.; Taskar, K.S.; Rudraraju, V.; Gril, B.; Bohn, K.A.; Adkins, C.E.; Roberts, A.; Thorsheim, H.R.; Gaasch, J.A.; Huang, S.; Palmieri, D.; Steeg, P.S.; Smith, Q.R. Heterogeneous blood-tumor barrier permeability determines drug efficacy in experimental brain metastases of breast cancer. *Clin. Cancer Res.*, **2010**, *16*, 5664-5668.
- [139] Ruoslahti, E.; Bhatia, S.N.; Sailor, M.J. Targeting of drugs and nanoparticles to tumors. *J. Cell. Biol.*, **2010**, *188*, 759-768.
- [140] Madhankumar, A.B.; Slagle-Webb, B.; Wang, X.; Yang, Q.X.; Antonetti, D.A.; Miller, P.A.; Sheehan, J.M.; Connor, J.R. Efficacy of interleukin-13 receptor-targeted liposomal doxorubicin in the intracranial brain tumor model. *Mol. Cancer Ther.*, **2009**, *8*, 648-654.
- [141] Steiniger, S.C.; Kreuter, J.; Khalansky, A.S.; Skidan, I.N.; Bobruskin, A.I.; Smirnova, Z.S.; Severin, S.E.; Uhl, R.; Kock, M.; Geiger, K.D.; Gelperina, S.E. Chemotherapy of glioblastoma in rats using doxorubicin-loaded nanoparticles. *Int. J. Cancer*, **2004**, *109*, 759-767.
- [142] Beier, C.P.; Schmid, C.; Gorka, T.; Kleinletzenberger, C.; Beier, D.; Grauer, O.; Steinbrecher, A.; Hirschmann, B.; Brawanski, A.; Dietmaier, C.; Jauch-Worley, T.; Kolbl, O.; Pietsch, T.; Proescholdt, M.; Rummele, P.; Muigg, A.; Stockhammer, G.; Hegi, M.; Bogdahn, U.; Hau, P. RNOP-09: pegylated liposomal doxorubicin and prolonged temozolomide in addition to radiotherapy in newly diagnosed glioblastoma--a phase II study. *BMC Cancer*, **2009**, *9*, 308-318.
- [143] Ananda, S.; Nowak, A.K.; Cher, L.; Dowling, A.; Brown, C.; Simes, J.; Rosenthal, M.A. Phase 2 trial of temozolomide and pegylated liposomal doxorubicin in the treatment of patients with glioblastoma multiforme following concurrent radiotherapy and chemotherapy. *J. Clin. Neurosci.*, **2011**, *18*, 1444-1448.
- [144] Huang, S.; Li, J.; Han, L.; Liu, S.; Ma, H.; Huang, R.; Jiang, C. Dual targeting effect of Angiopep-2-modified, DNA-loaded nanoparticles for glioma. *Biomaterials*, **2011**, *32*, 6832-6838.
- [145] Jin, J.; Bae, K.H.; Yang, H.; Lee, S.J.; Kim, H.; Kim, Y.; Joo, K.M.; Seo, S.W.; Park, T.G.; Nam, D.H. *In vivo* specific delivery of c-Met siRNA to glioblastoma using cationic solid lipid nanoparticles. *Bioconjug. Chem.*, **2011**, *22*, 2568-2572.
- [146] Spitzenberger, T.J.; Heilman, D.; Diekmann, C.; Batakova, E.V.; Kabanov, A.V.; Gendelman, H.E.; Elmquist, W.F.; Persidsky, Y. Novel delivery system enhances efficacy of antiretroviral therapy in animal model for HIV-1 encephalitis. *J. Cereb. Blood Flow Metab.*, **2007**, *27*, 1033-1042.
- [147] Pereira de Oliveira, M.; Garcion, E.; Venisse, N.; Benoit, J.P.; Couet, W.; Olivier, J.C. Tissue distribution of indinavir administered as solid lipid nanocapsule formulation in mdr1a (+/+) and mdr1a (-/-) CF-1 mice. *Pharm. Res.*, **2005**, *22*, 1898-1905.
- [148] Kuo, Y.C.; Lee, C.L. Methylmethacrylate-sulfopropylmethacrylate nanoparticles with surface RMP-7 for targeting delivery of antiretroviral drugs across the blood-brain barrier. *Colloids Surf. B Biointerfaces*, **2011**, *90*, 75-82.

- [149] Mahajan, S.D.; Roy, I.; Xu, G.; Yong, K.T.; Ding, H.; Aalinkeel, R.; Reynolds, J.; Sykes, D.; Nair, B.B.; Lin, E.Y.; Prasad, P.N.; Schwartz, S.A. Enhancing the delivery of anti retroviral drug "Saquinavir" across the blood brain barrier using nanoparticles. *Curr. HIV Res.*, **2010**, *8*, 396-404.
- [150] Parboosing, R.; Maguire, G.E.; Govender, P.; Kruger, H.G. Nanotechnology and the treatment of HIV infection. *Viruses*, **2012**, *4*, 488-520.
- [151] Jimenez, J.L.; Clemente, M.I.; Weber, N.D.; Sanchez, J.; Ortega, P.; de la Mata, F.J.; Gomez, R.; Garcia, D.; Lopez-Fernandez, L.A.; Munoz-Fernandez, M.A. Carbosilane dendrimers to transfect human astrocytes with small interfering RNA targeting human immunodeficiency virus. *BioDrugs*, **2010**, *24*, 331-343.
- [152] Fazil, M.; Shadab; Baboota, S.; Sahni, J.K.; Ali, J. Nanotherapeutics for Alzheimer's disease (AD): Past, present and future. *J. Drug Target.*, **2011**, *20*, 97-113.
- [153] Jaruszewski, K.M.; Ramakrishnan, S.; Poduslo, J.F.; Kandimalla, K.K. Chitosan enhances the stability and targeting of immunonanovehicles to cerebro-vascular deposits of Alzheimer's disease amyloid protein. *Nanomedicine*, **2011**, *8*, 250-260.
- [154] Mathew, A.; Fukuda, T.; Nagaoka, Y.; Hasumura, T.; Morimoto, H.; Yoshida, Y.; Maekawa, T.; Venugopal, K.; Kumar, D.S. Curcumin loaded-PLGA nanoparticles conjugated with Tet-1 peptide for potential use in Alzheimer's disease. *PLoS One*, **2012**, *7*, 32616-32626.
- [155] Re, F.; Cambianica, I.; Sesana, S.; Salvati, E.; Cagnotto, A.; Salmona, M.; Couraud, P.O.; Moghimi, S.M.; Masserini, M.; Sancini, G. Functionalization with ApoE-derived peptides enhances the interaction with brain capillary endothelial cells of nanoliposomes binding amyloid-beta peptide. *J. Biotechnol.*, **2011**, *156*, 341-346.
- [156] Md, S.; Haque, S.; Sahni, J.K.; Baboota, S.; Ali, J. New non-oral drug delivery systems for Parkinson's disease treatment. *Expert. Opin. Drug Deliv.*, **2011**, *8*, 359-374.
- [157] Loscher, W.; Luna-Tortos, C.; Romermann, K.; Fedrowitz, M. Do ATP-binding cassette transporters cause pharmacoresistance in epilepsy? Problems and approaches in determining which antiepileptic drugs are affected. *Curr. Pharm. Des.*, **2011**, *17*, 2808-2828.
- [158] Lazarowski, A.; Czornyj, L.; Lubienieki, F.; Girardi, E.; Vazquez, S.; D'Giano, C. ABC transporters during epilepsy and mechanisms underlying multidrug resistance in refractory epilepsy. *Epilepsia*, **2007**, *48*, 140-149.
- [159] Bennewitz, M.F.; Saltzman, W.M. Nanotechnology for delivery of drugs to the brain for epilepsy. *Neurotherapeutics*, **2009**, *6*, 323-336.
- [160] Wang, S.; Jiang, T.; Ma, M.; Hu, Y.; Zhang, J. Preparation and evaluation of anti-neuroexcitation peptide (ANEP) loaded N-trimethyl chitosan chloride nanoparticles for brain-targeting. *Int. J. Pharm.*, **2009**, *386*, 249-255.
- [161] Miladi, I.; Le Duc, G.; Kryza, D.; Berniard, A.; Mowat, P.; Roux, S.; Taleb, J.; Bonazza, P.; Perriat, P.; Lux, F.; Tillement, O.; Billorey, C.; Janier, M. Biodistribution of ultra small gadolinium-based nanoparticles as theranostic agent: Application to brain tumors. *J. Biomater. Appl.*, **2012**, doi: 10.1177/0885328212454315.

## FEATURE ARTICLE

# The cross-talk between canonical and non-canonical Wnt-dependent pathways regulates P-glycoprotein expression in human blood–brain barrier cells

Martha L Pinzón-Daza<sup>1,2</sup>, Iris C Salaroglio<sup>1</sup>, Joanna Kopecka<sup>1</sup>, Ruth Garzón<sup>2</sup>, Pierre-Olivier Couraud<sup>3</sup>, Dario Ghigo<sup>1,4</sup> and Chiara Riganti<sup>1,4</sup>

In this work, we investigate if and how transducers of the ‘canonical’ Wnt pathway, i.e., Wnt/glycogen synthase kinase 3 (GSK3)/ $\beta$ -catenin, and transducers of the ‘non-canonical’ Wnt pathway, i.e., Wnt/RhoA/RhoA kinase (RhoAK), cooperate to control the expression of P-glycoprotein (Pgp) in blood–brain barrier (BBB) cells. By analyzing human primary brain microvascular endothelial cells constitutively activated for RhoA, silenced for RhoA or treated with the RhoAK inhibitor Y27632, we found that RhoAK phosphorylated and activated the protein tyrosine phosphatase 1B (PTP1B), which dephosphorylated tyrosine 216 of GSK3, decreasing the GSK3-mediated inhibition of  $\beta$ -catenin. By contrast, the inhibition of RhoA/RhoAK axis prevented the activation of PTP1B, enhanced the GSK3-induced phosphorylation and ubiquitination of  $\beta$ -catenin, and reduced the  $\beta$ -catenin-driven transcription of Pgp. The RhoAK inhibition increased the delivery of Pgp substrates like doxorubicin across the BBB and improved the doxorubicin efficacy against glioblastoma cells co-cultured under a BBB monolayer. Our data demonstrate that in human BBB cells the expression of Pgp is controlled by a cross-talk between canonical and non-canonical Wnt pathways. The disruption of this cross-talk, e.g., by inhibiting RhoAK, downregulates Pgp and increases the delivery of Pgp substrates across the BBB.

*Journal of Cerebral Blood Flow & Metabolism* (2014) **34**, 1258–1269; doi:10.1038/jcbfm.2014.100; published online 4 June 2014

**Keywords:** blood–brain barrier;  $\beta$ -catenin; glycogen synthase kinase 3; P-glycoprotein; RhoA kinase; Wnt

## INTRODUCTION

The blood–brain barrier (BBB), a peculiar microvascular endothelium in the central nervous system, limits the delivery of drugs, xenobiotics, and toxic catabolites into the brain parenchyma, owing to the absence of fenestrations, the abundance of tight junctions and adherens junctions, and the presence of efflux transporters belonging to the ATP binding cassette family.<sup>1</sup> P-glycoprotein (Pgp) is one of the ATP binding cassette transporters present on the luminal side of BBB cells: it effluxes back into the bloodstream several chemotherapeutic drugs (e.g., anthracyclines, taxanes, Vinca alkaloids, epipodophyllotoxins, topotecan, methotrexate, imatinib, dasatinib, lapatinib, gefitinib, sorafenib, erlotinib), analgesics, anti-epileptics, anti-retrovirals, and antibiotics.<sup>1</sup>

The Wnt signaling has a central role in regulating the expression of Pgp in BBB cells<sup>2,3</sup> and relies on the simultaneous activation of different intracellular transducers. In the so-called ‘Wnt canonical pathway’, the soluble Wnt proteins bind to the Frizzled receptor and the low-density lipoprotein receptor-related protein-5 and -6 co-receptors, reduces the activity of glycogen synthase kinase 3 (GSK3), allowing the release of  $\beta$ -catenin from the cytosolic adenomatous polyposis coli–axin complex and its translocation into the nucleus. Here  $\beta$ -catenin binds to the T-cell factor/lymphoid

enhancer factor and induces the transcription of target genes, such as *mdr1*, which encodes for Pgp.<sup>4,5</sup> We recently demonstrated that the disruption of the Wnt3 canonical pathway downregulates the Pgp expression in human BBB cells.<sup>6</sup>

A plethora of intracellular transducers is involved in the so-called ‘non-canonical Wnt pathways’. By interacting with Frizzled, Wnt recruits Disheveled, stimulates the small GTPases RhoA and Rac, activates RhoA kinase (RhoAK), mitogen-activated protein kinase kinases, mitogen-activated protein kinases, and Jun N-terminal kinase.<sup>4,7</sup> By interacting with the co-receptors ROR2 and RYK, Wnt enhances the activity of phospholipase C, increases the intracellular calcium, activates protein kinase C and calmodulin kinases.<sup>4</sup> Wnt canonical and non-canonical pathways are often reciprocally modulated, with either cooperative or antagonistic effects.<sup>8,9</sup>

The Wnt non-canonical transducers RhoA and RhoAK regulate the integrity of tight junctions and the paracellular transport of substrates across BBB,<sup>10</sup> as well as the activity of Pgp.<sup>11</sup> It is not known whether Wnt/RhoA/RhoAK pathway controls also the expression of Pgp.

Aim of this work is to investigate if there are cross-talk mechanisms between the Wnt/GSK3/ $\beta$ -catenin canonical pathway and the Wnt/RhoA/RhoAK non-canonical pathway in human BBB

<sup>1</sup>Department of Oncology, School of Medicine, University of Turin, Turin, Italy; <sup>2</sup>Unidad de Bioquímica, Facultad de Ciencias Naturales y Matemáticas, Universidad del Rosario, Bogotá, Colombia; <sup>3</sup>Institut Cochin, Centre National de la Recherche Scientifique UMR 8104, Institut National de la Santé et de la Recherche Médicale (INSERM) U567, Université René Descartes, Paris, France and <sup>4</sup>Center for Experimental Research and Medical Studies, University of Turin, Turin, Italy. Correspondence: Professor D Ghigo, Department of Oncology, University of Turin, via Santena 5/bis, Turin 10126, Italy. E-mail: dario.ghigo@unito.it

This work has been supported by grants from Compagnia di San Paolo, Italy (Neuroscience Program; grant 2008.1136), Italian Association for Cancer Research (AIRC; grant MFAG 11475), Italian Ministry of University and Research (Future in Research FIRB 2012 Program; grant RBF1250Q1) to CR. MLP-D and RG are recipients of a ERACOL Erasmus Mundus fellowship provided by EU. JK is recipient of a ‘Mario and Valeria Rindi’ fellowship provided by Italian Foundation for Cancer Research (FIRC).

Received 24 December 2013; revised 19 March 2014; accepted 13 April 2014; published online 4 June 2014

cells, and how these cross-talks control the expression of Pgp and the delivery of Pgp substrates across BBB.

## MATERIALS AND METHODS

### Chemicals

The plasticware for cell cultures was from Falcon (Becton Dickinson, Franklin Lakes, NJ, USA). Wnt activators (WntA) [2-amino-4-(3,4-(methylene-dioxy)benzylamino)-6-(3-methoxyphenyl)pyrimidine] and Y27632 were purchased from Calbiochem (San Diego, CA, USA). Human recombinant Dickkopf-1 (Dkk-1) was from R&D Systems (Minneapolis, MN, USA). Rho activator II, a synthetic derivative of cytotoxic necrotizing factor from *Escherichia coli* that maintains RhoA constitutively activated,<sup>12</sup> was from Cytoskeleton (Denver, CO, USA). The electrophoresis reagents were obtained from Bio-Rad Laboratories (Hercules, CA, USA). The protein content of cell lysates was assessed with the BCA kit from Sigma Chemicals (St Louis, MO, USA). When not otherwise specified, all the other reagents were purchased from Sigma Chemicals.

### Cells

The hCMEC/D3 cells, a primary human brain microvascular endothelial cell line that retains the BBB characteristics *in vitro*,<sup>13</sup> were seeded at 50,000/cm<sup>2</sup> density, grown for 7 days up to confluence in Petri dishes or Transwell devices (0.4 μm diameter pore size, Corning Life Sciences, Corning, France), and cultured as previously reported.<sup>13</sup>

The primary human glioblastoma cells (CV17, 01010627, Nov3) were obtained from surgical samples of patients from the Neuro-Oncology Center, Vercelli, Italy and the DIBIT San Raffaele Scientific Institute, Milan, Italy. The tumor diagnosis was performed according to WHO guidelines. The U87-MG cell line was purchased from ATCC (Manassas, VA, USA). The cells were cultured as already reported.<sup>6</sup> The experimental protocols were approved by the Bioethics Committee ('Comitato di Bioetica d'Ateneo'), University of Turin, Italy.

In co-culture experiments, 500,000 (for intracellular doxorubicin accumulation, cytotoxicity assays and cell cycle analysis) or 1,000 (for proliferation assay) glioblastoma cells were added in the lower chamber of Transwell devices 4 days after seeding hCMEC/D3 cells in the Transwell insert. After 3 days of co-culture, the medium of the upper chamber was replaced with fresh medium or with medium containing Y27632 and doxorubicin, alone or in combination, as detailed in the Figure legends.

### Western Blot Analysis

The cells were rinsed with lysis buffer (50 mmol/L Tris, 10 mmol/L EDTA, 1% v/v Triton X-100), supplemented with the protease inhibitor cocktail set III (80 μmol/L aprotinin, 5 mmol/L bestatin, 1.5 mmol/L leupeptin, 1 mmol/L pepstatin; Calbiochem), 2 mmol/L phenylmethylsulfonyl fluoride and 1 mmol/L NaVO<sub>4</sub>, then sonicated and centrifuged at 13,000 g for 10 minutes at 4°C. A quantity of 20 μg protein extracts were subjected to SDS–PAGE and probed with the following antibodies: anti-GSK3 (BD Biosciences, Franklin Lakes, NJ, USA); anti-phospho(Tyr216)GSK3 (BD Biosciences); anti-β-catenin (BD Biosciences); anti-phospho(Ser33/Ser37/Thr41)β-catenin (Cell Signaling Technology, Danvers, MA, USA); anti-claudin 3 (Invitrogen Life Technologies, Monza, Italy); anti-claudin 5 (Invitrogen Life Technologies); anti-occludin (Invitrogen Life Technologies); anti-zonula occludens-1 (Invitrogen Life Technologies); anti-protein tyrosine phosphatase 1B (PTP1B; Abcam, Cambridge, UK); anti-phospho(Ser50)PTP1B (Abcam); anti-Pgp (clone C219, Calbiochem); anti-multidrug resistance-related protein 1 (MRP1; Abcam); anti-breast cancer resistance protein (BCRP; Santa Cruz Biotechnology, Santa Cruz, CA, USA); anti-caspase-3 (C33, GeneTex, Hsinhu City, Taiwan); anti-β-tubulin (Santa Cruz Biotechnology), followed by a peroxidase-conjugated secondary antibody (Bio-Rad). The membranes were washed with Tris-buffered saline-Tween 0.1% v/v, and the proteins were detected by enhanced chemiluminescence (Bio-Rad).

To assess the presence of ubiquitinated β-catenin, 100 μg of proteins from whole-cell extracts were immunoprecipitated with the anti-β-catenin antibody, using the PureProteome protein A and protein G Magnetic Beads (Millipore, Billerica, MA, USA). The immunoprecipitated proteins were separated by SDS–PAGE and probed with an anti-ubiquitin antibody (Enzo Life Science, Farmingdale, NY, USA), followed by a peroxidase-conjugated secondary antibody.

A quantity of 10 μg of nuclear extracts, obtained with the Nuclear Extraction Kit (Active Motif, Rixensart, Belgium), was subjected to western blot analysis using an anti-β-catenin antibody. To check the equal control

loading in nuclear fractions, the samples were probed with an anti-TATA-binding protein (TBP/TFIID) antibody (Santa Cruz Biotechnology). To exclude any cytosolic contamination of nuclear extracts, we verified that β-tubulin was undetectable in nuclear samples (not shown).

The densitometric analysis of western blots was performed with the ImageJ software (<http://rsb.info.nih.gov/ij/>) and expressed as arbitrary units, where '1 unit' is the mean band density of untreated hCMEC/D3 cells.

### Chromatin Immunoprecipitation

The chromatin immunoprecipitation experiments were performed using the Magna ChIP A/G Chromatin Immunoprecipitation Kit (Millipore). The samples were immunoprecipitated with 5 μg of an anti-β-catenin antibody or with no antibody. The immunoprecipitated DNA was washed and eluted twice with 100 μL of elution buffer (0.1 mol/L NaHCO<sub>3</sub>, 1% w/v SDS), the cross-linking was reversed by incubating the samples at 65°C for 6 hours. The samples were then treated with 1 μL proteinase K for 1 hour at 55°C. The DNA was eluted in 50 μL of H<sub>2</sub>O and analyzed by quantitative real-time PCR (qRT–PCR). The putative β-catenin site on *mdr1* promoter was validated by the MatInspector software (<http://www.genomatix.de/>); the primers sequences were: 5'-CGATCCGCTAAGAACAAG-3'; 5'-AGCACAAATGAAGGAAGGAG-3'. As negative control, the immunoprecipitated samples were subjected to PCR with primers matching a region 10,000 bp upstream the *mdr1* promoter, using the following primers: 5'-GTGGTGCCTGAGGAAGAGAG-3'; 5'-GCAACAAGTAGGCACAAGCA-3'. The qRT–PCR was carried out using an IQ SYBR Green Supermix (Bio-Rad); the data were analyzed with a Bio-Rad Software Gene Expression Quantitation (Bio-Rad).

### qRT–PCR

Total RNA was extracted and reverse transcribed using the QuantiTect Reverse Transcription Kit (Qiagen, Hilden, Germany). The qRT–PCR was performed with the IQ SYBR Green Supermix (Bio-Rad). The same cDNA preparation was used to quantify the genes of interest and the housekeeping gene β-actin. The primer sequences, designed with the Primer3 software (<http://frodo.wi.mit.edu/primer3/>), were: for *mdr1*: 5'-TGCTGGAGCGTTCTACG-3'; 5'-ATAGGCAATGTTCTCAGCAATG-3'; for β-actin: 5'-GCTATCCAGGCTGTGCTATC-3'; 5'-TGTCACGCAGATTTC-3'. The relative quantification was performed by comparing each PCR product with the housekeeping PCR product, using the Bio-Rad Software Gene Expression Quantitation (Bio-Rad).

### RhoA and RhoA Kinase Activity

To evaluate the RhoA activity, the RhoA-GTP-bound fraction, taken as an index of monomeric G-proteins activation,<sup>11</sup> was measured using the G-LISA RhoA Activation Assay Biochem Kit (Cytoskeleton), according to the manufacturer's instructions. The absorbance was read at 450 nm, using a Packard EL340 microplate reader (Bio-Tek Instruments, Winooski, VT, USA). For each set of experiments, a titration curve was prepared, using serial dilutions of the Rho-GTP positive control of the kit. The data were expressed as U absorbance/mg cell proteins. The RhoAK activity was measured using the CycLex Rho Kinase Assay Kit (CycLex, Nagano, Japan), following the manufacturer's instructions. For each set of experiments, a titration curve was set, using serial dilutions of recombinant RhoAK (MBL, Woburn, MA, USA). The data were expressed as U absorbance/mg cell proteins.

### RhoA Small Interfering RNA Transfection

A quantity of 200,000 cells were transfected with 400 nmol/L of 20 to 25 nucleotide non-targeting scrambled small interfering RNAs (Control siRNA-A, Santa Cruz Biotechnology) or specific RhoA siRNAs (Santa Cruz Biotechnology), as reported previously.<sup>14</sup> To verify the silencing efficacy, 48 hours after the transfection, the cells were lysed and checked for the expression of RhoA by western blotting, using an anti-RhoA antibody (Santa Cruz Biotechnology).

### Protein Tyrosine Phosphatase 1B Activity

To measure the activity of endogenous PTP1B in cell lysates, the PTP1B Inhibitor Screening Assay kit (Abcam) was used. Cells untreated or treated with RhoA activator II, Y27632 or both, were washed twice in ice-cold PBS, detached by trypsin/EDTA, rinsed with 0.5 mL of PTP1B assay buffer provided by the kit and sonicated. Cell lysate (200 μL), each containing

100  $\mu$ g proteins, were transferred into a 96-wells plate, in the presence of 100  $\mu$ mol/L PTP1B substrate from the kit. The plates were incubated for 30 minutes at 37°C, then 100  $\mu$ L of the Red Assay reagent of the kit was added for 20 minutes. The absorbance at 620 nm was read using a Packard EL340 microplate reader.

The activity of purified PTP1B was measured in a cell-free system: 5 U of human recombinant PTP1B protein (Abcam), diluted in 100  $\mu$ L of reaction buffer (10 mmol/L Tris/HCl, 50 mmol/L NaCl, 2 mmol/L dithiothreitol, 1 mmol/L MnCl<sub>2</sub>; pH 7.5), was incubated for 10 minutes at 37°C, with 10  $\mu$ g of a recombinant peptide from human GSK3 containing phosphorylated tyrosine 216 (Abcam). To test if RhoAK affects the dephosphorylation of GSK3 by PTP1B, in a parallel set of experiments, PTP1B protein was preincubated for 30 minutes at 37°C with 10 U of human recombinant RhoAK (MBL), diluted in 100  $\mu$ L of the Rho Kinase buffer (from CycLex Rho Kinase Assay Kit) containing 25 mmol/L ATP. When indicated, 10  $\mu$ mol/L of the RhoAK inhibitor Y27632 was added. After this preincubation step, a 10  $\mu$ L aliquot from each sample was removed and used to measure the phosphorylation of PTP1B on serine 50 by western blot analysis. The remaining sample was incubated for 10 minutes at 37°C with the phospho(Tyr 216)-GSK3 peptide, as reported above. In all samples, the reaction was stopped by adding 100  $\mu$ L of the Red Assay reagent from the PTP1B Inhibitor Screening Assay kit; the absorbance at 620 nm was read after 20 minutes. For each set of experiments, a titration curve was prepared, using serial dilutions of the phosphate standard from the PTP1B Inhibitor Screening Assay kit. Data were expressed as nmol phosphate/mL. The activity of endogenous PTP1B was then expressed as percentage of the activity of PTP1B of each sample versus the activity of PTP1B measured in untreated cells. The activity of purified PTP1B was expressed as percentage of the activity of PTP1B measured after the preincubation step with RhoAK versus the activity of PTP1B measured without the preincubation step with RhoAK.

#### Permeability Assays Across Blood–Brain Barrier

The permeability to dextran–fluorescein isothiocyanate (molecular weight 70 kDa), [<sup>14</sup>C]-sucrose (molecular weight: 342.30 Da; 589 mCi/mmol; PerkinElmer, Waltham, MA, USA), [<sup>14</sup>C]-inulin (molecular weight range: 5.0 to 5.5 kDa; 10 mCi/mmol; PerkinElmer), sodium fluorescein (molecular weight: 376.27 Da) was taken as a parameter of tight junction integrity<sup>11,15</sup> and measured as previously reported.<sup>6,16</sup>

To measure the permeability coefficient of doxorubicin across the BBB monolayer, wild-type or RhoA-silenced hCMEC/D3 cells were grown for 7 days up to confluence in 6-multiwell Transwell devices, and treated as reported under the Results section. Doxorubicin (5  $\mu$ mol/L) was added in the upper Transwell chamber for 3 hours, then the medium in the lower chamber was collected and the amount of doxorubicin was measured fluorimetrically, using an LS-5 Spectrofluorimeter (PerkinElmer). The excitation and emission wavelengths were 475 nm and 553 nm, respectively. The fluorescence was converted in nmol doxorubicin/cm<sup>2</sup>, using a calibration curve prepared previously. The permeability coefficients were calculated as reported earlier.<sup>17</sup>

#### Intratumor Doxorubicin Accumulation in Co-Culture Models

After 3 days of co-culture, doxorubicin (5  $\mu$ mol/L for 3 hours) or Y27632 (10  $\mu$ mol/L for 3 hours) followed by doxorubicin (5  $\mu$ mol/L for 3 hours) were added to the upper chamber of a Transwell insert containing an hCMEC/D3 cell monolayer. Then glioblastoma cells were collected from the lower chamber, rinsed with PBS, re-suspended in 0.5 mL ethanol/HCl 0.3 N (1:1 v/v) and sonicated. A 50  $\mu$ L aliquot was used to measure the protein content; the remaining sample was used to quantify fluorimetrically the intracellular doxorubicin content, as described above. The results were expressed as nmol doxorubicin/mg cell proteins.

For fluorescence microscope analysis, the glioblastoma cells in the lower chamber were seeded on sterile glass coverslips and treated as reported above. At the end of the incubation period, the cells were rinsed with PBS, fixed in 4% w/v paraformaldehyde for 15 minutes, washed three times with PBS and incubated with 4',6-diamidino-2-phenylindole dihydrochloride for 3 minutes at room temperature in the dark. The cells were washed three times with PBS and once with water, then the slides were mounted with 4  $\mu$ L of Gel Mount Aqueous Mounting and examined with a Leica DC100 fluorescence microscope (Leica Microsystems, Wetzlar, Germany). For each experimental point, a minimum of five microscopic fields were examined.

#### Cytotoxicity, Cell Cycle Analysis and Cell Proliferation of Glioblastoma Cells in Co-Culture Models

For cytotoxicity, apoptosis, and cell cycle analysis, after 3 days of co-culture, doxorubicin (5  $\mu$ mol/L for 24 hours) or Y27632 (10  $\mu$ mol/L for 3 hours) followed by doxorubicin (5  $\mu$ mol/L for 24 hours) were added to the upper chamber of Transwell inserts containing an hCMEC/D3 cell monolayer.

The release of lactate dehydrogenase in the supernatant of glioblastoma cells, used as an index of cell damage and necrosis, was measured spectrophotometrically as described earlier.<sup>18</sup> The apoptosis of glioblastoma cells was assessed by analyzing the cleavage of caspase-3 by western blotting, as described above. For cell cycle distribution, the glioblastoma cells were washed twice with fresh PBS, incubated in 0.5 mL of ice-cold 70% v/v ethanol for 15 minutes, then centrifuged at 1,200 g for 5 minutes at 4°C and rinsed with 0.3 mL of citrate buffer (50 mmol/L Na<sub>2</sub>HPO<sub>4</sub>, 25 mmol/L sodium citrate, 1% v/v Triton X-100), containing 10  $\mu$ g/mL propidium iodide and 1 mg/mL RNase (from bovine pancreas). After 15-minute incubation in the dark, the intracellular fluorescence was detected by a FACSCalibur flow cytometer (Becton Dickinson). For each analysis, 10,000 events were collected and analyzed by the Cell Quest software (Becton Dickinson).

To monitor the long-term cell proliferation, 1,000 glioblastoma cells were seeded in the lower chamber of Transwell, containing confluent hCMEC/D3 cells in the insert. This time was considered 'day 0' in the proliferation assay. After 3 days of co-culture, the upper chamber of the Transwell insert was filled with fresh medium or medium containing 10  $\mu$ mol/L Y27632 for 3 hours, 5  $\mu$ mol/L doxorubicin for 24 hours, 10  $\mu$ mol/L Y27632 for 3 hours followed by 5  $\mu$ mol/L doxorubicin for 24 hours. The treatments were repeated every 7 days, for 4 weeks. At day 7, 14, 21, and 28 the glioblastoma cells were collected, transferred into a 96-wells plate, fixed with 4% w/v paraformaldehyde and stained with 0.5% w/v crystal violet solution for 10 minutes at room temperature. The plate was washed three times in water, then 100  $\mu$ L of 0.1 mmol/L sodium citrate in 50% v/v ethanol was added to each well and the absorbance was read at 570 nm. The absorbance units were converted into the number of cells, according to a titration curve obtained with serial cell dilutions of each cell line. To check if the hCMEC/D3 cells retained BBB properties, the permeability to dextran and inulin was measured weekly in a parallel set of Transwell. No significant changes in the permeability coefficients were detected during the whole experiment (not shown).

#### Pgp ATPase Assay

The rate of ATP hydrolysis was measured spectrophotometrically on Pgp immunoprecipitated from the membrane of hCMEC/D3 cells as described previously.<sup>11</sup>

#### Statistical Analysis

All data in the text and figures are provided as means  $\pm$  s.d. The results were analyzed by a one-way analysis of variance. A  $P < 0.05$  was considered significant.

## RESULTS

### Wnt Controls the GSK3/ $\beta$ -Catenin and RhoA/RhoA Kinase Activities in Human Blood–Brain Barrier Cells

The hCMEC/D3 cells exhibited a GSK3 constitutively phosphorylated on tyrosine 216, i.e., activated, and a  $\beta$ -catenin constitutively phosphorylated on serine 33, serine 37 and threonine 41 (Figure 1A), i.e., primed for ubiquitination. Notwithstanding, we detected in the untreated hCMEC/D3 cells a basal amount of  $\beta$ -catenin translocated into the nucleus (Figure 1B) and bound to the promoter of *mdr1* gene (Figure 1C), which encodes for Pgp. In line with previous findings obtained on hCMEC/D3 cells and primary human brain microvascular endothelial cells,<sup>6</sup> the Wnt activator WntA decreased the phosphorylation/activation of GSK3, strongly reduced the phosphorylation of  $\beta$ -catenin (Figure 1A), increased the nuclear translocation and the binding of  $\beta$ -catenin to the *mdr1* promoter (Figures 1B and 1C); the Wnt inhibitor Dkk-1 produced opposite effects (Figures 1A–C). In keeping with these results, WntA increased and Dkk-1 decreased the mRNA level of *mdr1* in hCMEC/D3 cells (Figure 1D). In parallel, Wnt modulated

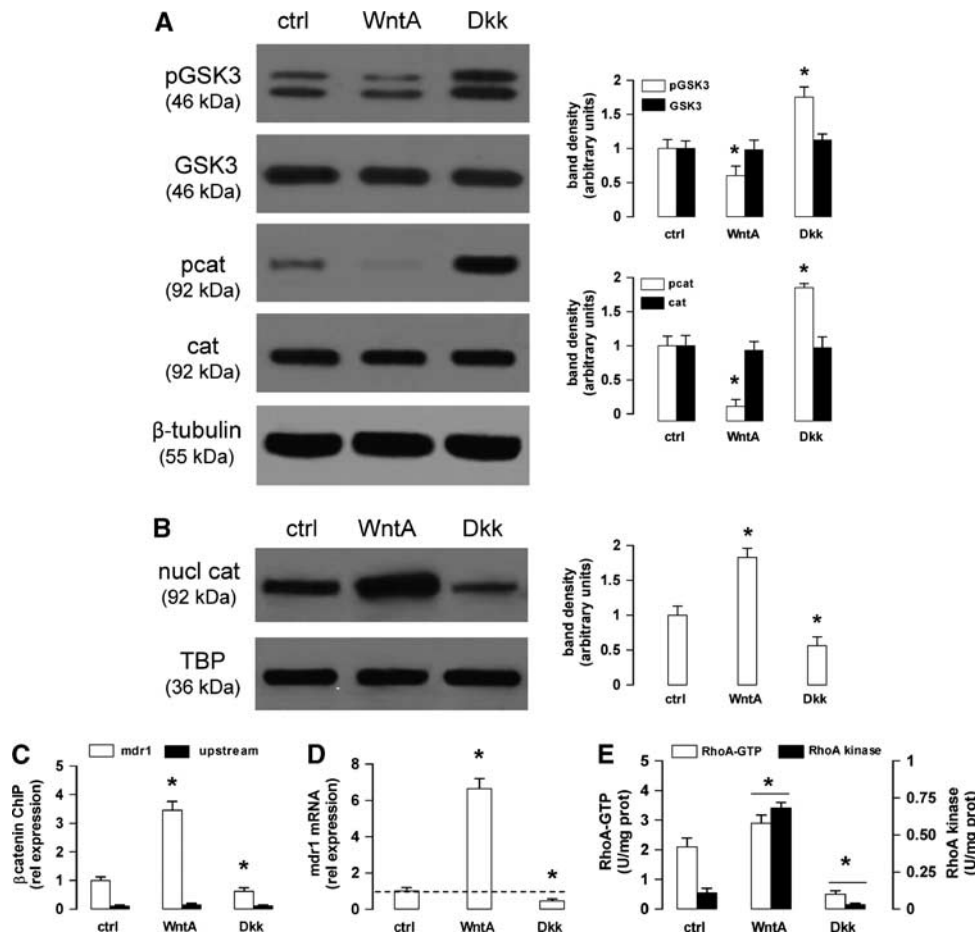


**Figure 1.** Wnt controls the  $\beta$ -catenin-induced transcription of P-glycoprotein (Pgp) and RhoA activity in human blood–brain barrier cells. The hCMEC/D3 cells were grown in fresh medium (ctrl), with the Wnt activator 2-amino-4-(3,4-(methylenedioxy)benzylamino)-6-(3-methoxyphenyl)pyrimidine (WntA; 20  $\mu$ mol/L for 24 hours) or the Wnt inhibitor Dickkopf-1 (Dkk-1) protein (Dkk; 1  $\mu$ g/mL for 24 hours). **(A)** Western blot analysis of phospho(Tyr216)GSK3 (glycogen synthase kinase 3) (pGSK3), GSK3, phospho(Ser33/Ser37/Thr41) $\beta$ -catenin (pcat),  $\beta$ -catenin (cat) in whole-cell lysates. The  $\beta$ -tubulin expression was used as a control of equal protein loading. The figure is representative of three experiments with similar results. The band density ratio between each protein and  $\beta$ -tubulin was expressed as arbitrary units. Versus ctrl cells:  $*P < 0.02$ . **(B)** Nuclear extracts were analyzed for the amount of  $\beta$ -catenin (nucl cat). The expression of TATA-binding protein (TBP) was used as a control of equal protein loading. The figure is representative of three experiments with similar results. The band density ratio between each protein and TBP was expressed as arbitrary units. Versus ctrl cells:  $*P < 0.02$ . **(C)** Chromatin Immunoprecipitation assay. The genomic DNA was extracted, immunoprecipitated with an anti- $\beta$ -catenin antibody and analyzed by quantitative real-time PCR (qRT–PCR), using primers for the  $\beta$ -catenin binding site on *mdr1* promoter (open bars) or for an upstream region (black bars), chosen as a negative control. Results are presented as means  $\pm$  s.d. ( $n = 4$ ). Versus ctrl:  $*P < 0.05$ . **(D)** The *mdr1* expression was detected by qRT–PCR. Data are presented as means  $\pm$  s.d. ( $n = 4$ ). Versus ctrl:  $*P < 0.02$ . **(E)** RhoA/RhoA kinase (RhoAK) activity. The samples were subjected to enzyme-linked immunosorbent assays to measure the amount of RhoA-GTP (open bars) and the activity of RhoAK (black bars). Data are presented as means  $\pm$  s.d. ( $n = 4$ ). Versus ctrl:  $*P < 0.05$ .

the activity of RhoA and RhoAK: as shown in Figure 1E, WntA increased and Dkk-1 decreased the GTP binding to RhoA and the activity of RhoAK. These data suggest that both Wnt/GSK3 canonical pathway and Wnt/RhoA/RhoAK non-canonical pathway are active in the hCMEC/D3 cells and vary their activity in response to Wnt activators and inhibitors at the same time.

#### RhoA Modulates the GSK3/ $\beta$ -Catenin-Driven Transcription of Pgp in Human Blood–Brain Barrier Cells

To investigate whether the activity of non-canonical Wnt/RhoA/RhoAK pathway controls the activity of canonical Wnt/GSK3 pathway in hCMEC/D3 cells, we constitutively activated RhoA with the RhoA activator II<sup>12</sup> (Figure 2A) and silenced RhoA (Figure 2B), respectively. The cells with active RhoA showed a reduced phosphorylation of GSK3 and  $\beta$ -catenin (Figure 2C), and an

increased  $\beta$ -catenin nuclear translocation (Figure 2D). By contrast, the RhoA-silenced cells exhibited a higher amount of phosphorylated GSK3 and  $\beta$ -catenin (Figure 2C), and a reduced  $\beta$ -catenin nuclear translocation (Figure 2D). These data suggest that the activity of the Wnt non-canonical transducer RhoA controls the activation of the Wnt canonical transducers GSK3/ $\beta$ -catenin in our model.

Of note for the aim of this work, the RhoA activation increased, while the RhoA silencing decreased the binding of  $\beta$ -catenin to *mdr1* promoter (Figure 2E) and the levels of *mdr1* mRNA (Figure 2F) in the hCMEC/D3 cells. The increase of *mdr1* expression induced by WntA or RhoA activator II was not paralleled by an increase in permeability to small molecules, such as sucrose and sodium fluorescein (Supplementary Figure 1), thus ruling out a Wnt- or RhoA-mediated increase of the monolayer passive permeability.

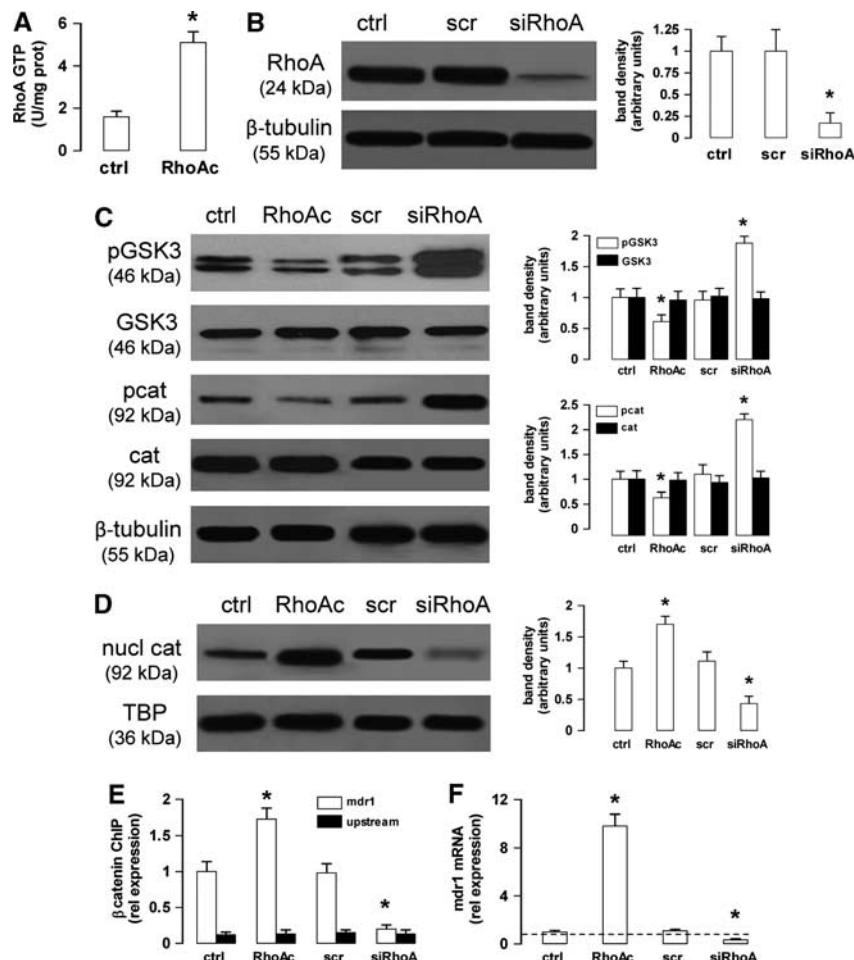


**Figure 2.** The RhoA activity controls the glycogen synthase kinase 3 (GSK3)/ $\beta$ -catenin-driven transcription of P-glycoprotein (Pgp) in human blood–brain barrier cells. **(A)** The hCMEC/D3 cells were grown in fresh medium in the absence (ctrl) or in the presence of the RhoA activator II (RhoAc; 5  $\mu$ g/mL for 3 hours), then the activity of RhoA was measured by an enzyme-linked immunosorbent assay. Data are presented as means  $\pm$  s.d. ( $n = 4$ ). Versus ctrl:  $*P < 0.005$ . **(B)** The cells were cultured for 48 hours with fresh medium (ctrl), treated with a non-targeting scrambled small interfering RNA (siRNA) (scr) or a RhoA-targeting specific siRNA pool (siRhoA). The expression of RhoA was measured in whole-cell lysates by western blotting. The  $\beta$ -tubulin expression was used as a control of equal protein loading. The figure is representative of three experiments with similar results. The band density ratio between each protein and  $\beta$ -tubulin was expressed as arbitrary units. Versus ctrl cells:  $*P < 0.005$ . **(C)** Western blot analysis of phospho(Tyr216)GSK3 (pGSK3), GSK3, phospho(Ser33/Ser37/Thr41) $\beta$ -catenin (pcat),  $\beta$ -catenin (cat) in whole-cell lysates of hCMEC/D3 cells treated as described in **(A)** and **(B)**. The  $\beta$ -tubulin expression was used as a control of equal protein loading. The figure is representative of three experiments with similar results. The band density ratio between each protein and  $\beta$ -tubulin was expressed as arbitrary units. Versus ctrl cells:  $*P < 0.05$ . **(D)** Nuclear extracts from cells treated as described in **(A)** and **(B)** were analyzed for the amount of  $\beta$ -catenin (nucl cat). The expression of TATA-binding protein (TBP) was used as a control of equal protein loading. The band density ratio between each protein and TBP was expressed as arbitrary units. Versus ctrl cells:  $*P < 0.005$ . **(E)** Cells were cultured as reported in **(A)** and **(B)**. After 3 hours (for the RhoAc II-treated cells) or 48 hours (for the scrambled- and RhoA-targeting siRNA-treated cells), the genomic DNA was extracted, immunoprecipitated with an anti- $\beta$ -catenin antibody and analyzed by quantitative real-time PCR (qRT-PCR), using primers for the  $\beta$ -catenin binding site on the *mdr1* promoter (open bars) or for an upstream region (black bars), chosen as a negative control. The ctrl bars in the figure correspond to the DNA extracted after 48 hours from hCMEC/D3 cells; the results were superimposable for the DNA extracted after 3 hours (not shown in the figure). Results are expressed as means  $\pm$  s.d. ( $n = 4$ ). Versus ctrl:  $*P < 0.01$ . **(F)** The cells were treated as detailed in **(A)** and **(B)**. After 3 hours (for the RhoAc II-treated cells) or 48 hours (for the scrambled- and RhoA-targeting siRNA-treated cells), the *mdr1* expression was detected by qRT-PCR. Data are presented as means  $\pm$  s.d. ( $n = 4$ ). Versus ctrl  $*P < 0.005$ .

The RhoA Kinase Inhibition Reduces the Pgp Transcription in Blood–Brain Barrier Cells, by Inhibiting the Protein Tyrosine Phosphatase 1B Activity and Increasing the Glycogen Synthase Kinase 3-Mediated Phosphorylation and Ubiquitination of  $\beta$ -Catenin

As in hCMEC/D3 cells, Wnt controls the activity of RhoA and its downstream effector RhoAK (Figure 1E), we next investigated whether RhoAK mediated the cross-talk between the Wnt/GSK3 canonical pathway and the Wnt/RhoA non-canonical pathway. Time-dependence experiments with the RhoAK inhibitor Y27632

showed that at 10  $\mu$ mol/L, this compound effectively inhibited the RhoAK activity at each time point considered (Supplementary Figure 2A) and decreased the  $\beta$ -catenin nuclear translocation at the time points from 3 to 24 hours (Supplementary Figure 2B). After 3 hours, when the reduction of RhoAK activity and  $\beta$ -catenin was maximal, Y27632 did not change the expression of claudin-3, claudin-5, occludin, zonula occludens-1 (Supplementary Figure 2C) and did not alter the permeability coefficient of dextran, inulin and sucrose (Supplementary Figure 2D), suggesting that the RhoAK inhibition did not affect the integrity of tight junctions and

the paracellular transport processes. In the light of these results, Y27632 was used at 10  $\mu$ mol/L for 3 hours in all the following experiments: in these conditions, Y27632 increased the phosphorylation of GSK3 and  $\beta$ -catenin (Figure 3A) and reduced the  $\beta$ -catenin nuclear translocation (Figure 3B), also in the presence of a constitutively activated RhoA (Figures 3A and 3B).

The tyrosine phosphatase PTP1B reduces the activity of GSK3 by dephosphorylating tyrosine 216, which is critical for the GSK3 activity.<sup>19</sup> PTP1B is in its turn activated by the phosphorylation on serine 50, operated by serine/threonine kinases.<sup>20</sup> We thus wondered whether RhoAK may modulate the GSK3 phosphorylation via PTP1B.

PTP1B was basally phosphorylated on serine 50 in the hCMEC/D3 cells (Figure 3C). Interestingly, the cells with activated RhoA had increased levels of phospho(Ser50)PTP1B, which was strongly reduced in cells treated with the RhoAK inhibitor Y27632. The latter also abolished the phosphorylation of PTP1B induced by active RhoA (Figure 3C). The endogenous activity of PTP1B was significantly increased in cells with activated RhoA and significantly decreased in Y27632-treated cells (Figure 3D). To test whether RhoAK, by phosphorylating PTP1B on serine 50, may decrease the phosphorylation of GSK3 on tyrosine 216, we set up a cell-free system and measured the activity of recombinant PTP1B protein, using as a substrate a synthetic peptide derived from GSK3, containing the phosphorylated tyrosine 216 (Figures 3E and 3F). PTP1B, when preincubated with the recombinant RhoAK in this cell-free system, was phosphorylated on serine 50, an effect that was prevented by Y27632 (Figure 3E). In keeping with this observation, the preincubation with RhoAK increased the PTP1B-mediated dephosphorylation of the recombinant phospho(Tyr 216)GSK3 peptide; such a dephosphorylation was significantly reduced by the RhoAK inhibitor Y27632 (Figure 3F).

These data suggest that RhoAK activates PTP1B, promotes the tyrosine dephosphorylation of GSK3 and its inhibition, whereas the RhoAK inhibition produces opposite effects.

As an active GSK3 promotes the phosphorylation of  $\beta$ -catenin, priming it for the subsequent ubiquitination and proteasomal degradation,<sup>4,5</sup> we next measured the  $\beta$ -catenin ubiquitination in the presence of RhoA/RhoAK activators or inhibitors. The untreated hCMEC/D3 cells showed a basal level of  $\beta$ -catenin ubiquitination (Figure 4A), which was in line with the basal phosphorylation of the protein on serine 33, serine 37, and threonine 41 (Figure 1A). The ubiquitination of  $\beta$ -catenin was reduced in cells with active RhoA and increased by the RhoA silencing or the RhoAK inhibitor Y27632 (Figure 4A). These data suggest that an active RhoAK prevents the ubiquitination of  $\beta$ -catenin and highlight the possibility to regulate the transcription of  $\beta$ -catenin-target genes by modulating the RhoAK activity. As the silencing of RhoA did (Figures 2E and 2F), also Y27632 decreased the binding of  $\beta$ -catenin to the *mdr1* promoter (Figure 4B) and the levels of *mdr1* mRNA (Figure 4C). Both RhoA silencing and RhoAK inhibition reduced the Pgp protein levels, whereas RhoA increased them; by contrast, these treatments did not change the amount of MRP1 and BCRP, two other ATP binding cassette transporters present on the luminal side of BBB cells<sup>1</sup> (Figure 4D).

To verify whether the inhibition of RhoA and RhoAK increases the delivery of Pgp substrates across the BBB, we used doxorubicin,<sup>21</sup> which exhibited a low permeability across the hCMEC/D3 cell monolayer (Figure 4E), owing to the high level of Pgp on the luminal side of these cells.<sup>22</sup> The doxorubicin permeability was further decreased by active RhoA, but it was increased by RhoA silencing or Y27632 (Figure 4E). The latter, which counteracted the effect of RhoA activator II on  $\beta$ -catenin ubiquitination (Figure 4A), also prevented the effects of RhoA activation on  $\beta$ -catenin binding to *mdr1* promoter (Figure 4B), *mdr1* transcription (Figure 4C), Pgp protein levels (Figure 4D) and doxorubicin permeability (Figure 4E).

### The Inhibition of RhoA Kinase Increases the Doxorubicin Delivery and Cytotoxicity in Human Glioblastoma Cells Co-Cultured with Blood–Brain Barrier Cells

As the inhibition of RhoAK increased the doxorubicin permeability across the hCMEC/D3 monolayer, we wondered whether priming the BBB cells with Y27632 improves the delivery of doxorubicin to glioblastoma cells grown under the BBB monolayer.

The doxorubicin accumulation within glioblastoma cells (CV17, 01010627, Nov3 and U87-MG) co-cultured with hCMEC/D3 cells was low, as evaluated by fluorimetric assays (Figure 5A) and fluorescence microscope analysis (Figure 5B). The pretreatment of the hCMEC/D3 cells with Y27632 significantly increased the doxorubicin retention within glioblastoma cells (Figures 5A and 5B). Doxorubicin alone did not produce significant cell damages in terms of release of lactate dehydrogenase in the extracellular medium of glioblastoma cells (Figure 5C), and induced weak signs of apoptosis, as suggested by the low level of cleaved caspase-3 (Figure 5D). When effective, the drug is expected to induce a G2/M-phase arrest, which was not observed in the 01010627 glioblastoma cells co-cultured under the hCMEC/D3 monolayer exposed to doxorubicin alone (Figure 5E). The exposure to Y27632 followed by doxorubicin strongly increased the release of lactate dehydrogenase (Figure 5C), the cleavage of caspase-3 (Figure 5D), the percentage of cells arrested in G2/M phase (Figure 5E). In parallel, such combination increased the amount of cells in pre-G1 phase, an index of apoptotic cells, and decreased the number of cells in S phase (Figure 5E). Of note, used at 10  $\mu$ mol/L for 3 hours, Y27632 alone was not cytotoxic for glioblastoma cells (Figures 5C–E). The repeated administration of Y27632 or doxorubicin as single agents on the luminal side of the hCMEC/D3 monolayer did not reduce the proliferation of 01010627 glioblastoma cells growing under this model of BBB (Figure 5F); only the pretreatment of hCMEC/D3 cells with Y27632 followed by doxorubicin significantly decreased the long-term proliferation of tumor cells (Figure 5F).

Interestingly, the pretreatment with Y27632 produced the same effects of verapamil, a strong inhibitor of Pgp activity in the hCMEC/D3 cells (Supplementary Figure 3A); when co-incubated with doxorubicin, verapamil increased the drug permeability across the BBB monolayer (Supplementary Figure 3B) and its accumulation in co-cultured glioblastoma cells (Supplementary Figure 3C), as well as lactate dehydrogenase release (Supplementary Figure 3D), caspase-3 activation (Supplementary Figure 3E), G2/M-arrest (Supplementary Figure 3F) in glioblastoma cells.

## DISCUSSION

In this work, we demonstrate that the expression of Pgp in human BBB cells is controlled by a cross-talk between the Wnt/GSK3 canonical pathway and the Wnt/RhoA/RhoAK non-canonical pathway. The activation of Wnt/GSK3/ $\beta$ -catenin axis is known to increase the expression of Pgp in hCMEC/D3 cells.<sup>2,3,6</sup> The activation of RhoA and RhoAK is known to enhance the Pgp activity in BBB cells.<sup>11</sup> It is not known: (1) whether the Wnt/RhoA/RhoAK axis controls also the Pgp expression; (2) whether the canonical and non-canonical Wnt pathways cooperate in regulating the Pgp levels in BBB cells.

We observed that the Wnt activation increases at the same time the activity of GSK3 and the activity of RhoA/RhoAK in hCMEC/D3 cells, while the Wnt inhibition reduces them. The positive cooperation between Wnt/GSK3 and Wnt/RhoA/RhoAK axis, which we detected in BBB cells, has been described in pulmonary aortic endothelial cells: here the bone morphogenetic protein 2 increases the activity of GSK3/ $\beta$ -catenin axis and at the same time recruits the Wnt-downstream effector Disheveled, which activates RhoA.<sup>23</sup> As WntA activates Disheveled, and Dkk-1 inhibits it in most mammalian cells,<sup>4</sup> it is likely that also in our model the changes in RhoA/RhoAK activity in response to WntA and Dkk-1 were due to the changes in Disheveled activity.

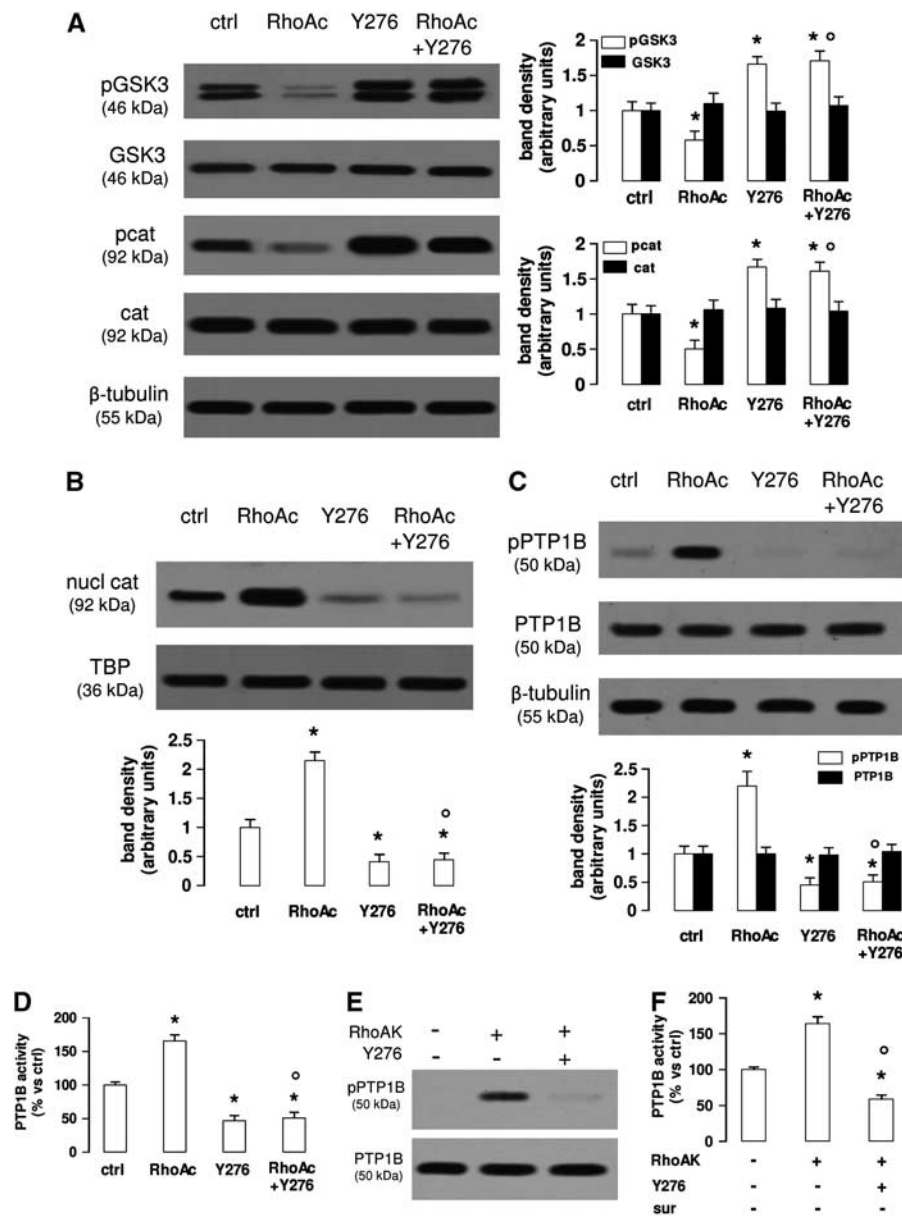


**Figure 3.** The RhoA kinase (RhoAK) inhibition increases the activation of glycogen synthase kinase 3 (GSK3), by decreasing the activity of protein tyrosine phosphatase 1B (PTP1B) in human blood-brain barrier cells. The hCMEC/D3 cells were grown in fresh medium (ctrl) or in medium containing the RhoA activator II (RhoAc; 5  $\mu$ g/mL for 3 hours) or the RhoAK inhibitor Y27632 (Y276; 10  $\mu$ mol/L for 3 hours), alone or co-incubated. **(A)** Western blot analysis of phospho(Tyr216)GSK3 (pGSK3), GSK3, phospho(Ser33/Ser37/Thr41) $\beta$ -catenin (pcat),  $\beta$ -catenin (cat) in whole-cell lysates. The  $\beta$ -tubulin expression was used as a control of equal protein loading. The figure is representative of three experiments with similar results. The band density ratio between each protein and  $\beta$ -tubulin was expressed as arbitrary units. Versus ctrl cells: \* $P$  < 0.05; versus RhoAc alone:  $^{\circ}P$  < 0.001. **(B)** The nuclear extracts were analyzed for the amount of  $\beta$ -catenin (nucl cat). The expression of TATA-binding protein (TBP) was used as a control of equal protein loading. The band density ratio between each protein and TBP was expressed as arbitrary units. Versus ctrl cells: \* $P$  < 0.002; versus RhoAc alone:  $^{\circ}P$  < 0.001. **(C)** Western blot analysis of phospho(Ser50)PTP1B (pPTP1B) and PTP1B. The  $\beta$ -tubulin expression was used as a control of equal protein loading. The figure is representative of three experiments with similar results. The band density ratio between each protein and  $\beta$ -tubulin was expressed as arbitrary units. Versus ctrl cells: \* $P$  < 0.005; versus RhoAc alone:  $^{\circ}P$  < 0.001. **(D)** The activity of endogenous PTP1B was measured in cell lysates, as reported under Materials and Methods. Data are presented as means  $\pm$  s.d. ( $n$  = 3). Versus ctrl: \* $P$  < 0.002; versus RhoAc alone:  $^{\circ}P$  < 0.001. **(E)** *In vitro* phosphorylation of PTP1B in the presence of RhoAK and Y27632. 5 U of human recombinant PTP1B were incubated in the absence (-) or in the presence of 10 U of human recombinant RhoAK, alone or in the presence of the RhoAK inhibitor Y27632 (Y276; 10  $\mu$ mol/L) for 30 minutes at 37°C, in a reaction buffer containing 25 mmol/L ATP. At the end of this incubation time, samples were resolved by SDS-PAGE and probed with anti-phospho(Ser50)PTP1B (pPTP1B) or anti-PTP1B antibodies. The figure is representative of three experiments with similar results. **(F)** The activity of purified PTP1B was measured in a cell-free system, using a recombinant phospho(Tyr 216)GSK3 peptide as substrate. When indicated, 10 U of RhoAK, alone or in the presence of Y27632 (Y276; 10  $\mu$ mol/L), were added in the reaction mix 30 minutes before adding the phospho(Tyr 216)GSK3 peptide. Suramin (sur; 10  $\mu$ mol/L), a known inhibitor of PTP1B, was added together with the phospho(Tyr 216)GSK3 peptide, as internal control. Data are presented as means  $\pm$  s.d. ( $n$  = 3). Versus PTP1B alone (-): \* $P$  < 0.002; versus RhoAK:  $^{\circ}P$  < 0.001.

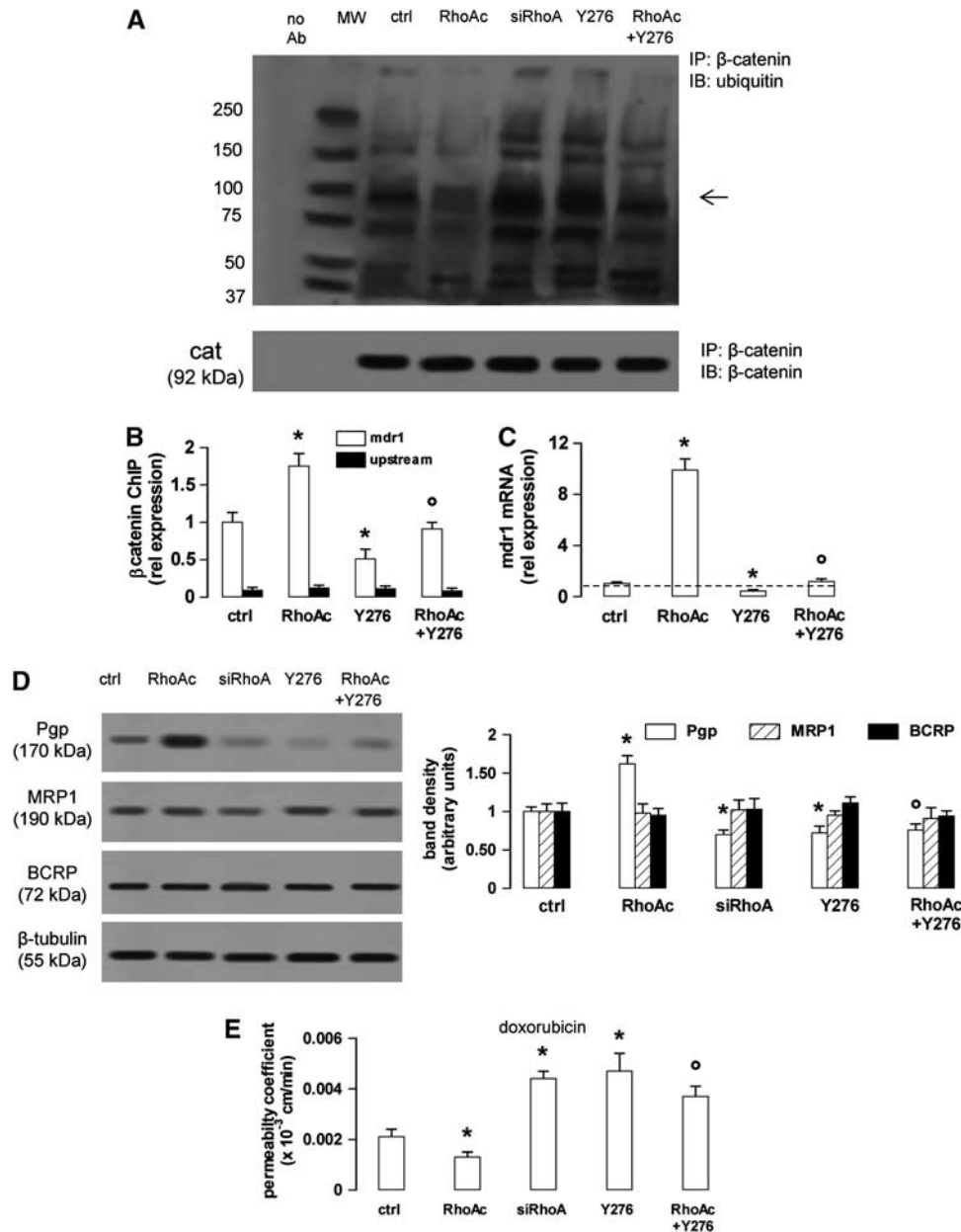


**Figure 4.** The RhoA kinase (RhoAK) inhibition enhances the ubiquitination of  $\beta$ -catenin, downregulates the  $\beta$ -catenin-induced transcription of P-glycoprotein (Pgp) and increases the doxorubicin permeability in human blood–brain barrier cells. The hCMEC/D3 cells were grown in fresh medium (ctrl), or in medium containing the RhoA activator II (RhoAc; 5  $\mu$ g/mL for 3 hours) or the RhoAK inhibitor Y27632 (Y276; 10  $\mu$ mol/L for 3 hours), alone or co-incubated. When indicated, the cells were treated with a non-targeting scrambled small interfering RNA (siRNA) or a RhoA-targeting specific siRNA (siRhoA) for 48 hours (panel **A**) or 72 hours (panels **D** and **E**). (**A**) Whole-cell lysates were immunoprecipitated (IP) with an anti- $\beta$ -catenin antibody, then immunoblotted (IB) with an anti-mono/polyubiquitin antibody or with an anti- $\beta$ -catenin antibody. Cells treated with non-targeting scrambled siRNA had the same level of ubiquitination than untreated (ctrl) cells (not shown). The figure is representative of three experiments with similar results. no Ab: samples immunoprecipitated without anti- $\beta$ -catenin antibody. MW, molecular weight markers. The 92 kDa band corresponding to the native  $\beta$ -catenin protein is indicated by the arrow. (**B**) Chromatin immunoprecipitation assay. The genomic DNA was extracted, immunoprecipitated with an anti- $\beta$ -catenin antibody and analyzed by qRT–PCR, using primers for the  $\beta$ -catenin-binding site on the *mdr1* promoter (open bars) or for an upstream region (black bars), chosen as a negative control. Results are expressed as means  $\pm$  s.d. ( $n = 4$ ). Versus ctrl:  $^*P < 0.05$ ; versus RhoAc:  $^{\circ}P < 0.01$ . (**C**) The *mdr1* expression was detected by qRT–PCR. Data are presented as means  $\pm$  s.d. ( $n = 4$ ). Versus ctrl:  $^*P < 0.005$ ; versus RhoAc:  $^{\circ}P < 0.001$ . (**D**) Western blot analysis of Pgp, multidrug resistance-related protein 1 (MRP1) and breast cancer resistance protein (BCRP) in the whole-cell lysates of hCMEC/D3 cells treated as described above. The  $\beta$ -tubulin expression was used as a control of equal protein loading. The figure is representative of three experiments with similar results. The band density ratio between each protein and  $\beta$ -tubulin was expressed as arbitrary units. Versus ctrl cells:  $^*P < 0.02$ ; versus RhoAc:  $^{\circ}P < 0.005$ . (**E**) Doxorubicin permeability. The cells were grown for 7 days up to confluence in Transwell inserts and incubated as reported above. At the end of the incubation period, doxorubicin (5  $\mu$ mol/L) was added in the upper chamber. After 3 hours the amount of drug recovered from the lower chamber was measured fluorimetrically. The permeability coefficient was calculated as reported under Materials and Methods. In cells treated with the non-targeting scrambled siRNA the permeability coefficient was  $0.0018 \pm 0.0002$  (not significant versus ctrl cells). Measurements were performed in duplicate and data are presented as means  $\pm$  s.d. ( $n = 3$ ). Versus ctrl:  $^*P < 0.05$ ; versus RhoAc:  $^{\circ}P < 0.02$ .

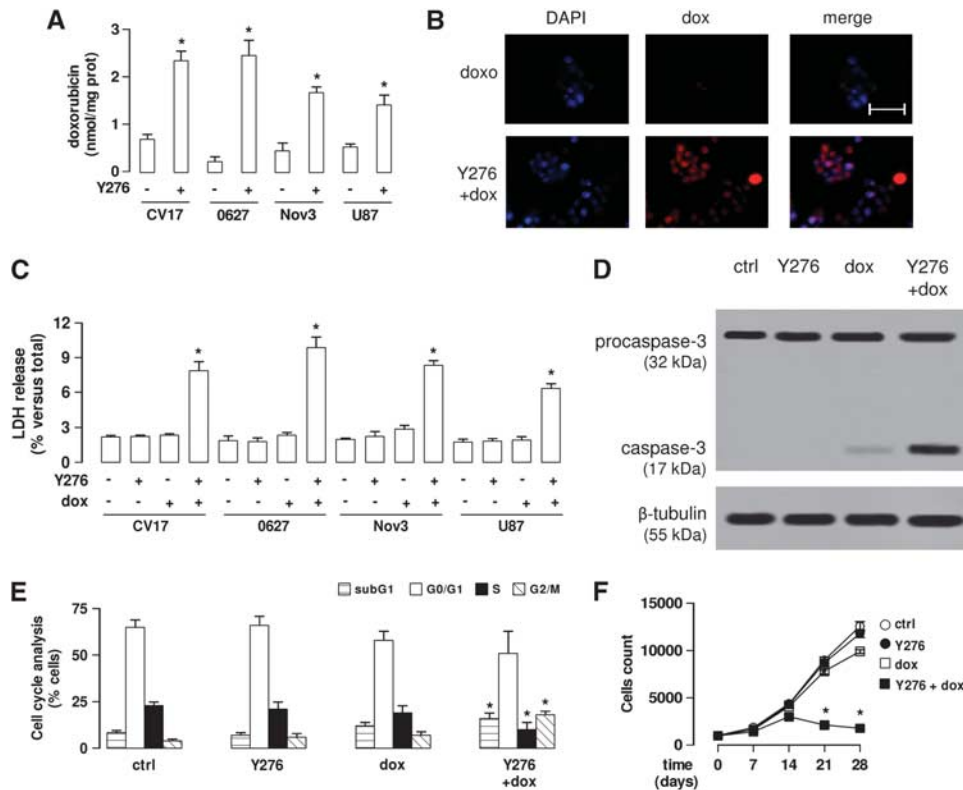


**Figure 5.** The RhoA kinase (RhoAK) inhibitor Y27632 increases the doxorubicin delivery and cytotoxicity in glioblastoma cells co-cultured with blood–brain barrier cells. The hCMEC/D3 cells were grown for 7 days up to confluence in Transwell inserts; CV17, 01010627, Nov3, and U87-MG cells were seeded at day 4 in the lower chamber. After 3 days of co-culture, the supernatant in the upper chamber was replaced with fresh medium without (– or ctrl) or with Y27632 (Y276; 10  $\mu$ mol/L for 3 hours). After this incubation time, doxorubicin (dox; 5  $\mu$ mol/L) was added in the upper chamber for 3 hours (panels A and B) or 24 hours (panels C–F), then the following investigations were performed. (A) Fluorimetric quantification of intracellular doxorubicin in glioblastoma cells. Data are presented as means  $\pm$  s.d. ( $n=4$ ). Versus untreated (–) cells:  $*P<0.001$ . (B) The 01010627 cells were seeded on sterile glass coverslips, treated as reported above, then stained with 4',6-diamidino-2-phenylindole dihydrochloride (DAPI) and analyzed by fluorescence microscopy to detect the intracellular accumulation of doxorubicin. Magnification:  $\times 63$  objective (1.4 numerical aperture);  $\times 10$  ocular lens. The micrographs are representative of three experiments with similar results. Scale bar, 20  $\mu$ m. (C) The glioblastoma cells were checked spectrophotometrically for the extracellular release of lactate dehydrogenase (LDH) activity. Data are presented as means  $\pm$  s.d. ( $n=4$ ). Versus untreated (–) cells:  $*P<0.001$ . (D) The whole-cell lysates from 01010627 cells were resolved by SDS–PAGE and immunoblotted with an anti-caspase 3 antibody (recognizing both pro-caspase and cleaved active caspase). The  $\beta$ -tubulin expression was used as a control of equal protein loading. The figure is representative of three experiments with similar results. (E) Cell cycle analysis. The distribution of the 01010627 cells in sub-G1, G0/G1, S, G2/M phase was analyzed by flow cytometry, as detailed under Materials and Methods. Data are presented as means  $\pm$  s.d. ( $n=4$ ). Versus ctrl:  $*P<0.005$ . (F) After 3 days of co-culture between hCMEC/D3 and 01010627 cells, the medium of the upper chamber was replaced with fresh medium (open circles) or medium containing Y27632 (Y276; 10  $\mu$ mol/L for 3 hours, solid circles), doxorubicin (dox; 5  $\mu$ mol/L for 24 hours, open squares), Y27632 (Y276; 10  $\mu$ mol/L for 3 hours) followed by doxorubicin (doxo; 5  $\mu$ mol/L for 24 hours, solid squares). Drug treatments were repeated every 7 days, as reported in the Materials and Methods section. The proliferation of glioblastoma cells was monitored weekly by crystal violet staining. Measurements were performed in triplicate and data are presented as means  $\pm$  s.d. ( $n=4$ ). Versus ctrl:  $*P<0.001$ .

It has not been clarified however whether the canonical Wnt pathway controls the activity of the non-canonical Wnt pathways or *vice versa*. In gastric cancer cells, the activation of RhoA in response to Wnt5a is dependent on the activation of the PI3K/Akt/GSK3 axis.<sup>24</sup> Our results demonstrated that an active RhoA decreases the activity of GSK3, prevents the GSK3-mediated phosphorylation of  $\beta$ -catenin, and favors its nuclear translocation and the subsequent transcription of Pgp, whereas the RhoA silencing produces opposite effects. We therefore hypothesize that the RhoA activity controls the GSK3/ $\beta$ -catenin axis in hCMEC/D3 cells. This hypothesis is in contrast with results obtained in murine cerebrovascular endothelial cells, where the activation of RhoA promotes the phosphorylation of  $\beta$ -catenin and reduces its transcriptional activity.<sup>9</sup> As murine and human brain microvascular cells have often striking differences in the expression and activity of Pgp,<sup>25</sup> it is not surprising that they also differ in the upstream

pathways controlling Pgp expression. For instance, the mechanism by which RhoA modulates GSK3 activity is quite different in murine and human cerebrovascular endothelial cells: in murine cells, RhoA controls the GSK3 activity in a PTEN- and protein kinase C $\delta$ -dependent way and changes the phosphorylation of GSK3 on serine 9.<sup>9</sup> This phosphorylation has inhibitory effects on the enzymatic activity of GSK3.<sup>26</sup> We cannot exclude that the RhoA activity may change the phosphorylation on serine 9 of GSK3 also in human hCMEC/D3 cells; however, we observed that in our model, the activation of RhoA decreases—and the silencing of RhoA increases—the phosphorylation of GSK3 on tyrosine 216, which is a proactivating phosphorylation.<sup>26</sup> When phosphorylated on tyrosine 216, GSK3 induces  $\beta$ -catenin phosphorylation and degradation. To our knowledge, this is the first work showing that RhoA activity modulates the phosphorylation on tyrosine 216 of GSK3.

We next looked for putative downstream effectors of RhoA responsible for this effect. We focused on RhoAK, whose activity followed the same trend of RhoA activity in response to WntA and Dkk-1 in hCMEC/D3 cells. Interestingly, the inhibition of RhoAK by Y27632 quickly decreased the nuclear translocation of  $\beta$ -catenin, with a maximal efficacy after 3 hours. At longer time points, nuclear  $\beta$ -catenin progressively re-accumulated in the nucleus, although it remained lower than in untreated cells: this may be due to the short half-life (i.e., less than 12 hours) of  $\beta$ -catenin,<sup>27</sup> which produces a fast re-synthesis of new  $\beta$ -catenin ready to translocate into the nucleus. After 3 hours, Y27632 effectively increased the phosphorylation on tyrosine 216 of GSK3 and the subsequent GSK3-induced phosphorylation of  $\beta$ -catenin; by acting downstream RhoA, Y27632 was effective even in cells with a constitutively activated RhoA. These data suggest that RhoAK likely controls the GSK3 activity by activating a tyrosine phosphatase, which recognizes GSK3 as substrate. PTP1B, which is activated by the phosphorylation on serine 50,<sup>20</sup> is one of these phosphatases.<sup>19</sup> Our results in hCMEC/D3 cells and in a cell-free system demonstrate that the RhoAK phosphorylates PTP1B on serine 50, promoting the dephosphorylation of GSK3 on tyrosine 216, an event that was fully abrogated by Y27632. These data suggest that the RhoAK, by activating PTP1B, inhibits the GSK3 activity, prevents the ubiquitination of  $\beta$ -catenin, and allows its nuclear translocation and transcriptional activity. Our results also explain previous observations, showing that Wnt3 stimulates the transcription of  $\beta$ -catenin-target genes and RhoA-target genes, with a putative RhoAK-dependent mechanism.<sup>8</sup>

Some  $\beta$ -catenin-target genes encode for proteins of adherens junctions and tight junctions; therefore, changes in RhoA/RhoAK activity may lead to the loss of BBB integrity.<sup>10</sup> In our experimental conditions, no changes occurred in the protein expression and functionality of tight junctions in the hCMEC/D3 cells treated with Y27632. By contrast, Y27632 was sufficient to reduce the  $\beta$ -catenin-driven transcription of Pgp. As different promoters have different sensitivity to the binding of  $\beta$ -catenin–T-cell factor complex, we might speculate that the promoter of Pgp is more sensitive than the promoter of other genes to the variations of  $\beta$ -catenin/T-cell factor binding.

Working at proper concentrations and incubation times, the RhoAK inhibitor increased the delivery of doxorubicin, a Pgp substrate with a very low permeability across the BBB.<sup>13</sup> Fasudil, the clinically prescribed analog of Y27632, is used to prevent vasospasms after subarachnoid hemorrhage,<sup>28</sup> to improve tissue perfusion during cerebral ischemia,<sup>29</sup> to prevent the progression of cerebral aneurysms.<sup>30</sup> Our work suggests that Fasudil might be used to improve the delivery of Pgp substrates through the BBB.

In the case of doxorubicin, a drug that is highly effective against glioblastoma cells *in vitro*<sup>31</sup> and ineffective in the presence of a competent BBB,<sup>6</sup> the pretreatment of hCMEC/D3 cells with Y27632 fully restored the doxorubicin delivery and cytotoxicity in glioblastoma cells. Repeated pulses of Y27632 followed by doxorubicin confirmed that this approach effectively reduced the long-term proliferation of glioblastoma cells grown under a BBB monolayer. However, Pgp is not the only transporter present on the luminal side of BBB that can efflux doxorubicin: also MRP1 and BCRP, which are detectable in the hCMEC/D3 cells,<sup>11</sup> meet these requisites,<sup>1</sup> but their expression did not change in cells with constitutively active RhoA, silenced for RhoA or treated with Y27632. We thus hypothesize that the changes in doxorubicin delivery after RhoA activation or inhibition were consequent to the expression change of Pgp in hCMEC/D3 cells. To further quantify the contribution of this transporter in doxorubicin permeability, we treated the hCMEC/D3 cells with the Pgp inhibitor verapamil, which produced the same effects—in terms of doxorubicin delivery and toxicity in glioblastoma cells—of Y27632. These results indirectly suggest that Pgp has a major role in limiting doxorubicin delivery in the central nervous system.

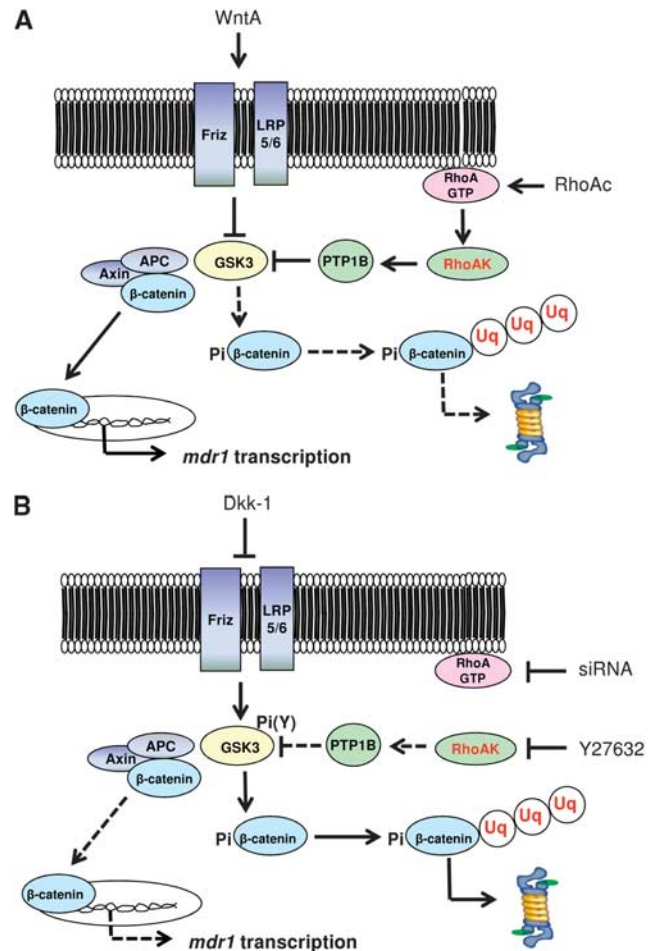


**Figure 6.** Cross-talk between Wnt/GSK3 pathway and Wnt/RhoA/Rho kinase (RhoAK) pathway and effects on P-glycoprotein (Pgp) expression in human blood–brain barrier (BBB) cells. **(A)** The Wnt activators (WntA) reduce the glycogen synthase kinase 3 (GSK3)-mediated phosphorylation and ubiquitination of  $\beta$ -catenin, decreasing its proteasomal degradation. In these conditions,  $\beta$ -catenin is released from the APC/axin complex, translocates into the nucleus, and activates the transcription of *mdr1* gene, which encodes for Pgp. The RhoA activation reduces as well the activity of GSK3: the active RhoA increases the activity of RhoAK, which induces the phosphorylation on serine 50 of protein tyrosine phosphatase 1B (PTP1B). After this phosphorylation, PTP1B dephosphorylates GSK3 on tyrosine 216 and inactivates it. Overall, the activation of the RhoA/RhoAK axis contributes to the transcription of  $\beta$ -catenin target genes, like *mdr1*. **(B)** The Wnt inhibitors (e.g., Dickkopf-1 (Dkk-1)) increase the GSK3-mediated phosphorylation and ubiquitination of  $\beta$ -catenin, priming it for the proteasomal degradation. The inhibition of RhoA (e.g., by RhoA small interfering RNA (siRNA)) or RhoAK (e.g., by Y27632) increases the GSK3 activity, by reducing the RhoAK-mediated phosphorylation of PTP1B on serine 50 and preventing the dephosphorylation of GSK3 on tyrosine 216. As a result, the nuclear translocation of  $\beta$ -catenin and its transcriptional activity are reduced, whereas the ubiquitination and proteasomal degradation of  $\beta$ -catenin are increased. These data lead to hypothesize the existence of a cross-talk between the Wnt/GSK3 canonical pathway and the Wnt/RhoA/RhoAK non-canonical pathway in human BBB cells. APC, adenomatous polyposis coli; Friz, Frizzled; LRP5/6, low density lipoprotein receptor-related protein 5/6; Pi, phosphate; Pi(Y), phosphotyrosine; RhoAc, RhoA activator II; RhoAK, RhoAK; Uq, ubiquitin. Continuous arrows indicate activated pathways; dotted arrows indicate inhibited pathways.

Although Pgp tightly cooperates with BCRP in controlling the delivery of several drugs across the BBB,<sup>32</sup> doxorubicin has high affinity for Pgp, which represents the main transporter of this drug in BBB cells.<sup>33</sup>

The downregulation of the canonical Wnt/GSK3/ $\beta$ -catenin pathway is known to reduce the Pgp expression and to induce chemosensitization in colon<sup>34</sup> and glioblastoma<sup>17</sup> tumor stem cells, neuroblastoma,<sup>35</sup> chronic myeloid leukemia,<sup>36</sup> and cholangiocarcinoma.<sup>37</sup> Also, the inhibition of the non-canonical Wnt3/RhoA/RhoAK pathway chemosensitizes multiple myeloma cells to doxorubicin.<sup>38</sup> We might speculate that the same cross-talk between canonical and non-canonical Wnt pathways, observed in BBB cells, cooperates in regulating the Pgp expression also in cancer cells, and may represent a critical target of therapeutic intervention for Pgp-rich tumors.

We suggest that the expression of Pgp is controlled by a cross-talk between canonical and non-canonical Wnt pathways in human BBB cells. A crucial regulator of this cross-talk is RhoAK, which inhibits the GSK3-induced phosphorylation of  $\beta$ -catenin by activating PTP1B. Targeted therapies against RhoA/RhoAK can disrupt the cross-talk and downregulate the Pgp expression (Figure 6). Improving the BBB permeability of anticancer drugs that are effluxed by Pgp thus enhancing their delivery to brain tumors is still an unsolved challenge.<sup>39</sup> Moreover, the high expression of Pgp on BBB cells decreases not only the delivery of chemotherapeutic agents, but also the passage of drugs used to treat infective diseases, neurodegenerative diseases, and epilepsy.<sup>40</sup> By unveiling a new mechanism that regulates Pgp expression in the BBB cells, our work may pave the way to preclinical investigations using RhoAK inhibitors as adjuvant tools in these central nervous system diseases.

## DISCLOSURE/CONFLICT OF INTEREST

The authors declare no conflict of interest.

## ACKNOWLEDGMENTS

The authors thank Mr Costanzo Costamagna, Department of Oncology, University of Turin for the technical assistance. We are grateful to Professor Davide Schiffer (Neuro-Biooncology Center, Vercelli, Italy) and Dr Rossella Galli (DIBIT, San Raffaele Scientific Institute, Milan, Italy) for providing the primary glioblastoma samples.

## REFERENCES

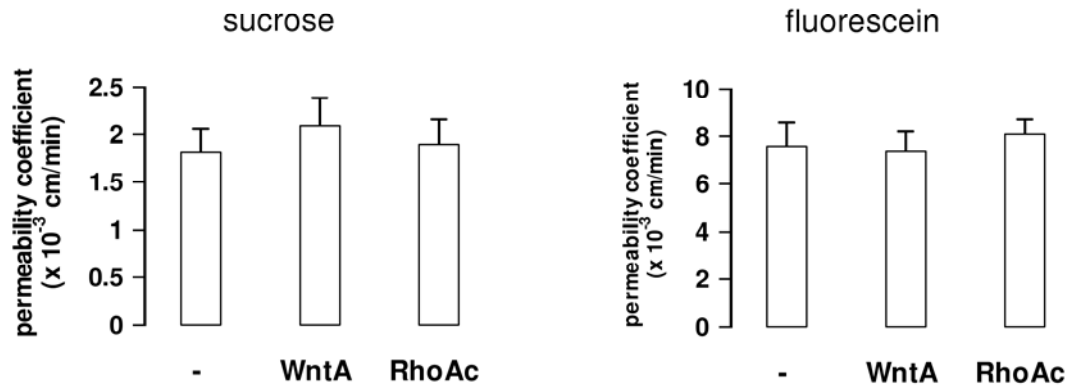
- Agarwal S, Sane R, Oberoi R, Ohlfest JR, Elmquist WF. Delivery of molecularly targeted therapy to malignant glioma, a disease of the whole brain. *Expert Rev Mol Med* 2011; **13**: e17.
- Lim JC, Kania KD, Wijesuriya H, Chawla S, Sethi JK, Pulaski L et al. Activation of  $\beta$ -catenin signalling by GSK-3 inhibition increases p-glycoprotein expression in brain endothelial cells. *J Neurochem* 2008; **106**: 1855–1865.
- Kania KD, Wijesuriya HC, Hladky SB, Barrand MA. Beta amyloid effects on expression of multidrug efflux transporters in brain endothelial cells. *Brain Res* 2011; **1418**: 1–11.
- Katoh M, Katoh M. WNT signalling pathway and stem cells signaling network. *Clin Cancer Res* 2007; **13**: 4042–4045.
- MacDonald BT, Tamai K, He X. Wnt/ $\beta$ -catenin signaling: components, mechanisms, and diseases. *Dev Cell* 2009; **17**: 9–26.
- Riganti C, Salaroglio IC, Pinzón-Daza ML, Caldera V, Campia I, Kopecka J et al. Temozolomide down-regulates P-glycoprotein in human blood-brain barrier cells by disrupting Wnt3-signalling. *Cell Mol Life Sci* 2014; **71**: 499–516.
- Tsuji T, Ohta Y, Kanno Y, Hirose K, Ohashi K, Mizuno K. Involvement of p114-RhoGEF and Lfc in Wnt-3a- and dishevelled-induced RhoA activation and neurite retraction in N1E-115 mouse neuroblastoma cells. *Mol Biol Cell* 2010; **21**: 3590–3600.
- Rossol-Allison J, Stemmler LN, Swenson-Fields KI, Kelly P, Fields PE, McCall SJ et al. Rho GTPase activity modulates Wnt3a/ $\beta$ -catenin signaling. *Cell Signal* 2009; **21**: 1559–1568.
- Chang CC, Lee PS, Chou Y, Hwang LL, Juan SH. Mediating effects of aryl-hydrocarbon receptor and RhoA in altering brain vascular integrity: the therapeutic potential of statins. *Am J Pathol* 2012; **181**: 211–221.
- Allen C, Srivastava K, Bayraktutan U. Small GTPase RhoA and its effector rho kinase mediate oxygen glucose deprivation-evoked *in vitro* cerebral barrier dysfunction. *Stroke* 2010; **41**: 2056–2063.
- Pinzón-Daza ML, Garzón R, Couraud PO, Romero IA, Weksler B, Ghigo D et al. The association of statins plus LDL receptor-targeted liposome-encapsulated doxorubicin increases the *in vitro* drug delivery across blood-brain barrier cells. *Brit J Pharmacol* 2012; **167**: 1431–1447.
- Flatau G, Lemichez E, Gauthier M, Chardin P, Paris S, Fiorentini C et al. Toxin-induced activation of the G protein p21 Rho by deamidation of glutamine. *Nature* 1997; **387**: 729–733.
- Weksler BB, Subileau EA, Perrière N, Charneau P, Holloway K, Leveque M et al. Blood-brain barrier-specific properties of a human adult brain endothelial cell line. *FASEB J* 2005; **19**: 1872–1894.
- Doublier S, Riganti C, Voena C, Costamagna C, Aldieri E, Pescarmona G et al. RhoA silencing reverts the resistance to doxorubicin in human colon cancer cells. *Mol Cancer Res* 2008; **6**: 1607–1620.
- Monnaert V, Betbeder D, Fenart L, Bricout H, Lenfant AM, Landry C et al. Effects of  $\gamma$ - and hydroxypropyl- $\gamma$ -cyclodextrins on the transport of doxorubicin across an *in vitro* model of blood-brain barrier. *J Pharmacol Exp Ther* 2004; **311**: 1115–1120.
- Eigenmann DE, Xue G, Kim KS, Moses AV, Hamburger M, Oufir M. Comparative study of four immortalized human brain capillary endothelial cell lines, hCMEC/D3, hBMEC, TY10, and BB19, and optimization of culture conditions, for an *in vitro* blood-brain barrier model for drug permeability studies. *Fluids Barriers CNS* 2013; **10**: e33.
- Siflinger-Birnboim A, Del Vecchio PJ, Cooper JA, Blumenstock FA, Shepard JM, Malik AB. Molecular sieving characteristics of the cultured endothelial monolayer. *J Cell Physiol* 1987; **132**: 111–117.
- Riganti C, Salaroglio IC, Caldera V, Campia I, Kopecka J, Mellai M et al. Temozolomide down-regulates P-glycoprotein expression in glioblastoma stem cells by interfering with the Wnt3a/GSK3/ $\beta$ -catenin pathway. *Neuro Oncol* 2013; **15**: 1502–1517.
- Mobasher MA, González-Rodríguez A, Santamaría B, Ramos S, Martín MÁ, Goya L et al. Protein tyrosine phosphatase 1B modulates GSK3/ $\beta$ /Nrf2 and IGF1R signaling pathways in acetaminophen-induced hepatotoxicity. *Cell Death Dis* 2003; **4**: e626.
- Moeslein FM, Myers MP, Landreth GE. The CLK family kinases, CLK1 and CLK2, phosphorylate and activate the tyrosine phosphatase, PTP-1B. *J Biol Chem* 1999; **274**: 26697–26704.
- Gottesman MM, Fojo T, Bates SE. Multidrug resistance in cancer: role of ATP-dependent transporters. *Nat Rev Cancer* 2002; **2**: 48–58.
- Tai LM, Loughlin AJ, Male DK, Romero IA. P-glycoprotein and breast cancer resistance protein restrict apical-to-basolateral permeability of human brain endothelium to amyloid- $\beta$ . *J Cereb Blood Flow Metab* 2009; **29**: 1079–1083.
- de Jesus Perez VA, Alastalo TP, Wu JC, Axelrod JD, Cooke JP, Amieva M et al. Bone morphogenetic protein 2 induces pulmonary angiogenesis via Wnt-beta-catenin and Wnt-RhoA-Rac1 pathways. *J Cell Biol* 2009; **184**: 83–99.
- Liu J, Zhang Y, Xu R, Du J, Hu Z, Yang L et al. PI3K/Akt-dependent phosphorylation of GSK3 $\beta$  and activation of RhoA regulate Wnt5a-induced gastric cancer cell migration. *Cell Signal* 2013; **25**: 447–456.
- Uchida Y, Ohtsuki S, Katsukura Y, Ikeda C, Suzuki T, Kamiie J et al. Quantitative targeted absolute proteomics of human blood-brain barrier transporters and receptors. *J Neurochem* 2011; **117**: 333–345.
- Jope RS, Johnson GV. The glamour and gloom of glycogen synthase kinase-3. *Trends Biochem Sci* 2004; **29**: 95–102.
- Bareiss S, Kim K, Lu Q. Delta-catenin/NPRAP: A new member of the glycogen synthase kinase-3beta signaling complex that promotes beta-catenin turnover in neurons. *J Neurosci Res* 2010; **88**: 2350–2363.
- Zoerle T, Ilodigwe DC, Wan H, Lakovic K, Sabri M, Ai J et al. Pharmacologic reduction of angiographic vasospasm in experimental subarachnoid hemorrhage: systematic review and meta-analysis. *J Cereb Blood Flow Metab* 2012; **32**: 1645–1658.
- Shin HK, Huang PL, Ayata C. Rho-kinase inhibition improves ischemic perfusion deficit in hyperlipidemic mice. *J Cereb Blood Flow Metab* 2014; **34**: 284–287.
- Eldawoody H, Shimizu H, Kimura N, Saito A, Nakayama T, Takahashi A et al. Fasudil, a Rho-kinase inhibitor, attenuates induction and progression of cerebral aneurysms: experimental study in rats using vascular corrosion casts. *Neurosci Lett* 2010; **470**: 76–80.
- Hau P, Fabel K, Baumgart U, Rummele P, Grauer O, Bock A et al. Pegylated liposomal doxorubicin-efficacy in patients with recurrent high-grade glioma. *Cancer* 2004; **100**: 1199–1207.
- Agarwal S, Hartz AM, Elmquist WF, Bauer B. Breast cancer resistance protein and P-glycoprotein in brain cancer: two gatekeepers team up. *Curr Pharm Des* 2011; **17**: 2793–2802.

- 33 Qu Q, Chu JW, Sharom FJ. Transition state P-glycoprotein binds drugs and modulators with unchanged affinity, suggesting a concerted transport mechanism. *Biochemistry* 2003; **42**: 1345–1353.
- 34 Chikazawa N, Tanaka H, Tasaka T, Nakamura M, Tanaka M, Onishi H *et al*. Inhibition of Wnt signaling pathway decreases chemotherapy-resistant side-population colon cancer cells. *Anticancer Res* 2010; **30**: 2041–2048.
- 35 Flahaut M, Meier R, Coulon A, Nardou KA, Niggli FK, Martinet D *et al*. The Wnt receptor FZD1 mediates chemoresistance in neuroblastoma through activation of the Wnt/beta-catenin pathway. *Oncogene* 2009; **28**: 2245–2256.
- 36 Corrêa S, Binato R, Du Rocher B, Castelo-Branco MT, Pizzatti L, Abdelhay E. Wnt/ $\beta$ -catenin pathway regulates ABCB1 transcription in chronic myeloid leukemia. *BMC Cancer* 2012; **12**: e303.
- 37 Shen DY, Zhang W, Zeng X, Liu CQ. Inhibition of Wnt/ $\beta$ -catenin signaling downregulates P-glycoprotein and reverses multi-drug resistance of cholangiocarcinoma. *Cancer Sci* 2013; **104**: 1303–1308.
- 38 Kobune M, Chiba H, Kato J, Kato K, Nakamura K, Kawano Y *et al*. Wnt3/RhoA/ROCK signaling pathway is involved in adhesion-mediated drug resistance of multiple myeloma in an autocrine mechanism. *Mol Cancer Ther* 2007; **6**: 1774–1784.
- 39 Serwer LP, James CD. Challenges in drug delivery to tumors of the central nervous system: an overview of pharmacological and surgical considerations. *Adv Drug Deliv Rev* 2012; **64**: 590–597.
- 40 Pinzón-Daza ML, Campia I, Kopecka J, Garzón R, Ghigo D, Riganti C. Nanoparticle- and liposome-carried drugs: new strategies for active targeting and drug delivery across blood-brain barrier. *Curr Drug Metab* 2013; **14**: 625–640.

Supplementary Information accompanies the paper on the Journal of Cerebral Blood Flow & Metabolism website (<http://www.nature.com/jcbfm>)

## Supplementary Figures legends

### Supplementary Figure 1

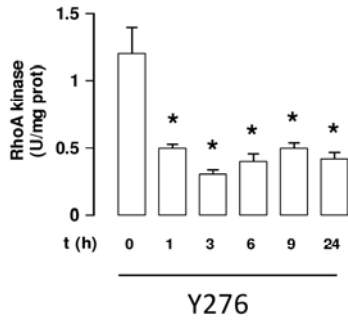


#### Supplementary Figure 1. Effects of Pgp inducers on small molecules permeability in human BBB cells

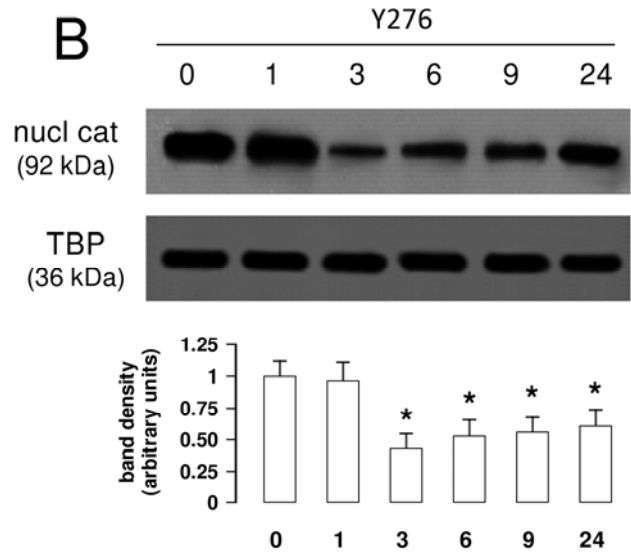
hCMEC/D3 cells were grown for 7 days up to confluence in Transwell inserts, then the medium in the upper chamber was replaced with fresh medium (-) or medium containing Wnt activator 2-amino-4-(3,4-(methylenedioxy)benzylamino)-6-(3-methoxyphenyl)pyrimidine (*WntA*; 20  $\mu\text{mol/L}$  for 24 h) and RhoA activator II (*RhoAc*; 5  $\mu\text{g/mL}$  for 3 h), chosen as Pgp inducers. At the end of the incubation period, 2  $\mu\text{Ci/mL}$  [<sup>14</sup>C]-sucrose or 10  $\mu\text{g/mL}$  sodium fluorescein were added in the upper chamber. After 3 h the amount of each compound recovered from the lower chamber was measured by liquid scintillation (for sucrose) or fluorimetrically (for sodium fluorescein). Permeability coefficients were calculated as reported under Materials and methods. Measurements were performed in duplicate and data are presented as means  $\pm$  SD (n = 3).

## Supplementary Figure 2

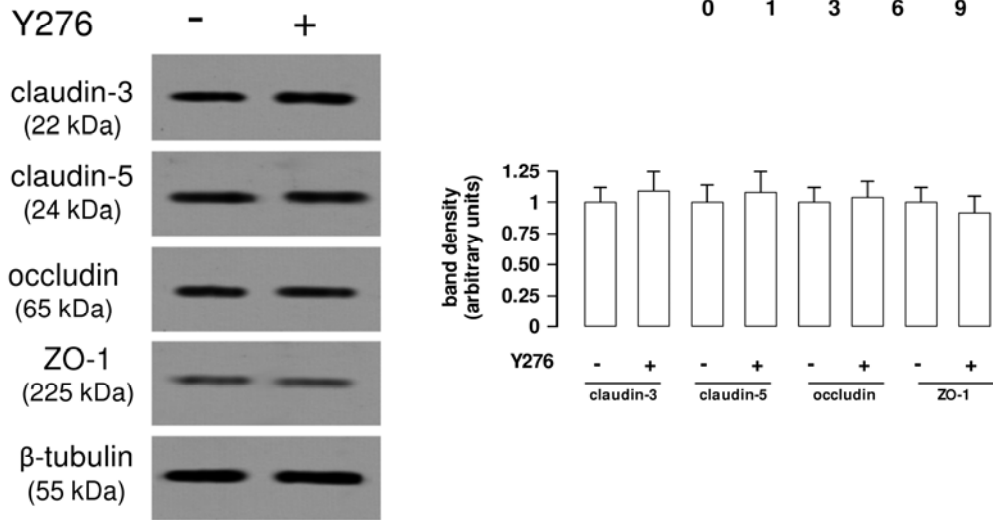
**A**



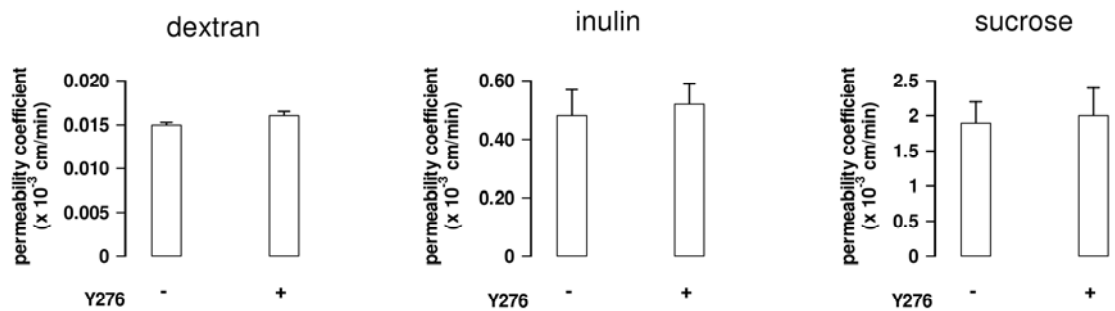
**B**



**C**



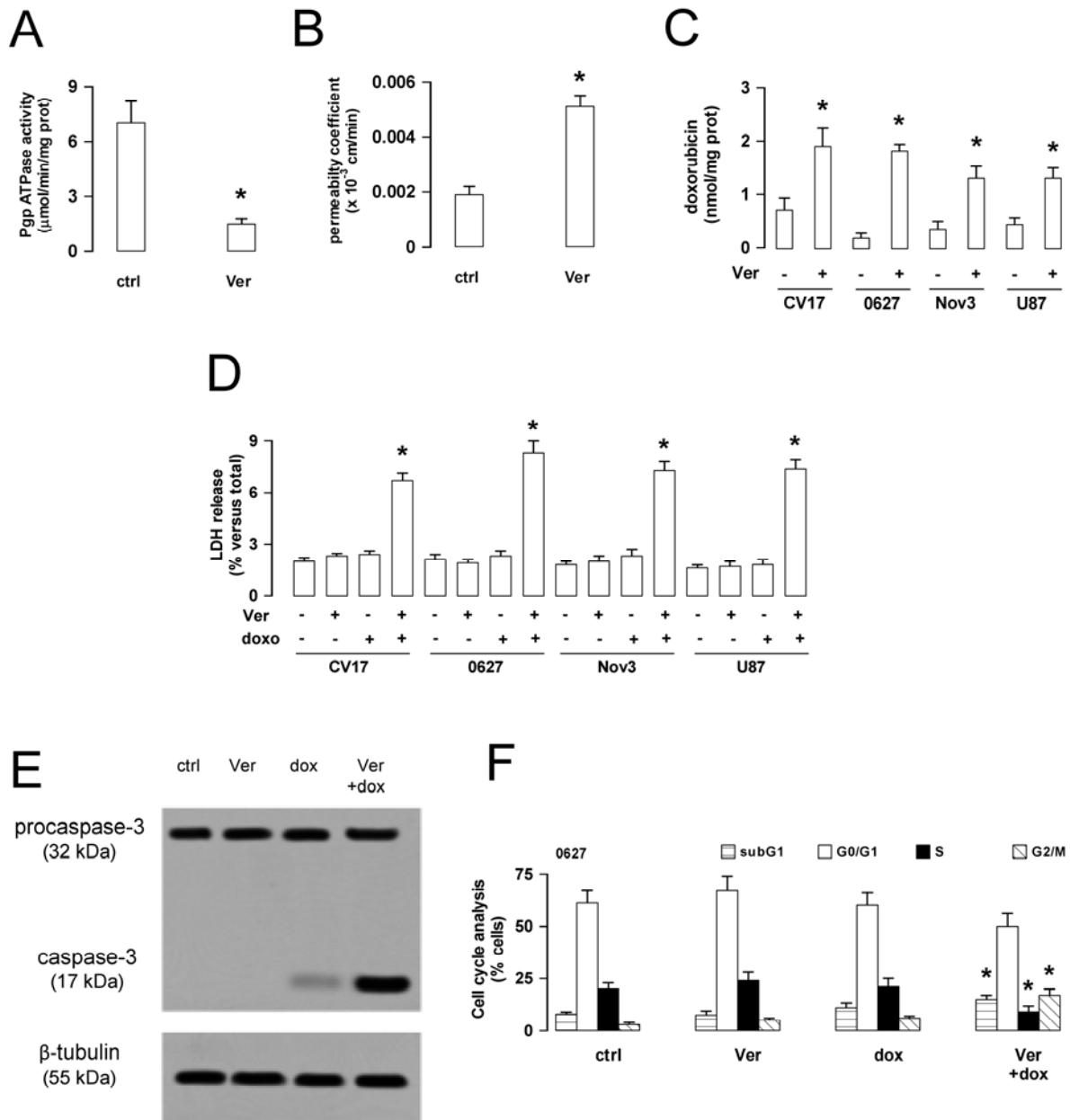
**D**



**Supplementary Figure 2. RhoA kinase inhibition decreases  $\beta$ -catenin translocation in human BBB cells**

hCMEC/D3 cells were cultured in fresh medium in the absence (0) or in the presence of 10  $\mu\text{mol/L}$  of RhoA kinase inhibitor Y27632 (Y276) for 1, 3, 6, 9, 24 h. **A.** RhoA kinase activity. Samples were subjected to ELISA assays to measure the activity of RhoA kinase. Data are presented as means  $\pm$  SD (n = 4). Versus *ctrl*: \* p < 0.001. **B.** Nuclear extracts were analyzed for the amount of  $\beta$ -catenin (*nucl cat*). The expression of TBP was used as control of equal protein loading. The figure is representative of 3 experiments with similar results. The band density ratio between each protein and TBP was expressed as arbitrary units. Versus *ctrl* cells: \* p < 0.01. **C.** hCMEC/D3 cells were cultured in fresh medium (-) or in the presence (+) of 10  $\mu\text{mol/L}$  of the RhoA kinase inhibitor Y27632 (Y276) for 3 h, then lysed and subjected to Western blot analysis for claudin-3, claudin-5, occludin, ZO-1.  $\beta$ -tubulin expression was used as control of equal protein loading. The figure is representative of 3 experiments with similar results. The band density ratio between each protein and  $\beta$ -tubulin was expressed as arbitrary units. **D.** hCMEC/D3 cells were grown for 7 days up to confluence in Transwell inserts, then the medium in the upper chamber was replaced with fresh medium (-) or medium containing (+) 10  $\mu\text{mol/L}$  of the RhoA kinase inhibitor Y27632 (Y276) for 3 h. At the end of the incubation period, 2  $\mu\text{mol/L}$  dextran-FITC, 2  $\mu\text{Ci/mL}$  [ $^{14}\text{C}$ ]-inulin, 2  $\mu\text{Ci/mL}$  [ $^{14}\text{C}$ ]-sucrose, were added in the upper chamber. After 3 h the amount of each compound recovered from the lower chamber was measured fluorimetrically (for dextran-FITC) or by liquid scintillation (for inulin and sucrose). Permeability coefficients were calculated as reported under Materials and methods. Measurements were performed in duplicate and data are presented as means  $\pm$  SD (n = 3).

### Supplementary Figure 3



### Supplementary Figure 3. Effects of verapamil on doxorubicin permeability and cytotoxicity in glioblastoma cells co-cultured with BBB cells

hCMEC/D3 cells were grown for 7 days up to confluence in Transwell inserts; CV17, 01010627, Nov3 and U87-MG cells were seeded at day 4 in the lower chamber. After 3 days of co-culture, supernatant in the upper chamber was replaced with fresh medium without (- or *ctrl*) or with verapamil (*Ver*; 10  $\mu\text{mol}/\text{L}$ ) for 3 h (panels **A-C**) or 24 h (panels **D-F**). Doxorubicin (*dox*; 5  $\mu\text{mol}/\text{L}$ )

was coi-incubated in the upper chamber for 3 h (panels **B-C**) or 24 h (panels **D-F**). **A.** ATPase activity was measured spectrophotometrically after immunoprecipitation of Pgp from membrane fractions. Measurements were performed in duplicate and data are presented as means  $\pm$  SD (n = 3). Versus *ctrl*: \* p < 0.005. **B.** Doxorubicin permeability coefficient was calculated as reported under Materials and methods. Measurements were performed in duplicate and data are presented as means  $\pm$  SD (n = 3). Versus *ctrl*: \* p < 0.001. **C.** Fluorimetric quantification of intracellular doxorubicin in glioblastoma cells. Data are presented as means  $\pm$  SD (n = 3). Versus untreated (-) cells: \* p < 0.01. **D.** Glioblastoma cells were checked spectrophotometrically for the extracellular release of LDH. Data are presented as means  $\pm$  SD (n= 4). Versus untreated (-) cells: \* p < 0.001. **E.** Whole cell lysates from 01010627 cells were resolved by SDS-PAGE and immunoblotted with an anti-caspase-3 antibody (recognizing both pro-caspase and cleaved active caspase).  $\beta$ -tubulin expression was used as control of equal protein loading. The figure is representative of 3 experiments with similar results. **F.** Cell cycle analysis. The distribution of 01010627 cells in sub-G1, G0/G1, S, G2/M phase was analyzed by flow cytometry, as detailed under Materials and methods. Data are presented as means  $\pm$  SD (n=4). Vs *ctrl*: \* p < 0.01.

# The “LDL-masked doxorubicin”: an effective strategy for drug delivery across hypoxic blood brain barrier

Martha L. Pinzón-Daza<sup>a,b</sup>, Joanna Kopecka<sup>a</sup>, Ivana Campia<sup>a</sup>, Ruth Garzon<sup>b</sup>, Chiara Riganti<sup>a,c,\*</sup>

<sup>a</sup> Department of Oncology, School of Medicine, University of Turin, via Santena 5/bis, 10126, Turin, Italy

<sup>b</sup> Unidad de Bioquímica, Facultad de Ciencias Naturales y Matemáticas, Universidad del Rosario, Quinta Mutis Carrera 24 #63C-69, Bogotá, Colombia

<sup>c</sup> Center for Experimental Research and Medical Studies, University of Turin, via Santena 5/bis, 10126, Turin, Italy

\* Author for correspondence: Chiara Riganti, email: chiara.riganti@unito.it  
Received Nov 19, 2013; Accepted Dec 20, 2013; Available Online Dec 20, 2013

## Abstract

The drug delivery across blood brain barrier (BBB) is hampered by the presence of ATP binding cassette transporters, such as P-glycoprotein (Pgp), which effluxes back into the bloodstream several drugs, e.g. anticancer agents like doxorubicin. Pgp is induced by the transcription factor hypoxia-inducible factor-1 $\alpha$  (HIF-1 $\alpha$ ). By using brain microvascular endothelial cells of murine and human origin cultured in normoxia and hypoxia, we observed that - despite species-specific differences, due to the differential basal activity of HIF-1 $\alpha$  - the delivery of Pgp substrates is severely reduced in hypoxic BBB cells. Besides increasing the expression of Pgp, however, HIF-1 $\alpha$  also increased the expression of low density lipoprotein receptor (LDLR), by activating the sterol regulatory element binding protein-2. The amount of LDLR was further enhanced by simvastatin in hypoxia. Combining simvastatin plus a “LDL-masked” liposomal doxorubicin is an effective strategy to improve the drug delivery across hypoxic BBB cells.

**Keywords:** Blood brain barrier; Hypoxia; Hypoxia-inducible factor-1 $\alpha$ ; P-glycoprotein; Low density lipoprotein receptor; Doxorubicin

**Abbreviations:** BBB, blood brain barrier; ABC, ATP binding cassette; Pgp, P-glycoprotein; MRP, multidrug resistance related protein; BCRP, breast cancer resistance protein; HIF-1 $\alpha$ , hypoxia-inducible factor-1 $\alpha$ ; FBS, fetal bovine serum; LDLR, low density lipoprotein receptor; TBS, Tris buffered saline; SREBP-2, sterol regulatory element binding protein-2; TBP, TATA-box binding protein; qRT-PCR, quantitative real time-PCR; HMGCoAR, 3-hydroxy-3-methylglutaryl-coenzyme A reductase; PBS, phosphate-buffered saline; apo-Lipodox, LDL-masked liposomal doxorubicin; LDH, lactate dehydrogenase; LRP1, LDLR-related protein 1; VLDLR, very low density lipoprotein receptor.

## 1. Introduction

The microvascular endothelium surrounding central nervous system, known as blood brain barrier (BBB), represents a natural barrier that limits the delivery of drugs, xenobiotics and toxic catabolites into brain parenchyma. The peculiarity of BBB includes the absence of fenestrations, the high number of tight junctions and adherens junctions, the presence of transmembrane efflux transporters belonging to the ATP binding cassette (ABC) transporters family, such as P-glycoprotein (Pgp/ABCB1), multidrug resistance related proteins (MRPs/ABCCs), breast cancer resistance protein (BCRP/ABCG2) [1]. ABC transporters are integral membrane transporters that hydrolyze ATP obtaining the driving force to pump substrates against their concentration gradient. Pgp and BCRP are the main transporters present on the luminal side of BBB and are involved in the efflux of different substrates, e.g. chemotherapeutic agents (such as anthracyclines, taxanes, Vinca alkaloids, epipodophyllotoxins, topotecan, methotrexate, imatinib, dasatinib, lapatinib, gefitinib, sorafenib, erlotinib), analgesics, anti-retrovirals, antibiotics, anti-epileptics, back into the bloodstream [2]. Given the broad spectrum of drugs transported, Pgp represents a major obstacle for the successful pharmacological therapy of brain tumors, such as glioblastoma multiforme, neurodegenerative diseases, infections, epilepsy [3].

Hypoxia is a condition commonly present in the bulk of solid tumors like glioblastoma or consequent to cardiovascular diseases like stroke. One of the main event occurring during hypoxia is the stabilization of the transcription factor hypoxia-inducible factor-1 $\alpha$  (HIF-1 $\alpha$ ), which is composed by two subunits:  $\beta$  subunit is constitutively synthesized;  $\alpha$  subunit undergoes an O<sub>2</sub>- and iron-dependent degradation in normoxia, while it is stabilized in hypoxia, when the  $\alpha$ - $\beta$  dimer is active as transcription factor [4]. Upon activation, HIF-1 $\alpha$  up-regulates several genes involved in cell proliferation, neo-angiogenesis, matrix remodeling and invasion, pH control, iron metabolism [5], glucose metabolism [6], lipid uptake [7], lipogenesis [8] and steroidogenesis [9,10].

In the last years, it has been reported that chronic hypoxia generates a progressive dysfunction of the neurovascular unit forming the BBB; such dysfunction has been implicated in the pathogenesis of various central nervous system diseases, including Alzheimer disease and amyotrophic lateral sclerosis [11]. Several studies demonstrated that hypoxia destabilizes the tight junctions, increases the paracellular leakage of substrates [12-14], changes the activity and expression of membrane transporters, such as the Na-K-Cl co-transporter [15] and the glucose transporters [16]. Notably, the promoter of Pgp gene has an hypoxia responsive element [17]. Repetitive exposures to low O<sub>2</sub> tension indeed increase the expression of Pgp in rat brain microvascular endothelial cells [18]. The increased expression of Pgp occurring in

hypoxia is expected to further limit the success of pharmacological therapy in diseases characterized by large hypoxic areas, such as glioblastoma.

Aim of this study is to analyze how the transport of Pgp substrates varies in normoxic and hypoxic BBB cells, and to design a strategy that allows an effective delivery also in hypoxia.

## 2. Experimental Details

### 2.1. Chemicals

Fetal bovine serum (FBS) and culture medium were purchased from Invitrogen Life Technologies (Carlsbad, CA). Plasticware for cell cultures was from Falcon (Becton Dickinson, Franklin Lakes, NJ). Simvastatin was purchased from Calbiochem (San Diego, CA). Electrophoresis reagents were obtained from Bio-Rad Laboratories (Hercules, CA). The protein content of cell lysates was assessed with the BCA kit from Sigma Chemical Co. (St. Louis, MO). When not otherwise specified, all the other reagents were purchased from Sigma Chemical Co.

### 2.2. Cells

bEND3 cells, a murine brain microvascular endothelial cell line, were purchased from ATCC (Manassas, VA) and cultured in DMEM medium, containing 10% v/v FBS, 1% v/v penicillin-streptomycin, 1% v/v L-glutamine. hCMEC/D3 cells, a primary human brain microvascular endothelial cell line, were a kind gift from Prof. Pierre-Olivier Couraud (Institut Cochin, Centre National de la Recherche Scientifique UMR 8104, INSERM U567, Paris, France) and were cultured according to [19]. Both bEND3 and hCMEC/D3 cells retain the BBB characteristics when cultured *in vitro*, as demonstrated by the measure of permeability coefficients of different substrates, by the trans-epithelial electric resistance value and by the expression profile of tight junction proteins [19-22]. Cells were seeded at 50,000/cm<sup>2</sup> density, and grown for 7 days up to confluence in Petri dishes or Transwell devices (0.4 μm diameter pore-size, Corning Life Sciences, Chorges, France), to allow the formation of a competent BBB.

C6 and U87-MG cells (from ATCC) were chosen as models of glioblastoma cells and were respectively cultured in HAMF12 medium and DMEM medium, with 10% v/v FBS, 1% v/v penicillin-streptomycin, 1% v/v L-glutamine. In co-culture experiments, 500,000 C6 cells were added in the lower chamber of Transwell devices, 4 days after seeding bEND3 cells in the Transwell insert; 500,000 U87-MG cells were added in the lower chamber of Transwell devices, 4 days after seeding hCMEC/D3 cells in the Transwell insert. After 3 days of co-culture the medium of the upper and lower chamber was replaced, and cells were used for the experimental assays.

When cultured in normoxic conditions, cells were maintained in a humidified atmosphere at 37°C, 5% CO<sub>2</sub> and 21% O<sub>2</sub>; when cultured in hypoxic conditions, cells were maintained in a humidified atmosphere at 37°C, 5% CO<sub>2</sub> and 2% O<sub>2</sub>, in a Heracell 150i incubator (Thermo Scientific, Waltham, MA).

### 2.3. Permeability assays

The permeability of doxorubicin, [<sup>3</sup>H]-vinblastine (0.25 mCi/mL, PerkinElmer, Waltham, MA), mitoxantrone, was taken as index of Pgp and BCRP activity [19]. bEND3 and hCMEC/D3 cells were seeded at 50,000/cm<sup>2</sup> and grown for 7

days up to confluence in 6-multiwell Transwell inserts; culture medium was replaced with fresh one and 5 μmol/L doxorubicin, 2 μCi/mL [<sup>3</sup>H]-vinblastine, 10 μmol/L mitoxantrone were added to the upper chamber of Transwell. After 3 h the medium in the lower chamber was collected. The amount of [<sup>3</sup>H]-vinblastine was measured using a Tri-Carb Liquid Scintillation Analyzer (PerkinElmer). Radioactivity was converted in nmol/cm<sup>2</sup>, using a previously prepared calibration curve. The amount of doxorubicin and mitoxantrone was measured fluorimetrically, using a LS-5 spectrofluorimeter (PerkinElmer). Excitation and emission wavelengths were: 475 nm and 553 nm (doxorubicin); 607 nm and 684 nm (mitoxantrone). Fluorescence was converted in nmol/cm<sup>2</sup>, using a calibration curve previously set. The permeability coefficients were calculated as reported [23].

### 2.4. Western blot

Cells were rinsed with lysis buffer (50 mmol/L Tris, 10 mmol/L EDTA, 1% v/v Triton-X100), supplemented with the protease inhibitor cocktail set III (80 μmol/L aprotinin, 5 mmol/L bestatin, 1.5 mmol/L leupeptin, 1 mmol/L pepstatin; Calbiochem), 2 mmol/L phenylmethylsulfonyl fluoride and 1 mmol/L Na<sub>3</sub>VO<sub>4</sub>, then sonicated and centrifuged at 13,000 x g for 10 min at 4°C. 20 μg of protein extracts were subjected to SDS-PAGE and probed with the following antibodies: anti-Pgp/ABCB1 (C219, Novus Biologicals, Cambridge, UK); anti-MRP1/ABCC1 (Abcam, Cambridge, UK); anti-MRP2/ABCC2 (Abcam); anti-MRP3/ABCC3 (Santa Cruz Biotechnology Inc., Santa Cruz, CA); anti-MRP4/ABCC4 (Abcam); anti-MRP5/ABCC5 (Santa Cruz Biotechnology Inc.); anti-MRP6/ABCC6 (Santa Cruz Biotechnology Inc.); anti-BCRP/ABCG2 (Santa Cruz Biotechnology Inc.); anti-low density lipoprotein receptor (LDLR; Abcam); anti-β-tubulin (Santa Cruz Biotechnology Inc.), followed by the peroxidase-conjugated secondary antibody (Bio-Rad). The membranes were washed with Tris buffered saline (TBS)-Tween 0.1% v/v, and proteins were detected by enhanced chemiluminescence (Bio-Rad).

10 μg of nuclear extracts, obtained with the Nuclear Extraction Kit (Active Motif, Rixensart, Belgium), were subjected to Western blot analysis using an HIF-1α (BD Bioscience, San Jose, CA) or an anti-sterol regulatory element binding protein-2 (SREBP-2, Santa Cruz Biotechnology Inc.) antibodies. To check the equal control loading in nuclear fractions, samples were probed with an anti-TATA-box binding protein (TBP/TFIID) antibody (Santa Cruz Biotechnology Inc.). To exclude any cytosolic contamination of nuclear extracts, we verified that β-tubulin was undetectable in nuclear samples (not shown).

In co-immunoprecipitation assays, 100 μg of proteins from nuclear extracts were immunoprecipitated with the anti-HIF-1α antibody, using the PureProteome protein A and protein G Magnetic Beads (Millipore, Billerica, MA). Immunoprecipitated proteins were separated by SDS-PAGE and probed with the anti-SREBP-2 antibody or with the anti-HIF-1α antibody (to verify the effective immunoprecipitation), followed by the peroxidase-conjugated secondary antibody.

The densitometric analysis of Western blots was performed with the ImageJ software (<http://rsb.info.nih.gov/ij/>) and expressed as arbitrary units, where "1 unit" (or "0 unit" in case of undetectable bands) is the mean band density of bEND3 cells grown at 21% O<sub>2</sub>.

### 2.5. HIF-1 $\alpha$ activity

Nuclear proteins were extracted using the Nuclear Extract Kit (Active Motif). The activity of HIF-1 $\alpha$  was assessed on 10  $\mu$ g of nuclear proteins with the TransAM™ HIF-1 Transcription Factor Assay Kit (Active Motif), following the manufacturer's instructions. Data were expressed as U absorbance/mg cell proteins. For each set of experiments, blank (with bis-distilled water), negative control (with mutated oligonucleotide) and competition assay (using 20 pmol of the wild type non-biotinylated oligonucleotide, in the presence of the nuclear extracts of bEND3 and hCMEC/D3 cells grown at 2% O<sub>2</sub> for 24 h) - were included. With mutated oligonucleotide, HIF-1 $\alpha$  activity was  $0.51 \pm 0.07$  U/mg cell proteins for bEND3 cells and  $0.63 \pm 0.09$  U/mg cell proteins for hCMEC/D3 cells; in the competition assay, HIF-1 $\alpha$  activity was  $1.02 \pm 0.14$  U/mg cell proteins for bEND3 cells and  $2.24 \pm 0.33$  U/mg cell proteins for hCMEC/D3 cells (n = 3).

### 2.6. Quantitative Real Time PCR (qRT-PCR)

Total RNA was extracted and reverse-transcribed using the QuantiTect Reverse Transcription Kit (Qiagen, Hilden, Germany). qRT-PCR was carried out with the IQ™ SYBR Green Supermix (Bio-Rad). The same cDNA preparation was used for the quantitation of *Pgp*, *3-hydroxy-3-methylglutaryl-coenzyme A reductase (HMGCoAR)* and *actin*, chosen as housekeeping gene. Primer sequences, designed with Primer3 software (<http://frodo.wi.mit.edu/primer3>), were: *Pgp*: 5'-TGCTGGAGCGTTCTACG-3'; 5'-ATAGGCAA TGTTCTCAGCAATG-3'; *HMGCoAR*: 5'-CGCAACCTC TATATCCGT-3'; 5'-GTAGCCGCCTATGCTC-3'; *actin*: 5'-GCTATCCAGGCTGTGCTATC-3'; 5'-TGTCACGCACGA TTTCC-3'. The relative quantitation of samples was performed by comparing each PCR product with the housekeeping PCR product, using the Software Gene Expression Quantitation (Bio-Rad).

### 2.7. De novo cholesterol synthesis

Cells were labeled with 1  $\mu$ Ci/mL [<sup>3</sup>H]acetate (3600 mCi/mmol; Amersham Bioscience, Piscataway, NJ) and the synthesis of radiolabeled cholesterol was measured as described [24]: after 24 h cells were washed twice with phosphate-buffered saline (PBS) and mechanically scraped in 200  $\mu$ L of PBS. 500  $\mu$ L of methanol and 1 mL of hexane were added to the cell suspension, which was stirred at room temperature for 1 h and then centrifuged at 2,000 x g for 5 min. The upper phase was transferred into a new test tube; the lower phase was supplemented with 1 mL of hexane and stirred overnight. After a 5 min centrifugation at 2,000 x g, the new upper phase was added to the previous one and the solvent was allowed to evaporate at room temperature for 24 h. Cellular lipid extracts produced by this separation were re-suspended in 30  $\mu$ L of chloroform and subjected to thin layer chromatography, using a 1:1 (v/v) ether/hexane solution as mobile phase. Each sample was spotted on pre-coated LK6D Whatman silica gels (Merck, Darmstadt, Germany) and allowed to run for 30 min. A solutions of cholesterol (10  $\mu$ g/mL) was used as standard. The silica gel plates were exposed for 1 h to a iodine-saturated atmosphere, then the migrated spots were cut out and their radioactivity was measured by liquid scintillation, using a Tri-Carb Liquid Scintillation Analyzer (PerkinElmer). The results were expressed as pmol [<sup>3</sup>H]cholesterol/mg cell proteins, according to the relative calibration curve.

### 2.8. "LDL-masked" liposomal doxorubicin (apo-Lipodox) preparation

"LDL-masked" liposomal doxorubicin (termed apo-Lipodox) was prepared using anionic pegylated liposomes (COATSOME EL-01-PA, NOF Corporation, Tokyo, Japan) as detailed in [25]. The size of the liposomes was evaluated by dynamic light scattering with an ALV-NIBS dynamic light scattering instrument (ALV-Laser, Langen, Germany), provided with a Ne-He laser and an ALV-5000 multiple tau digital correlator. The scattered light intensity was recorded for 30 s on liposome suspensions at 37°C. The hydrodynamic radius of liposomes was evaluated by using both the cumulant method and the CONTIN algorithm [26]. The mean radius of apo-Lipodox was  $72.44 \pm 23.17$  nm; the polydispersity index was 0.189.

The intraliposomal doxorubicin was measured on a 5  $\mu$ L aliquot of apo-Lipodox, diluted 1:100 into a 1:1 v/v solution of ethanol/HCl 0.3 N, and sonicated. The fluorescence of doxorubicin was detected fluorimetrically as reported above. The encapsulation efficiency was  $86 \pm 7$  %. Apo-Lipodox was stocked at 4°C at a concentration of 0.5 mmol/L.

### 2.9. Intratumor doxorubicin delivery and cytotoxicity in co-culture models

The intratumor doxorubicin delivery was measured as previously described [27]. After 3 days of co-culture, doxorubicin (5  $\mu$ mol/L) was added to the upper chamber of Transwell inserts containing bEND3 or hCMEC/D3 cells monolayer. After 3 h, C6 and U87-MG glioblastoma cells were collected from the lower chamber, rinsed with PBS, re-suspended in 0.5 mL ethanol/HCl 0.3 N (1:1 v/v), and sonicated. A 50  $\mu$ L aliquot was used to measure the protein content, the remaining sample was used to quantify fluorimetrically the intracellular doxorubicin content, as described above. Results were expressed as nmol doxorubicin/mg cell proteins.

For cytotoxicity assays, 5  $\mu$ mol/L doxorubicin was added to the upper chamber of Transwell inserts. After 24 h, both cell culture medium and glioblastoma cells from the lower chamber were collected. The activity of lactate dehydrogenase (LDH) in cell supernatant, used as index of cell damage and necrosis, and the activity of LDH in cell lysates were measured spectrophotometrically as described earlier [28]. Both intracellular and extracellular enzyme activity were expressed in  $\mu$ mol NADH oxidized/min/dish, then extracellular LDH activity was calculated as percentage of the total LDH activity in the dish.

### 2.10. Statistical analysis

All data in text and figures are provided as means  $\pm$  SD. The results were analyzed by a one-way Analysis of Variance (ANOVA). A  $p < 0.05$  was considered significant.

## 3. Results

### 3.1. Hypoxia lowers the delivery of *Pgp* substrates across murine, but not human BBB cells

To evaluate how hypoxia affects the delivery of substrates of *Pgp* and BCRP, two ABC transporters highly expressed on the luminal side of BBB cells [2], we measured the permeability coefficient of doxorubicin and vinblastine (two *Pgp* substrates), and mitoxantrone (a BCRP substrate). In

normoxia, hCMEC/D3 cells had a lower transport of doxorubicin and – at lesser extent – of vinblastine, than bEND3 cells; no differences in the transport of mitoxantrone were detected between normoxic bEND3 and hCMEC/D3 cells (Figure 1A). Hypoxia reduced the permeability of Pgp substrates only in murine bEND3 cells; surprisingly it did not further reduce the transport of doxorubicin and vinblastine in human hCMEC/D3 cells. In parallel, we did not detect any significant variations in the permeability of mitoxantrone in both cell lines in hypoxic conditions (Figure 1A). To explain such differences, we examined the ABC transporters present in murine and human BBB cells in normoxia and hypoxia: as shown in Figure 1B, normoxic human hCMEC/D3 cells were richer of Pgp, MRP1, MRP2 and MRP6 compared with normoxic murine bEND3 cells. Hypoxia did not produce significant differences in the expression of ABC transporters in both cell lines, with the exception of Pgp, which was significantly increased in murine bEND3 cells (Figure 1B). By contrast, in hCMEC/D3 cells, where the amount of Pgp in normoxic conditions was comparable to the amount of Pgp in hypoxic bEND3 cells, Pgp was not further increased by hypoxia (Figure 1B).

These results suggest that species-specific differences occur for the transport of Pgp substrates under hypoxic conditions, because of the different basal levels of Pgp and the different modulation of Pgp in response to hypoxia.

### 3.2. Hypoxia induces the HIF-1 $\alpha$ -driven transcription of Pgp in murine, but not in human BBB cells

HIF-1 $\alpha$  is one of the main factor activated by hypoxia [4] and it is a strong inducer of Pgp [17]. We therefore analyzed its activation in murine and human BBB cells cultured in normoxia and hypoxia, by measuring the amount of HIF-1 $\alpha$  in nuclear extracts and the binding of the translocated HIF-1 $\alpha$  to a DNA target sequence containing an hypoxia responsive element (Figure 2A-B). As expected, HIF-1 $\alpha$  was undetectable in the nucleus of bEND3 cells (Figure 2A) and the DNA binding activity was very low (Figure 2B) under normoxic conditions. Hypoxia increased both the nuclear translocation and activity of HIF-1 $\alpha$  in bEND3 cells. The same results were obtained by treating cells with CoCl<sub>2</sub> (Figure 2A-B), used as a chemical inducer of HIF-1 $\alpha$  [29]. Surprisingly, HIF-1 $\alpha$  was constitutively translocated in the nucleus and bound to DNA in normoxic hCMEC/D3 cells; we did not detect any further increase in hCMEC/D3 cells grown in an hypoxic environment or treated with CoCl<sub>2</sub> (Figure 2A-B).

In keeping with the differential activity of HIF-1 $\alpha$ , normoxic bEND3 cells had a lower expression of Pgp mRNA than normoxic hCMEC/D3 cells (Figure 2C); whereas hypoxia and CoCl<sub>2</sub> significantly increased Pgp transcription in murine BBB cells, they did not change the Pgp transcription in human BBB cells, which had the same Pgp mRNA levels in normoxia and hypoxia (Figure 2C). The difference in HIF-1 $\alpha$  translocation and activation may explain the differences in Pgp expression and in permeability of Pgp substrates, observed between murine and human BBB cells in normoxia and hypoxia.

### 3.3. When activated, HIF-1 $\alpha$ promotes the nuclear translocation and the transcriptional activity of SREBP-2 in both murine and human BBB cells

Recently, we demonstrated a direct correlation between the expression of Pgp and the activity of mevalonate

pathway, the metabolic cascade which produces cholesterol [30]. Most genes of the mevalonate pathway, including the pace-maker enzyme HMGCoAR, are under the transcriptional control of the SREBP-2 factor. The latter is activated by low levels of intracellular cholesterol, but also by the interaction with other transcription factors like HIF-1 $\alpha$  [9]. We thus wonder whether the differential activation of HIF-1 $\alpha$  between normoxic and hypoxic murine and human BBB cells may change the activity of SREBP-2 and the expression of HMGCoAR.

Interestingly, when activated - i.e. in hypoxic bEND3 cells, in normoxic and hypoxic hCMEC/D3 cells -, nuclear HIF-1 $\alpha$  co-immunoprecipitated with SREBP-2 (Figure 3A). The interaction with HIF-1 $\alpha$  was paralleled by a change in the nuclear levels of SREBP-2: normoxic bEND3 cells have a detectable levels of nuclear SREBP-2, which was significantly increased in hypoxic conditions (Figure 3B). hCMEC/D3 cells, which had a constitutive activation of HIF-1 $\alpha$  in normoxia and hypoxia (Figure 2A-B), had a constitutively high nuclear level of SREBP-2 (Figure 3B). In line with the differential nuclear translocation of HIF-1 $\alpha$ /SREBP-2 complex, normoxic bEND3 cells had lower HMGCoAR mRNA levels than hypoxic cells (Figure 3C); by contrast, in hCMEC/D3 cells the transcription of HMGCoAR was unchanged in normoxia and hypoxia, and was similar to that measured in hypoxic bEND3 cells (Figure 3C).

This experimental set pointed out that the differential activity of HIF-1 $\alpha$  in murine and human BBB cells not only explains the differences in Pgp expression, but also determines a different transcription of SREBP-2 target genes.

The changes in HMGCoAR expression determined a different metabolic flux through the mevalonate pathway, measured as rate of *de novo* cholesterol synthesis (Figure 4A): compared with normoxic bEND3 cells, hypoxic bEND3 cells had a higher cholesterol synthesis; in hCMEC/D3 cells the mevalonate pathway activity was high either in normoxia or in hypoxia, and again was superimposable to the activity measured in hypoxic bEND3 cells (Figure 4A). Independently from the basal rate of cholesterol synthesis, in both cell lines in normoxia and hypoxia, the activity of the mevalonate pathway was significantly reduced by the HMGCoAR inhibitor simvastatin (Figure 4A).

Another target gene of SREBP-2 is LDLR, whose expression is also increased when intracellular cholesterol levels decrease [31]. In our models, the expression of LDLR varied in accord to the activation of SREBP-2/HIF-1 $\alpha$  complex: indeed normoxic bEND3 cells, which had undetectable nuclear translocation of HIF-1 $\alpha$  (Figure 2A) and low nuclear levels of SREBP-2 (Figure 3B), had a small amount of LDLR (Figure 4B). Such amount was increased by hypoxia, which increased in parallel the nuclear levels of HIF-1 $\alpha$  (Figure 2A) and SREBP-2 (Figure 3B). Normoxic and hypoxic hCMEC/D3 cells, characterized by high amounts of nuclear HIF-1 $\alpha$  (Figure 2A) and SREBP-2 (Figure 3B), were characterized as well by a high expression of LDLR (Figure 4B). Of note, the expression of LDLR was sensitive to the intracellular variations of cholesterol: indeed simvastatin, which reduced the synthesis of cholesterol (Figure 4A), increased the expression of LDLR in all the experimental conditions (Figure 4B).

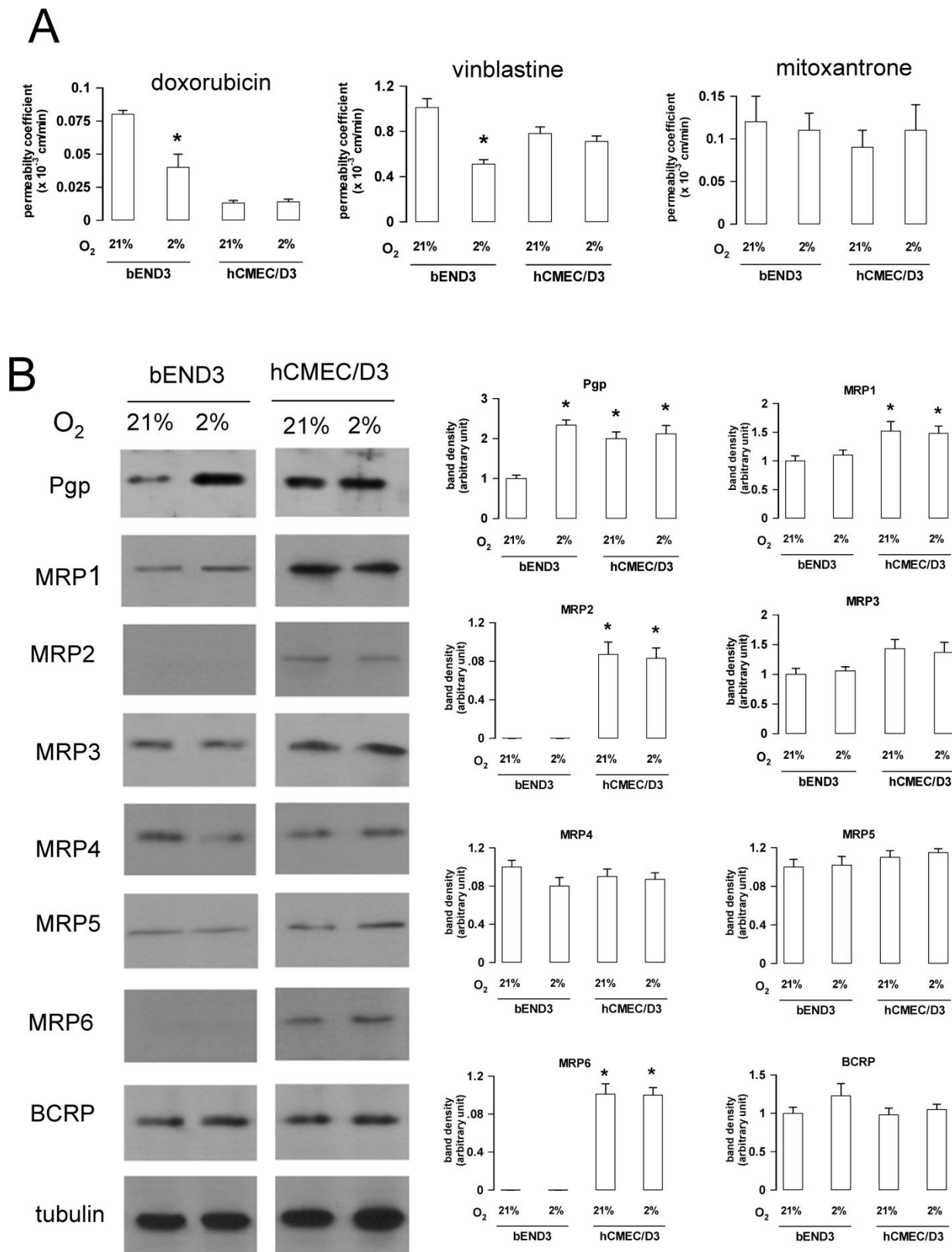


**Figure 1.** Hypoxia reduces the delivery of Pgp substrates and increases Pgp expression in murine, but not in human BBB cells. **A.** bEND3 and hCMEC/D3 cells were grown for 7 days up to confluence in Transwell inserts, in normoxic (21% O<sub>2</sub>) or hypoxic (2% O<sub>2</sub>) conditions, then the medium in the upper chamber was replaced with medium containing 5 μmol/L doxorubicin, 2 μCi/mL [<sup>3</sup>H]-vinblastine, 10 μmol/L mitoxantrone. After 3 h the amount of each compound recovered from the lower chamber was measured fluorimetrically (for doxorubicin and mitoxantrone) or by liquid scintillation (for vinblastine). Permeability coefficients were calculated as reported under Experimental Details. Measurements were performed in duplicate and data are presented as means ± SD (n = 3). For each cell line, permeability at 2% O<sub>2</sub> versus permeability at 21% O<sub>2</sub>: \* p < 0.05. **B.** Cells were grown for 7 days in normoxic (21% O<sub>2</sub>) or hypoxic (2% O<sub>2</sub>) conditions, then lysed and subjected to Western blot analysis for Pgp, MRP1, MRP2, MRP3, MRP4, MRP5, MRP6, BCRP. β-tubulin expression was used as control of equal protein loading. The figure is representative of 3 experiments with similar results. The band density ratio between each protein and β-tubulin was expressed as arbitrary units. Versus bEND3 cells at 21% O<sub>2</sub>: \* p < 0.05.

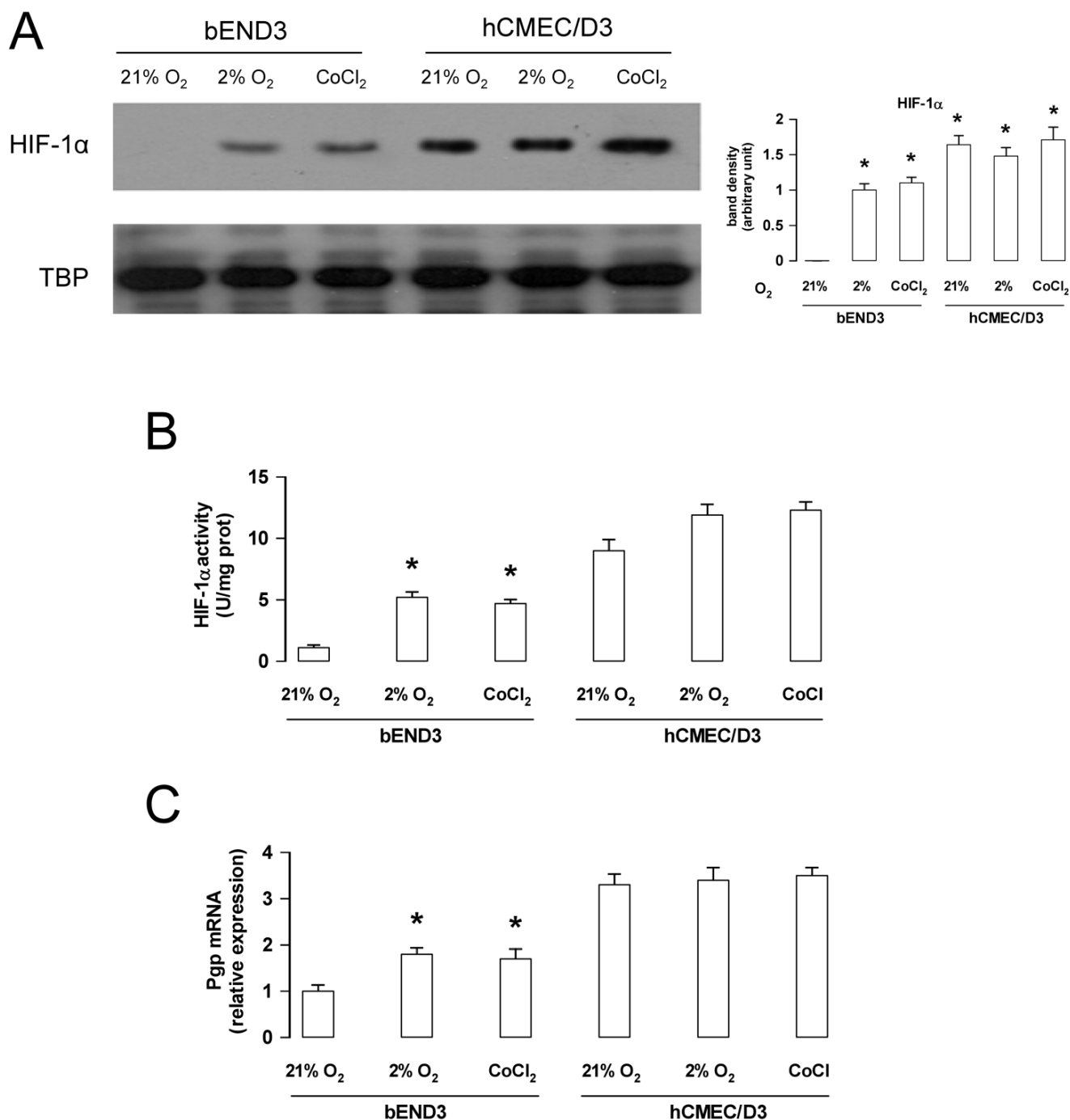


**Figure 2.** Murine, but not human BBB cells are sensitive to the hypoxia induced activation of HIF-1α and transcription of *Pgp*. bEND3 and hCMEC/D3 cells were grown for 7 days up to confluence in normoxic (21% O<sub>2</sub>) or hypoxic (2% O<sub>2</sub>) conditions, then subjected to the following investigations. When indicated, cells grown at 21% O<sub>2</sub> were incubated with CoCl<sub>2</sub> (10 μmol/L for the last 24 h), chosen as a chemical activator of HIF-1α. A. Nuclear extracts were analyzed for the amount of HIF-1α by Western blotting. The expression of TBP was used as control of equal protein loading. The band density ratio between HIF-1α and TBP was expressed as arbitrary units. Versus bEND3 cells at 21% O<sub>2</sub>: \* *p* < 0.001. B. HIF-1α activity was measured in nuclear extracts by ELISA assay. Data are presented as means ± SD (n = 3). For each cell line, versus 21% O<sub>2</sub>: \* *p* < 0.005. C. *Pgp* mRNA levels were detected in triplicate by qRT-PCR. Data are presented as means ± SD (n = 4). For each cell line, versus 21% O<sub>2</sub>: \* *p* < 0.02.

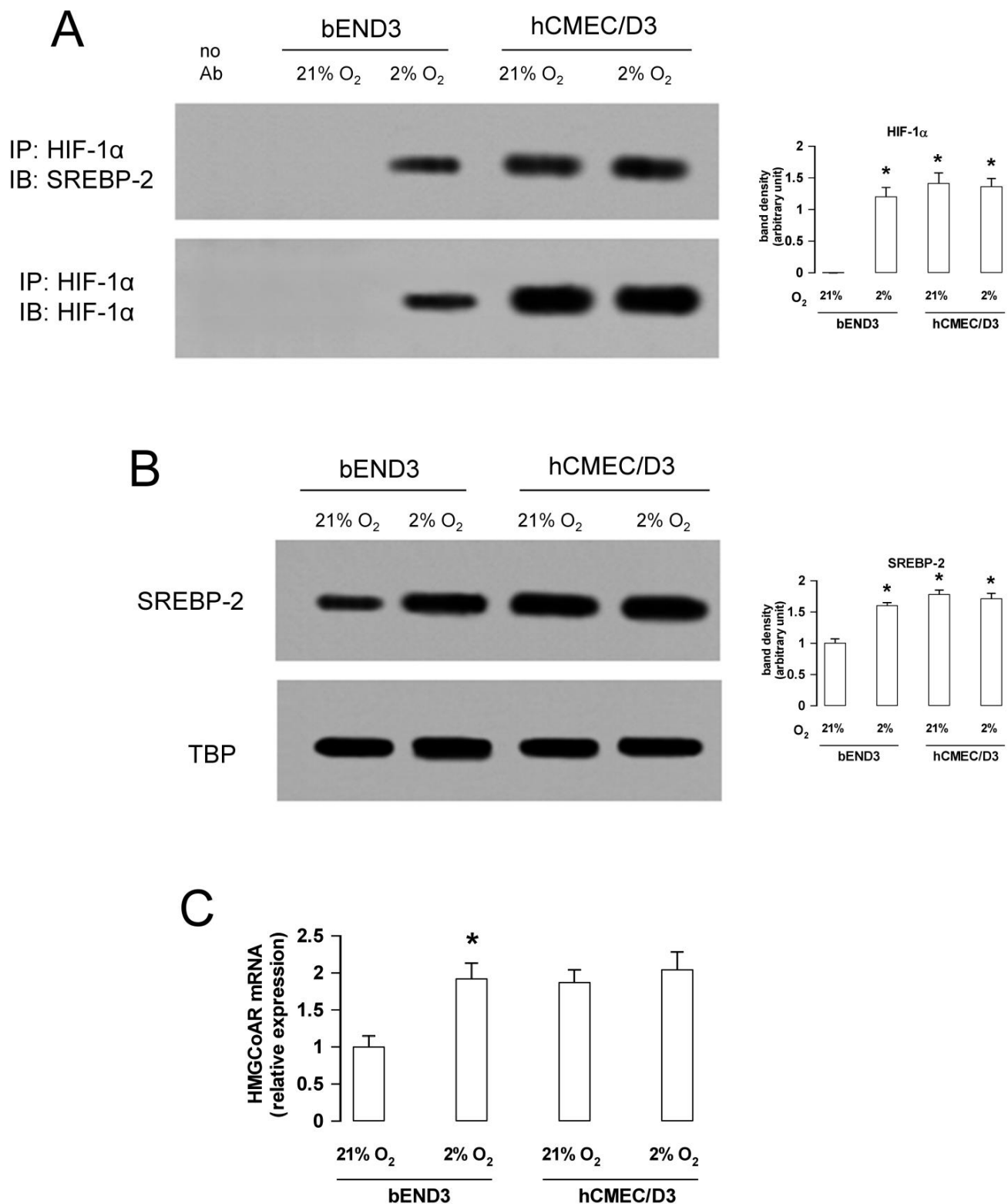
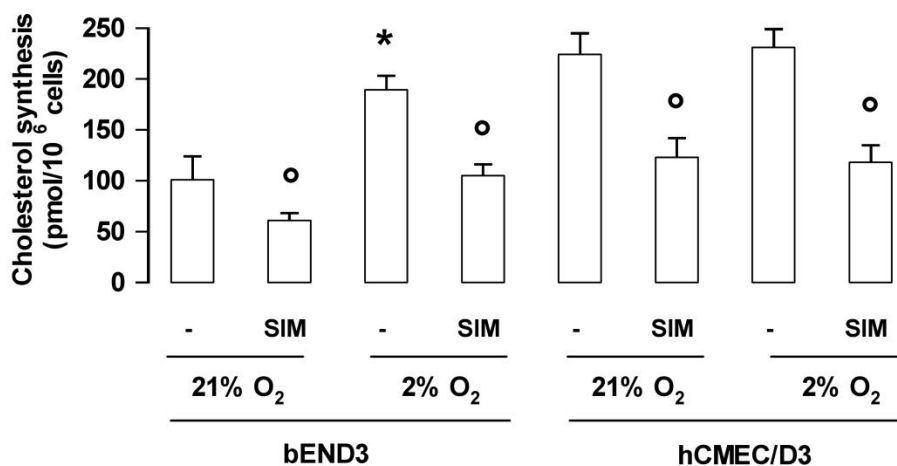


**Figure 3.** HIF-1α co-immunoprecipitates with SREBP-2, increases the nuclear translocation of SREBP-2 and the transcription of *HMGCAR* in murine and human BBB cells. bEND3 and hCMEC/D3 cells were grown for 7 days up to confluence in normoxic (21% O<sub>2</sub>) or hypoxic (2% O<sub>2</sub>) conditions, then subjected to the following investigations. A. Nuclear extracts were immunoprecipitated (IP) with an anti-HIF-1α antibody, then immunoblotted (IB) with an anti-SREBP-2 antibody or with an anti-HIF-1α antibody. The figure is representative of 3 experiments with similar results. *no Ab*: hypoxic hCMEC/D3 nuclear extracts immunoprecipitated without the anti-HIF-1α antibody. The band density ratio between HIF-1α (after IP for HIF-1α + IB for SREBP-2) and HIF-1α (after IP for HIF-1α + IB for HIF-1α) was expressed as arbitrary units. Versus bEND3 cells at 21% O<sub>2</sub>: \* *p* < 0.001. B. Nuclear extracts were analyzed for the amount of SREBP-2 by Western blotting. The expression of TBP was used as control of equal protein loading. The band density ratio between SREBP-2 and TBP was expressed as arbitrary units. Versus bEND3 cells at 21% O<sub>2</sub>: \* *p* < 0.005. C. *HMGCAR* mRNA levels were detected in triplicate by qRT-PCR. Data are presented as means ± SD (n = 4). For each cell line, versus 21% O<sub>2</sub>: \* *p* < 0.01.

A



B

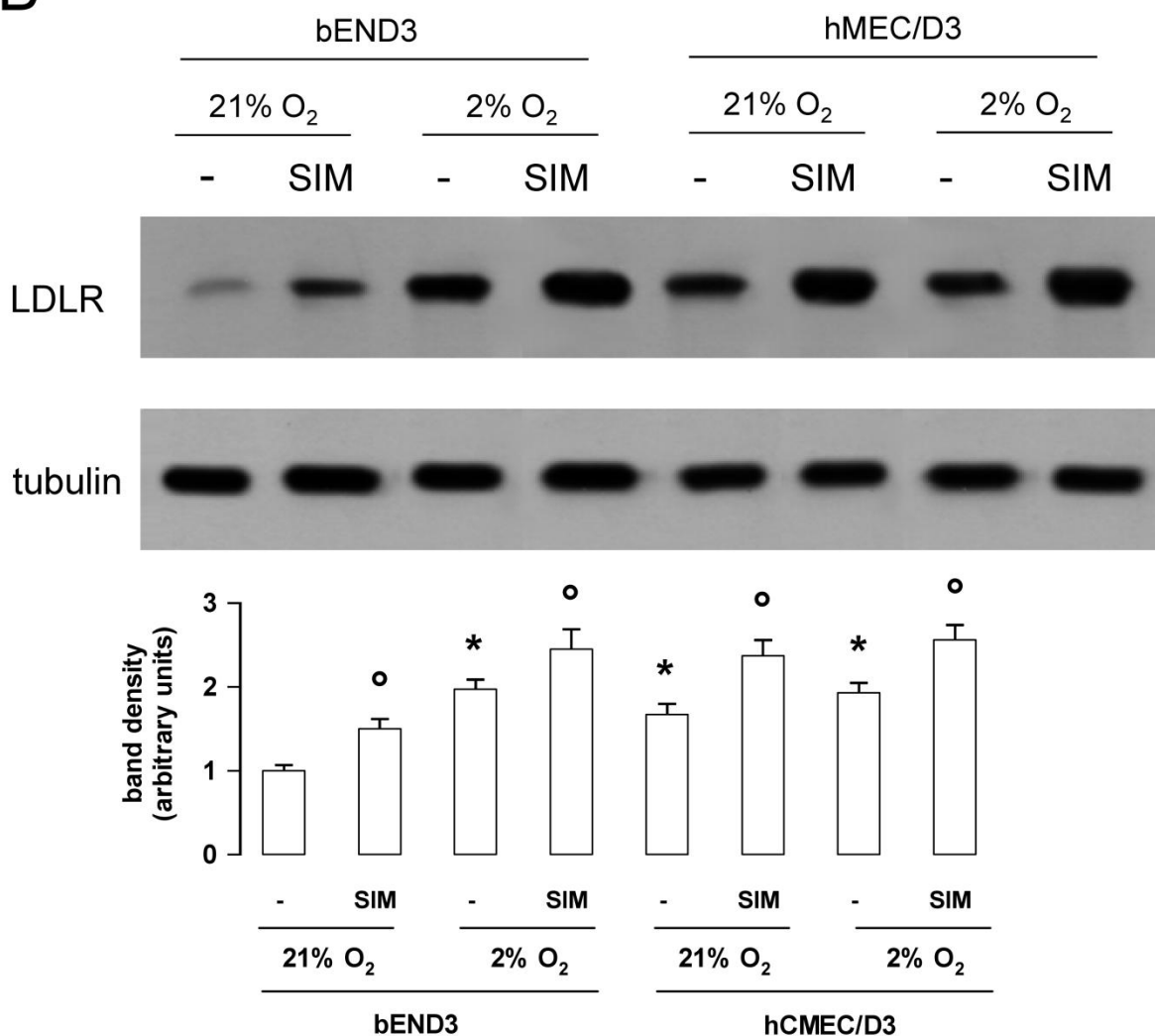


**Figure 4.** BBB cells with activated HIF-1 $\alpha$  have increased synthesis of cholesterol and expression of LDLR, two events that are modulated by simvastatin. bEND3 and hCMEC/D3 cells were grown for 7 days up to confluence in normoxic (21% O<sub>2</sub>) or hypoxic (2% O<sub>2</sub>) conditions, in fresh medium (-). When indicated, the HMGCoAR inhibitor simvastatin (10  $\mu$ mol/L; SIM) was added in the last 24 h. A. Cells were radiolabeled 24 h with [<sup>3</sup>H]acetate, then the *de novo* synthesis of cholesterol was measured in duplicate as described under Experimental Details. Data are presented as means  $\pm$  SD (n=3). For each cell line, versus 21% O<sub>2</sub>: \* p < 0.02; SIM-treated cells versus untreated (-) cells: <sup>o</sup> p < 0.05. B. Cells were lysed and subjected to Western blot analysis for LDLR.  $\beta$ -tubulin expression was used as control of equal protein loading. The figure is representative of 3 experiments with similar results. The band density ratio between LDLR and  $\beta$ -tubulin was expressed as arbitrary units. Versus untreated bEND3 cells at 21% O<sub>2</sub>: \* p < 0.05; for each cell line, SIM-treated cells versus untreated (-) cells: <sup>o</sup> p < 0.05.

Overall, these data suggest that the activity of SREBP-2 is controlled by HIF-1 $\alpha$  in BBB cells. Despite the different activation of HIF-1 $\alpha$  between murine and human BBB cells in normoxia and hypoxia, the metabolic responses controlled by the HIF-1 $\alpha$ /SREBP-2 axis - such as the synthesis of cholesterol and the expression of LDLR - are sensitive to simvastatin.

### 3.4. The association of simvastatin plus a “LDL-masked” liposomal doxorubicin increases the doxorubicin delivery across BBB also in the presence of activated HIF-1 $\alpha$

We previously showed that the association of simvastatin, which decreases the activity of Pgp and increases the exposure of LDLR in hCMEC/D3 cells, followed by a “LDL-masked” liposomal doxorubicin (apo-Lipodox), improves doxorubicin delivery across BBB cells [25]. Here, we tested the efficacy of this strategy in normoxic and hypoxic bEND3 and hCMEC/D3 cells, and we verified whether this strategy was effective also when HIF-1 $\alpha$  was activated: in these conditions, BBB cells had indeed high levels of Pgp (Figure 1B), but also high levels of LDLR (Figure 4B), which is crucial for the LDLR-mediated endocytosis of apo-Lipodox [25].

In normoxic bEND3 cells, when Pgp expression (Figure 1B), HIF-1 $\alpha$  activity (Figure 2B) and LDLR levels (Figure 4B) were relatively low, doxorubicin permeability was slightly increased by the treatment of “simvastatin plus apo-Lipodox” (Figure 5A). In hypoxic bEND3 cells, when Pgp expression (Figure 1B), HIF-1 $\alpha$  activity (Figure 2B) and LDLR levels (Figure 4B) were increased, the permeability of free doxorubicin was lower, but doxorubicin delivery was significantly improved by the association of “simvastatin plus apo-Lipodox” (Figure 5A). hCMEC/D3 cells had high levels of Pgp (Figure 1B), high activity of HIF-1 $\alpha$  (Figure 2B) and high expression of LDLR (Figure 4B) in normoxia and hypoxia; these cells had indeed a very low delivery of free doxorubicin, which was significantly increased by the sequential treatment with “simvastatin plus apo-Lipodox” in both normoxic and hypoxic conditions (Figure 5A).

apo-Lipodox alone slightly improved the drug delivery in all the experimental conditions, but no significant differences with free doxorubicin were observed (Figure 5A).

To verify whether the increased delivery of doxorubicin obtained with the sequential treatment “simvastatin plus apo-Lipodox” was sufficient to reach cytotoxic concentrations for tumor cells, we set-up co-culture models of BBB cells (bEND3 or hCMEC/D3 cells), and glioblastoma cells (C6 or U87-MG cells, respectively) in Transwell devices. Free doxorubicin, apo-Lipodox alone or apo-Lipodox preceded by simvastatin were applied in the Transwell insert, facing the luminal side of BBB cells: in both models, the intra-glioblastoma content of doxorubicin in normoxia was significantly lower with free doxorubicin and apo-Lipodox alone, compared with the intracellular content of doxorubicin obtained with “simvastatin plus apo-Lipodox” (Figure 5B). In hypoxia, the intratumor doxorubicin measured after the treatment with free doxorubicin or apo-Lipodox alone was even lower in C6 cells co-cultured with bEND3 cells; the doxorubicin content in hypoxic U87-MG cells co-cultured with hCMEC/D3 cells was as low as in normoxic cells. Only the treatment with “simvastatin plus apo-Lipodox” increased the intratumor drug content (Figure 5B). In line with the doxorubicin accumulation, free doxorubicin did not produce

any cytotoxic effect on glioblastoma cells in normoxia and in hypoxia (Figure 5C). apo-Lipodox was moderately cytotoxic in C6 cells co-cultured with bEND3 cells in normoxic and hypoxic conditions, but was ineffective against U87-MG cells co-cultured with hCMEC/D3 cells. Simvastatin alone was not cytotoxic; by contrast, the scheme “simvastatin plus apo-Lipodox” was the only effectively cytotoxic approach in both co-culture models, either in normoxia or hypoxia (Figure 5C).

## 4. Discussion

In this work we investigated how the delivery of Pgp substrates, such doxorubicin and vinblastine, varies in normoxic and hypoxic BBB. To our surprise, murine and human cells showed a widely different behavior: while in murine bEND3 cells the delivery of Pgp substrates was decreased after long term-culture (i.e. 7 days) in hypoxia, in human hCMEC/D3 cells the permeability of Pgp substrates was lower than in bEND3 cells also in normoxic conditions and was not further reduced by hypoxia. This trend can be explained by the different levels of Pgp, which was more expressed in normoxic human BBB cells than in normoxic murine BBB cells; moreover, Pgp increased in hypoxic murine BBB cells, but not in hypoxic human BBB cells. This is not the first time that murine and human brain microvascular cells show striking differences in the expression and activity of Pgp [32]; however, what emerged from our data is that there is a species-specific regulation of Pgp expression in BBB cells exposed to hypoxia.

Other ABC transporters had a different expression between bEND3 and hCMEC/D3 cells: for instance, MRP2 and MRP6 were undetectable in the former and present in the latter. However, in this case no differences occurred in each cell population between normoxic and hypoxic cells, leading to exclude a differential hypoxia-dependent regulation of these transporters.

Since HIF-1 $\alpha$  is a strong inducer of Pgp, we analyzed the expression levels of nuclear HIF-1 $\alpha$  (i.e. the activated form of the protein) and its DNA binding capacity, as index of its transcriptional activity. While murine BBB cells have HIF-1 $\alpha$  active only in hypoxia (either physically induced by low O<sub>2</sub> tension or chemically induced by CoCl<sub>2</sub>), as it occurs in most mammalian cells [4], in human hCMEC/D3 cells HIF-1 $\alpha$  was active in normoxia as well as in hypoxia. The activity of HIF-1 $\alpha$  correlated with the mRNA and protein levels of Pgp, suggesting that the different expression of Pgp between murine and human BBB cells in normoxia and hypoxia was likely due to the differential activity of HIF-1 $\alpha$ .

Previous works on cancer cells have reported the constitutive activation of HIF-1 $\alpha$  in normoxia, in consequence of the increased rate of its synthesis, stimulated by autocrine growth factors and cytokines [33]. Moreover, the phosphorylation on serine, e.g. by RhoA kinase [34] and MAP kinases [35], promotes HIF-1 $\alpha$  stabilization, which is associated to its activation even in normoxic conditions [30]. We did not investigate the phosphorylation status of HIF-1 $\alpha$  in this work; worth of note, we previously detected a basal activity of RhoA/RhoA kinase axis in normoxic hCMEC/D3 cells [25]: we cannot exclude that the active RhoA kinase may promote the stabilization of HIF-1 $\alpha$  in normoxic hCMEC/D3 cells, as it occurs in solid tumors [30].

Our data may explain previous findings showing that Pgp did not change its expression in hypoxic hCMEC/D3 cells

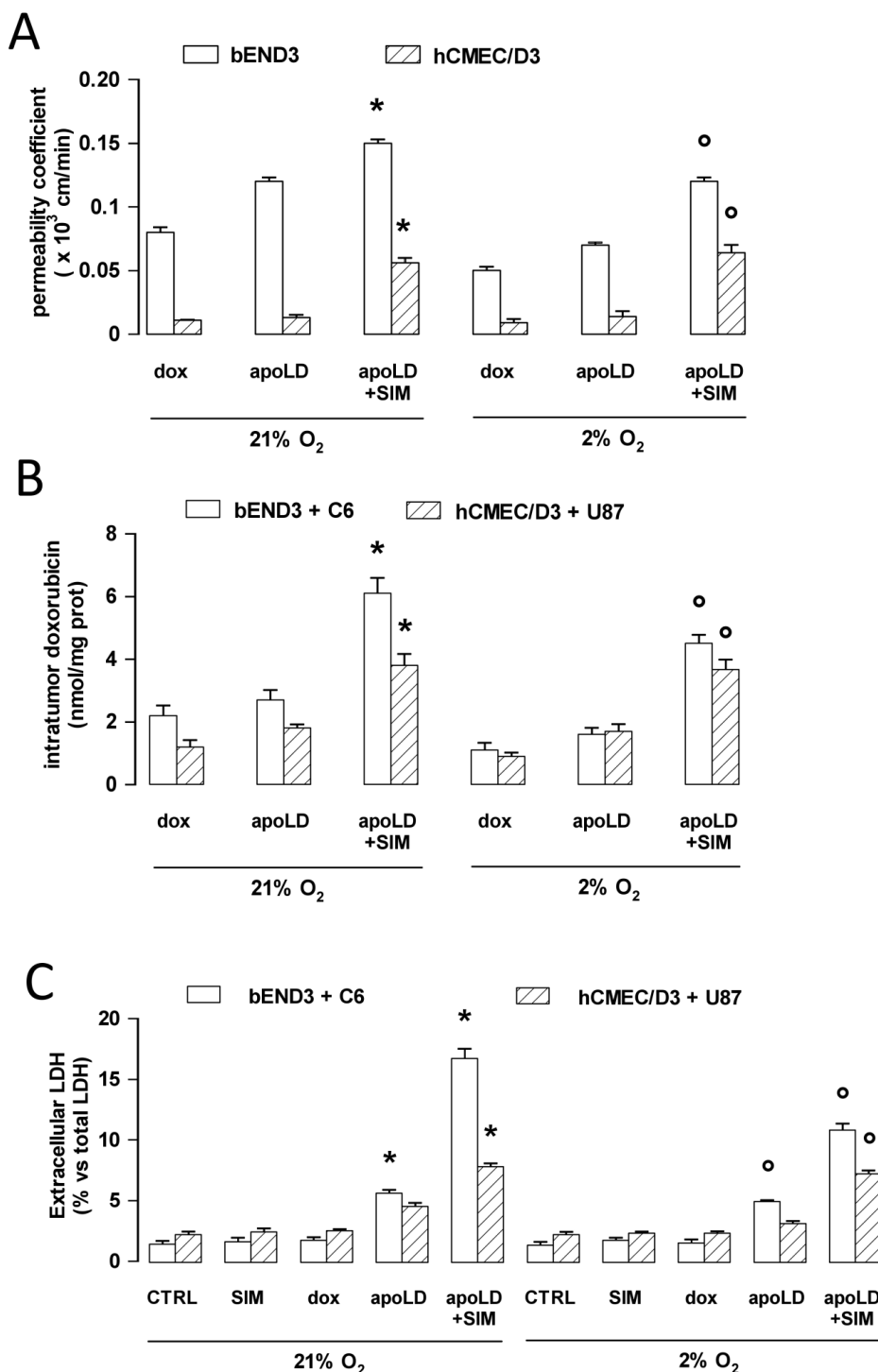


**Figure 5.** The combination of simvastatin plus “LDL-masked” liposomal doxorubicin effectively increases the drug delivery and cytotoxicity against co-cultured hypoxic glioblastoma cells. bEND3 and hCMEC/D3 cells were grown for 7 days up to confluence in normoxic (21% O<sub>2</sub>) or hypoxic (2% O<sub>2</sub>) conditions in Transwell inserts. A. Permeability of doxorubicin across BBB monlayer. 5 μmol/L doxorubicin (dox) or apo-Lipodox (apoLD) were added for 3 hour in the upper chamber. When indicated, the incubation with apo-Lipodox was preceded by a 24 h pre-treatment with 10 μmol/L simvastatin (apoLD+SIM). The amount of doxorubicin recovered from the lower chamber was measured fluorimetrically. Permeability coefficients were calculated as reported under Experimental Details. Measurements were performed in duplicate and data are presented as means ± SD (n = 3). For each cell line, versus dox at 21% O<sub>2</sub>: \* p < 0.001; versus dox at 2% O<sub>2</sub>: <sup>o</sup> p < 0.002. B. bEND3 and hCMEC/D3 cells were grown for 7 days up to confluence in Transwell inserts; C6 and U87-MG cells were seeded at day 4 in the lower chamber. After 3 days of co-culture, the medium of the upper chamber was replaced with medium containing 5 μmol/L doxorubicin (dox) or apo-Lipodox (apoLD); when indicated, the incubation with apo-Lipodox was preceded by a 24 h pre-treatment with 10 μmol/L simvastatin (apoLD+SIM). After 3 h the intraglioblastoma doxorubicin content was measured fluorimetrically. Data are presented as means ± SD (n = 4). For each cell line, versus dox at 21% O<sub>2</sub>: \* p < 0.001; versus dox at 2% O<sub>2</sub>: <sup>o</sup> p < 0.001. C. Cells were left untreated for 7 days (CTRL), treated with 10 μmol/L simvastatin for the last 24 h (SIM) or with doxorubicin, apo-Lipodox, simvastatin plus apo-Lipodox, as detailed in panel B. After 24 h, the release of LDH was measured spectrophotometrically in the culture supernatant of glioblastoma cells, as index of doxorubicin-induced cytotoxicity. Data are presented as means ± SD (n = 4). For each cell line, versus untreated (CTRL) cells at 21% O<sub>2</sub>: \* p < 0.001; versus untreated (CTRL) cells at 2% O<sub>2</sub>: <sup>o</sup> p < 0.001.

[36]: for instance, in the work of Patak and colleagues, HIF-1 $\alpha$  was expressed in normoxic hCMEC/D3 cells, increased after 4 h of hypoxia and returned to basal levels after 24 h. Another study reported a very small increase of HIF-1 $\alpha$  in hypoxic hCMEC/D3 cells after 24 h, without appreciable changes in Pgp expression towards normoxic cells [37]. As many transcription factors, also HIF-1 $\alpha$  is subjected to temporal fluctuations of its expression. In our work, we cultured hCMEC/D3 cells for 7 days in hypoxia and in relatively mild hypoxic conditions (i.e. 2% O<sub>2</sub>), in order to mimic the constant hypoxia present in microvascular endothelial cells within the bulk of glioblastoma. It is conceivable that in our experimental conditions, hCMEC/D3 cells became adapted to the hypoxic environment and HIF-1 $\alpha$  became insensitive to the periodic fluctuations observed during shorter pulses of hypoxia.

These data suggest that there are marked species-specific differences in Pgp expression and transcription in cells, and that the response of BBB cells of murine and human origin to normoxic and hypoxic environment may widely differ. Given such variability, the results of permeability assays for Pgp substrates obtained on murine BBB cells may not be reproducible in human BBB models; therefore, great caution is needed in the comparison of permeability results from BBB models of different species.

On the other hand, independently from the species examined, our data suggest that high levels of HIF-1 $\alpha$  are associated with high levels of Pgp, and limit the delivery of Pgp substrate across BBB.

We therefore investigated how to improve the drug delivery in BBB cells with high levels of HIF-1 $\alpha$  and Pgp. We previously observed that cancer cells with a constitutive activation of HIF-1 $\alpha$  have also an increased metabolic flux through the mevalonate pathway [30]. This pathway supplies cells with high levels of cholesterol, which increases activity [38, 39] and expression of Pgp [30]. Also in bEND3 and hCMEC/D3 cells, the activation of HIF-1 $\alpha$  was associated with increased synthesis of cholesterol and increased transcription of the pace-maker enzyme HMGCoAR.

*HMGCoAR* promoter has an hypoxia responsive element; it has been shown that in human hepatocytes HIF-1 $\alpha$  up-regulates the transcription of *HMGCoAR* by binding to the gene promoter and by activating the transcription factor SREBP-2 [9]. We found that, when active, HIF-1 $\alpha$  co-immunoprecipitated with SREBP-2, favored the nuclear translocation of SREBP-2 and the transcription of *HMGCoAR*. These events were detected in hypoxic bEND3 cells, in normoxic and hypoxic hCMEC/D3 cells. By contrast, in normoxic bEND3 cells, where HIF-1 $\alpha$  was undetectable, the nuclear levels of SREBP-2 and the mRNA levels of *HMGCoAR* were lower. The activation of HIF-1 $\alpha$ /SREBP-2 axis determined the rate of cholesterol synthesis. To the best of our knowledge, there are no other reports showing that the rate of cholesterol synthesis is dependent on the activity of HIF-1 $\alpha$  in BBB cells.

Note of worthy for the aim of this work, the activation of HIF-1 $\alpha$  may lower the delivery of Pgp substrates across BBB with at least two mechanisms: 1) by increasing Pgp expression, because of the up-regulation of *Pgp* gene transcription [17]; 2) by increasing Pgp activity, because of the higher amount of cholesterol synthesized and incorporated in plasma membrane [38, 39].

Besides the increase of cholesterol synthesis, another consequence of HIF-1 $\alpha$ /SREBP-2 activation was the enhanced

expression of LDLR, which is constitutively present on BBB cells [40] and is further increased by the activation of SREBP-2 or by the decrease of intracellular cholesterol exerted by statins [31]. Also in our models of BBB cells, higher was the activity of SREBP-2, higher was the expression of LDLR; on the other hand, when the synthesis of cholesterol was lowered by simvastatin, LDLR expression was further enhanced. This situation reflects a dysregulated cholesterol homeostasis and is typical of cells with activated HIF-1 $\alpha$ , which have high levels of LDLR that allows the uptake of extracellular cholesterol, notwithstanding the high levels of intracellular cholesterol [30, 39]. We previously observed this altered homeostasis of cholesterol in cancer cells overexpressing HIF-1 $\alpha$  and Pgp [30, 39]; this is the first time that such metabolic condition is described in BBB cells. HIF-1 $\alpha$  has been reported to increase the expression of LDLR-related protein 1 (LRP1) and very low density lipoprotein receptor (VLDLR) in renal cancer cells [41] and in cardiomyocytes, where LDLR was concurrently down-regulated [42]. However, in these works, only the activity of HIF-1 $\alpha$  has been considered, without analyzing whether SREBP-2 was also changed. In the light of our results, we propose that the HIF-1 $\alpha$ -induced activation of SREBP-2 was the actual driving force in up-regulating LDLR in BBB cells.

Since the LDLR-triggered endocytosis may be exploited to enhance the uptake of nanoparticle sensed as physiological LDL [25, 39], the high level of LDLR following HIF-1 $\alpha$  activation represents a paradoxical "Achille's heel" of hypoxic BBB cells. We previously found that in normoxic hCMEC/D3 cells the administration of simvastatin, which increased the exposure of LDLR, followed by a LDL-masked liposomal doxorubicin ("apo-Lipodox") increased the delivery of doxorubicin, a drug which otherwise will be effluxed by Pgp, and the drug cytotoxicity against glioblastoma cells cultured under competent BBB [25]. Here we demonstrated that the same strategy was effective in BBB cells with activated HIF-1 $\alpha$ , i.e. hypoxic bEND3 cells, normoxic and hypoxic hCMEC/D3 cells. The use of classical Pgp inhibitor such as cyclosporine A to improve the drug delivery across hypoxic BBB cells was not a good strategy, because of the potential delivery of cyclosporine A into brain parenchyma, where the compound induces neurotoxicity [43]. By contrast, the treatment scheme "simvastatin plus apo-Lipodox" appears more promising: on the one hand, simvastatin alone did not induce any cytotoxicity; on the other hand, the association "simvastatin plus apo-Lipodox" was the only strategy that grants an effective delivery of cytotoxic amounts of doxorubicin into hypoxic glioblastoma cells.

Doxorubicin is a typical substrates of Pgp and is effective against glioblastoma *in vitro*; however, the efflux via Pgp at BBB level strongly reduces its *in vivo* efficacy and clinical use [44]. Our work shows that doxorubicin might overcome such limitation, if encapsulated in a "LDL-masked" liposome and preceded by treatment with a statin.

## 5. Conclusions

Pgp effluxes back into the bloodstream a variety of drugs potentially useful for brain tumors, neurodegenerative diseases, infective diseases and epilepsy. Chronic hypoxia is involved in the pathogenesis of many of these morbidities [11]; moreover, the increased expression of Pgp observed in hypoxic conditions further reduces the success of

pharmacological therapies in such diseases. Our work puts light on the metabolic changes occurring in BBB cells during hypoxia and proposes an effective strategy to improve drug delivery across BBB cells exposed to hypoxic environment and/or with an activated HIF-1 $\alpha$ . Such approach is flexible, since several drugs can be loaded into “LDL masked” liposomes, and might be advantageous in a broad spectrum of central nervous system diseases.

### Acknowledgments

We are indebted with Prof. Pierre-Olivier Couraud (Institut Cochin, Centre National de la Recherche Scientifique UMR 8104 and INSERM U567, Université René Descartes, Paris, France) for having provided hCMEC/D3 cells. We are grateful to Mr. Costanzo Costamagna (Department of Oncology, University of Turin, Italy) for the technical assistance and to Prof. Dario Ghigo (Department of Oncology, University of Turin, Italy) for the fruitful discussion.

This work has been supported by grants from Compagnia di San Paolo, Italy (Neuroscience Program; grant 2008.1136).

Martha Leonor Pinzón-Daza is recipient of a ERACOL Erasmus Mundus fellowship. Joanna Kopecka is recipient of a “Mario and Valeria Rindi” fellowship provided by Italian Foundation for Cancer Research (FIRC).

### References

1. S. Agarwal, R. Sane, R. Oberoi, J. R. Ohlfest, W. F. Elmquist, *Expert Rev. Mol. Med.* 13 (2011) 17.
2. S. Agarwal, A. M. Hartz, W. F. Elmquist, B. Bauer, *Curr. Pharm. Des.* 17 (2011) 2793.
3. M. L. Pinzón-Daza, I. Campia, J. Kopecka, R. Garzón, D. Ghigo, C. Riganti, *Curr. Drug Metab.* 14 (2013) 625.
4. C. Brahimi-Horn, N. Mazure, J. Pouyssegur, *Cell. Signal.* 17 (2005) 1.
5. J. L. O'Donnell, M. R. Joyce, A. M. Shannon, J. Harmey, J. Geraghty, D. Bouchier-Hayes, *Cancer Treat. Rev.* 32 (2006) 407.
6. J. Q. Chen, J. Russo, *Biochim. Biophys. Acta* 1826 (2012) 370.
7. M. Cruet, S. J. Wüst, P. Spielmann, T. F. Lüscher, R. H. Wenger, C. M. Matter, *Atherosclerosis* 229 (2013) 110.
8. L. Li, B. Liu, L. Håversen, E. Lu, L. U. Magnusson, M. Ståhlman, J. Borén, G. Bergström, M. C. Levin, L. M. Hultén, *PLoS One* 7 (2012) 42360.
9. V. Pallottini, B. Guantario, C. Martini, P. Totta, I. Filippi, F. Carraro, A. Trentalance, *J. Cell. Biochem.* 104 (2008) 701.
10. D. Hala, L. H. Petersen, D. Martinovic, D. B. Huggett, *J. Exp. Biol.* 215 (2012) 1753.
11. B. V. Zlokovic BV, *Nat. Rev. Neurosci.* 12 (2011) 723.
12. Y. A. Kim, S. L. Park, M. Y. Kim, S. H. Lee, E. J. Baik, C. H. Moon, Y. S. Jung, *Neurosci. Lett.* 468 (2010) 254.
13. J. Yan, B. Zhou, S. Taheri, H. Shi, *PLoS One* 6 (2011) 27798.
14. C. M. Zehendner, L. Librizzi, M. de Curtis, C. R. Kuhlmann, H. J. Luhmann, *PLoS One* 6 (2011) 16760.
15. B. K. Wallace, K. A. Jelks, M. E. O'Donnell, *Am. J. Physiol. Cell Physiol.* 302 (2012) C505.
16. M. Espinoza-Rojo, K. I. Iturralde-Rodríguez, M. E. Cháñez-Cárdenas, M. E. Ruiz-Tachiquín, P. Aguilera, *Cent. Nerv. Syst. Agents Med. Chem.* 10 (2010) 317.
17. K. M. Comerford, T. J. Wallace, J. Karhausen, N. A. Louis, M. C. Montalto, S. P. Colgan, *Cancer Res.* 62 (2002) 3387.
18. L. Xiao-Dong, Y. Zhi-Hong, Y. Hui-Wen, *Neurosci. Lett.* 432 (2008) 184.
19. B. B. Weksler, E. A. Subileau, N. Perrière, P. Charneau, K. Holloway, M. Leveque, H. Tricoire-Leignel, A. Nicotra, S. Bourdoulous, P. Turowski, D. K. Male, F. Roux, J. Greenwood, I. A. Romero, P. O. Couraud, *FASEB J.* 19 (2005) 1872.
20. R. C. Brown, A. P. Morris, R. G. O'Neil, *Brain Res.* 1130 (2007) 17.
21. L. Bao, H. Shi, *Chem. Res. Toxicol.* 23 (2010) 1726.
22. A. Inamura, Y. Adachi, T. Inoue, Y. He, N. Tokuda, T. Nawata, S. Shirao, S. Nomura, M. Fujii, E. Ikeda, Y. Owada, M. Suzuki, *Neurochem. Res.* 38 (2013) 1641.
23. Siflinger-Birboim, P. J. Del Vecchio, J. A. Cooper, F. A. Blumenstock, J. M. Shepard, A. B. Malik, *J. Cell. Physiol.* 132 (1987) 111.
24. Campia, E. Gazzano, G. Pescarmona, D. Ghigo, A. Bosia, C. Riganti, *Cell. Mol. Life Sci.* 66 (2009) 1580.
25. M. L. Pinzón-Daza, R. Garzón, P. O. Couraud, I. A. Romero, B. Weksler, D. Ghigo, A. Bosia, C. Riganti, *Brit. J. Pharmacol.* 167 (2012) 1431.
26. S. W. Provencher, *Comput. Phys. Commun.* 27 (1982) 213.
27. Riganti, I. C. Salaroglio, M. L. Pinzón-Daza, V. Caldera, I. Campia, J. Kopecka, M. Mellai, L. Annovazzi, P. O. Couraud, A. Bosia, D. Ghigo, D. Schiffer, *J. Cell. Mol. Life Sci.* (2013) doi: 10.1007/s00018-013-1397-y.
28. Riganti, I. C. Salaroglio, V. Caldera, I. Campia, J. Kopecka, M. Mellai, L. Annovazzi, A. Bosia, D. Ghigo, D. Schiffer, *Neuro Oncol.* 15 (2013) 1502.
29. S. Bae, H. J. Jeong, H. J. Cha, K. Kim, Y. M. Choi, I. S. An, H. J. Koh, D. J. Lim, S. J. Lee, S. An, *Int. J. Mol. Med.* 30 (2012) 1180.
30. Riganti, B. Castella, J. Kopecka, I. Campia, M. Coscia, G. Pescarmona, A. Bosia, D. Ghigo, M. Massaia, *PLoS One* 8 (2013) 60975.
31. J. K. Liao, U. Laufs, *Annu. Rev. Pharmacol. Toxicol.* 45 (2005) 89.
32. Y. Uchida, S. Ohtsuki, Y. Katsukura, C. Ikeda, T. Suzuki, J. Kamiie, T. Terasaki, *J. Neurochem.* 117 (2011) 333.
33. J. J. Haddad, H. L. Harb, *Int. Immunopharmacol.* 5 (2005) 461.
34. K. Takata, K. Morishige, T. Takahashi, K. Hashimoto, S. Tsutsumi, L. Yin, T. Ohta, J. Kawagoe, K. Takahashi, H. Kurachi, *Mol. Cancer Ther.* 7 (2008) 1551.
35. V. Sharma, D. Dixit, N. Koul, V. S. Mehta, E. Sen, *J. Mol. Med.* 89 (2011) 123.
36. P. Patak, F. Jin, S. T. Schäfer, E. Metzen, D. M. Hermann, *Exp. Transl. Stroke Med.* 3 (2011) 12.
37. C. Lindner, A. Sigrüner, F. Walther, U. Bogdahn, P. O. Couraud, G. Schmitz, F. Schlachetzki, *Exp. Transl. Stroke Med.* 4 (2012) 9.
38. J. Troost, J. Lindenmaie, W. E. Haefeli, J. Weiss, *Mol. Pharmacol.* 66 (2004) 1332.
39. J. Kopecka, I. Campia, P. Olivero, G. Pescarmona, D. Ghigo, A. Bosia, C. Riganti, *J. Control. Release* 149 (2011) 196.
40. A. Ambruosi, A. S. Khalansky, H. Yamamoto, S. E. Gelperina, D. J. Begley, J. Kreuter, *J. Drug Target.* 14 (2006) 97.
41. J. P. Sundelin, M. Ståhlman, A. Lundqvist, M. Levin, P. Parini, M. E. Johansson, J. Borén, *PLoS One* 7 (2012) 48694.
42. R. Cal, J. Castellano, E. Revuelta-López, R. Aledo, M. Barriga, J. Farré, G. Vilalur, L. Nasarre, L. Hove-Madsen, L. Badimon, V. Llorente-Cortés, *Cardiovasc. Res.* 94 (2012) 469.
43. S. Dohgu, T. Nishioku, N. Sumi, F. Takata, S. Nakagawa, M. Naito, T. Tsuruo, A. Yamauchi, H. Shuto, Y. Kataoka, *Cell. Mol. Neurobiol.* 27 (2007) 889.
44. P. Hau, K. Fabel, U. Baumgart, P. Rummele, O. Grauer, A. Bock, C. Dietmaier, W. Dietmaier, J. Dietrich, C. Dudel, F. Hubner, T. Jaucj, E. Drechsel, I. Kleiter, C. Wismeth, A. Zellner, A. Brawanski, A. Steinbrecher, J. Marienhagen, U. Bogdahn, *Cancer* 100 (2004) 1199.

**Cite this article as:**

Martha L. Pinzòn-Daza *et al.*: The “LDL-masked doxorubicin”: an effective strategy for drug delivery across hypoxic blood brain barrier. **ScienceJet** 2014, **3**: 49

# Temozolomide down-regulates P-glycoprotein in human blood–brain barrier cells by disrupting Wnt3 signaling

Chiara Riganti · Iris C. Salaroglio · Martha L. Pinzòn-Daza · Valentina Caldera · Ivana Campia · Joanna Kopecka · Marta Mellai · Laura Annovazzi · Pierre-Olivier Couraud · Amalia Bosia · Dario Ghigo · Davide Schiffer

Received: 30 December 2012 / Revised: 30 May 2013 / Accepted: 31 May 2013 / Published online: 15 June 2013  
© Springer Basel 2013

**Abstract** Low delivery of many anticancer drugs across the blood–brain barrier (BBB) is a limitation to the success of chemotherapy in glioblastoma. This is because of the high levels of ATP-binding cassette transporters like P-glycoprotein (Pgp/ABCB1), which effluxes drugs back to the bloodstream. Temozolomide is one of the few agents able to cross the BBB; its effects on BBB cells permeability and Pgp activity are not known. We found that temozolomide, at therapeutic concentration, increased the transport of Pgp substrates across human brain microvascular endothelial cells and decreased the expression of Pgp. By methylating

the promoter of *Wnt3* gene, temozolomide lowers the endogenous synthesis of Wnt3 in BBB cells, disrupts the Wnt3/glycogen synthase kinase 3/ $\beta$ -catenin signaling, and reduces the binding of  $\beta$ -catenin on the promoter of *mdr1* gene, which encodes for Pgp. In co-culture models of BBB cells and human glioblastoma cells, pre-treatment with temozolomide increases the delivery, cytotoxicity, and antiproliferative effects of doxorubicin, vinblastine, and topotecan, three substrates of Pgp that are usually poorly delivered across BBB. Our work suggests that temozolomide increases the BBB permeability of drugs that are normally effluxed by Pgp back to the bloodstream. These findings may pave the way to new combinatorial chemotherapy schemes in glioblastoma.

**Electronic supplementary material** The online version of this article (doi:10.1007/s00018-013-1397-y) contains supplementary material, which is available to authorized users.

C. Riganti (✉) · I. C. Salaroglio · M. L. Pinzòn-Daza · I. Campia · J. Kopecka · A. Bosia · D. Ghigo  
Department of Oncology, University of Turin, Via Santena, 5/bis, 10126 Turin, Italy  
e-mail: chiara.riganti@unito.it

C. Riganti · A. Bosia · D. Ghigo  
Research Center On Experimental Medicine (CeRMS), University of Turin, Via Santena, 5/bis, 10126 Turin, Italy

M. L. Pinzòn-Daza  
Unidad de Bioquímica, Facultad de Ciencias Naturales y Matemáticas, Universidad del Rosario, Carrera 6, Bogotá, Colombia

V. Caldera · M. Mellai · L. Annovazzi · D. Schiffer  
Neuro-bio-oncology Center, Policlinico di Monza Foundation, Via Pietro Micca 29, 13100 Vercelli, Italy

P.-O. Couraud  
Institut Cochin, Centre National de la Recherche Scientifique UMR 8104, Institut National de la Santé et de la Recherche Médicale (INSERM) U567, Université René Descartes, 22 rue Méchain, 75014 Paris, France

**Keywords** Blood–brain barrier · Temozolomide · P-glycoprotein · Wnt3 · Glioblastoma multiforme

## Abbreviations

GBM	Glioblastoma multiforme
CNS	Central nervous system
BBB	Blood–brain barrier
TMZ	Temozolomide
ABC	ATP-binding cassette
BAT	Brain-adjacent to tumor
Pgp	P-glycoprotein
MRP	Multidrug resistance-related protein
BCRP	Breast cancer resistance protein
LRP	Low-density lipoprotein receptor-related protein
GSK3	Glycogen synthase kinase 3
TCF/IEF	T cell factor/lymphoid enhancer factor
Dkk-1	Dickkopf-1
HBMECs	Human brain microvascular endothelial cells
FCS	Fetal calf serum

BSA	Bovine serum albumin
FITC	Fluorescein isothiocyanate
ZO-1	Zonula occludens-1
TBP	TATA-box binding protein
qRT-PCR	Quantitative real-time PCR
ChIP	Chromatin immunoprecipitation
MSP	Methylation-specific PCR
DAPI	4',6-Diamidino-2-phenylindole dihydrochloride
LDH	Lactate dehydrogenase

## Introduction

Glioblastoma multiforme (GBM) accounts for 65 % of primary central nervous system (CNS) tumors in the adult population. Adjuvant chemotherapy is, along with maximal surgical resection and radiation therapy, a standard therapeutic approach in disseminated GBM that almost universally fails [1]. The failure of this approach is due to the highly invasive phenotype of GBM, its strong chemoresistance, and the low delivery of anti-neoplastic drugs across the blood–brain barrier (BBB) [1]. First-line therapy in GBM is the systemic administration of the alkylating agent temozolomide (TMZ, online resource 1), one of the few drugs to show good permeability across the BBB [2]. In systemic circulation, TMZ is rapidly converted into its active metabolite 3-methyl-(triazen-1-yl)imidazole-4-carboxamide (MTIC, online resource 1) [3], the chemical entity that likely reaches BBB in vivo. Therapeutic protocols currently in use [4] aim either to increase the cumulative dose of TMZ or prolong the duration of the treatment. Until now, however, no treatment protocol has been curative [1]. Since the prognosis of GBM is still poor, alternative approaches have been the object of intensive investigation [2]. The topoisomerase I inhibitors irinotecan and topotecan have shown excellent anti-tumor activity in vitro and significant efficacy in vivo when administered with TMZ or bevacizumab [5]. Topotecan, however, does not cross the BBB and achieves maximal efficacy only when administered by convection-enhanced delivery [6]. Doxorubicin is highly effective against GBM cells in vitro, as well, but its clinical use is limited by low delivery across BBB [7].

The greatest hurdle for many promising anti-GBM drugs is the BBB, the peculiar brain microvascular endothelium, devoid of fenestrations and pinocytotic vesicles, and rich in tight junctions, adherent junctions and drug efflux transporters of the ATP-binding cassette (ABC) family [8]. The BBB is disrupted in the core of GBM, but is intact in the “brain-adjacent to tumor” (BAT) area, where invasive GBM cells lay scattered in the non-transformed brain parenchyma. BAT is a critical zone for targeting chemotherapy because it contains cells that will either spread to other areas of the CNS or cause local relapse. Since the

BAT is surrounded by a competent BBB, the delivery of chemotherapeutic drugs to this area is marginal [8]. Alternative strategies—such as the osmotic opening of tight junctions with mannitol [9] or ultrasound [10]—have been devised in vivo, to overcome the low permeability of the BBB, with some success. Inhibitors of the ABC transporters present on the luminal side of BBB cells, such as P-glycoprotein (Pgp/ABCB1), multidrug resistance-related protein 1 (MRP1/ABCC1) and breast cancer resistance protein (BCRP/ABCG2) [8], have also been used [11]. To date, however, no safe or satisfactory strategies to bypass the ABC transporter-mediated drug efflux have been devised.

Pgp/ABCB1 transports a number of chemotherapeutic agents, such as anthracyclines, taxanes, vinca alkaloids, teniposide/etoposide, topotecan, methotrexate, imatinib, dasatinib, lapatinib, gefitinib, sorafenib, erlotinib, and mediates the efflux of several analgesics, anti-epileptics, anti-retrovirals, and antibiotics [8]. In BBB cells, Pgp/ABCB1 is up-regulated by different stimuli, such as tumor necrosis factor  $\alpha$  [12] and ligands of pregnane X receptor, constitutive androstane receptor [13], aryl hydrocarbon receptor [14].

Recent data show that the activation of the Wnt-canonical pathway, critical for angiogenesis in brain [15] and acquisition of BBB properties [16], up-regulates Pgp/ABCB1 in human BBB cells [17, 18]. In the Wnt-canonical pathway, the binding of soluble Wnt proteins on Frizzled receptor and low-density-lipoprotein receptor related protein-5 and -6 (LRP5/IRP6) co-receptors decreases the activity of the enzyme glycogen synthase kinase 3 (GSK3). By doing so, Wnt allows  $\beta$ -catenin to move from the cytosolic APC/axin complex into the nucleus, where it binds to the T-cell factor/lymphoid enhancer factor (TCF/IEF) and induces the transcription of target genes, such as *mdr1*, which encodes for Pgp/ABCB1 [19].

While several determinants have been reported to up-regulate Pgp/ABCB1 in BBB cells, determinants that down-regulate Pgp/ABCB1 are poorly known. There is some evidence that specific polymorphisms of Pgp/ABCB1 change the delivery of TMZ across BBB [20], but the relation between TMZ and Pgp/ABCB1 is still controversial. In this study, we asked the question whether a clinically achievable dose of TMZ can affect the permeability and the activity/expression of ABC transporters in human BBB cells. We found that TMZ specifically down-regulates Pgp/ABCB1 by interfering with the Wnt/GSK3/ $\beta$ -catenin signaling.

## Materials and methods

### Chemicals

Plasticware for cell cultures was from Falcon (Becton–Dickinson, Franklin Lakes, NJ, USA). TMZ, doxorubicin,

mitoxantrone, vinblastine, and topotecan were obtained by Sigma Chemical Co. (St. Louis, MO, USA). WntA [2-amino-4-(3,4-(methylenedioxy)benzylamino)-6-(3-methoxyphenyl)pyrimidine] was purchased from Calbiochem (San Diego, CA, USA). Human recombinant Dickkopf-1 (Dkk-1) was from R&D Systems (Minneapolis, MN, USA). Electrophoresis reagents were obtained from Bio-Rad Laboratories (Hercules, CA, USA); the protein content of cell lysates was assessed with the BCA kit from Sigma Chemical Co. When not otherwise specified, all the other reagents were purchased from Sigma Chemical Co.

## Cells

The immortalized hCMEC/D3 cells, a primary human brain microvascular endothelial cell line that retains the BBB characteristics *in vitro*, were cultured as reported [21]. Cells were seeded at 50,000/cm<sup>2</sup> density and were grown for 7 days up to confluence in Petri dishes and Transwell (0.4- $\mu$ m diameter pores-size, Corning Life Sciences, Chorges, France). Primary human brain microvascular endothelial cells (HBMECs) were purchased from PromoCell GmbH (Heidelberg, Germany) and cultured in the endothelial cell growth medium MV (PromoCell GmbH), supplemented with 5 % *v/v* fetal calf serum (FCS), 0.4 % *v/v* endothelial cell growth supplement (PromoCell GmbH), 10 ng/ml EGF, 90  $\mu$ g/ml heparin, and 1  $\mu$ g/ml hydrocortisone.

Primary human GBM cells (CV17, 01010627) were obtained from surgical samples of patients from the Department of Neuroscience, Neurosurgical Unit, University of Turin, Italy. The pathological diagnosis was performed according to WHO guidelines. Cells were cultured in DMEM-F12 medium, supplemented with 1 mol/l HEPES, 0.3 mg/ml glucose, 75  $\mu$ g/ml NaHCO<sub>3</sub>, 2 mg/ml heparin, 2 mg/ml bovine serum albumin (BSA), 2 mmol/l progesterone, 20 ng/ml EGF, 10 ng/ml bFGF. U87-MG cells (ATCC, Rockville, MD) were used as GBM reference cell line and cultured as reported above.

In co-culture experiments, 500,000 (for intracellular doxorubicin accumulation, PCR and cytotoxicity assays) or 1,000 (for proliferation assay) GBM cells were added in the lower chamber of Transwell 4 days after seeding hCMEC/D3 cells or HBMECs in Transwell inserts. After 3 days of co-culture the medium of the upper chamber was replaced with fresh medium with or without TMZ, doxorubicin, vinblastine or topotecan, alone or in combination as detailed below.

## Permeability coefficient across the BBB cells

The permeability to dextran-fluorescein isothiocyanate (FITC, molecular weight 70 kDa), [<sup>14</sup>C]-sucrose (589 mCi/mmol; PerkinElmer, Waltham, MA, USA),

[<sup>14</sup>C]-inulin (10 mCi/mmol; PerkinElmer) was taken as a parameter of tight junction integrity [21, 22]. The permeability to doxorubicin, [<sup>3</sup>H]-vinblastine (0.25 mCi/ml, PerkinElmer), mitoxantrone, was taken as index of ABC transporters activity [21]. hCMEC/D3 cells, seeded at 50,000/cm<sup>2</sup> and grown for 7 days up to confluence in six-multiwell Transwell inserts, were incubated at day 4 with or without TMZ (50  $\mu$ mol/l for 72 h). Then the culture medium was replaced in both chambers, 2  $\mu$ mol/l dextran-FITC, 2  $\mu$  Ci/ml [<sup>14</sup>C]-sucrose, 2  $\mu$  Ci/ml [<sup>14</sup>C]-inulin, 5  $\mu$ mol/l doxorubicin, 2  $\mu$  Ci/ml [<sup>3</sup>H]-vinblastine, 10  $\mu$ mol/l mitoxantrone were added to the upper chamber of Transwell. After 3 h, the medium in the lower chamber was collected. The amount of [<sup>14</sup>C]-sucrose, [<sup>14</sup>C]-inulin or [<sup>3</sup>H]-vinblastine was measured using a tri-carb liquid scintillation analyzer (PerkinElmer). Radioactivity was converted in nmol/cm<sup>2</sup>, using a calibration curve previously prepared. The amount of dextran-FITC, doxorubicin, and mitoxantrone present in the lower chamber was measured fluorometrically, using a LS-5 spectrofluorometer (PerkinElmer). Excitation and emission wavelengths were: 494 and 518 nm (dextran-FITC), 475 and 553 nm (doxorubicin), 607 and 684 nm (mitoxantrone). Fluorescence was converted in nmol/cm<sup>2</sup>, using a calibration curve previously set. The permeability coefficients were calculated as reported [23]. In time- and temperature-dependence experiments, the Transwell inserts were incubated at 4, 15, and 37 °C, and treated as reported above; aliquots of the medium from the lower chamber were collected every 30 min up to 3 h. The amount of doxorubicin or vinblastine in the lower chamber was quantified as described earlier. When indicated, a 25 % *w/v* solution of mannitol, used to increase the leakage of solutes through the BBB tight junctions, was co-incubated in the upper chamber.

For TMZ permeability, hCMEC/D3 cells seeded in Transwell inserts as reported above were incubated for 72 h with 0.7  $\mu$  Ci/ml [<sup>3</sup>H]-TMZ (Moravek Biochemical Inc., Brea, CA, USA), equivalent to 10  $\mu$ mol/l TMZ, in the presence of increasing concentrations (50, 100, and 200  $\mu$ M) of cold TMZ. After this incubation period, the amount of [<sup>3</sup>H]-TMZ in the lower chamber was measured by liquid count scintillation. The results were expressed as the percentage of [<sup>3</sup>H]-TMZ recovered in the lower chamber after 72 h versus [<sup>3</sup>H]-TMZ added in the upper chamber at time 0, taking into account the concentration of cold TMZ added in the upper chamber at time 0.

## Rhodamine 123 and Hoechst 33342 accumulation

hCMEC/D3 cells were grown up to confluence in Petri dishes and incubated in the absence or presence of TMZ, as reported above. Cells were washed with PBS, detached with cell dissociation solution (Sigma), centrifuged at

13,000 × *g* for 5 min and re-suspended in 0.5 ml culture medium containing 5 % v/v FCS. A 50-μl aliquot was taken away, sonicated and used for the measurement of the protein content. Twenty μmol/l of rhodamine 123 or 50 μmol/l Hoechst 33342 were added to the remaining sample. After 10 min at 37 °C, cells were washed three times with PBS and re-suspended in 1 ml PBS. The intracellular fluorescence of rhodamine 123 (index of Pgp/ABCB1 and MRP1/ABCC1 activity) and Hoechst 33342 (index of BCRP/ABCG2 activity) was measured fluorometrically, using a LS-5 spectrofluorometer (PerkinElmer). Excitation and emission wavelengths were: 488 and 520 nm for rhodamine 123, 370 and 450 nm for Hoechst 33342. Fluorescence was converted in nmol/mg cell proteins using a calibration curve previously set.

#### Western-blot analysis

Cells were rinsed with lysis buffer (50 mmol/l Tris, 10 mmol/l EDTA, 1 % w/v Triton-X100), supplemented with the protease inhibitor cocktail set III (80 μmol/l aprotinin, 5 mmol/l bestatin, 1.5 mmol/l leupeptin, 1 mmol/l pepstatin; Calbiochem), 2 mmol/l phenylmethylsulfonyl fluoride and 1 mmol/l sodium orthovanadate, then sonicated and centrifuged at 13,000 × *g* for 10 min at 4 °C. 20 μg of protein extracts were subjected to SDS-PAGE and probed with the following antibodies: anti-claudin 3 (Invitrogen Life Technologies, Monza, Italy); anti-claudin 5 (Invitrogen Life Technologies); anti-occludin (Invitrogen Life Technologies); anti-zonula occludens-1 (ZO-1; Invitrogen Life Technologies); anti-Pgp/ABCB1 (clone C219, Cabiochem), anti-MRP1/ABCC1 (Abcam, Cambridge, MA, USA), anti-BCRP/ABCG2 (Santa Cruz Biotechnology Inc., Santa Cruz, CA, USA), anti-Wnt3 (Abcam); anti-GSK3 (BD Biosciences, Franklin Lakes, NJ, USA); anti-phospho(Tyr216)GSK3 (BD Biosciences); anti-β-catenin (BD Biosciences); anti-phospho(Ser33/37/Thr41)β-catenin (Cell Signalling Technology Inc., Danvers, MA, USA); anti-β-tubulin (Santa Cruz Biotechnology Inc). This procedure was followed by the exposure to a peroxidase-conjugated secondary antibody (Bio-Rad). The membranes were washed with Tris buffer saline-Tween 0.1 % v/v, and proteins were detected by enhanced chemiluminescence (PerkinElmer).

Cytosol/nucleus separation was performed as reported [24]. Ten μg of cytosolic or nuclear extracts were subjected to Western-blot analysis using the anti-β-catenin antibody. To check the equal control loading in cytosolic and nuclear fractions, samples were probed respectively with an anti-β-tubulin or an anti-TATA-box binding protein (TBP/TFIID) antibody (Santa Cruz Biotechnology Inc). To exclude any cytosolic contamination of nuclear extracts or vice versa, we verified that β-tubulin was undetectable in

nuclear samples and TBP was undetectable in cytosolic samples.

The densitometric analysis of Western blots was performed with ImageJ software (<http://rsb.info.nih.gov/ij/>) and expressed as arbitrary units, where “1 unit” is the mean band density in untreated cells.

#### Quantitative real-time PCR (qRT-PCR)

Total RNA was extracted and reverse-transcribed using the QuantiTect Reverse Transcription Kit (Qiagen, Hilden, Germany). qRT-PCR was carried out using IQ SYBR Green Supermix (Bio-Rad), according to the manufacturer's instructions. The same cDNA preparation was used to quantify the genes of interest and the housekeeping gene β-actin. Primer sequences, designed with the Primer3 software (<http://frodo.wi.mit.edu/primer3>), are reported in online resource 2. The relative quantification was performed by comparing each PCR product with the housekeeping PCR product using Bio-Rad software gene expression quantitation (Bio-Rad).

#### Chromatin immunoprecipitation (ChIP)

ChIP experiments were performed using the Magna ChIP A/G chromatin immunoprecipitation kit (Millipore, Billerica, MA, USA). Samples were immunoprecipitated with 5 μg of anti-β-catenin antibody or with no antibody. The immunoprecipitated DNA was washed and eluted twice with 100 μl of elution buffer (0.1 M NaHCO<sub>3</sub>, 1 % w/v SDS), the cross-linking was reversed by incubating the samples at 65 °C for 6 h. Samples were then treated with 1 μl proteinase K for 1 h at 55 °C. The DNA was eluted in 50 μl of H<sub>2</sub>O and analyzed by PCR. The putative β-catenin site on *mdr1* promoter was validated by the MatInspector software (<http://www.genomatix.de/>). Primers sequences, designed with the Primer3 software (<http://frodo.wi.mit.edu/primer3>), are reported in online resource 2. PCR products were visualized on a 3 % agarose gel, stained with 0.05 % v/v ethidium bromide. As negative control, immunoprecipitated samples were subjected to PCR with primers matching a region 10,000 bp upstream the *mdr1* promoter. In this condition, no PCR product was detected (not shown).

#### Flow cytometry analysis

Cells were washed with PBS, detached with cell dissociation solution, and re-suspended at 5 × 10<sup>5</sup> cells/ml in 1 ml of culture medium containing 5 % v/v FCS. Samples were washed with 0.25 % w/v BSA-PBS, incubated with the primary antibody for Frizzled (Santa Cruz Biotechnology Inc.) or LRP6 (Abcam) for 45 min at 4 °C, then washed

twice and incubated with secondary FITC-conjugated antibody for 30 min at 4 °C. After washing and fixing in paraformaldehyde 2 % w/v, the surface amount of Frizzled or LRP6 was detected on 100,000 cells by a FACSCalibur system, using the Cell Quest software (Becton–Dickinson). Control experiments included incubation of cells with non-immune isotypic antibody, followed by the secondary antibody.

#### Promoter methylation assay

Genomic DNA (1 µg) was subjected to bisulphite modification using the Methyl Easy Xceed kit (Human Genetics Signatures, Randwick, Australia), following the manufacturer's instructions. *Wnt3* promoter sequence was obtained using the UCSC Genome Browser (<http://genome.ucsc.edu/>). The CpG islands localization on *Wnt3* promoter and the design of primers for methylation-specific PCR (MSP) was performed with Methprimer software (<http://www.urogene.org/methprimer>). Primers specific for methylated and unmethylated *Wnt3* promoter are reported in online resource 2. MSP was performed with AmpliTaq gold DNA polymerase (Applied Biosystems, Carlsbad, CA, USA), including universally methylated (CpGenome, Millipore) and unmethylated DNA samples (Human Genetics Signatures) as control. PCR products were visualized on a 3 % w/v agarose gel, stained with 0.05 % v/v ethidium bromide.

#### Generation of Wnt3-silenced cells

A total of 300,000 hCMEC/D3 cells were treated with Turbofectin 8.0 (Origene Technologies Inc., Rockville, MD, USA) and 1 µg of 29-mer shRNA *Wnt3* construct in pGFP-C-shLenti-vector (Origene Technologies Inc.) or non-targeting 29-mer scrambled shRNA cassette in pGFP-C-shLenti Vector (Origene Technologies Inc.), used as control. Twenty-four hours after the transfection, the green fluorescent cells were sorted by flow cytometry analysis. Forty-eight hours after the transfection, the cells were transferred in puromycin-containing medium to select clones stably silenced for *Wnt3*. The silencing efficacy was controlled every two passages by qRT-PCR and Western-blot analysis of *Wnt3*.

#### Intracellular doxorubicin accumulation in co-culture models

After 3 days of co-culture, 5 µmol/l doxorubicin for 24 h or 50 µmol/l TMZ for 72 h plus 5 µmol/l doxorubicin in the last 24 h were added to the upper chamber of Transwell inserts containing hCMEC/D3 cells monolayer. Then, the GBM cells were collected from the lower chamber, rinsed with PBS, re-suspended in 0.5 ml ethanol/HCl 0.3 N (1:1

v/v) and sonicated. A 50-µl aliquot was used to measure the protein content and the remaining sample was used to quantify fluorometrically the intracellular doxorubicin content as described above. Results were expressed as nmol doxorubicin/mg cell proteins.

For fluorescence microscope analysis, the GBM cells in the lower chamber were seeded on sterile glass coverslips and treated as reported above. At the end of the incubation period, cells were rinsed with PBS, fixed in 4 % w/v paraformaldehyde for 15 min, washed three times with PBS, and incubated with 4',6-diamidino-2-phenylindole dihydrochloride (DAPI) for 3 min at room temperature in the dark. Cells were washed three times with PBS and once with water and then the slides were mounted with 4 µl of gel mount aqueous mounting and examined with a Leica DC100 fluorescence microscope (Leica Microsystems GmbH, Wetzlar, Germany). For each experimental point, a minimum of five microscopic fields were examined.

#### Cytotoxicity assays in co-culture models

After 3 days of co-culture, the upper chamber of the Transwell inserts containing hCMEC/D3 cells was filled with fresh medium or with medium containing: 50 µmol/l TMZ for 72 h, 5 µmol/l doxorubicin for 24 h, 50 µmol/l TMZ for 72 h plus 5 µmol/l doxorubicin in the last 24 h, 20 nmol/l vinblastine for 24 h, 50 µmol/l TMZ for 72 h plus 20 nmol/l vinblastine in the last 24 h, 10 µmol/l topotecan for 24 h, 50 µmol/l TMZ for 72 h plus 10 µmol/l topotecan in the last 24 h. According to preliminary experiments, 50 µmol/l TMZ for 72 h did not produce any significant toxicity in GBM cells or in hCMEC/D3 cells. The concentration of doxorubicin, vinblastine, and topotecan was chosen on the basis of previous works, showing that at these concentrations each drug reduced the survival of GBM cells—in the absence of BBB cells—to less than 20 % [25–27].

The release of lactate dehydrogenase (LDH) in cell supernatant, used as index of cell damage and necrosis, was measured spectrophotometrically as described earlier [28]. Results were expressed as percentage of extracellular LDH versus total (intracellular plus extracellular) LDH. The activation of caspase 3, as index of apoptosis, was assessed in cells lysates as reported [29]. The amount of the hydrolyzed DEVD-7-amino-4-methylcumarine, a substrate of caspase 3, was measured fluorometrically. Results were expressed as nmol/mg cell protein using a calibration curve prepared with standard solutions of amino-4-methylcumarine.

#### Proliferation assays in co-culture models

GBM cells (1,000) were seeded in the lower chamber of Transwell, containing confluent hCMEC/D3 cells in the

insert. This time was considered “day 0” in the proliferation assay. After 3 days of co-culture, the upper chamber of the Transwell inserts was filled with fresh medium or medium containing: 50  $\mu\text{mol/l}$  TMZ for 72 h, 5  $\mu\text{mol/l}$  doxorubicin for 24 h, 50  $\mu\text{mol/l}$  TMZ for 72 h plus 5  $\mu\text{mol/l}$  doxorubicin in the last 24 h, 20 nmol/l vinblastine for 24 h, 50  $\mu\text{mol/l}$  TMZ for 72 h plus 20 nmol/l vinblastine in the last 24 h, 10  $\mu\text{mol/l}$  topotecan for 24 h, 50  $\mu\text{mol/l}$  TMZ for 72 h plus 10  $\mu\text{mol/l}$  topotecan in the last 24 h. The treatments were repeated every 7 days, for 4 weeks. At day 7, 14, 21, and 28, GBM cells were collected, transferred into a 96-well plate, fixed with 4 % w/v paraformaldehyde, and stained with 0.5 % w/v crystal violet solution for 10 min at room temperature. The plate was washed three times in water, and then 100  $\mu\text{l}$  of 0.1 mmol/l sodium citrate in 50 % v/v ethanol was added to each well and the absorbance was read at 570 nm. The absorbance units were converted into cell number, according to a titration curve obtained with serial cells dilutions of each cell line. To check that hCMEC/D3 cells retain BBB properties, the permeability to dextran and inulin was measured weekly in a parallel set of Transwell. No significant changes in the permeability coefficients were detected during the whole experiment (data not shown).

#### Statistical analysis

All data in text and figures are provided as mean  $\pm$  SD. The results were analyzed by a one-way analysis of variance (ANOVA). A  $p$  value  $<0.05$  was considered significant.

## Results

### Temozolomide increases the transport of Pgp/ABCB1 substrates through hCMEC/D3 BBB cells monolayer

We investigated whether 50  $\mu\text{mol/l}$  TMZ (equivalent to 9.7  $\mu\text{g/ml}$ , a concentration that is clinically achievable in blood) [30] may affect the transport of other molecules through hCMEC/D3 monolayer.

As shown in Fig. 1a (upper panels), the permeability of molecules that have a paracellular diffusion in case of tight junctions leakage, such as dextran, inulin, and sucrose, widely varied in hCMEC/D3 cells, but was compatible with intact tight junctions [21]. The permeability coefficients followed this rank order: inulin  $>$  sucrose  $>$  dextran 70. TMZ did not affect the permeability of these compounds (Fig. 1a, upper panels). Also the permeability of ABC transporters substrates displayed major differences: among the substrates of Pgp/ABCB1 and MRP1/ABCC1 proteins, doxorubicin was almost 100-fold less transported than vinblastine across the hCMEC/D3 monolayer. When we analyzed the transport of doxorubicin and vinblastine at earlier time points,

it increased linearly in a temperature- and time-dependent manner (online resource 3a). In the presence of mannitol, an agent that disrupts the tight junctions as shown by the increased permeability of inulin (online resource 3b), we did not detect significant changes in doxorubicin and vinblastine transport (online resource 3c). These results suggest that paracellular leakage contributed minimally to the transport of doxorubicin and vinblastine across the hCMEC/D3 monolayer. Because of their high hydrophobicity, doxorubicin and vinblastine are expected to enter by passive diffusion [31, 32], and then to be effluxed back by Pgp/ABCB1 and MRP1/ABCC1. Of note, the permeability of doxorubicin and vinblastine was significantly higher in hCMEC/D3 cells pre-treated with TMZ (Fig. 1a, lower panels). By contrast, the permeability of mitoxantrone, a substrate of BCRP/ABCG2 with a permeability coefficient between doxorubicin and vinblastine in hCMEC/D3 cells, was unaffected by TMZ (Fig. 1a, lower panels).

Congruent with these results, TMZ increased the intracellular accumulation of rhodamine 123, which is effluxed by Pgp/ABCB1 and MRP1/ABCC1, and did not change the accumulation of Hoechst 33342, which is effluxed by BCRP/ABCG2 (online resource 4).

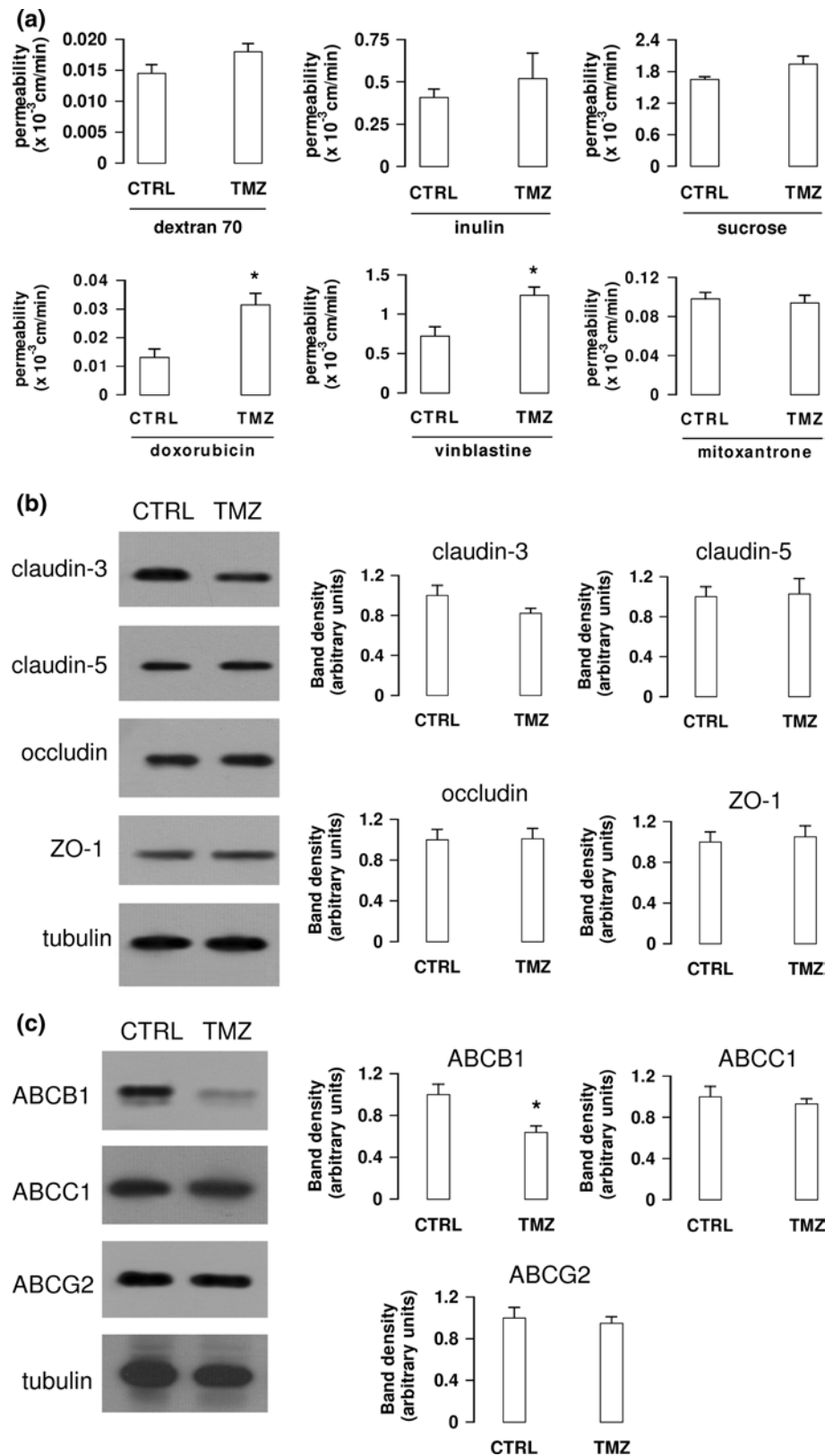
When we analyzed the expression of typical tight junctions proteins in cells exposed to TMZ we detected a small decrease of claudin-3. Claudin-5, occludin, and ZO-1 did not change (Fig. 1b). hCMEC/D3 cells constitutively expressed Pgp/ABCB1, MRP1/ABCC1, and BCRP/ABCG2 (Fig. 1c). Of note, TMZ decreased the amount of Pgp/ABCB1, without affecting the other two proteins (Fig. 1c). The decrease of Pgp/ABCB1 exerted by TMZ was dose-dependent (online resource 5a). We next measured the transport of [ $^3\text{H}$ ]-TMZ across hCMEC/D3 monolayer in the presence of increasing concentrations of unlabeled TMZ, sufficient to significantly reduce Pgp/ABCB1: as shown in the online resource 5b, the amount of [ $^3\text{H}$ ]-TMZ in the lower chamber of Transwell was about 100 % of the amount added in the upper chamber, independently of the decrease of Pgp/ABCB1 induced by TMZ itself. These results suggest that Pgp/ABCB1 played a minor role in the transport of TMZ across hCMEC/D3 monolayer and that TMZ did not enhance its own delivery by decreasing Pgp/ABCB1.

Under our experimental conditions, TMZ (50  $\mu\text{mol/l}$  for 72 h) showed no toxicity on hCMEC/D3 cells, as measured by LDH release (as described below) and caspase-3 activity (not shown).

Temozolomide down-regulates the transcription of *mdr1* gene by disrupting the Wnt/GSK3/ $\beta$ -catenin pathway in hCMEC/D3 BBB cells

To clarify the molecular mechanisms by which TMZ decreases Pgp/ABCB1 protein, we asked the questions of

**Fig. 1** Effects of temozolomide on permeability coefficients, tight junction markers, and ABC transporters in blood–brain barrier hCMEC/D3 cells. **a** hCMEC/D3 cells were grown for 7 days up to confluence in Transwell inserts, without (*CTRL*) or with temozolomide (*TMZ*; 50  $\mu\text{mol/l}$  for the last 72 h). At the end of the incubation period, 2  $\mu\text{mol/l}$  dextran-FITC, 2  $\mu\text{Ci/ml}$  [ $^{14}\text{C}$ ]-inulin, 2  $\mu\text{Ci/ml}$  [ $^{14}\text{C}$ ]-sucrose, 5  $\mu\text{mol/l}$  doxorubicin, 2  $\mu\text{Ci/ml}$  [ $^3\text{H}$ ]-vinblastine, 10  $\mu\text{mol/l}$  mitoxantrone were added in the upper chamber. After 3 h, the amount of the drug recovered from the lower chamber was measured fluorometrically (for dextran-FITC, doxorubicin, and mitoxantrone) or by liquid scintillation (for inulin, sucrose, and vinblastine). Permeability coefficients were calculated as reported under the “Materials and methods” section. Measurements were performed in duplicate and data are presented as mean  $\pm$  SD ( $n = 3$ ). vs. *CTRL*: \* $p < 0.02$ . **b** hCMEC/D3 cells were incubated without (*CTRL*) or with temozolomide (*TMZ*; 50  $\mu\text{mol/l}$  for 72 h), then lysed and subjected to Western-blot analysis for claudin-3, claudin-5, occludin, ZO-1.  $\beta$ -tubulin expression was used as control of equal protein loading. The figure is representative of three experiments with similar results. The band density ratio between each protein and  $\beta$ -tubulin was expressed as arbitrary units. **c** hCMEC/D3 cells, treated as reported in **b**, were subjected to Western-blot analysis for Pgp/ABCB1, MRP1/ABCC1, and BCRP/ABCG2.  $\beta$ -tubulin expression was used as control of equal protein loading. The figure is representative of three experiments with similar results. The band density ratio between each protein and  $\beta$ -tubulin was expressed as arbitrary units. vs. *CTRL*: \* $p < 0.05$



whether decreased gene transcription could be accountable and which transcription factors could be the targets of the drug. TMZ lowered the mRNA levels of *mdr1* (Fig. 2a)

and decreased the binding of  $\beta$ -catenin, a known inducer of Pgp/ABCB1 in hCMEC/D3 cells [16], to the *mdr1* promoter (Fig. 2b).

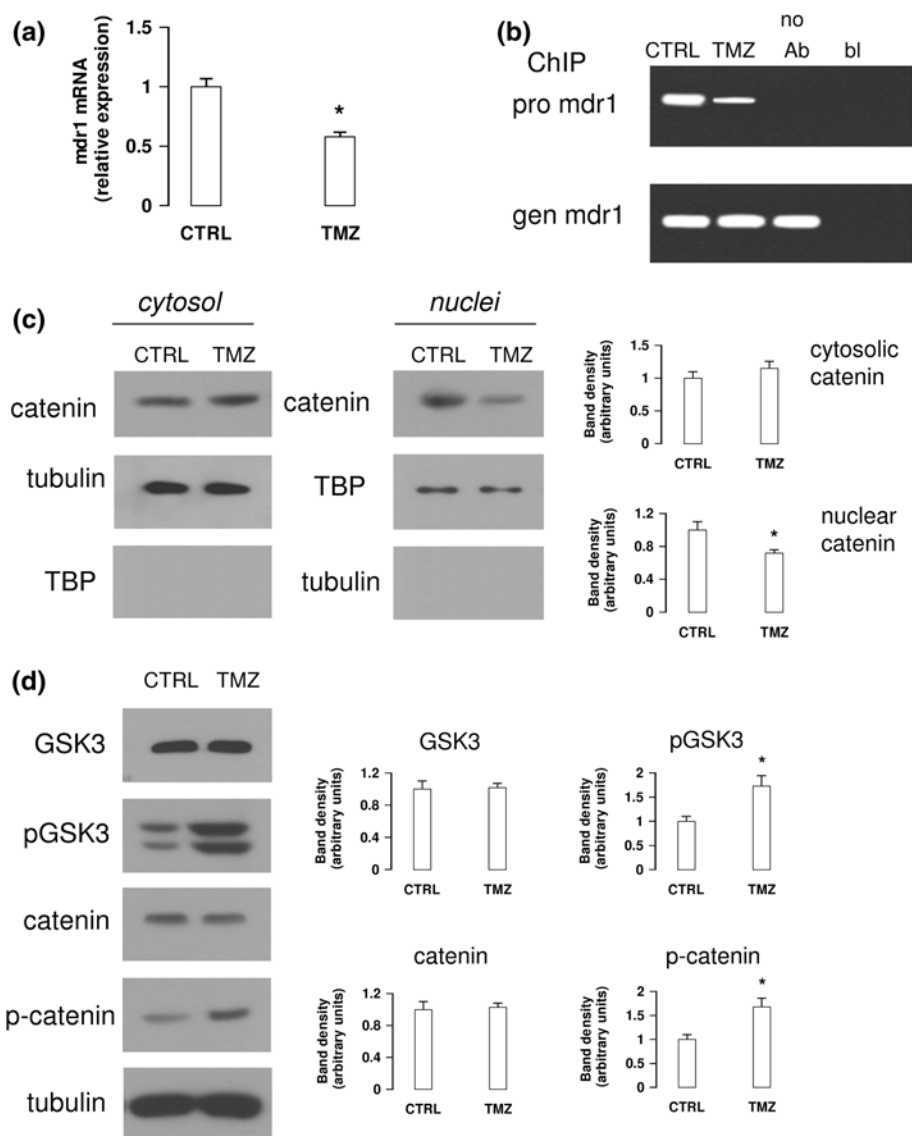


**Fig. 2** Effects of temozolomide on *mdr1* expression and GSK3/ $\beta$ -catenin pathway in hCMEC/D3 cells. hCMEC/D3 cells were grown in fresh medium (CTRL) or in the presence of temozolomide (TMZ; 50  $\mu$ mol/l for 48 h), then subjected to the following investigations. **a** Total RNA was extracted and reverse-transcribed and the expression of *mdr1* gene was detected by qRT-PCR. The expression level in untreated cells was considered “1”. Data are presented as mean  $\pm$  SD ( $n = 3$ ). vs. CTRL: \* $p < 0.002$ . **b** Chromatin immunoprecipitation of  $\beta$ -catenin on *mdr1* promoter (*pro*) in hCMEC/D3 cells. *gen* PCR product from genomic DNA. *no Ab* precipitated samples without anti- $\beta$ -catenin antibody. *bl* blank. The figure is representative of three experiments with similar results. **c** Nuclear and cytosolic extracts were

analyzed for the amount of  $\beta$ -catenin. The expression of  $\beta$ -tubulin and TBP was used as control of equal protein loading for cytosolic and nuclear samples, respectively, and to verify the efficacy of the nucleus–cytosol separation. The band density ratio between each protein and  $\beta$ -tubulin/TBP was expressed as arbitrary units. vs. CTRL: \* $p < 0.05$ . The figure is representative of three experiments with similar results. **d** Western-blot analysis of phospho(Ser33/37/Thr41) $\beta$ -catenin,  $\beta$ -catenin in whole-cell lysates.  $\beta$ -tubulin expression was used as control of equal protein loading. The figure is representative of three experiments with similar results. The band density ratio between each protein and  $\beta$ -tubulin was expressed as arbitrary units. vs. CTRL: \* $p < 0.02$

In hCMEC/D3 cells,  $\beta$ -catenin was detectable in both cytosolic and nuclear extracts under basal conditions (Fig. 2c); TMZ decreased the amount of  $\beta$ -catenin present in the nucleus (Fig. 2c). In parallel the drug increased the active form of GSK3—i.e., phospho(Tyr216)GSK3—, and the amount of serine 33/37/threonine 41-phosphorylated

$\beta$ -catenin (Fig. 2d). As a whole, these data suggest that TMZ may reduce the amount of  $\beta$ -catenin active as transcription factor.

In hCMEC/D3 cells, the activity of GSK3 is controlled by the Wnt canonical pathway [17, 18]. The presence of Wnt proteins in endothelial cells is restricted to some

antigens of the large Wnt family, such as Wnt2b, Wnt3, Wnt4, and Wnt5 [33]. The first three are associated to the canonical GSK3/ $\beta$ -catenin pathway [34–36].

We wanted to validate the hypotheses that (1) the Wnt/GSK3/ $\beta$ -catenin axis controls the expression of the *mdr1* gene in hCMEC/D3 and (2) TMZ down-regulates the expression of Pgp/ABCB1 by interfering with this axis. We therefore treated cells with the Wnt activator WntA, the Wnt antagonist Dkk-1, and the GSK3 inhibitor LiCl. As shown in Fig. 3a, WntA decreased the phosphorylation of GSK3, whereas Dkk-1 produced the opposite effect. The phosphorylation of  $\beta$ -catenin, which was low in untreated hCMEC/D3 cells, was not significantly reduced by WntA and was increased by Dkk-1. LiCl did not change the phosphorylation of GSK3 on tyrosine 216, but slightly reduced the phosphorylation of  $\beta$ -catenin on serine 33/37/threonine 41, suggesting that it effectively inhibited the activity of GSK3. The nuclear translocation of  $\beta$ -catenin (Fig. 3b) and its binding on *mdr1* promoter (Fig. 3c) was increased by WntA and LiCl, and reduced by Dkk-1. Indeed, hCMEC/D3 cells treated with Dkk-1 had lower levels of *mdr1* mRNA (Fig. 3d) and Pgp/ABCB1 protein (Fig. 3e). Cells treated with WntA or LiCl had higher amounts of *mdr1* mRNA and Pgp/ABCB1 protein (Fig. 3d–e). Congruent with this trend, Dkk-1 increased, and WntA and LiCl decreased the permeability of doxorubicin, chosen as a Pgp/ABCB1 substrate, across the hCMEC/D3 monolayer (Fig. 3f). Interestingly, TMZ mimicked the effects of Dkk-1 and counteracted the effects of WntA and LiCl on  $\beta$ -catenin phosphorylation (Fig. 3a), nuclear translocation (Fig. 3b) and *mdr1* promoter binding (Fig. 3c), on *mdr1* mRNA (Fig. 3d) and Pgp/ABCB1 levels (Fig. 3e), and on doxorubicin permeability (Fig. 3f). These findings suggested that TMZ reduced *mdr1* transcription by inhibiting the Wnt/GSK3/ $\beta$ -catenin axis.

#### Temozolomide lowers the synthesis of Wnt3 in hCMEC/D3 BBB cells

TMZ did not change the surface amount of the Wnt receptor Frizzled and Wnt co-receptor LRP6 (online resource 6), leading to exclude interference with the Wnt3 signaling on the cell surface.

We asked the question, then, of whether TMZ down-regulated the endogenous synthesis of one or more Wnts proteins. We did not detect Wnt2b and Wnt4 in hCMEC/D3 cells (data not shown). Wnt3 was instead detectable at protein (Fig. 4a) and mRNA (Fig. 4b) level. Notably, TMZ reduced both Wnt3 protein and mRNA (Fig. 4a, b).

Since TMZ is an alkylating agent that methylates DNA [4], we asked the question of whether it might cause the methylation of the *Wnt3* promoter. *Wnt3* promoter has indeed several CpG islands (online resource 7), usually

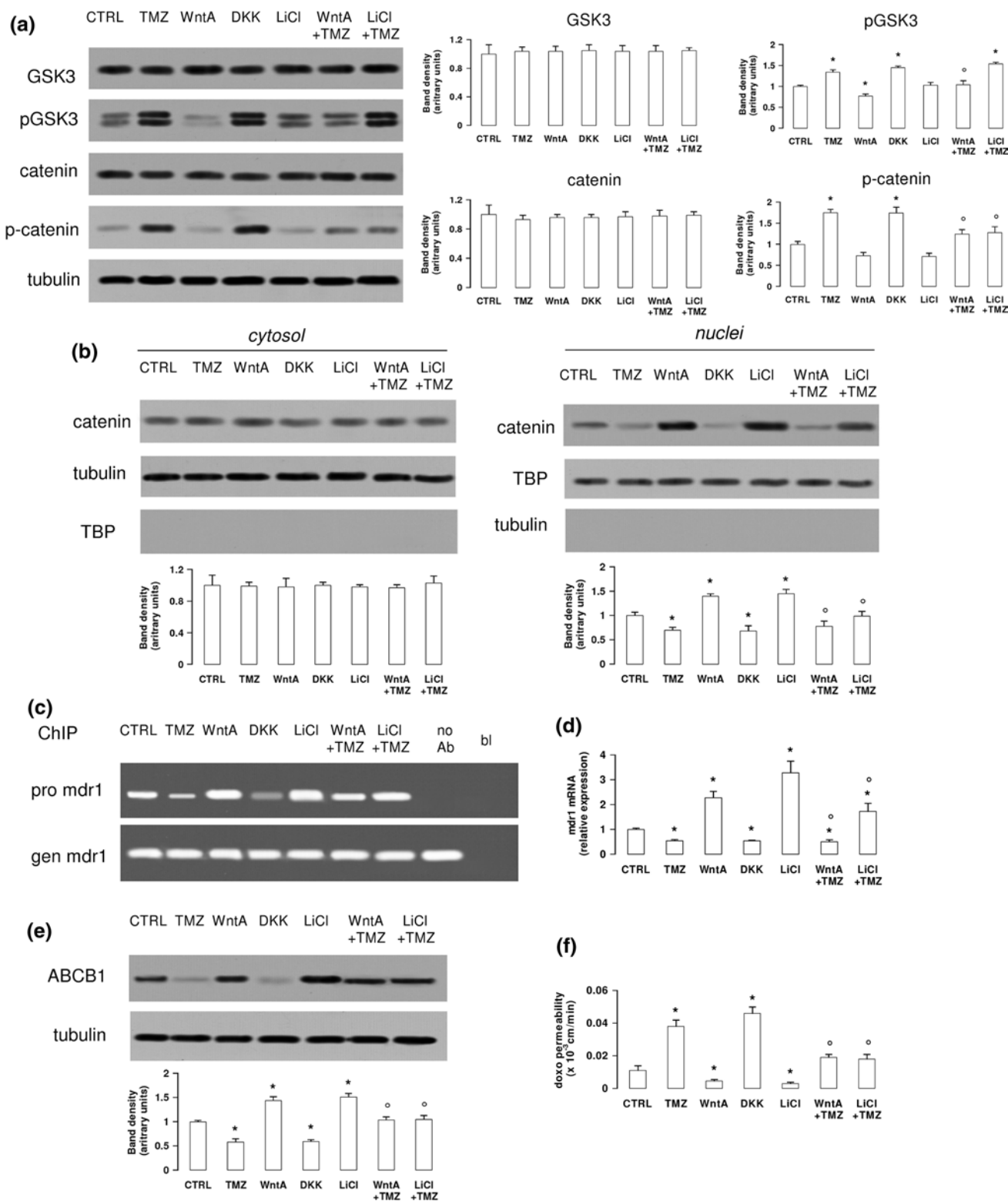
methylated in infrequently transcribed genes and unmethylated in highly transcribed ones. MSP PCR assays showed that Wnt3 promoter was fully unmethylated in hCMEC/D3 cells (Fig. 4c). TMZ decreased the amount of unmethylated promoter and induced the appearance of a methylated band (Fig. 4c), thus appearing to be a good candidate for the epigenetic down-regulation of Wnt3.

To confirm that Wnt3 was a critical controller of *mdr1* expression in our model, we permanently silenced Wnt3 in hCMEC/D3 cells; silencing produced a 90 % reduction in *Wnt3* mRNA (Fig. 5a) and made the Wnt3 protein undetectable by Western blotting (Fig. 5b). The depletion of the Wnt3 protein significantly increased the amount of phospho(Tyr216)GSK3 and phospho(Ser33/37/Thr41) $\beta$ -catenin (Fig. 5c), prevented the binding of  $\beta$ -catenin on *mdr1* promoter (Fig. 5d) and markedly reduced the expression of Pgp/ABCB1 (Fig. 5e). Additionally, Wnt3-depleted hCMEC/D3 cells showed a higher permeability to doxorubicin than wild-type cells (Fig. 5f).

#### Temozolomide increases the anti-tumor efficacy of Pgp/ABCB1 substrates in glioblastoma-hCMEC/D3 co-culture models

Since TMZ decreased the amount and activity of Pgp/ABCB1 in BBB cells, we next asked the question of whether the efficacy of anti-cancer drugs commonly effluxed by this transporter would be improved. With this goal in mind, we cultured hCMEC/D3 cells, treated or not with TMZ, in Transwell inserts, containing different GBM cell lines (CV17, 01010627, U87-MG) in the lower chamber. Without pre-treatment with TMZ, doxorubicin was applied in the upper chamber, facing the luminal side of hCMEC/D3 monolayer, which expresses high amounts of Pgp/ABCB1 [37]. As expected, doxorubicin was poorly delivered to GBM cells in the lower chamber (Fig. 6a). Pre-treatment of hCMEC/D3 cells with TMZ significantly increased the intratumor amount of doxorubicin (Fig. 6a). The typical nuclear red fluorescence of doxorubicin [28] was undetectable in 01010627 GBM cells recovered from the lower chamber of the co-cultures, whereas pre-treatment of hCMEC/D3 cells with TMZ restored the nuclear accumulation of doxorubicin in GBM cells (Fig. 6b). Interestingly, TMZ decreased the expression levels of *mdr1* also in the GBM cells cultured in the lower chamber (online resource 8), as it did in hCMEC/D3 cells.

Under the experimental conditions used, neither TMZ nor doxorubicin alone induced detectable cytotoxicity, measured as extracellular release of LDH and activation of caspase 3 (Fig. 6c), in GBM cells. The TMZ-doxorubicin combination produced cytotoxic effects in all the tumor cell lines analyzed (Fig. 6c). The rate of proliferation of the three GBM cell lines was not affected by



the addition of doxorubicin in the upper chamber of the Transwell (Fig. 6d). TMZ applied in the upper chamber reduced the proliferation rate of all tumor cell lines in a time-dependent way; of note, its antiproliferative effect was significantly enhanced when TMZ was followed by

doxorubicin (Fig. 6d). Under these conditions TMZ and doxorubicin, alone or in combination, did not induce any significant cytotoxicity (online resource 9a) and did not affect cell proliferation (online resource 9b) in hCMEC/D3 cells.

**Fig. 3** Effects of temozolomide and Wnt modulators on *mdr1* expression in hCMEC/D3 cells. hCMEC/D3 cells were grown in fresh medium (*CTRL*) or with temozolomide (*TMZ*; 50  $\mu\text{mol/l}$  for 48 h), Wnt activator 2-amino-4-(3,4-(methylene dioxy)benzyl amino)-6-(3-methoxyphenyl)pyrimidine (*WntA*; 20  $\mu\text{mol/l}$  for 24 h), Wnt inhibitor recombinant Dkk-1 protein (*DKK*; 1  $\mu\text{g/ml}$  for 24 h), GSK3 inhibitor LiCl (*LiCl*; 10  $\text{mmol/l}$  for 24 h). When co-incubated, WntA and LiCl were added to TMZ in the last 24 h. **a** Western-blot analysis of phospho(Tyr216)GSK3, GSK3, phospho(Ser33/37/Thr41) $\beta$ -catenin,  $\beta$ -catenin in whole cell lysates.  $\beta$ -tubulin expression was used as control of equal protein loading. The figure is representative of three experiments with similar results. The band density ratio between each protein and  $\beta$ -tubulin was expressed as arbitrary units. vs. *CTRL*: \* $p < 0.02$ ; vs. *WntA* or *LiCl* alone:  $^{\circ}p < 0.05$ . **b** Nuclear and cytosolic extracts were analyzed for the amount of  $\beta$ -catenin. The expression of  $\beta$ -tubulin and TBP was used as control of equal protein loading for cytosolic and nuclear samples respectively, and to verify the efficacy of the nucleus–cytosol separation. The band density ratio between each protein and  $\beta$ -tubulin/TBP was expressed as arbitrary units. vs. *CTRL*: \* $p < 0.05$ ; vs. *WntA* or *LiCl* alone:  $^{\circ}p < 0.005$ . The figure is representative of three experiments with similar results. **c** Chromatin immunoprecipitation of  $\beta$ -catenin on *mdr1* promoter (*pro*) in hCMEC/D3 cells. *gen* PCR product from genomic DNA. *no Ab* precipitated samples without anti- $\beta$ -catenin antibody. *bl* blank. The figure is representative of three experiments with similar results. **d** *mdr1* expression was detected in triplicate by qRT-PCR. Data are presented as mean  $\pm$  SD ( $n = 4$ ). vs. *CTRL*: \* $p < 0.02$ ; vs. *WntA* or *LiCl*:  $^{\circ}p < 0.05$ . **e** Western-blot analysis of Pgp/ABCB1.  $\beta$ -tubulin expression was used as control of equal protein loading. The figure is representative of three experiments with similar results. The band density ratio between each protein and  $\beta$ -tubulin was expressed as arbitrary units. vs. *CTRL*: \* $p < 0.01$ ; vs. *WntA* or *LiCl* alone:  $^{\circ}p < 0.02$ . **f** Doxorubicin permeability. hCMEC/D3 cells were grown for 7 days up to confluence in Transwell inserts and treated as reported above. At the end of the incubation period, 5  $\mu\text{mol/l}$  doxorubicin was added in the upper chamber. After 3 h, the amount of the drug recovered from the lower chamber was measured fluorometrically. Permeability coefficient was calculated as reported under the “Materials and methods” section. Measurements were performed in duplicate and data are presented as mean  $\pm$  SD ( $n = 3$ ). vs. *CTRL*: \* $p < 0.001$ ; vs. *WntA* or *LiCl* alone:  $^{\circ}p < 0.005$

The chemosensitizing properties of TMZ were not limited to doxorubicin. In the same co-culture models, vinblastine and topotecan, two other substrates of Pgp/ABCB1, did not increase the extracellular LDH (online resource 10a), did not activate the caspase 3 (online resource 10b) and did not decrease cell proliferation (online resource 10c) of GBM cells, when applied in the upper chamber of the Transwell. Only the pre-treatment of hCMEC/D3 cells with TMZ followed by vinblastine and topotecan exerted significant cytotoxicity (online resource 10a–b) and reduced the proliferation (online resource 10c) of GBM cells cultured under the BBB monolayer. The combination of TMZ plus vinblastine or TMZ plus topotecan (online resource 10c) were significantly more effective in reducing cell proliferation after 21 and 28 days ( $p < 0.02$ ) than TMZ alone (Fig. 6d).

Notably, the same permeabilizing effects induced by TMZ in wild-type BBB cells was obtained after Wnt3

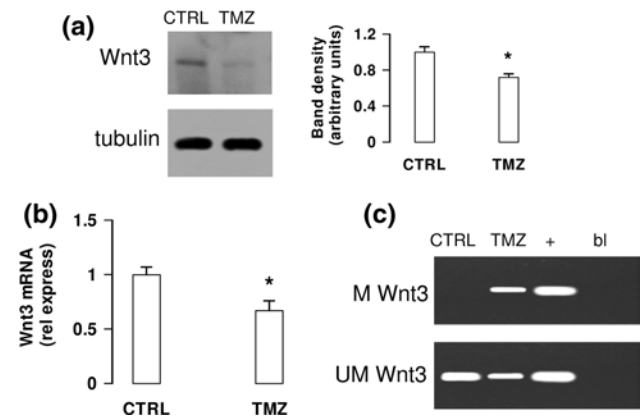


**Fig. 4** Effects of temozolomide on Wnt3 synthesis in hCMEC/D3 cells. hCMEC/D3 cells were grown in the absence (*CTRL*) or in the presence of temozolomide (*TMZ*; 50  $\mu\text{mol/l}$  for 48 h) in Western-blot experiments, 24 h in qRT-PCR and MSP experiments, then subjected to the following investigations. **a** Western-blot analysis of Wnt3 in whole cell lysates.  $\beta$ -tubulin expression was used as control of equal protein loading. The figure is representative of three experiments with similar results. The band density ratio between Wnt3 and  $\beta$ -tubulin was expressed as arbitrary units. vs. *CTRL*: \* $p < 0.05$ . **b** Total RNA was extracted and reverse-transcribed, then the expression of *Wnt3* gene was detected by qRT-PCR. The expression level in untreated cells was considered “1”. Data are presented as mean  $\pm$  SD ( $n = 3$ ). vs. *CTRL*: \* $p < 0.05$ . **c** Methylation of *Wnt3* promoter. Genomic DNA was subjected to bisulfite modification, followed by PCR with specific primers for methylated (*M*) and unmethylated (*UM*) *Wnt3* promoter. The figure is representative of three experiments with similar results. + positive controls with a universal methylated or unmethylated genome sequence, respectively. *bl* blank

depletion: indeed, Wnt3-silenced hCMEC/D3 monolayer allowed a higher delivery (Fig. 6e) and toxicity (Fig. 6f) of doxorubicin in the co-cultured 01010627 GBM cells.

Temozolomide downregulates the Wnt3/GSK3/ $\beta$ -catenin/ABCB1 axis and increases the efficacy of doxorubicin in co-cultures of human primary BBB cells and glioblastoma cells

We then asked the question of whether the effects of TMZ could also occur in primary cells extracted from human brain microvessels, i.e., HBMECs.

We found that the promoter of *Wnt3* was fully unmethylated in HBMECs and that TMZ induced the partial methylation of the promoter (Fig. 7a). This was followed by the decrease of Wnt3 mRNA (Fig. 7b) and protein (Fig. 7c), the increase of phospho(Tyr216)GSK3 and phospho(Ser33/37/Thr41) $\beta$ -catenin (Fig. 7c), the reduction of the  $\beta$ -catenin binding on *mdr1* promoter (Fig. 7d), the decrease of Pgp/ABCB1 protein (Fig. 7e). In co-cultures of HBMECs and primary GBM 01010627 cells, the intratumor delivery of doxorubicin was low (Fig. 7f). Neither doxorubicin nor TMZ induced significant cytotoxicity, measured in terms

of extracellular release of LDH and activation of the caspase 3, in GBM cells co-cultured with HBMECs (Fig. 7g). By contrast, the addition of TMZ on the luminal side of HBMECs, at a concentration that did not induce cytotoxicity (online resource 11a) and did not reduce the proliferation (online resource 11b) of endothelial cells, significantly increased the delivery of doxorubicin and cytotoxicity in GBM cells (Fig. 7f, g).

## Discussion

While the effect of TMZ on GBM cells is well known, no studies have yet investigated the effects of the drug on BBB cells. To explore this issue, we exposed human immortalized brain microvascular endothelial cells hCMEC/D3 and primary brain microvascular endothelial cells HBMECs to TMZ, at a concentration found in the blood of patients [30]. At this concentration, the drug did not induce any detectable cytotoxic effect on BBB cells, but was able to increase the permeability of substrates of Pgp/ABCB1 across the BBB monolayer. Unlike other permeabilizing strategies [9, 10], TMZ did not affect the integrity of tight junctions, as the permeability to dextran, inulin, and sucrose, as well as the expression of claudin-5, occludin and ZO-1 did not change. Only claudin-3 was slightly reduced by TMZ: since Wnt3/ $\beta$ -catenin has been reported to up-regulate claudin-3 in mouse brain microvascular endothelial cells [35], this effect may be caused by the decrease in Wnt3 signaling induced by TMZ. However, as it appears from the permeability assay, the isolated decrease of claudin-3 was not sufficient enough for the functional impair of the tight junctions in hCMEC/D3 cells.

The reduction of Pgp/ABCB1 caused the increase in the permeability of doxorubicin and vinblastine elicited by TMZ. To the best of our knowledge, this effect of TMZ was not described before. This observation may have a strong impact on what we know about drug delivery to CNS, as Pgp/ABCB1 is abundantly localized on the luminal side of BBB cells [37] and recognizes a broad spectrum of substrates. Among these substrates, more specifically, is the majority of anticancer drugs [8], prevented from reaching therapeutic concentrations in CNS via this mechanism. The half-life of TMZ in plasma is short and the drug is chemically converted into its active metabolite MTIC [3]; it is conceivable that such a chemical conversion occurs also in our experimental system and that MTIC is the actual responsible for the effects on BBB cells.

The effect of TMZ was specific for Pgp/ABCB1, since the activity and expression of MRP1/ABCC1 and BCRP/ABCG2, two other ABC transporters present on BBB cells [8, 11, 37], were not affected. The decrease of Pgp/ABCB1 without changes in other ABC

transporters is of particular interest. Indeed, mice knocked down for Pgp/ABCB1 have a compensatory increase of BCRP/ABCG2 in BBB, suggesting cooperation between these transporters [11]. Our study was performed by treating cells with a single dose of TMZ for 72 h; we did not investigate whether different experimental conditions (e.g., repetitive treatments with the drug or longer treatment periods) affect the expression of ABC transporters other than Pgp/ABCB1. The antitumor effects of TMZ, in terms of alkylating efficacy and DNA damages, are significantly stronger when the drug is administered repetitively within the same day than when the drug is administered as single dose [4]. We cannot exclude a priori that prolonged or repetitive administrations of TMZ might exert a stronger decrease in Pgp/ABCB1, thereby triggering a progressive increase in BCRP/ABCG2. When BCRP/ABCG2 is increased in response to the decrease of Pgp/ABCB1, drugs that are dual substrates of these transporters are not more delivered through the BBB [11]. Notwithstanding, the down-regulation of Pgp/ABCB1 results in the increased delivery of drugs, which have higher affinity for Pgp/ABCB1 than for BCRP/ABCG2 [11]. This is the case of doxorubicin and vinblastine, which are more transported across hCMEC/D3 monolayer upon the down-regulation of Pgp/ABCB1 induced by TMZ.

It has been reported that Pgp/ABCB1 is under the transcriptional control of  $\beta$ -catenin, whose activity is regulated by Wnt/GSK3/ $\beta$ -catenin axis in hCMEC/D3 cells [17, 18]. In our hands, untreated hCMEC/D3 cells had  $\beta$ -catenin constitutively bound on the promoter of *mdr1* gene and Pgp/ABCB1 constitutively expressed. In contrast, cells treated with TMZ showed increased activity of GSK3 and increased amounts of phosphorylated  $\beta$ -catenin. The phosphorylation-dependent degradation of  $\beta$ -catenin resulted in a decrease of its nuclear translocation and binding on the *mdr1* promoter. The results with activators and inhibitors of the Wnt canonical pathway suggested that TMZ down-regulated Pgp/ABCB1 acting like a Wnt-pathway inhibitor. Of note, the same effect of Wnt/GSK3/ $\beta$ -catenin axis in controlling the expression of Pgp/ABCB1 and the same effect of TMZ occurred in primary HBMECs. Unlike previous observations, that showed that the inhibitor of GSK3 6-bromoindirubin-3'-oxime up-regulated the transcription of MRP2/ABCC2, MRP4/ABCC4 and BCRP/ABCG2, and the inhibitor of  $\beta$ -catenin quercetin produced the opposite effects [17], we did not find any change in the expression of BCRP/ABCG2 in hCMEC/D3 cells after TMZ. This discrepancy could owe to the different stimuli used. Quercetin inhibited the binding of TCF to its DNA target sequences [38], therein reducing the transcriptional activity of  $\beta$ -catenin/TCF complex. TCF is paramount in the activation of certain promoters, less so in the activation of others. We hypothesized that the transcription of *bcrp* gene may be tightly dependent

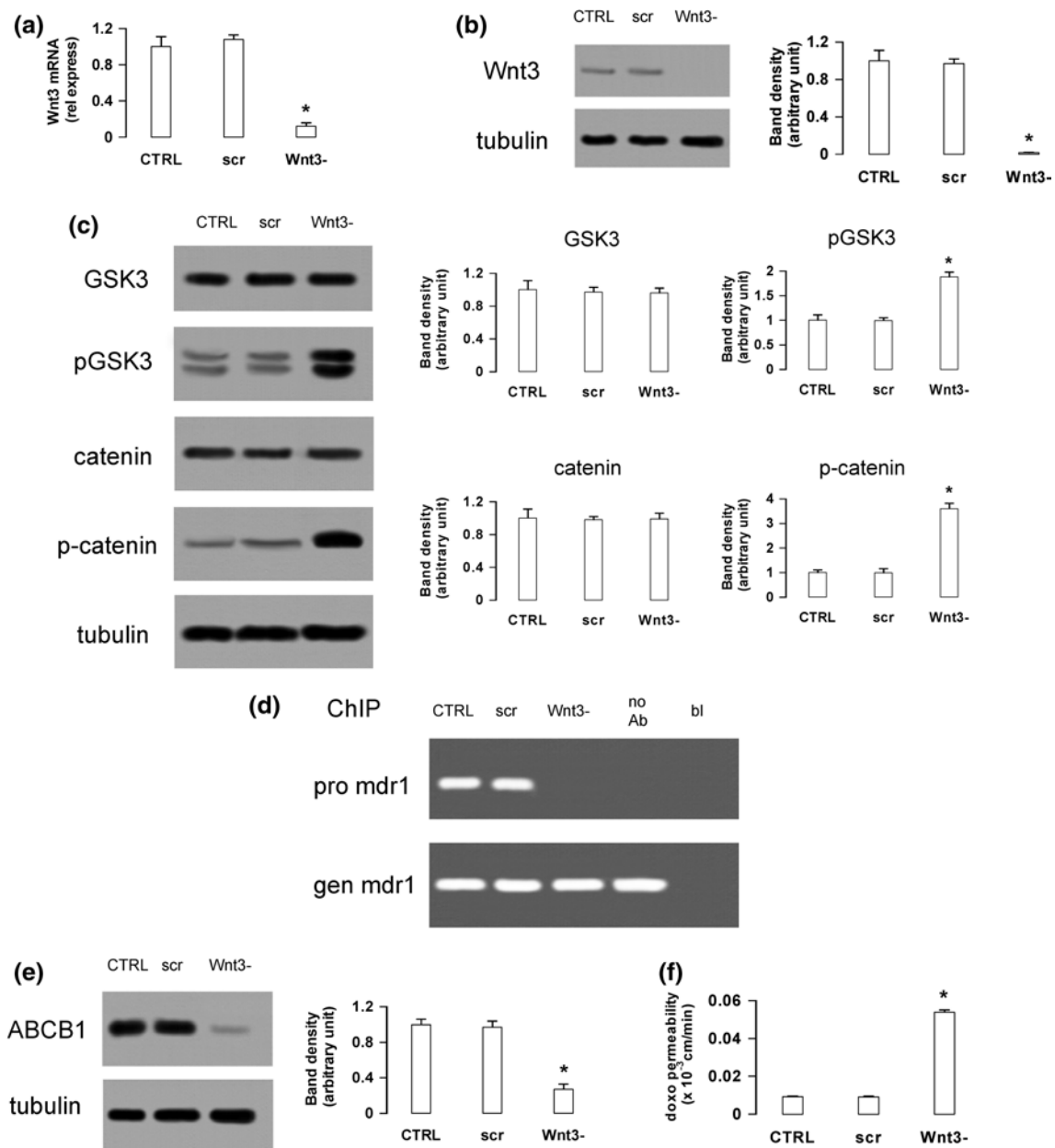
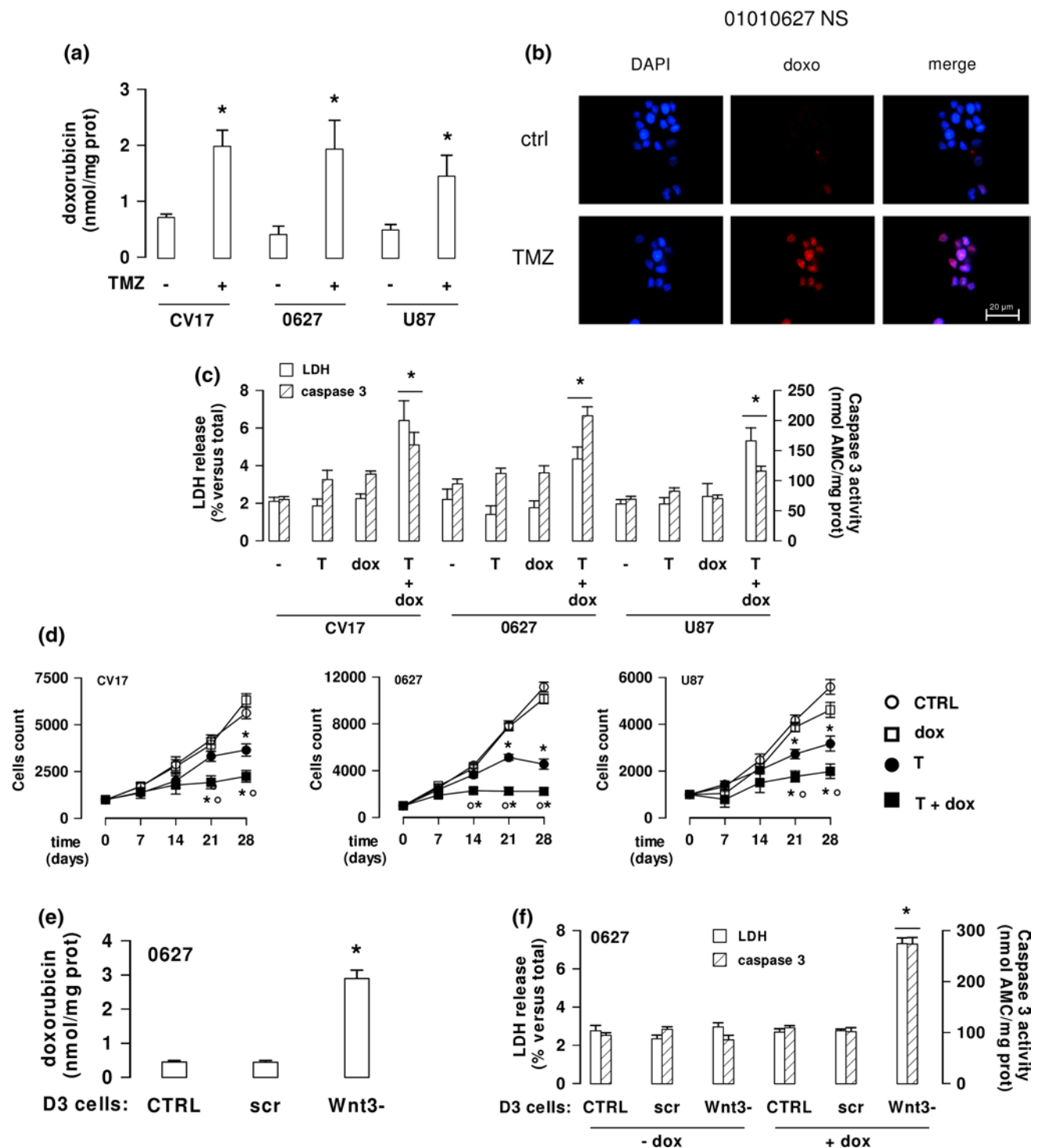


**Fig. 5** Effects of Wnt3 silencing on *mdr1* expression in hCMEC/D3 cells. Wild-type hCMEC/D3 cells (*CTRL*), cells stably transfected with a non-targeting 29-mer scrambled shRNA (*scr*) or stably silenced for Wnt3 (*Wnt3-*) were subjected to the following investigations. **a** Wnt3 qRT-PCR. Total RNA was extracted and reverse-transcribed, the expression of *Wnt3* gene was detected by qRT-PCR. The expression level in untreated cells was considered “1”. Data are presented as mean  $\pm$  SD ( $n = 3$ ). vs. *CTRL*: \* $p < 0.001$ . **b** Western-blot analysis of Wnt3 in whole cell lysates.  $\beta$ -tubulin expression was used as control of equal protein loading. The figure is representative of three experiments with similar results. The band density ratio between Wnt3 and  $\beta$ -tubulin was expressed as arbitrary units. vs. *CTRL*: \* $p < 0.001$ . **c** Western-blot analysis of phospho(Tyr216)GSK3, GSK3, phospho(Ser33/37/Thr41) $\beta$ -catenin,  $\beta$ -catenin in whole cell lysates.  $\beta$ -tubulin expression was used as control of equal protein loading. The figure is representative of three experiments with similar results. The band density ratio between each

protein and  $\beta$ -tubulin was expressed as arbitrary units. vs. *CTRL*: \* $p < 0.01$ . **d** Chromatin immunoprecipitation of  $\beta$ -catenin on *mdr1* promoter (*pro*) in hCMEC/D3 cells. *gen* PCR product from genomic DNA. *no Ab* precipitated samples without anti- $\beta$ -catenin antibody. *bl* blank. The figure is representative of three experiments with similar results. **e** Western-blot analysis of Pgp/ABCB1.  $\beta$ -tubulin expression was used as control of equal protein loading. The figure is representative of three experiments with similar results. The band density ratio between each protein and  $\beta$ -tubulin was expressed as arbitrary units. vs. *CTRL*: \* $p < 0.002$ . **f** Doxorubicin permeability. hCMEC/D3 cells were grown for 7 days up to confluence in Transwell inserts, then 5  $\mu$ mol/l doxorubicin was added in the upper chamber. After 3 h, the amount of the drug recovered from the lower chamber was measured fluorometrically. Permeability coefficient was calculated as reported under the “Materials and methods” section. Measurements were performed in duplicate and data are presented as mean  $\pm$  SD ( $n = 3$ ). vs. *CTRL*: \* $p < 0.001$



on the whole  $\beta$ -catenin/TCF complex, whereas the transcription of *mdr1* gene may be less so. Although we did not measure the amount of TCF in hCMEC/D3 cells treated with TMZ and we cannot exclude that the drug may also interfere with the formation of the  $\beta$ -catenin/TCF complex, our data strongly suggest that TMZ down-regulated  $\beta$ -catenin at an upstream level, by preventing its nuclear translocation

and the subsequent association with TCF. Alternatively, we may speculate that the down-regulation of *bcrp* gene due to the lower activation of  $\beta$ -catenin is masked by the simultaneous compensatory up-regulation of *bcrp*, consequent to the decrease of Pgp/ABCB1 [11]. The sum of these two events may leave unchanged the levels of BCRP/ABCG2 protein in cells treated with TMZ.

**◀ Fig. 6** Effects of temozolomide on doxorubicin delivery and cytotoxicity in glioblastoma cells co-cultured with hCMEC/D3 cells. hCMEC/D3 cells were grown for 7 days up to confluence in Transwell inserts; CV17, 01010627, and U87-MG cells were seeded at day 4 in the lower chamber. After 3 days of co-culture, supernatant in the upper chamber was replaced with fresh medium without (–) or with temozolomide (50  $\mu\text{mol/l}$  for 72 h; *TMZ* or *T*). 5  $\mu\text{mol/l}$  doxorubicin (*dox*) was added in the upper chamber in the last 24 h, then the following investigations were performed. **a** Fluorimetric quantification of intracellular doxorubicin in GBM cells. Measurements were performed in duplicate and data are presented as mean  $\pm$  SD ( $n = 4$ ). vs. untreated cells:  $*p < 0.05$ . **b** 01010627 cells were seeded on sterile glass coverslips, treated as reported above, then stained with DAPI and analyzed by fluorescence microscopy to detect the intracellular accumulation of doxorubicin. Magnification: 63 $\times$  objective (1.4 numerical aperture); 10 $\times$  ocular lens. The micrographs are representative of three experiments with similar results. **c** The culture supernatant of GBM cells was checked spectrophotometrically for the extracellular activity of LDH (*open bars*), the cell lysates were analyzed fluorometrically for the activity of caspase 3 (*hatched bars*). Measurements were performed in duplicate and data are presented as mean  $\pm$  SD ( $n = 4$ ). vs. untreated cells:  $*p < 0.05$ . **d** After 3 days of co-culture, the medium of the upper chamber was replaced with fresh medium (*open circles*) or medium containing 50  $\mu\text{mol/l}$  temozolomide for 72 h (*solid circles*, *T*), 5  $\mu\text{mol/l}$  doxorubicin for 24 h (*open squares*, *dox*), 50  $\mu\text{mol/l}$  temozolomide for 72 h plus 5  $\mu\text{mol/l}$  doxorubicin in the last 24 h (*solid squares*, *T + dox*). Drug treatments were repeated every 7 days, as reported in the “Materials and methods” section. The proliferation of GBM cells was monitored weekly by crystal violet staining. Measurements were performed in triplicate and data are presented as mean  $\pm$  SD ( $n = 4$ ). vs. untreated cells (*CTRL*):  $*p < 0.01$ . *T + dox* vs. *T* alone:  $^{\circ}p < 0.05$ . **e–f** Wild-type hCMEC/D3 cells (*CTRL*), cells stably transfected with a non-targeting 29-mer scrambled shRNA (*scr*) or stably silenced for Wnt3 (*Wnt3-*) were grown for 7 days up to confluence in Transwell inserts; 01010627 GBM cells were seeded at day 4 in the lower chamber. After 3 days of co-culture, supernatant in the upper chamber was replaced with fresh medium without (*-dox*) or with 5  $\mu\text{mol/l}$  doxorubicin (*+dox*) for 24 h. The intracellular doxorubicin in GBM cells was measured fluorometrically (**e**). Measurements were performed in duplicate and data are presented as mean  $\pm$  SD ( $n = 3$ ). vs. untreated cells:  $*p < 0.001$ . The culture supernatant of GBM cells was checked spectrophotometrically for the extracellular activity of LDH (*open bars*, **f**), the cell lysates were analyzed fluorometrically for the activity of caspase 3 (*hatched bars*, **panel f**). Measurements were performed in duplicate and data are presented as mean  $\pm$  SD ( $n = 3$ ). vs. untreated cells:  $*p < 0.001$

Our results are in agreement with other reports showing that Wnt signaling is involved in the Pgp-mediated chemoresistance in tumors. The Frizzled-1 receptor of Wnt, necessary for the activation of  $\beta$ -catenin pathway, is present at high levels in neuroblastoma [19] and breast cancers [39] overexpressing Pgp/ABCB1, where the silencing of Frizzled-1 down-regulated the *mdr1* gene. However, we did not detect any change in the expression levels of Frizzled in hCMEC/D3 cells exposed to TMZ. We therefore moved our focus on the levels of Wnt ligands produced by endothelial cells, which are able to bind Frizzled receptors and activate the GSK3/ $\beta$ -catenin axis. Wnt3 was present in both hCMEC/D3 and HBMEC cells; the results in Wnt3-silenced hCMEC/D3 cells supported the hypothesis that Wnt3 was a

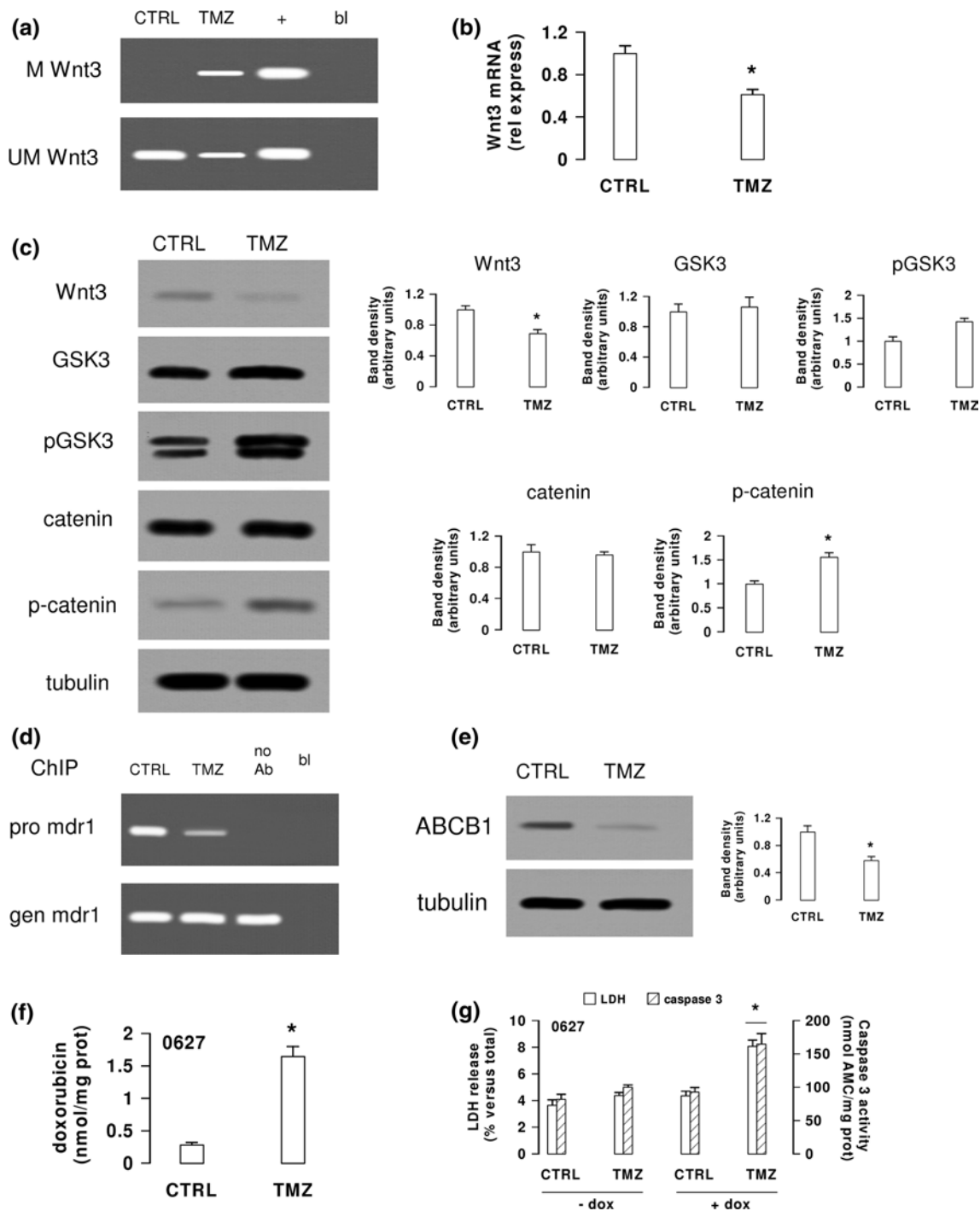
critical controller of *mdr1* transcription, since its depletion produced a 70 % decrease in Pgp/ABCB1 protein.

Interestingly, TMZ decreased Wnt3 protein and mRNA, leading us to hypothesize that the drug down-regulated the transcription of Wnt3 gene in BBB cells. As an alkylating agent, TMZ methylates guanine on O<sup>6</sup> position and induces a DNA mismatch repair response that produces double-strand breaks, if not repaired by the O<sup>6</sup> methyl guanine methyltransferase enzyme. However, the vast majority of the methylations caused by TMZ are other methylations, usually not cytotoxic [4]. The consequences of these non-toxic methylations have not yet been investigated. We found that TMZ methylates the promoter of *Wnt3* gene, which is rich in CpG islands. Untreated hCMEC/D3 and HBMEC cells express a fully unmethylated promoter, which is consistent with the constitutive transcription of Wnt3: the promoter’s methylation induced by TMZ may explain the decrease of Wnt3, suggesting that TMZ is an epigenetic down-regulator of *Wnt3* gene.

Of note, TMZ administered on the luminal side of hCMEC/D3 cells also decreased the *mdr1* levels in GBM cells growing under hCMEC/D3 monolayer: this means that the drug crossed—as expected—the BBB, and acted on both endothelial and tumor cells, increasing at the same time the permeability of BBB cells and the chemosensitivity of GBM cells. Experimental findings obtained in our laboratory suggest that TMZ down-regulates Pgp/ABCB1 in GBM cells with a Wnt3a-dependent mechanism (Riganti, unpublished data).

In view of our results, we think that clinically achievable doses of TMZ may facilitate the subsequent passage of anticancer drugs, not commonly used in the therapy of GBM because they are rapidly effluxed through the BBB by Pgp/ABCB1. Using doxorubicin as a prototype, we indeed observed in co-culture models of hCMEC/D3 or HBMEC with GBM cells that the pre-treatment of BBB cells with TMZ significantly increased the delivery of doxorubicin, induced marked cytotoxicity, and reduced the proliferation of GBM cells. The increased permeability of doxorubicin induced by TMZ was likely triggered by the down-regulation of the Wnt3/GSK3/ $\beta$ -catenin/Pgp axis in BBB cells, since the same effect was achieved by depleting Wnt3 in hCMEC/D3 cells.

Several strategies that increase the delivery of doxorubicin to GBMs, such as encapsulating the drug in PEGylated liposomes [7, 40] or loading it in BBB-targeting nanoparticles [41, 42], are under intensive investigations. Our approach is different as we studied a drug already commonly used in GBM therapy, like TMZ. The pharmacokinetics, the pharmacodynamic effects and the side effects of TMZ and doxorubicin are well known. The combination of TMZ and doxorubicin is new and requires appropriate studies of pharmacokinetics and safety



pharmacology. The results of the present study are paving the way to other studies on the antitumor efficacy of this new drug combination in orthotopic animal models of human glioblastoma.

The same chemosensitizing effects of TMZ that we describe here were obtained with two other substrates of Pgp/ABCB1, vinblastine, and topotecan. While the former is not currently used in GBM therapy, the latter has received a great deal of interest in the last few years.

Although topotecan does not cross the BBB [6], it has a very low  $IC_{50}$  against GBM cells in vitro [27, 43] and has been proposed as an effective agent when administered by convection-enhanced delivery [6]. If the results obtained in our co-culture models will be confirmed in vivo, this might open the door for new therapeutic protocols based on the pre-treatment with TMZ followed by systemic administration of topotecan. Our findings may also explain the clinical observation that the topoisomerase I inhibitors produce

◀ **Fig. 7** Effects of temozolomide in primary human brain microvascular endothelial cells co-cultured with primary human glioblastoma cells. **a** Methylation of *Wnt3* promoter. HBMECs were grown in the absence (*CTRL*) or in the presence of temozolomide (*TMZ*; 50  $\mu\text{mol/l}$ , for 24 h), then genomic DNA was subjected to bisulfite modification, followed by PCR with specific primers for methylated (*M*) and unmethylated (*UM*) *Wnt3* promoter. The figure is representative of three experiments with similar results. + positive controls with a universal methylated or unmethylated genome sequence, respectively. *bl* blank. **b** *Wnt3* mRNA levels. Cells were incubated in the absence (*CTRL*) or in the presence of temozolomide (*TMZ*; 50  $\mu\text{mol/l}$ , for 48 h). Total RNA was extracted and reverse-transcribed, the expression of *Wnt3* gene was detected by qRT-PCR. The expression level in untreated cells was considered “1”. Data are presented as mean  $\pm$  SD ( $n = 3$ ). vs. *CTRL*: \* $p < 0.02$ . **c** Western-blot analysis of Wnt3 signaling. Cells were incubated as reported in **b**, then lysed and subjected to the Western-blot analysis of Wnt3, phospho(Tyr216)GSK3, GSK3, phospho(Ser33/37/Thr41) $\beta$ -catenin,  $\beta$ -catenin in whole-cell lysates.  $\beta$ -tubulin expression was used as control of equal protein loading. The figure is representative of three experiments with similar results. The band density ratio between each protein and  $\beta$ -tubulin was expressed as arbitrary units. vs. *CTRL*: \* $p < 0.05$ . **d** Chromatin immunoprecipitation of  $\beta$ -catenin on *mdr1* promoter (*pro*) in cells incubated as reported in **b** *gen* PCR product from genomic DNA. *no Ab* precipitated samples without anti- $\beta$ -catenin antibody. *bl* blank. The figure is representative of three experiments with similar results. **e** Cells were incubated for 72 h without (*CTRL*) or with temozolomide (*TMZ*; 50  $\mu\text{mol/l}$ ), then lysed and subjected to Western-blot analysis for Pgp/ABC1.  $\beta$ -tubulin expression was used as control of equal protein loading. The figure is representative of three experiments with similar results. The band density ratio between each protein and  $\beta$ -tubulin was expressed as arbitrary units. vs. *CTRL*: \* $p < 0.01$ . **f** HBMECs were grown for 7 days up to confluence in Transwell inserts; 01010627 GBM cells were seeded at day 4 in the lower chamber. After 3 days of co-culture, supernatant in the upper chamber was replaced with fresh medium without (*CTRL*) or with temozolomide (50  $\mu\text{mol/l}$  for 72 h; *TMZ*); 5  $\mu\text{mol/l}$  doxorubicin (*dox*) was added in the upper chamber in the last 24 h. GBM cells were then collected and analyzed for the intracellular amount of doxorubicin by a fluorimetric assay. Measurements were performed in duplicate and data are presented as mean  $\pm$  SD ( $n = 3$ ). vs. untreated cells (*CTRL*): \* $p < 0.001$ . **g** Co-cultures of HBMECs and 01010627 cells were set up as detailed in **f**. At the end of the incubation period, the culture supernatant of GBM cells was checked spectrophotometrically for the extracellular activity of LDH (*open bars*), the cell lysates were analyzed fluorimetrically for the activity of caspase 3 (*hatched bars*). Measurements were performed in duplicate and data are presented as mean  $\pm$  SD ( $n = 3$ ). vs. untreated cells: \* $p < 0.005$

significant benefits in patients with recurrent gliomas when used in combination with TMZ [5].

In conclusion, we describe a novel role of TMZ in BBB cells, as a down-regulator of the expression of Pgp/ABC1 at clinically achievable concentrations. Beside opening the door for new treatment protocols, our results might have important implications for the eradication of GBM cells in the BAT area, where tumor cells lay surrounded by intact BBB [8], cannot be completely removed by surgery or efficiently radiated and almost never are reached by effective concentrations of chemotherapeutic drugs. The use of TMZ in association with doxorubicin, topotecan, or vinblastine

may become a successful strategy for eradicating GBM cells from BAT area and preventing recurrence.

**Acknowledgments** We are indebted to Prof. Michele Lanotte (Department of Neuroscience, Neurosurgical Unit, University of Turin) and to Dr. Rossella Galli (San Raffaele Scientific Institute, Milan) for providing the primary glioblastoma samples. We are grateful to Costanzo Costamagna (Department of Oncology, University of Turin) for the technical assistance and to Dr. Oriana Monzeglio (Neuro-bio-oncology Center, Policlinico di Monza Foundation) for the technical suggestions with methylation promoter assay. This work has been supported by grants from Compagnia di San Paolo, Italy (Neuroscience Program; grant 2008.1136) and Italian Association for Cancer Research (AIRC; MFAG 11475) to Chiara Riganti. Martha Leonor Pinzón-Daza is recipient of a ERACOL Erasmus Mundus fellowship. Joanna Kopecka is recipient of a “Mario and Valeria Rindi” fellowship provided by Italian Foundation for Cancer Research (FIRC).

**Conflict of interest** None.

## References

- Bai RY, Staedke V, Riggins GJ (2011) Molecular targeting of GBM: drug discovery and therapies. *Trends Mol Med* 17:301–332
- Serwer LP, James CD (2012) Challenges in drug delivery to tumors of the central nervous system: an overview of pharmacological and surgical considerations. *Adv Drug Deliv Rev* 64:590–597
- Saleem A, Brown GD, Brady F, Aboagye EO, Osman S, Luthra SK, Ranicar AS, Brock CS, Stevens MF, Newlands E, Jones T, Price P (2003) Metabolic activation of temozolomide measured in vivo using positron emission tomography. *Cancer Res* 63:2409–2415
- Wick W, Plattan M, Weller M (2009) New (alternative) temozolomide regimens for the treatment of glioma. *Neuro Oncol* 11:69–79
- Vredenburgh JJ, Desjardins A, Reardon DA, Peters KB, Herndon JE 2nd, Marcello J, Kirkpatrick JP, Sampson JH, Bailey L, Threan S, Friedman AH, Bigner DD, Friedman HS (2011) The addition of bevacizumab to standard radiation therapy and temozolomide followed by bevacizumab, temozolomide, and irinotecan for newly diagnosed glioblastoma. *Clin Cancer Res* 17:4119–4124
- Lopez KA, Tannenbaum AM, Assanah MC, Linskey K, Yun J, Kangarlou A, Gil OD, Canoli P, Bruce JN (2011) Convection-enhanced delivery of topotecan into PDGF-driven model of glioblastoma prolongs survival and ablates both tumor-initiating cells recruited glial progenitors. *Cancer Res* 71:3963–3971
- Hau P, Fabel K, Baumgart U, Rummele P, Grauer O, Bock A, Dietmaier C, Dietmaier W, Dietrich J, Dudel C, Hubner F, Jaucj T, Drechsel E, Kleiter I, Wismeth C, Zellner A, Brawanski A, Steinbrecher A, Marienhagen J, Bogdahan U (2004) PEGylated liposomal doxorubicin-efficacy in patients with recurrent high-grade glioma. *Cancer* 100:1199–1207
- Agarwal S, Sane R, Oberoi R, Ohlfest JR, Elmquist WF (2011) Delivery of molecularly targeted therapy to malignant glioma, a disease of the whole brain. *Expert Rev Mol Med* 13:e17
- Guillaume DJ, Doolittle ND, Gahramanov S, Hedrick NA, Delashaw JB, Neuwelt EA (2010) Intra-arterial chemotherapy with osmotic blood–brain barrier disruption for aggressive oligodendroglial tumors: results of a phase I study. *Neurosurgery* 66:48–58

10. Liu H-L, Hua M-Y, Chen P-Y, Chu P-C, Pan C-H, Yang H-W, Wang C-Y, Wang J-J, Yen T-C, Wei K-C (2010) Blood-brain barrier disruption with focused ultrasound enhanced delivery of chemotherapeutic drugs for glioblastoma treatment. *Radiology* 255:415–425
11. Agarwal S, Hartz AM, Elmquist WF, Bauer B (2011) Breast cancer resistance protein and P-glycoprotein in brain cancer: two gatekeepers team up. *Curr Pharm Des* 17:2793–2802
12. Poller B, Drewe J, Krähenbühl S, Huwylar J, Gutmann H (2010) Regulation of BCRP (ABCG2) and P-glycoprotein (ABCB1) by cytokines in a model of the human blood-brain barrier. *Cell Mol Neurobiol* 30:63–70
13. Chan GNY, Hoque MT, Cummins CL, Bendayan R (2011) Regulation of P-glycoprotein by orphan nuclear receptors in human brain microvessel endothelial cells. *J Neurochem* 118:163–175
14. Wang X, Hawkins BT, Miller DS (2011) Aryl hydrocarbon receptor-mediated up-regulation of ATP-driven xenobiotic efflux transporters at the blood-brain barrier. *FASEB J* 25:644–652
15. Daneman R, Agalliu D, Zhoy L, Kuhnert F, Kuo CJ, Barres BA (2009) Wnt/ $\beta$ -catenin signalling is required for CNS, but not non-CNS, angiogenesis. *Proc Natl Acad Sci USA* 106:641–646
16. Liebner S, Plate KH (2010) Differentiation of the brain vasculature: the answer came blowing by the Wnt. *J Angiogenesis Res* 2:1–10
17. Lim JC, Kania KD, Wijesuriya H, Chawla S, Sethi JK, Pulaski L, Romero IA, Couraud PO, Weksler BB, Hladky SB, Barrand MA (2008) Activation of  $\beta$ -catenin signalling by GSK-3 inhibition increases p-glycoprotein expression in brain endothelial cells. *J Neurochem* 106:1855–1865
18. Kania KD, Wijesuriya HC, Hladky SB, Barrand MA (2011) Beta amyloid effects on expression of multidrug efflux transporters in brain endothelial cells. *Brain Res* 1418:1–11
19. Flahaut M, Meier R, Coulon A, Nardou KA, Niggli FK, Martinet D, Beckmann JS, Joseph J-M, Muhlethaler-Mottet A, Gross N (2009) The Wnt receptor FZD1 mediates chemoresistance in neuroblastoma through activation of the Wnt/ $\beta$ -catenin pathway. *Oncogene* 28:2245–2256
20. Schaich M, Kestel L, Pfirrmann M, Robel K, Illmer T, Kramer M, Dill C, Ehninger G, Schackert G, Krex D (2009) A MDR1 (ABCB1) gene single nucleotide polymorphism predicts outcome of temozolomide treatment in GBM patients. *Ann Oncol* 20:175–181
21. Weksler BB, Subileau EA, Perrière N, Charneau P, Holloway K, Leveque M, Tricoire-Leignel H, Nicotra A, Bourdoulous S, Turowski P, Male DK, Roux F, Greenwood J, Romero IA, Couraud PO (2005) Blood-brain barrier-specific properties of a human adult brain endothelial cell line. *FASEB J* 19:1872–1874
22. Monnaert V, Betbeder D, Fenart L, Bricout H, Lenfant AM, Landry C, Cecchelli R, Monflier E, Tilloy S (2004) Effects of  $\gamma$ - and hydroxy propyl- $\gamma$ -cyclodextrins on the transport of doxorubicin across an in vitro model of blood-brain barrier. *J Pharmacol Exp Ther* 311:1115–1120
23. Siflinger-Bimboim A, Del Vecchio PJ, Cooper JA, Blumenstock FA, Shepard JM, Malik AB (1987) Molecular sieving characteristics of the cultured endothelial monolayer. *J Cell Physiol* 132:111–117
24. Campia I, Gazzano E, Pescarmona G, Ghigo D, Bosia A, Riganti C (2009) Digoxin and ouabain increase the synthesis of cholesterol in human liver cells. *Cell Mol Life Sci* 66:1580–1594
25. Broadley KW, Hunn MK, Farrand KJ, Price KM, Grasso C, Miller RJ, Hermans IF, McConnell MJ (2011) Side population is not necessary or sufficient for a cancer stem cell phenotype in glioblastoma multiforme. *Stem Cells* 29:452–461
26. Liu Y, Yang G, Bu X, Liu G, Ding J, Li P, Jia W (2011) Cell-type-specific regulation of raft-associated Akt signalling. *Cell Death Dis* 2:e145
27. Carcaboso AM, Elmeliogy MA, Shen J, Juel SJ, Zhang ZM, Calabrese C, Tracey L, Waters CM, Stewart CF (2010) Tyrosine kinase inhibitor gefitinib enhances topotecan penetration of gliomas. *Cancer Res* 70:4499–4508
28. Kopecka J, Campia I, Olivero P, Pescarmona G, Ghigo D, Bosia A, Riganti C (2011) A LDL-masked liposomal-doxorubicin reverses drug resistance in human cancer cells. *J Contr Rel* 149:196–205
29. Pinzón-Daza ML, Garzón R, Couraud PO, Romero IA, Weksler B, Ghigo D, Bosia A, Riganti C (2012) The association of statins plus LDL receptor-targeted liposome-encapsulated doxorubicin increases the in vitro drug delivery across blood-brain barrier cells. *Brit J Pharmacol* 167:1431–1447
30. Portnow J, Badie B, Chen M, Liu A, Blanchard S, Synold TW (2009) The neuro-pharmacokinetics of temozolomide in patients with resectable brain tumors: potential implications for the current approach to chemoradiation. *Clin Cancer Res* 15:7092–7098
31. Dalmark M, Storm HH (1981) A Fickian diffusion transport process with features of transport catalysis. Doxorubicin transport in human red blood cells. *J Gen Physiol* 78:349–364
32. Ito S, Woodland C, Sarkadi B, Hockmann G, Walker SE, Koren G (1999) Modeling of P-glycoprotein-involved epithelial drug transport in MDCK cells. *Am J Physiol* 277:F84–F96
33. Goodwin AM, Sullivan KM, D'Amore PA (2006) Cultured endothelial cells display endogenous activation of the canonical Wnt signalling pathway and express multiple ligands, receptors, and secreted modulators of Wnt signalling. *Dev Dyn* 235:3110–3120
34. Fu L, Zhang C, Zhang LY, Dong SS, Lu LH, Chen J, Dai Y, Li Y, Kong KL, Kwong DL, Guan XY (2011) Wnt2 secreted by tumor fibroblasts promotes tumor progression in oesophageal cancer by activation of the Wnt/ $\beta$ -catenin signalling pathway. *Gut* 60:1635–1643
35. Liebner S, Corada M, Bangsow T, Babbage J, Taddei A, Czupalla CJ, Reis M, Felici A, Wolburg H, Fruttiger M, Taketo MM, von Melchner H, Plate KH, Gerhardt H, Dejana E (2008) Wnt/ $\beta$ -catenin signalling controls development of the blood-brain barrier. *J Cell Biol* 183:409–417
36. Bernardi H, Gay S, Fedon Y, Vernus B, Bonniou A, Bacou F (2011) Wnt4 activates the canonical  $\beta$ -catenin pathway and regulates negatively myostatin: functional implication in myogenesis. *Am J Physiol Cell Physiol* 300:C1122–C1138
37. Tai LM, Loughlin AJ, Male DK, Romero IA (2009) P-glycoprotein and breast cancer resistance protein restrict apical-to-basolateral permeability of human brain endothelium to amyloid- $\beta$ . *J Cereb Blood Flow Metab* 29:1079–1083
38. Park CH, Chang JY, Hahn ER, Park S, Kim HK, Yang CH (2005) Quercetin, a potent inhibitor against  $\beta$ -catenin/Tcf signalling in SW480 colon cancer cells. *Biochem Biophys Res Commun* 328:227–234
39. Zhang H, Zhang Z, Wu X, Li W, Su W, Su P, Cheng H, Xiang L, Gao P, Zhou G (2012) Interference of Frizzled 1 (FD1) reverses multidrug resistance in breast cancer cells through the Wnt/ $\beta$ -catenin pathway. *Cancer Lett* 323:106–113
40. Ananda S, Nowak AK, Cher L, Dowling A, Brown C, Simes J, Rosenthal MA, Cooperative Trials Group for Neuro-Oncology (COGNO) (2011) Phase 2 trial of temozolomide and PEGylated liposomal doxorubicin in the treatment of patients with glioblastoma multiforme following concurrent radiotherapy and chemotherapy. *J Clin Neurosci* 18:1444–1448
41. Steiniger SC, Kreuter J, Khalansky AS, Skidan IN, Bobruskin AI, Smirnova ZS, Severin SE, Uhl R, Kock M, Geiger KD, Gelperina SE (2004) Chemotherapy of glioblastoma in rats using doxorubicin-loaded nanoparticles. *Int J Cancer* 109:759–767
42. Wohlfart S, Khalansky AS, Gelperina S, Begley D, Kreuter J (2011) Kinetics of transport of doxorubicin bound to nanoparticles across the blood-brain barrier. *J Control Rel* 154:103–107
43. Yount G, Yang Y, Wong B, Wang H-J, Yang L-X (2007) A novel camptothecin analog with enhanced antitumor activity. *Anticancer Res* 27:3173–3178

## Supplementary Material

# Temozolomide down-regulates P-glycoprotein in human blood-brain barrier cells by disrupting Wnt3-signaling.

Chiara Riganti<sup>1,2</sup>, Iris C. Salaroglio<sup>1</sup>, Martha L. Pinzón-Daza<sup>1,3</sup>, Valentina Caldera<sup>4</sup>, Ivana Campia<sup>1</sup>, Joanna Kopecka<sup>1</sup>, Marta Mellai<sup>4</sup>, Laura Annovazzi<sup>4</sup>, Pierre-Olivier Couraud<sup>5</sup>, Amalia Bosia<sup>1,2</sup>, Dario Ghigo<sup>1,2</sup>, Davide Schiffer<sup>4</sup>

<sup>1</sup> *Department of Oncology, University of Turin, Via Santena, 5/bis, 10126, Turin, Italy*

<sup>2</sup> *Research Center on Experimental Medicine (CeRMS), University of Turin, Via Santena, 5/bis, 10126, Turin, Italy*

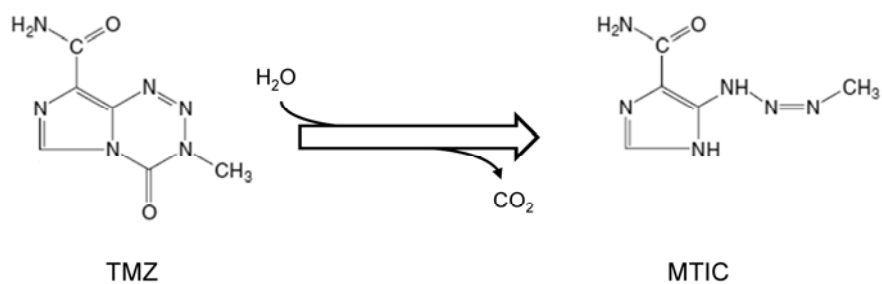
<sup>3</sup> *Unidad de Bioquímica, Facultad de Ciencias Naturales y Matemáticas, Universidad del Rosario, Carrera 6, Bogotá, Colombia*

<sup>4</sup> *Neuro-bio-oncology Center, Policlinico di Monza Foundation, Via Pietro Micca 29, 13100, Vercelli, Italy*

<sup>5</sup> *Institut Cochin, Centre National de la Recherche Scientifique UMR 8104, Institut National de la Santé et de la Recherche Médicale (INSERM) U567, Université René Descartes, 22 rue Méchain, 75014 Paris, France*

**Corresponding author:** Dr. Chiara Riganti, Department of Oncology, University of Turin, Via Santena 5/bis, 10126 Turin, Italy - Phone: +39-11-6705857; fax: +39-11-6705845; e-mail: chiara.riganti@unito.it

## Online Resource 1



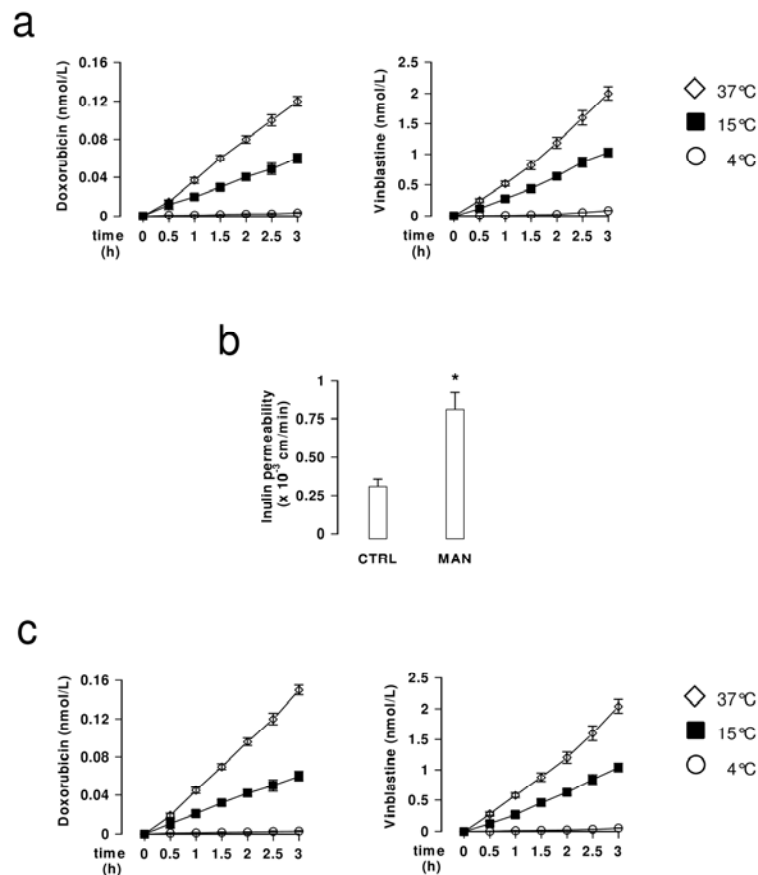
**Online Resource 1. Chemical structure of temozolomide (TMZ) and its metabolite 3-methyl-(triazen-1-yl)imidazole-4-carboxamide (MTIC).**

## Online Resource 2

**Primers sequences of quantitative Real Time-PCR (qRT-PCR), chromatin immunoprecipitation (ChIP) and methylation specific PCR (MSP).**

Gene	Assay	Forward primer (5'-3')	Reverse primer (5'-3')
<i>mdr1</i>	qRT-PCR	TGCTGGAGCGGTTCTACG	ATAGGCAATGTTCTCAGCAATG
<i>Wnt2b</i>	qRT-PCR	GTGTCCTGGCTGGTTCCTTA	GAAGCTGGTGCAAAGGAAAG
<i>Wnt3</i>	qRT-PCR	ACGAGAACTCCCCCACTTT	GATGCAGTGGCATTTCCT
<i>Wnt4</i>	qRT-PCR	GCTGTGACAGGACAGTGCAT	GCCTCATGTTGTGGAGGTT
<i>β-actin</i>	qRT-PCR	GCTATCCAGGCTGTGCTATC	TGTCACGCACGATTTC
<i>mdr1</i> (promoter)	ChIP	CGATCCGCCTAAGAACAAAG	AGCACAAATTGAAGGAAGGAG
<i>mdr1</i> (upstream sequence)	ChIP	GTGGTGCTGAGGAAGAGAG	GCAACAAGTAGGCACAAGCA
<i>mdr1</i> (genomic)	ChIP	GACCAAGCTCTCCTTGCATC	AGGGAAGTCTGGCAGCTGTA
<i>Wnt3</i> promoter (methylated)	MSP	GAATTTTATTGAGGTTGTGGGTTAC	TTATCAAAAATCAAATCGATATCGA
<i>Wnt3</i> promoter (unmethylated)	MSP	ATTTTATTGAGGTTGTGGGTTATGT	TATCAAAAATCAAATCAATATCAAA

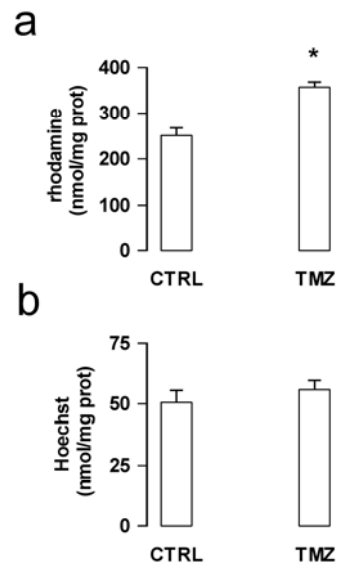
## Online Resource 3



### Online Resource 3. Time- and temperature-dependence in the transport of doxorubicin and vinblastine across hCMEC/D3 monolayer.

**a.** hCMEC/D3 cells were grown for 7 days up to confluence in Transwell inserts, then 5  $\mu\text{mol/L}$  doxorubicin or 2  $\mu\text{Ci/mL}$  [ $^3\text{H}$ ]-vinblastine (equivalent to 10.8  $\mu\text{mol/L}$ ) were added in the upper chamber. Plates were incubated at 4°C, 15°C and 37°C. From each plate, aliquots of 100  $\mu\text{L}$  from the lower chamber medium were collected at fixed time point up to 3 h. The amount of the drug was measured fluorimetrically (for doxorubicin) or by liquid scintillation (for vinblastine). Measurements were performed in duplicate and data are presented as means  $\pm$  SD ( $n = 3$ ). **b.** hCMEC/D3 cells were grown for 7 days up to confluence in Transwell inserts, then 2  $\mu\text{Ci/mL}$  [ $^{14}\text{C}$ ]-inulin was added in the upper chamber, in the absence (*CTRL*) or presence of 25% w/v mannitol (*MAN*), chosen as tight junctions-disrupting agent. After 3 h the amount of inulin in the lower chamber was quantified by liquid scintillation. Measurements were performed in duplicate and data are presented as means  $\pm$  SD ( $n = 2$ ). Vs *CTRL*: \*  $p < 0.02$ . **c.** hCMEC/D3 cells were treated as reported in **a**, in the presence of 25% w/v mannitol (*MAN*) in the upper chamber. The amount of the drug was measured fluorimetrically (for doxorubicin) or by liquid scintillation (for vinblastine). Measurements were performed in duplicate and data are presented as means  $\pm$  SD ( $n = 3$ ).

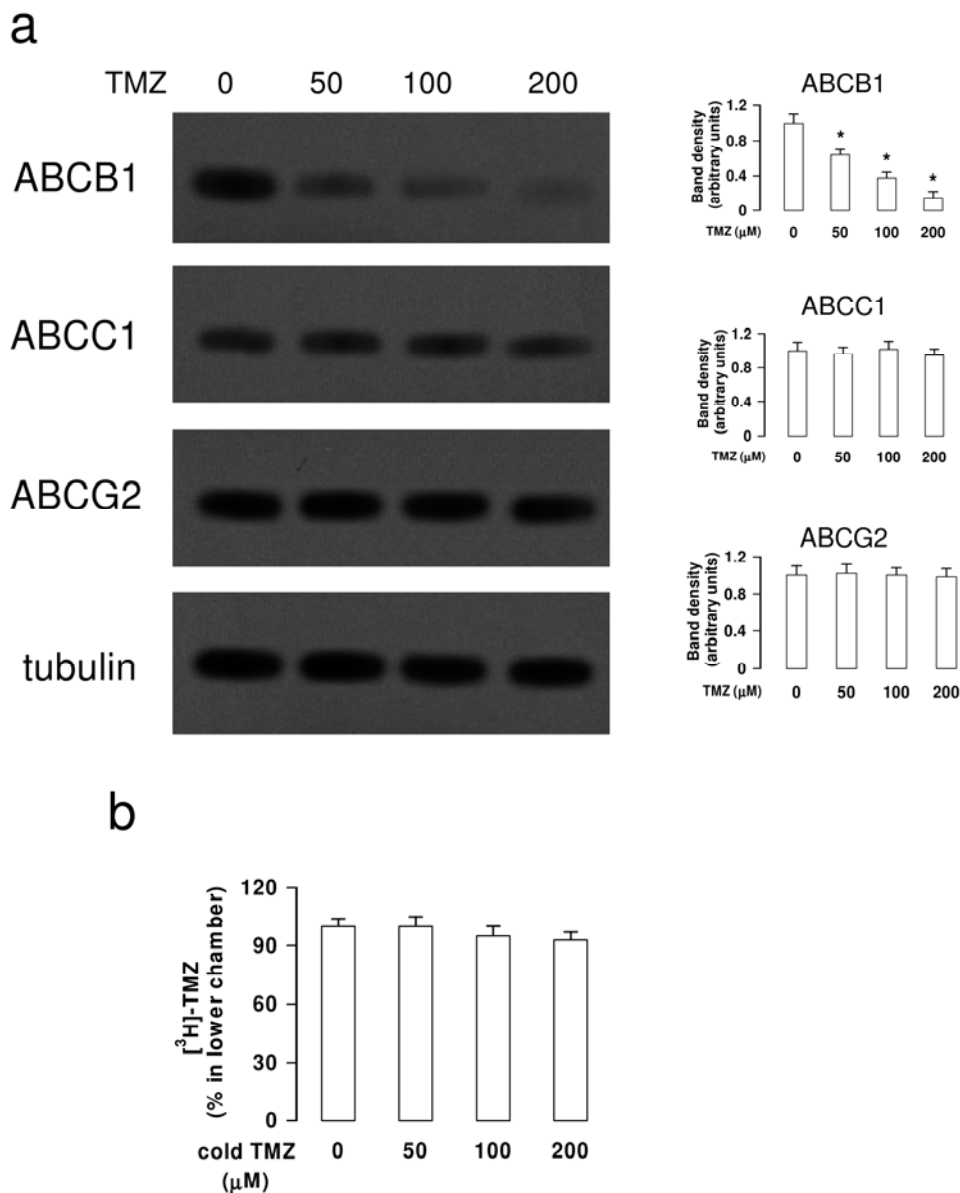
## Online Resource 4



### Online Resource 4. Intracellular accumulation of rhodamine 123 and Hoechst 33342 by hCMEC/D3 cells.

hCMEC/D3 cells were grown in fresh medium (*CTRL*) or with 50  $\mu\text{mol/L}$  temozolomide (*TMZ*) for 72 h, then incubated with the Pgp/ABCB1 substrate rhodamine 123 (panel **a**) or the BCRP/ABCG2 substrate Hoechst 33342 (panel **b**). The intracellular retention of rhodamine 123 and Hoechst 33342 was measured in duplicate fluorimetrically, as reported under Materials and methods. Data are presented as means  $\pm$  SD ( $n=4$ ). Vs *CTRL*: \*  $p < 0.005$ .

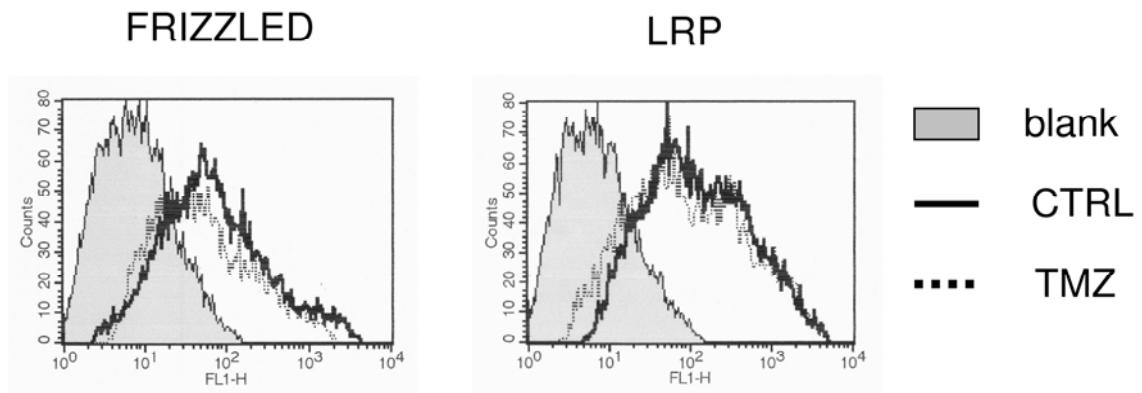
Online Resource 5



**Online Resource 5. Effect of temozolomide on its own transport across hCMEC/D3 monolayer.**

**a.** hCMEC/D3 cells were grown in fresh medium (0) or with 50, 100 or 200 μmol/L temozolomide (TMZ) for 72 h, then subjected to the Western blot analysis of Pgp/ABCB1, MRP1/ABCC1, BCRP/ABCG2. β-tubulin expression was used as control of equal protein loading. The figure is representative of 3 experiments with similar results. The band density ratio between each protein and β-tubulin was expressed as arbitrary units. Vs untreated cells (0): \* p < 0.05. **b.** hCMEC/D3 cells were cultured in Transwell device for 7 days up to confluence, then incubated as reported in **a**, in the presence of 0.7 μC/mL (equivalent to 10 μmol/L) [<sup>3</sup>H]-temozolomide. After this incubation period, the amount of [<sup>3</sup>H]-temozolomide in the lower chamber was measured by liquid count scintillation. Results were expressed as percentage of [<sup>3</sup>H]-temozolomide recovered in the lower chamber versus [<sup>3</sup>H]-temozolomide added in the upper chamber at time 0. Data are presented as means ± SD (n=3).

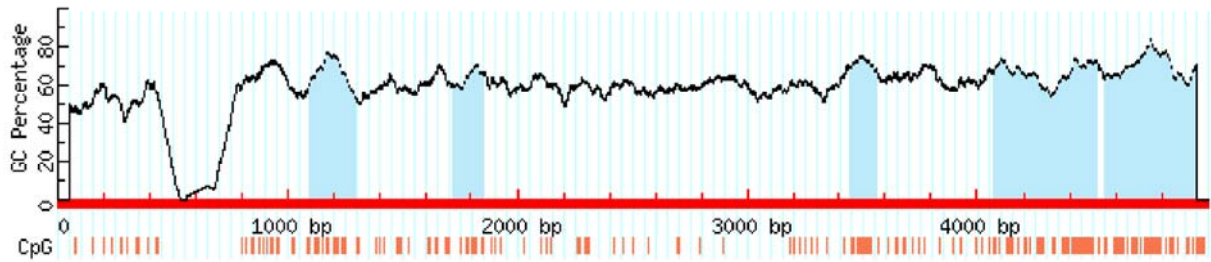
## Online Resource 6



### Online Resource 6. Effects of temozolomide on the expression of Frizzled and LRP6 in hCMEC/D3 cells.

hCMEC/D3 cells were incubated for 72 h in fresh medium (*CTRL*) or with 50  $\mu\text{mol/L}$  temozolomide (*TMZ*). Flow cytometry analysis of surface Frizzled (left panel) and LRP6 (right panel) in cells untreated (*continuous line*) or treated with temozolomide (*dotted line*). Grey peak: cells treated with anti-isotypic antibody. The figures shown here are representative of 3 similar experiments, performed in triplicate.

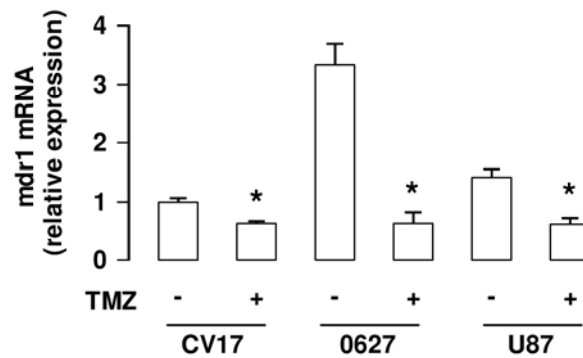
## Online Resource 7



### Online Resource 7. Localization of CpG islands on the promoter of *Wnt3* gene.

CpG islands localization on *Wnt3* promoter, according to Methprimer software (<http://www.urogene.org/methprimer>). As input the promoter sequence (from -5,000 bps to 0 bps) obtained by the UCSC Genome Browser (<http://genome.ucsc.edu/>) was used.

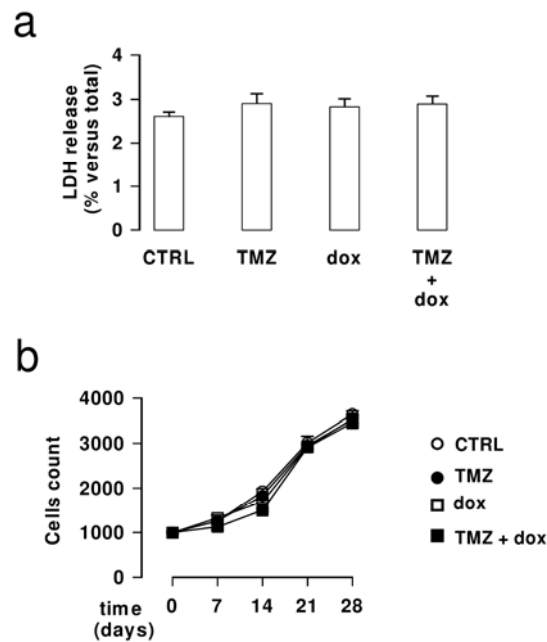
## Online Resource 8



### Online Resource 8. Effects of temozolomide on *mdr1* expression in glioblastoma cells co-cultured with hCMEC/D3 cells.

hCMEC/D3 cells were grown for 7 days up to confluence in Transwell inserts; CV17, 01010627 and U87-MG cells were seeded at day 4 in the lower chamber. After 3 days of co-culture, the supernatant in the upper chamber was replaced with fresh medium without (-) or with temozolomide (50  $\mu\text{mol/L}$  for 48 h; *TMZ*). Total RNA was extracted and reverse-transcribed, the expression of *mdr1* gene was detected by qRT-PCR. The expression level in untreated CV17 cells was considered "1". Data are presented as means  $\pm$  SD (n = 3). Vs untreated cells: \* p < 0.02.

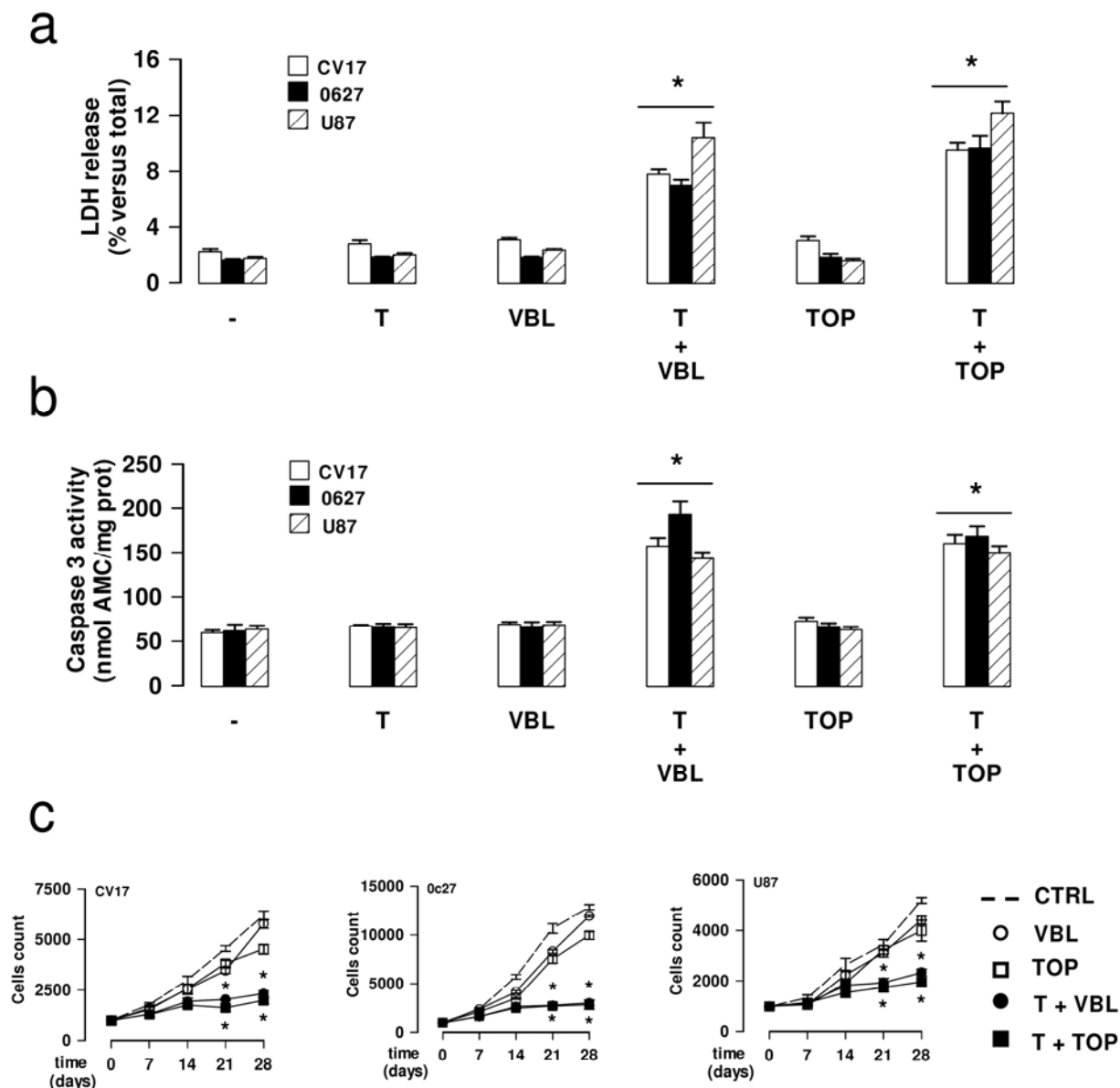
## Online Resource 9



### Online Resource 9. Effects of temozolomide and doxorubicin on cell survival of hCMEC/D3 cells.

**a.** hCMEC/D3 were cultured 7 days up to confluence, then incubated in fresh medium (CTRL), or medium containing 50  $\mu\text{mol/L}$  temozolomide for 72 h (TMZ), 5  $\mu\text{mol/L}$  doxorubicin for 24 h (dox), or 50  $\mu\text{mol/L}$  temozolomide for 72 h plus 5  $\mu\text{mol/L}$  doxorubicin in the last 24 h. The culture supernatant of cells was checked spectrophotometrically for the extracellular activity of LDH, taken as an index of cytotoxicity. Measurements were performed in duplicate and data are presented as means  $\pm$  SD ( $n=3$ ). **b.** 1,000 hCMEC/D3 were seeded at day 0 in 96-wells plates. After 4 days, the medium was replaced with fresh medium (open circles, CTRL) or medium containing 50  $\mu\text{mol/L}$  temozolomide for 72 h (solid circles, TMZ), 5  $\mu\text{mol/L}$  doxorubicin for 24 h (open squares, dox), 50  $\mu\text{mol/L}$  temozolomide for 72 h plus 5  $\mu\text{mol/L}$  doxorubicin in the last 24 h (solid squares, TMZ + dox). Drug treatments were repeated every 7 days. Cell proliferation was monitored on day 7, 14, 21 and 28 by crystal violet staining. Measurements were performed in triplicate and data are presented as means  $\pm$  SD ( $n=3$ ).

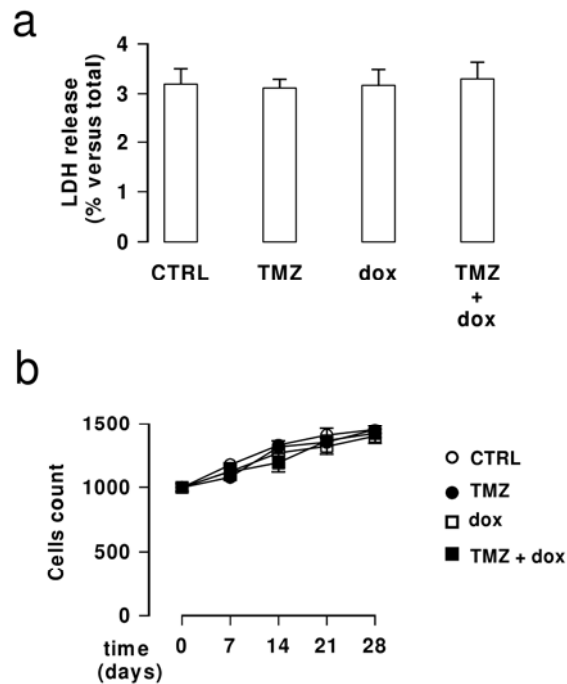
## Online Resource 10



### Online Resource 10. Effective cytotoxicity of the combination temozolomide plus vinblastine and topotecan on glioblastoma cells co-cultured with hCMEC/D3 cells.

hCMEC/D3 cells were grown for 7 days up to confluence in Transwell inserts; CV17, 01010627 and U87-MG cells were seeded at day 4 in the lower chamber. After 3 days of co-culture, the supernatant in the upper chamber was replaced with fresh medium without (-) or with temozolomide (50  $\mu\text{mol/L}$  for 72 h; *T*). 20 nmol/L vinblastine (*VBL*) or 10  $\mu\text{mol/L}$  topotecan (*TOP*) was added in the upper chamber of Transwell in the last 24 h, then the following investigations were performed. **a.** The culture supernatant of glioblastoma cells was checked for the extracellular activity of LDH. Measurements were performed in duplicate and data are presented as means  $\pm$  SD ( $n=4$ ). Vs untreated cells: \*  $p < 0.02$ . **b.** The activation of caspase-3 was measured fluorimetrically in glioblastoma cells lysates. Measurements were performed in duplicate and data are presented as means  $\pm$  SD ( $n=4$ ). Vs untreated cells: \*  $p < 0.01$ . **c.** After 3 days of co-culture, the medium of the upper chamber was replaced with fresh medium (*dashed line*) or medium containing 20 nmol/L vinblastine for 24 h (*open circles, VBL*), 10  $\mu\text{mol/L}$  topotecan for 24 h (*open squares, TOP*), 50  $\mu\text{mol/L}$  temozolomide for 72 h plus 20 nmol/L vinblastine in the last 24 h (*solid circles, T + VBL*), 50  $\mu\text{mol/L}$  temozolomide for 72 h plus 10  $\mu\text{mol/L}$  topotecan in the last 24 h (*solid squares, T + TOP*). Drug treatments were repeated every 7 days, as reported in the Materials and methods section. The proliferation of glioblastoma cells was monitored weekly by crystal violet staining. Measurements were performed in triplicate and data are presented as means  $\pm$  SD ( $n=4$ ). Vs untreated cells (*CTRL*): \*  $p < 0.02$ .

## Online Resource 11



### Online Resource 11. Effects of temozolomide and doxorubicin on cell survival of primary human brain microvascular endothelial cells.

**a.** HBMECs were cultured 7 days up to confluence, then incubated in fresh medium (CTRL), or medium containing 50  $\mu\text{mol/L}$  temozolomide for 72 h (TMZ), 5  $\mu\text{mol/L}$  doxorubicin for 24 h (dox), or 50  $\mu\text{mol/L}$  temozolomide for 72 h plus 5  $\mu\text{mol/L}$  doxorubicin in the last 24 h. The culture supernatant of cells was checked spectrophotometrically for the extracellular activity of LDH, taken as an index of cytotoxicity. Measurements were performed in duplicate and data are presented as means  $\pm$  SD ( $n=3$ ). **b.** 1,000 HBMECs were seeded at day 0 in 96-wells plates. After 4 days, the medium was replaced with fresh medium (open circles, CTRL) or medium containing 50  $\mu\text{mol/L}$  temozolomide for 72 h (solid circles, TMZ), 5  $\mu\text{mol/L}$  doxorubicin for 24 h (open squares, dox), 50  $\mu\text{mol/L}$  temozolomide for 72 h plus 5  $\mu\text{mol/L}$  doxorubicin in the last 24 h (solid squares, TMZ + dox). Drug treatments were repeated every 7 days. Cell proliferation was monitored on day 7, 14, 21 and 28 by crystal violet staining. Measurements were performed in triplicate and data are presented as means  $\pm$  SD ( $n=3$ ).